PROBABILISTIC ANALYSIS
OF
FAILURES MECHANISMS
OF
LARGE DAMS

II

PROBABILISTIC ANALYSIS

OF

FAILURES MECHANISMS OF LARGE DAMS

Proefschrift

ter verkrijging van de graad van doctor

aan de Technische Universiteit Delft,

op gezag van de Rector Magnificus prof. ir. K.C.A.M. Luyben,

voorzitter van het College voor Promoties,

in het openbaar te verdedigen op dinsdag 7 Oktober 2014 om 10:00 uur

door

GHOLAMREZA SHAMS GHAHFAROKHI

Master in Civil Engineering Hydraulic

Amirkabir University of Technology (Tehran Polytechnic)

geboren Khorramabad – IRAN

Dit proefschrift is goedgekeurd door de promotor:

Prof. drs. ir. J.K. Vrijling

Prof. dr. ir. P.H.A.J.M. van Gelder

Samenstelling promotiecommissie:

Rector Magnificus,	voorzitter
Prof. drs. ir. J. K. Vrijling,	Technische Universiteit Delft, promotor
Prof. dr. ir. P.H.A.J.M. van Gelder,	Technische Universiteit Delft, promotor
Prof. dr. ir. S. N. Jonkman,	Technische Universiteit Delft
Prof. dr. ir. M. Kok,	Technische Universiteit Delft
Prof. M. R. Maheri,	Shiraz University, Iran
Prof. ir. C. A. Willemse,	SBM Schiedam B.V, Nederland
Dr. ir. G. Hoffmans,	Deltares, Nederland
Prof. ir. T. Vellinga,	Technische Universiteit Delft

To my family

&

In memory of my mother

Summary

Risk and reliability analysis is presently being performed in almost all fields of engineering depending upon the specific field and its particular area. Probabilistic risk analysis (PRA), also called quantitative risk analysis (QRA) is a central feature of hydraulic engineering structural design.

Actually, probabilistic methods, which consider resistance and load parameters as random variables, are more suitable than conventional deterministic methods to determine the safety level of a hydraulic structure. In fact, hydraulic variables involved in hydraulic structures, such as discharge, flow depth and velocity, are stochastic in nature, which maybe represented by relevant probability distributions. Therefore, the optimal design of hydraulic structures needs to be modelled by probabilistic methods.

Reliability analysis methods are being adopted for use to develop risk management programs. Implementing the programs will ensure that safety is maintained to a robust and acceptable level. Any simple reliability analysis should include the following steps:

The main work carried out relates to three different subjects in the general area of dam structures failure. These included the probabilistic methods work on:

- o *Geometry of plunge pool downstream of flip bucket spillway*
- o *Evaluation of superelevation in open channel bends*
- o *Hydrodynamic loading on buildings by floods*

1. Geometry of plunge pool downstream of flip bucket spillway

Extreme scouring can gradually undermine the foundations of structures such as spillway and body dams and the areas downstream of dams. Extensive plunge pools downstream of flip bucket spillway structures, which are caused by jets of different configurations, form an important field of research.

The plunge pool mechanism is more complex because of difficulties arising from the modelling of bed rock and sediment load flow in and around the scour hole caused by the jet

effect of the flow downstream of flip bucket spillway. The experimental study of plunge pool has been limited to the consideration of variables involved in the plunge pool geometry.

The reliability-based assessment of the geometry of the plunge pool downstream of a flip bucket spillway. Experimental data obtained from a model of a flip bucket spillway has been used to develop a number of equations for the prediction of scour geometry downstream from a flip bucket spillway of a large dam structure. The accuracy of the developed equations was examined both through statistical and experimental procedures with satisfactory results.

2. *Evaluation of superelevation in open channel bends*

The so-called centrifugal force caused by flow around a curve results in a rise in the water surface at the outside wall and a depression of the surface along the inside wall. This phenomenon is called superelevation. The problems associated with flow through open channel bends deserve special attention in hydraulic engineering. Water surface slopes have been frequently reported to be a function of the curvature. But due to the difficulties in operation, the theoretical basis of superelevation has been discussed in depth in the literature. Furthermore, experience indicates that existing theory does not lead to good results at the present status.

Superelevation in the Ziaran Flume (Iran) has led to severe erosion of the bank and has undermined the structure. Therefore, this study aims to cast light on the cause of overtopping by superelevation. By means of direct observation on the flume's hydraulic performance, during full discharge, and from generalization of the field data, a more reliable prediction method of the magnitude of superelevation has become possible. The probabilistic analysis is shown to have several advantages in comparison with deterministic analysis methods.

3. *Hydrodynamic loadings on buildings by floods*

Assessing the vulnerability of buildings in flood-prone areas is a key issue when evaluating the risk induced by flood events, particularly because of its proved direct influence on the loss of life during catastrophes. Hydrodynamic loads are caused by water flowing along, against and around a structural element or system. Hydrodynamic loads are basically of the lateral type and are related to direct impulsive loads by the moving mass of water, and to drag forces as the water flows around the obstruction. Where application of hydrodynamic loads is required, the loads shall be calculated or estimated by recognized engineering and reliable methods.

A comprehensive methodology for risk assessment of buildings subjected to flooding is nevertheless still missing. A new set of experiments has been performed in this thesis with the aim of shedding more light on dynamics of flood induced loads and their effects on buildings with state of the art benchmarks. In this research, an overview is given of flood induced load on buildings, the new experimental work is then presented, together with results from preliminary analysis. Initial results suggest that use of existing prediction methods might be unsafe and that impulsive loading might be critical for both the assessment of the vulnerability of existing structures and the design of new flood-proof buildings.

The research presented in this thesis is focused on developing and applying probabilistic design, safety, system reliability and risk based design in the field of hydraulic structures design in the open channel bends, plunge pool downstream of flip bucket spillway and dam break analysis. Probabilistic design approach is a powerful tool in reliability assessment of

civil hydraulic engineering. Uncertainty and risk are central features of hydraulic engineering. Hydraulic design is subject to uncertainties due to the randomness of natural phenomena, data sample limitations and errors, modelling reliability and operational variability. Uncertainties can be measured in terms of the probability density function, confidence interval, or statistical moment such as standard deviation or coefficient of variation of the stochastic parameters.

Outcomes from this thesis are beneficial to the design of hydraulic structures in many ways; not only minimizing cost, but also educating and providing valuable knowledge for structural operators. Probabilistic methods and reliability analysis can increase the quality and value of the achievements compared to traditional dam engineering approaches. Since the goal is to avoid the dam failures by reducing risk to almost zero with optimum cost, dam safety risk analysis has a key role in modern dam safety programs. It is hoped that illustrations provided in this thesis are applicable to other civil engineering structures of similar concerns.

Gholamreza Shams Ghahfarokhi

October 2014, Delft

X

Samenvatting

Risico- en betrouwbaarheidsanalyses worden momenteel in bijna alle gebieden van de techniek uitgevoerd, afhankelijk van het specifieke gebied en haar specialisatie. Probabilistische risicoanalyse (Probabilistic Risk Analysis - PRA), ook wel kwantitatieve risicoanalyse (Quantitative Risk Analysis - QRA) genaamd, is een wezenlijk onderdeel binnen de constructieve waterbouwkunde.

Probabilistische methoden, die de variabelen weerstand en belasting als stochastische variabelen in acht nemen, zijn beter geschikt dan conventionele deterministische methoden om het veiligheidsniveau van een waterbouwkunde constructies te bepalen. In feite, zijn hydraulische variabelen, die van invloed zijn op waterbouwkundige constructies, zoals afvoer, stroom-diepte en stroomsnelheid, van nature stochastisch, welke door relevante kansverdelingen gerepresenteerd kunnen worden. Het optimale ontwerp van waterbouwkundige constructies moet daarom gemodelleerd worden door probabilistische methoden.

Betrouwbaarheidsanalyse methoden maken onderdeel uit van de ontwikkeling en toepassing van risicomanagement programma's. Uitvoering van deze programma's zal garanderen dat de veiligheid op een robuust en aanvaardbaar niveau wordt gehandhaafd. Een eenvoudige betrouwbaarheidsanalyse moet de volgende stappen bevatten:

Het uitgevoerde onderzoek is gerelateerd aan drie verschillende onderwerpen binnen het domein van constructief falen van dammen. Deze onderwerpen zijn de probabilistische benadering van:

- o *Geometrie van de plunge pool benedenstrooms van de flip bucket spillway*
- o *Evaluatie van superelevatie in open kanaal bochten*
- o *Hydrodynamische belastingen op gebouwen door overstromingen*

1. Geometrie van de plunge pool benedenstrooms van de flip bucket spillway

Extreme erosie kan geleidelijk de fundamenten van constructies, zoals noodoverlaten en dammen, en het gebied van dammen stroomafwaarts, ondermijnen. De 'plons' poelen

stroomafwaarts van flip-bucket noodoverlaat constructies, die worden veroorzaakt door stromen van verschillende configuraties, vormen een belangrijk gebied van onderzoek.

Het 'plons' poel mechanisme is complex vanwege de moeilijkheden die voortvloeien uit de modellering van "bed rock" en sediment belasting in en rond het poel-gat, veroorzaakt door het 'jet-effect' van de stroomafwaartse stroming van de "flip-bucket" noodoverlaat. De experimentele studies van de 'plons' poel zijn beperkt tot de geometrische variabelen.

Het onderwerp van dit onderzoek is de betrouwbaarheidsgebaseerde beoordeling van de geometrie van de 'plons' poel, stroomafwaarts van een zgn. 'ski jump bucket'. De experimentele gegevens, verkregen middels een schaalmodel van een 'flip-bucket' noodoverlaat, zijn gebruikt om een aantal vergelijkingen te ontwikkelen voor de voorspelling van de erosie- geometrie, stroomafwaarts van de 'flip bucket' noodoverlaat van een grote dam constructie. De nauwkeurigheid van de ontwikkelde vergelijkingen is zowel via statistische als experimentele procedures onderzocht, met bevredigende resultaten.

2. *Evaluatie van superelevatie in open kanaal bochten*

De zogenaamde centrifugale kracht veroorzaakt door stroming in een kromming, resulteert in een stijging van het wateroppervlak aan de buitenmuur en een daling van het oppervlak langs de binnen muur. Dit verschijnsel heet scheluwte. De problemen met stroming door open kanaal bochten verdienen speciale aandacht in de waterbouw. De hellingen van water oppervlakten worden vaak gemodelleerd als een functie van de kromming. De theoretische basis van scheluwte is zeer diepgaand bediscussieerd in de literatuur. Uit ervaring is geconcludeerd dat de bestaande theorie in de huidige situatie niet tot gewenste resultaten leidt.

Scheluwte in de Ziaran stroomgoot (Iran) heeft tot ernstige erosie van de oever en tot ondermijning van de constructie geleid. Deze studie beoogt een licht te werpen op de oorzaak van overtopping ten gevolge van scheluwte. Door directe observatie van de hydraulische prestaties van de goot tijdens volledige afvoer van water en door generalisatie van de veld data, is een betrouwbaarder methode van de voorspelling van de omvang van scheluwte mogelijk geworden. De probabilistische analyse toont verschillende voordelen ten opzichte van en in vergelijking met de deterministische analyses.

3. *Hydrodynamische belastingen op gebouwen door overstromingen*

Beoordeling van de kwetsbaarheid van gebouwen in overstromingsgevoelige gebieden is een belangrijk aspect in de evaluatie van risico bij overstroming, in het bijzonder door de bewezen directe invloed op het verlies van mensenlevens tijdens rampen. Hydrodynamische belastingen zijn het resultaat van stromend water langs, tegen en rond een rigide constructief element of systeem. Hydrodynamische belastingen zijn in principe lateraal en zijn gerelateerd aan directe impact belastingen en aan sleepkrachten van de stroming rond de obstructie. Goede rekenmodellen voor hydrodynamische belastingen op constructies zijn beschikbaar.

Een alomvattende methodologie voor de evaluatie van het overstromingsrisico van gebouwen is niettemin nog afwezig. Een nieuwe reeks van experimenten, met het doel om meer licht te werpen op de dynamische effecten van door overstromingen veroorzaakte belastingen op gebouwen, is binnen dit promotie-onderzoek volgens de nieuwste methoden verricht. Daartoe is in dit onderzoek een overzicht gegeven van door overstromingen veroorzaakte belastingen op gebouwen en worden de analyses en resultaten van het nieuwe experimentele werk gepresenteerd. De resultaten suggereren dat het gebruik van bestaande voorspellingsmethoden onveilig kunnen zijn en dat impact belastingen cruciaal kunnen zijn voor zowel de

beoordeling van de kwetsbaarheid van bestaande constructies als voor het ontwerp van nieuwe overstromingsresistente gebouwen.

Het promotie-onderzoek is gericht op het ontwikkelen en toepassen van een probabilistisch en risico-gebaseerd ontwerp, gericht op veiligheid en betrouwbaarheid van waterbouwkundige constructies. Een probabilistische ontwerpbenadering is een krachtig hulpmiddel in de betrouwbaarheidsanalyse van de civiele waterbouw. Onzekerheden en risico's zijn centrale kenmerken van de waterbouw. Hydraulisch ontwerp is onderhevig aan onzekerheden en de willekeur ten gevolge van natuurlijke fenomenen, de beperkingen en fouten van experimentele data, de modelleringsbetrouwbaarheid en de operationele variabiliteit. Onzekerheden dienen te worden gemeten in termen van kansdichtheidsfuncties, betrouwbaarheidsintervallen, statistische momenten, zoals standaarddeviatie, of de variatiecoëfficiënt van de stochastische parameters.

De resultaten van deze thesis zijn nuttig voor het ontwerpen van waterbouwkundige constructies op meerdere manieren. Niet alleen worden de kosten geminimaliseerd, maar toegevoegde bijdragen zijn ook het opleiden en verstrekken van waardevolle kennis aan waterbouwkundig ingenieurs. Probabilistische methoden en betrouwbaarheidsanalyse kunnen de kwaliteit en waarde van de resultaten verhogen in vergelijking met traditionele benaderingen van dam technologie. Aangezien het doel is om dam falen te voorkomen door een optimale risicokosten vermindering tot bijna nul, hebben dam veiligheid en risicoanalyse een belangrijke rol in moderne programma's van dam veiligheid. De cases in deze thesis kunnen hopelijk ook van toepassing zijn op andere civieltechnische constructies met eenzelfde problematiek.

Gholamreza Shams Ghahfarokhi

Oktober 2014, Delft

Contents

CHAPTER 1

INTRODUCTION

Natural hazards are threatening modern societies around the world with almost non-stop intervals. Every year many natural disasters happen of which flooding comes close to the top of these disasters in terms of loss of life and economic damage. People do not want these disasters to happen again and are trying to minimize the damage as much as possible. Technical engineering measures and probabilistic methods can be effective in the fight against flooding (United Nations, 2004).

Hydraulic structures are built to store water and make it available for irrigation, drinking water supply, energy production and flood reduction. While hydraulic structures originally provided flood protection for agricultural lands, other facilities as diverse as industrial, commercial and residential now rely on flood protection as well.

In river areas people live on the natural higher grounds while the lower areas are generally used for cultivation. As a result, the regular floods deposited fertile silt on the land which enabled the land to keep pace with the naturally rising sea level.

The rise in population meant that increasing numbers of lower lying areas were taken into use. In addition, a rise in population is often accompanied by a rise in human activities in flood prone areas, often resulting in an increase of society, cultural and economic values of the land. This means that more property and life may be at risk due to flooding and in need of protection.

In summary, densely populated, highly developed but low lying areas if affected by flooding, could lead to loss of life, economy and culture and a disruption of society. Therefore, hydraulic structures and flood defence systems and models are needed.

1.1 DAM SAFETY

1.1.1 Overview of Dams

Dams are artificial structures built to confine water in a reservoir. Dams are built for many multifunction goals including irrigation, flood control, navigation, hydroelectric, water storage for potable water supply, livestock water supply and recreation.

1.1.2 Failure Mode / Mechanisms

A failure mode mechanism describes how element or component failures must occur to cause loss of the sub-system or system function. In this regard, failure modes are not unique features of the system but tools of how the system is modelled. Failure effects at a lower level in the system become the failure modes at the next highest level in the system. In general, the system is broken down into sub-systems to a level where there is a thorough understanding of the failure modes of the elementary sub-systems.

General failure mode categories have been presented in Figure 1-1 and Figure 1-2 for dams and while these categories are often too general for definitive risk analysis for a dam, they are useful for comparative analysis because they are at a sufficiently generalised level to permit broad comparisons between dams and dam components. Dam failures can result from any one, or a combination, of the following causes:

- *Extended periods of rainfall;*
- *Flooding and inundation, which cause most failures;*
- *Insufficient spillway capacity results in excess overtopping and can be divided into ;*
  - *Out-of-channel flow may be caused by the superelevation, size of the channel, obstructions, its gradient, cross-waves, steps or pools or bulking through air entrainment Water is not contained in the spillway channel when it overflows from the reservoir. This can cause erosion of the embankment if the spillway channel is located close to it. (Figure 1-3).*
  - *Inadequate energy dissipation is not restricted to the toe of the spillway, and scour or erosional features can also develop further up the structure.(Figure 1-4);*
- *External erosion and internal erosion caused by foundation leakage or piping;*
- *Improper design and Improper construction materials;*
- *Cracks at the top of the embankments;*
- *Animal burrows;*
- *Human failure;*
- *Structural failure caused stress or instability from material used in dam constrictions;*
- *Landslides into reservoirs;*
- *High winds, which can cause significant wave action and result in substantial erosion;*
- *Insufficient maintenance, including to control and repair internal seepage problems, or valves, gates, remove trees and other operational components;*
- *Earthquake damage due to seismic induced hydrodynamic forces*
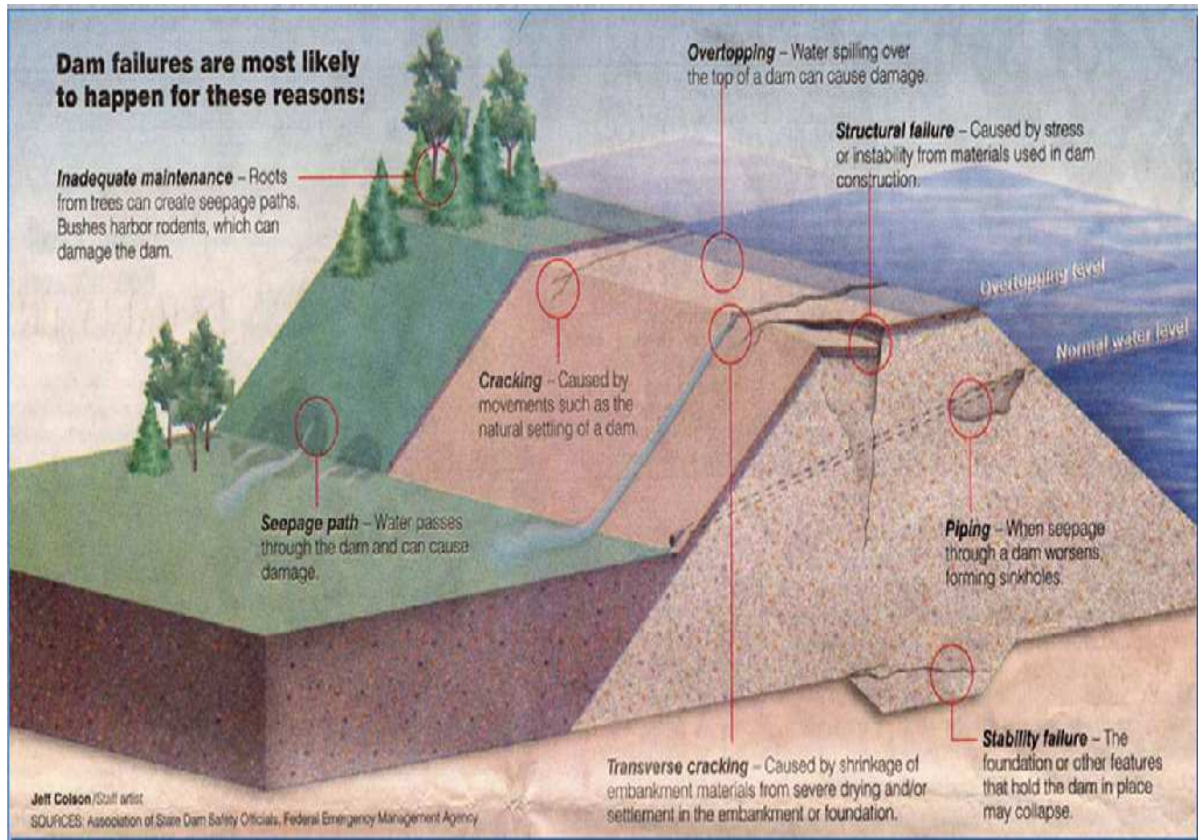
Figure 1-1. Anatomy of dam failure mechanisms, Zebell, (2012)
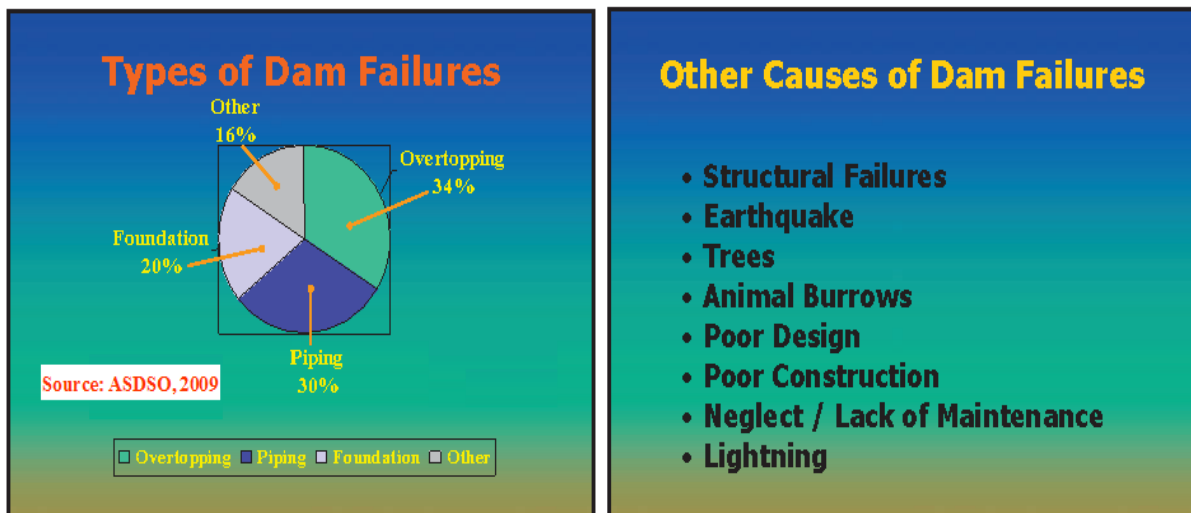
Figure 1-2. Causes of dam failure, Harrington (2012)
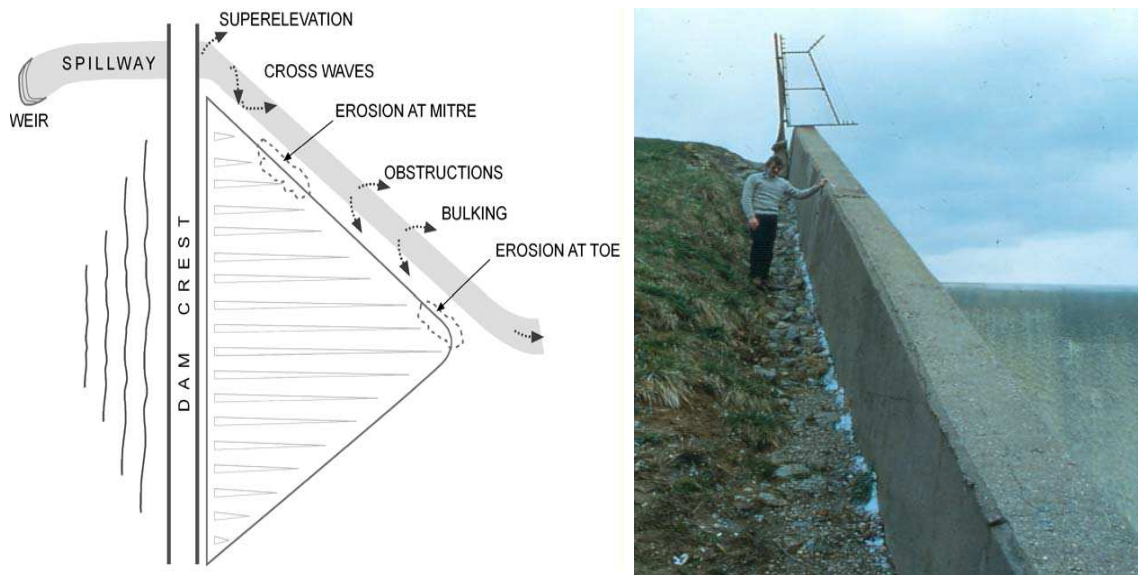
Figure 1-3. Out-of-channel flow phenomena by in spillway, Almog, 2011, (left). Erosion adjacent to a spillway wall, NC. DENR, 2007 (right).

1.1.3   Plunge Pools

For at least 80 years plunge pools have been used in modern dam construction to dissipate energy by jet impact. High dams are built for flood retention to store water and make it available for irrigation, drinking water supply and energy production. These structures include by-pass channels or orifices to control the water level in the reservoir. In case the storage limit is reached during a critical flood, water has to be released; a further uncontrolled water level rise may be threatening dam safety. The discharges release water that is stored a few dozen meters higher than the river downstream. The potential energy of the water is converted into the kinetic energy of the flows passing through channel spillways or orifices. The velocities reached by such flows are largely in excess of the corresponding flow velocities in natural floods in the downstream reach and may produce uncontrolled erosion of the riverbed and banks. Therefore, part of this kinetic energy has to be dissipated locally, so that restitution velocities become lower.

The direct impact of falling jets on the riverbed downstream of high dams is often used as a solution for the dissipation of water energy from floods. In these cases, the assessment of the formation of scour is mandatory for dam safety as the scour hole might compromise the foundation of the dam. It is a complex water-air-rock interaction problem.

For large dams, scaled physical model tests are often performed. The results are combined with prototype observations in order to develop empirical formulae for ultimate scour prediction. The applicability of empirical methods is limited to the range of tested parameters and it does not represent the complex interaction between a highly aerated water jet and the rock. Also, correction factors have been added in previous research to account for jet aeration, two-phase pool flow, as well as local rock characteristics but are limited to the conditions for which they were obtained. Therefore, the use of empirical methods is often limited to the preliminary stages of a project.
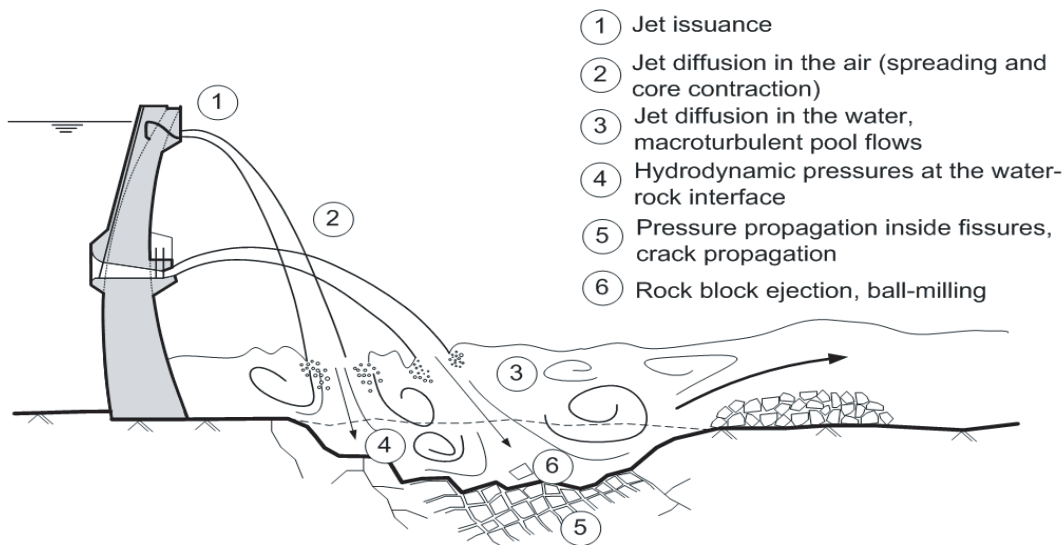
Figure 1-4. Schematic process in plunge pool, Manso (2009)

The process of plunge pool can be divided into six different phases (see Figure 1.4): (1) jet issuance, (2) jet diffusion in the air, (3) turbulence shear-layer diffusion in plunge pool, (4) dynamic pressure at the interface between the water and the rock, (5) hydraulic fracturing of the rock, (6) dynamic uplift of the rock blocks, and finally the disintegration and transport of them.

A comprehensive review and discussion about scouring and also the relation with foundation stability downstream of dams can be found in Schleiss and Bollaert (2002) or other published literature. The hydrodynamic pressures generated by the impact of the jet at the pool bottom can cause the failure of reinforced concrete structures built to confine energy dissipation (e.g. stilling basin or lined plunge pools) and are the driving agent for scour progression in unlined plunge pools (Manso, 2006).

Displacement of large concrete slabs by differential pressure fluctuations has been investigated experimentally for stilling basin under the influence of hydraulic jumps, as well as under the impact of falling jets.

In unlined plunge pools, the rock mass should first disintegrate before the loose blocks can be removed. Unlined pools are highly heterogeneous by nature, whereas lined pools are the results of engineering design. There is increasing interest in the definition of dynamic impact pressures at the pool bottom, for typical prototype conditions of jet velocity, turbulence and pool depths. Figure 1-8 shows the spillway and plunge pool Theodore Roosevelt dam in during and after construction.

Figure 1-5. Karun III arch dam in Iran, H = 205 m, maximum discharge capacity of 18000 (m^3/s) through chute and overfall spillways and orifices (IWPCO, 2006).

A recent example of the combination of solutions is presented in Figure 1-5 for the Karun III HEPP dam project in Iran (IWPCO, 2006). All spillway flows are discharged into a $400\,m$ long, $50\,m$ wide, concrete lined plunge pool, as well as a $60\,m$ high tail pond dam ($45\,m$ from foundation to Ogee crest). The analysis of the dynamic pressures generated by the multiple spillways and outlet jets is of utmost importance for the design of the lining structure and drainage system, as well as for the definition of the tail pond dam height and of the operation guidelines for flood routing.

1.1.3.1 *Previous Research*

Systematic research on the jets has been going on since the 1920's. Based on experimental data with air jets, Albertson (1948) set the foundations of the theory of free jet diffusion. Abramovich (1963) developed analytical solutions for typical jet applications, based on potential flow theory. Soon afterwards the first studies with plunging jets appeared (Henderson et al., 1970; Hartung and Hausler, 1973), Henderson et al. (1970), McKeogh and Elsawy (1980); McKeogh and Ervine (1981); Ervine and Falvey (1987); Sene (1988); Bin (1993).

The trajectory of jets in the air was studied by Martins (1977). A review on this topic was presented in Melo (2001). The development of the jet in the air has been discussed by, amongst others, Kraatz (1965); Henderson et al. (1970); Ervine and Falvey (1987). The influence of the issuance conditions were studied by Ervine and Falvey (1987); Zaman (1999); Burattini et al. (2004). However, the development of aerated core jets such as those issued from ski-jump spillways is barely documented.

1.1.3.2 *Estimation of Scour*

Several methods exist to estimate the ultimate scour, i.e. the scour depth that corresponds to an equilibrium situation. The scour estimation methods can be divided into hydrodynamic methods (Hartung and Hausler, 1973), empirical methods derived from model or prototype observations (Martins, 1973a; Mason and Arumugam, 1985), semi-empirical methods (Spurr,

1985; Annandale, 1995) and physically based methods (Yuditskii, 1963; Bollaert, 2002; Bollaert and Schleiss, 2005). Formulae for scour development both in time and space have been proposed based on experimental tests with mobile bed (Rajaratnam and Mazurek, 2002, 2003), compared with numerical simulation (Salehi-Neyshabouri et al., 2003) and development of the influence of upstream turbulence on local scour holes (Hoffmans and Verheij 1993, 1997, 2003, 2011).

1.1.3.3   *Rock Bed*

High-velocity plunging jets, coming from hydraulic artificial or natural structures, can result in scouring of the rock riverbed or the dam toe foundation (see Figure 1-6). Assessment of the extent of scour is necessary to ensure the safety of the dam and to guarantee the stability of its abutments. Plunge pools are a highly dynamic and multi complex process which is governed by the interaction with water, rock and air.

To estimate potential scour different methods can be used but the most common method is the use of a hydraulic scale model. However, it is nearly impossible to fully simulate the process above in a hydraulic scale model and therefore the model often consists of a downstream bed with different material which only makes it possible to simulate a part of the last phase (the transport of the rock block from the plunge pool). This usage of a fully erodible bed to estimate scour results in what is called the ultimate or maximum scour (Khatsuria, 2005).

1.1.3.4   *Mobile Bed*

Most research on plunge pool scour has been conducted with uniform grain sized material, simulating a fully disintegrated rock foundation. The predominant sediment transport mechanism is the shear stress generated by the laterally expanding wall jets (see Figure 1-7).

Rajaratnam and Mazurek (2002, 2003) presented results of tests with non-cohesive bed material and provided empirical relations for the scour profiles and its development in time, for different jet velocities and angles of impact. Pool profiles are presented as a function of a Froude number that accounts for the grain size. Scour growth follows a logarithmic law. The expressions proposed by these authors have wide applicability for scour assessment downstream of structures in alluvial riverbeds.

Figure 1-6. Plunge pool at Gebidem dam (left) [1]. A spillway failure caused by erosion, Harrington, 2012 (right).
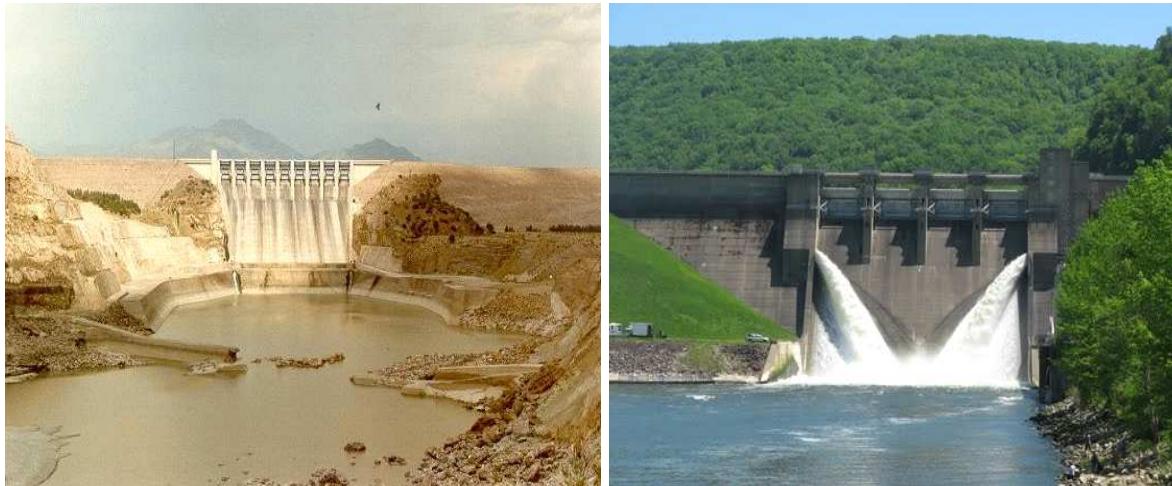
Figure 1-7. Plunge pool Tarbela Dam on the Indus River in Pakistan (left) [2]. Kinzua dam and plunge pool, on the Mississippi River, Pennsylvania, United State (right) [3].

Figure 1-8. Spillway and plunge pool Theodore Roosevelt dam in during and after construction, Phoenix, Arizona, United State, 1996, [4].

1.1.4   Superelevation

When a permanent flow moves around a curved channel, the water level increases at the outside edge of the channel and a corresponding decrease in level occurs at the inside edge of the channel. The superelevation is defined as the difference in elevation of water surface between inside and outside wall of the bend at a given section in the channel. The centrifugal forces act on the bend channel and fluid particles. The detail of superelevation is shown in Figure 1-9.
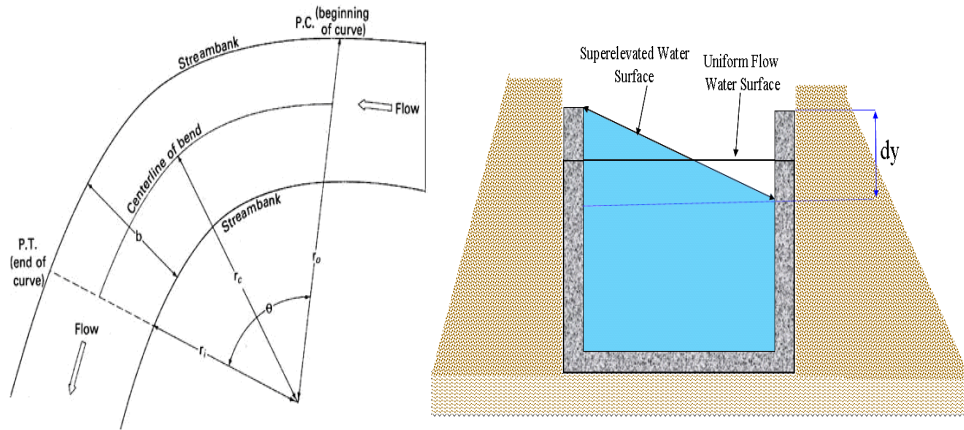
Figure 1-9. Superelevation dy in open channel bends

At extreme flow and overtopping the foundation of the bank walls can be undercut by scouring which results in failure of the protection wall. Especially walls in channel bends are endangered because of the increased erosion and scouring action in bends. Failure of the foundation and consequently of the protection wall, will allow uncontrolled lateral bank erosion, which will result in serious destruction of buildings and infrastructures.

On the floor of the natural channel the secondary flow transport sand, silt and gravel across the channel and deposits the solids near the inside wall. This process can lead to the formation of a meander or a point bar. The turbulence plays a more important role in the flow in a channel bend for superelevation increased (see Figure 1-10).
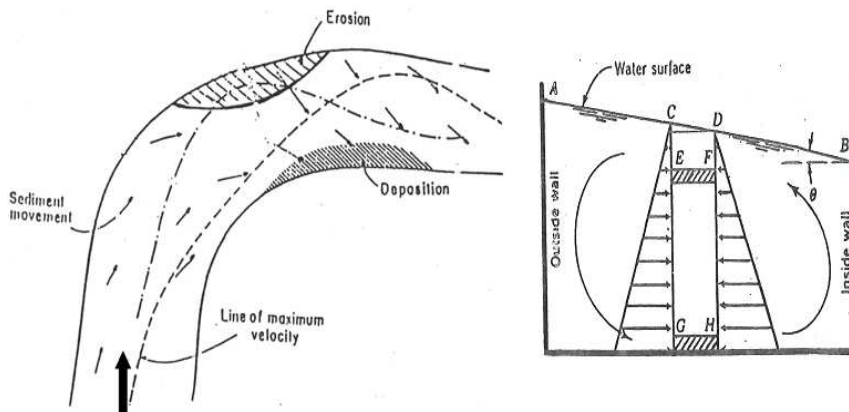
Figure 1-10. Velocity direction, secondary flow in the open channel (Shams, 1998)

1.1.4.1   Previous Research

Flow in open channel bends is commonly encountered in both natural and artificial channel systems in hydraulic design practice. It is characterised by flow separation, secondary flows, energy losses and water surface variations caused by the bend curvature. The first work on mathematical modelling of flow in curved channels is based on the assumption of laminar flow (e.g. Boussinesq (1868), Dean (1927) and many others). Many earlier bend flow studies Shukry (1949), Rozovskii (1957), Ippen & Drinker (1962), Kalkwijk and Vriend (1980), Vriend (1973, 1976, 1977, 1979 & 1981), Ikeda (1975), Gottlib (1976), Falcon (1979), Dietrich and Smith (1983), Odgaard (1989) and Blanckaert and Graf (2001, 2004) provided and they were often obtained in the central portion of the flow.

1.1.5   Dam Break

According to Yang and Jing (2010), a dam-break flow is a catastrophic dam failure, which can correspond to an uncontrolled release of water due to a dam, a channel or other types of hydraulic structure failures. The resulting rapid increase of discharge creates serious floods, with sharp gradient wave fronts and significant impact forces on structures or obstacles. Numerical and analytical models were used to predict dam break flow conditions. Also, with numerical models being capable of predicting more complex dam-break flows (see Figure 1-12 and Figure 1-13).

1.1.5.1   Previous Research

In the natural channels, flow is typically quite complex. Many researchers developed two-dimensional hydrodynamic models, and simulated unsteady flows, to predict flood propagation along in the channel and floodplains.

A number of models have been recently developed to simulate natural flows such as flash floods (Hogg and Pritchard 2004), floods with sediment transport (Pritchard 2005), snow avalanches (Bartelt 1999), debris flows (Huang and Garcia 1997, Iverson 1997) and lava flows (Griffiths 2000).

In recent years, many numerical methods have also been developed to simulate dam-break flows, including the characteristics method (Katopodes and Strelkoff 1978, 1979), finite difference method (Aureli 2000, Macchione and Morelli 2003, Liang 2007), discrete finite element method (Cockburn 2000, Dawson and Martinez- Canales 2000) and finite-volume method (Zhou et al. 1996, Wang and Liu 2001, Medina et al. 2008).

1.1.5.2   Riverine Floods

The forces generated during a riverine flood include hydrostatic, hydrodynamic, buoyancy, and the forces generated by the impact of waterborne debris (Caraballo-Nadal, 2006). These forces are illustrated in Figure 1-11.

The summary of the flood actions on a building is (Kelman et, al 2004):

- o *Hydrostatic forces (actions resulting from the water's presence, horizontal)*
- o *Hydrodynamic forces (actions resulting from the water's motion, horizontal)*
- o *Buoyancy forces (vertical)*

o *Erosion forces (water moving soil)*

o *Debris forces (actions from solids in the water)*

The Coastal Construction Manual (FEMA, 2000) recommends different contact time values according to the stiffness of the object and type of construction material, and debris.
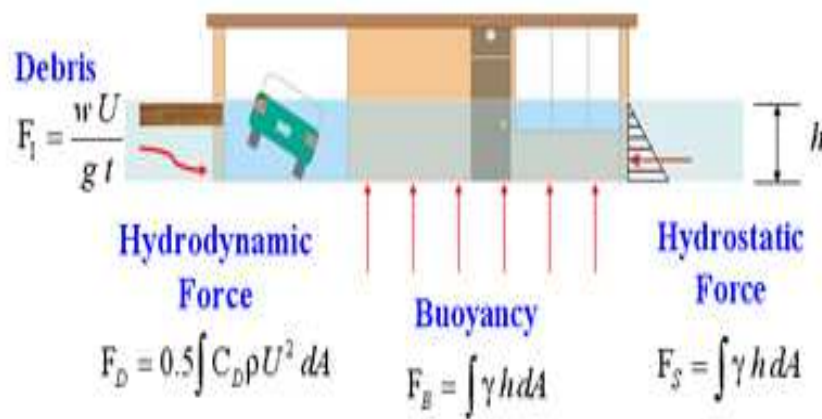
Figure 1-11. Typical forces generated by flooding (Caraballo-Nadal, 2006)

Figure 1-12. Dam break in the Shih-Kang Dam Taiwan, 1999 (left) [5]. Catastrophic dam-break flow in Delhi Dam, Maquoketa River, Iowa, United State, 2010 (right) [6].

Figure 1-13. Failure of the Auburn Cofferdam on the American River, 1986 (left) [7]. Teton Dam collapse, Idaho, United States, 1976 (right) [8].

1.1.5.3 Physical Model

The physical experiment model built at the Hydraulic Laboratory of the Delft University of Technology is shown in Figure 1.14. For the physical model tests, it was assumed that the dam or hydraulic structures failed immediately since the motivation for the physical model tests study were to see how the flood moved to downstream. These tests gave additional insights in the flood pressures (see chapter 8).

Figure 1-14. Photo of model structure housing force

1.2 PROBABILISTIC APPROACH IN HYDRAULIC ENGINEERING

In the last century, mathematical and statistical knowledge improved. Combined with the introduction in practice of structural fluid and soil mechanics the approach for hydraulic structural design became more and more scientific. The hydraulic load on a hydraulic structure could be predicted more accurately and the strength of the structure could be calculated. In the Netherlands after the disaster in 1953 a statistical approach to the storm surge levels was chosen and an extrapolated storm surge level formed the basis for dike design.

Probabilistic design approach is a powerful tool in reliability of civil hydraulic engineering. In hydraulic engineering, stress and load parameters are described by statistical distribution functions. Risk and reliability analysis is presently being performed in almost all fields of engineering, depending upon the specific field and its particular area. Since 1980, the development and application of reliability theory made it possible to assess the flooding risks taking into account the multiple failure mechanisms of the hydraulic structure. Dutch hydraulic designers were among the first to apply this theory in the practical design of structures.

In 1979 a project was started to apply the probabilistic methods to the design of dikes in general (Vrijling, 2001), water defence system (Vrijling 2000, 2001, 2002), Risk assessment system of natural hazards (Van Gelder et, al 2010) and reliability based and risk based design of flood defences system (Van Gelder 2000, Jonkman et, al 2008). Recently, the approach was applied on many Dutch polders or dikes.

Probabilistic design with risk based design concepts are considered the most modern approaches in the filed of hydraulic structural design. Advantages of the methods are that they allow the designer to take into account the uncertainties of the input parameters as random

variables, and to describe the hydraulic structure as a system, including various structural components and its protected area. Moreover, for each system component various possible failure modes can be considered. These all help to determine the probability of flooding of a protected area and judge its acceptability in view of the consequences of the protected area. Thus, probabilistic approach is apparently an essential tool for the analysis and design of hydraulic structures.

Uncertainty and risk are central features of hydraulic engineering. Uncertainties can be measured in terms of the probability density function, confidence intervals, or statistical moments such as standard deviation or coefficient of variation of the stochastic parameters.

In recent years, reliability and probabilistic hydraulic structural design and analysis of self elevating hydraulic units has been the subject of various research programs . Due to the complexity of the type of the structure and environmental conditions, no complete agreement has been achieved as the best choice for the analysis method.

As hydraulic structures are installed in deeper water and more severe environmental conditions, an improved understanding of interaction of the upstream and downstream flow and current with these structures remains important as:

o *There is a greater need to demonstrate safety and reliability, requiring more complete and accurate models.*

o *Costs are to be reduced and one way of achieving that is through the application of better technology.*

Analysis for probabilistic design of hydraulic structures requires integration of hydraulic, hydrodynamic and structural mechanics data and innovative use of theoretical and experimental technique. The model development in probabilistic methods is presented in Figure 1-15.
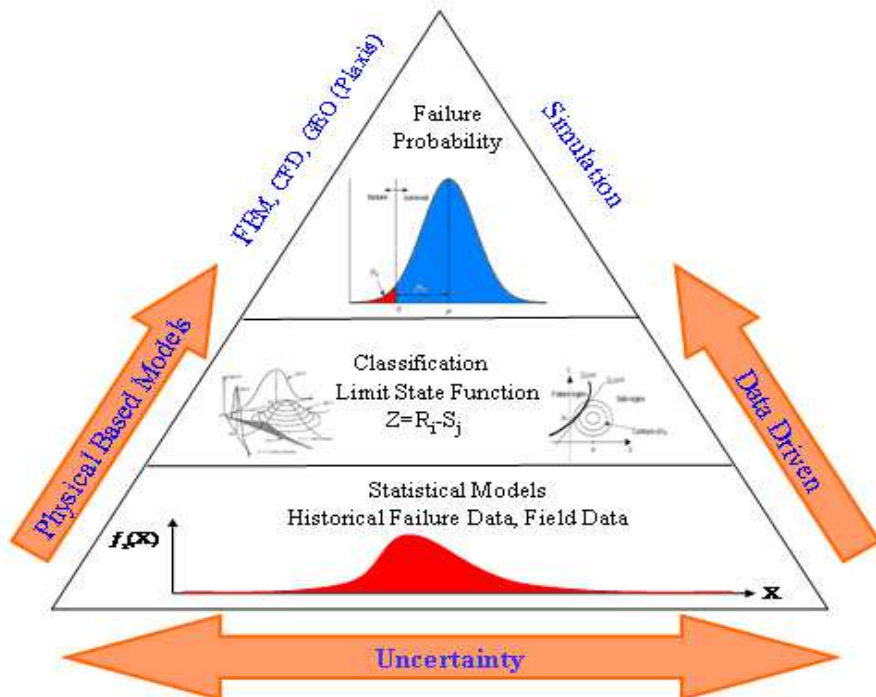
Figure 1-15. Model development in probabilistic methods

1.2.1   **Statistics and Engineering**

Engineering Design of Experiments is a methodology for formulating scientific and engineering problems using statistical models. According to Van der Heijden (2004), a designer for classification and estimation needs to find the best answer to this question: how can the information that is needed to design a hydraulic system to operate in the real world be inferred in usable form. Good design processing of the measurement is possible only if some knowledge and understanding of the environment and the system is present. Modelling certain aspects of that environment like objects, physical modelling or events is a necessary task for the engineer.

According to Van der Heijden (2004), parameter estimation is the process of attributing a parametric description to an object, a physical process or an event based on measurements that are obtained from that object (or process, or event). The measurements are made available by a sensory system. Figure 1-16 gives an overview.
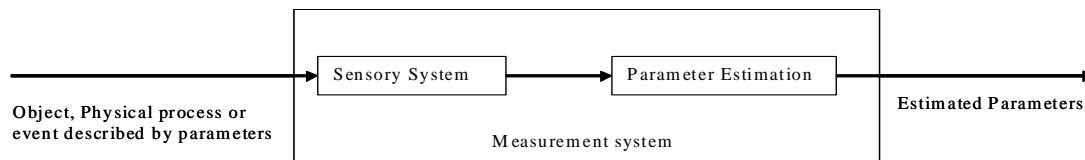
Figure 1-16. Parameter estimation presses (Van der Heijden, 2004)

1.3   GOALS OF THE THESIS

The goals of this thesis are to investigate:

   o *Geometry of plunge pool downstream of flip bucket spillway*
   o *Evaluation of superelevation in open channel bends*
   o *Hydrodynamic loading on buildings by floods*

1.4   OUTLINE OF THIS THESIS

The research presented in this thesis is focused on developing and application of probabilistic design, safety, system reliability and risk based design in the fields of hydraulic structures design. This dissertation has been organized into 9 chapters. The introductory material thus far includes the first chapter. The contents of the following chapters are briefly summarized below.

Methods and application of statistical techniques to analysis environmental data are presented in Chapter 2. The probabilistic methods are discussed and the significant parameters are reviewed. The proposed methodology for system reliability has been selected and the accuracy of proposed system reliability formulation in component reliability and system reliability has been verified for limit state functions for structural components. Methods concerning data management and parameter estimation methods are presented. This chapter explains the least-squares estimation and validation of a general linear model to observation. Three estimation principles, which lead to the weighted least squares estimation, the best linear unbiased estimation (BLUE) and the maximum likelihood estimation, will be

discussed. Equivalent expressions for estimators are determined using the model of condition equations afterward. The last part of this chapter deals with hypotheses testing to find misspecifications (with respect to data) in a linear model.

In chapter 3, the theoretical backgrounds of failure mechanisms of large dams are presented. A description of the hydraulic structures (concrete dams) in general and the load estimation and failure modes are presented in this chapter. A survey of various load and resistance models and techniques for failure probability calculation in large dams is also provided.

Chapter 4 deals briefly with the theoretical framework for fluid flows and includes an overview of some of the previous knowledge of relevant processes. Methods and application of deterministic technique to analyse geometry of plunge pool are presented in this chapter. A literature review in the deterministic plunge pool modeling of hydraulic structures is also presented in Chapter 4.

In Chapter 5, the theoretical background of deterministic design analysis is reviewed and investigated. Also, a literature review in the deterministic modelling for superelevation in open channel bends under hydraulic conditions is presented.

In Chapter 6, application of the theoretical methods that were given in Chapter 2 and 4 are made for the case study of design geometry of plunge pool down stream of flip bucket spillway. The weakest link of the system and dominant failure mode for geometry of plunge pool are found. A set of optimal geometry dimensionless for plunge pool design are presented in accordance with analysis results from the reliability based design model. This case study is completed with a full Probabilistic description of scour hole development downstream of a flip bucket spillway.

In chapter 7, application of the probabilistic methods, reliability analysis and design hydraulic structures that were given in Chapter 2 and 5 are made for evaluation of superelevation in open channel bend. An extensive overview of risk analysis method, economic risk evaluations and reliability based design models are discussed in this chapter. The economic risk based approach for optimal design in open channel bend is also discussed.

In Chapter 8 methods and application of statistical techniques to analyses physical laboratory data and dam break analyses are presented. A case study that contains a description of a physical laboratory test system and experimental program to investigate flood-induced loading and dam break on buildings are presented.

Chapter 9 provides conclusion and recommendations of this thesis. These include remarks regarding the methodology on the suitability of the proposed probabilistic approaches in design of hydraulic structures. The limitation of the present work is also highlighted. The recommendations presented are hoped to be further improved and incorporated in future researches on this topic.
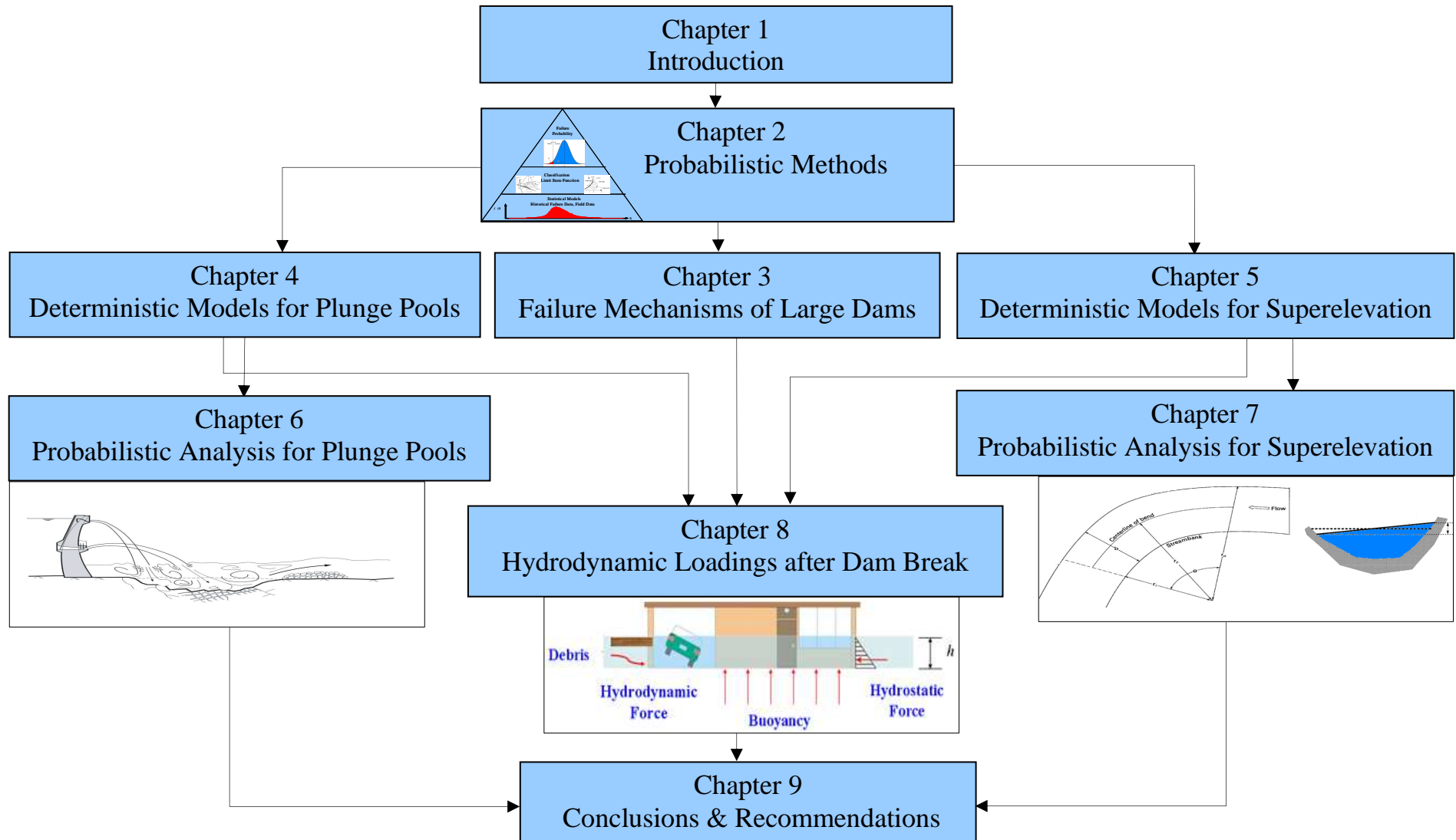
Figure 1-17. Schematic outline of the thesis

CHAPTER 2

PROBABILISTIC METHODS

The Probabilistic Method is a powerful tool in tackling many problems in engineering science. It belongs to those areas of engineering which have experienced a most impressive growth in the past few decades. This method in solving engineering problems is useful because it provides a better understanding of failure mechanisms and occurrence probabilities compared to other techniques. The complex hydraulic engineering problems with dimensionless analysis condition usually are analysis with least square techniques presented for instance in Azmathullah (2005); Shams et al. (2008). It provides an implicit approximation to the limit state function (LSF) that is far more accurate than other approaches.

This chapter contains the methodology of the thesis. Probabilistic methods will be fully utilized throughout the analysis. The methods however are too wide to be discussed in one single chapter. The basic ideas about probabilistic methods will be covered when discussing tools of reliability analysis. Following this, readers will be introduced to the theory of least squares estimation methods. In addition it provides an introduction to the estimation methods, with emphasis on least square methodology.

2.1 TOOLS OF RELIABILITY ANALYSIS

Probabilistic design methods are well known but their application is generally limited to difficult cases and to the development of design codes. The application of the probabilistic design methods offers the designer a way to unify the design of structures, dikes, dunes, mechanical, equipment and management systems. For this reason, there is a growing interest in the use of these methods (Van Gelder, 2000).

The tools available to the engineer for performing a reliability analysis fall into three broad categories. First there are the methods of direct reliability analysis. These propagate the uncertainties in properties, geometries, loads, water levels, etc. through analytical models to obtain probabilistic descriptions of the behaviour of a structure or system. The second category includes event trees, fault trees, and influence diagrams, which describe the interaction among events and conditions in an engineering system. The third group includes other statistical techniques. In particular, some problems are so poorly defined that it is useless to try to formulate mechanical models and the engineer must rely on simple statistics. (Van Gelder 1996).

2.1.1   Limit State Function

A model that applies to the failure of an engineering system can be described as the load S (external forces or demands) on the system exceeding the resistance R (strength, capacity, or supply) of the system equation (2.1) (Vrijling 2001).

$$Z(x_i) = Strength - Load = R_{r_i} - S_{s_j} = R(r_1, r_2, ..., r_i) - S(s_1, s_2, ..., s_j) \qquad (2.1)$$

The reliability P_S is described as the probability of safe operation, in which the resistance of the structure exceeds or equals to the load, that is,

$$P_s = P(Z > 0) = P(S \le R) \qquad (2.2)$$

In which P_f denotes the failure probability and can be computed as:

$$P_f = P(Z < 0) = P(R < S) = 1 - P_s \qquad (2.3)$$

The definitions of reliability and failure probability (equations (2.2) and (2.3)) are equally applicable to individual system components as well as total system reliability. The graph of Figure 2-1 shows Z=0 line of some hypothetical stochastic variables.
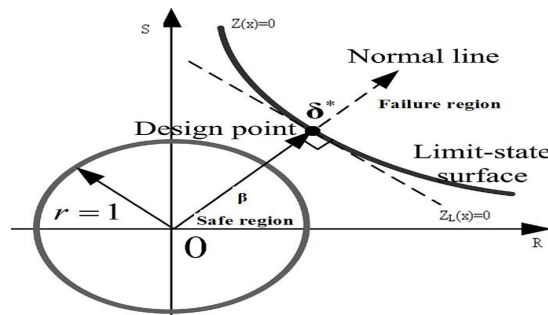
Figure 2-1. Reliability function

In the reliability function, the strength and load variables are assumed stochastic variables. A stochastic variable is a variable, which is defined by a cumulative distribution function (CDF) and a probability density function (PDF) shown in Figure 2-2.

The probability distribution F_x returns the probability that the variable is less than x. The probability density function is the first derivative of the probability distribution (Van Gelder 1996). If the distribution of the density of all the strength and load variables is known it is possible to estimate the probability that the load has a value x and that the strength has a value less than x (Figure 2-3).
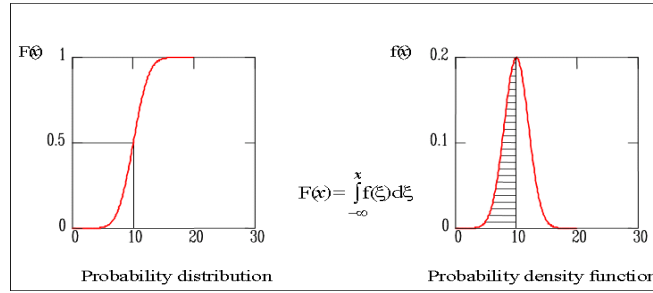
Figure 2-2. Probability distribution and Probability density function

The failure probability is the probability that $S = x$ and $R \leq x$ for every value of x. So

$$\left. \begin{array}{l} P(S = x) = f_S(x)dx \\ P(R \leq x) = F_R(x) \end{array} \right\} \Rightarrow P(S = x \cap R \leq x) = f_S(x)F_R(x) \tag{2.4}$$
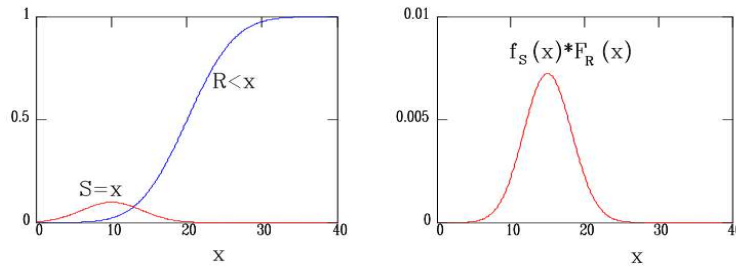
Figure 2-3. Components of the failure probability

We have to compute the sum of the probabilities for all possible values of x:

$$P_f = \int_{-\infty}^{\infty} f_S(x)F_R(x)dx \tag{2.5}$$

This method can be applied when the strength and the load are independent of each other. Figure 2-4 gives the joint probability density function for the strength and the load for a certain failure mode in which the strength and the load are not independent. The strength is plotted on the horizontal axis and the load is plotted on the vertical axis. The contours give the combinations of the strength and the load with the same probability density. In the area ($Z < 0$) the value of the reliability function is less then zero and the element will fail. (Van Gelder 1996).

The failure probability can by determined by summation of the probability density of all the combinations of strength and load in this area.

$$P_f = \int\int_{Z \langle 0} f_{RS}(r,s)drds = \int....\int_{Z \langle 0} \int f_{RS}(x_1, x_2, ..., x_n)dx_1dx_2....dx_n \tag{2.6}$$

In a real case, the strength and the load in the reliability function are nearly always functions of multiple variables. For instance, the load can consist of the water level and the significant wave height. In this case, the failure probability is less simple to evaluate. Nevertheless, with numerical methods, such as numerical integration and Monte Carlo simulation, it is possible to solve the integral:

$$P_f = \iint..\iint_{Z < 0} f_{r_1, r_2, ..., r_n, s_1, s_2, ..., s_m}(r_1, r_2, ..., r_n, s_1, s_2, ..., s_m)\, dr_1\, dr_2...r_n\, ds_1\, ds_2...ds_m \tag{2.7}$$
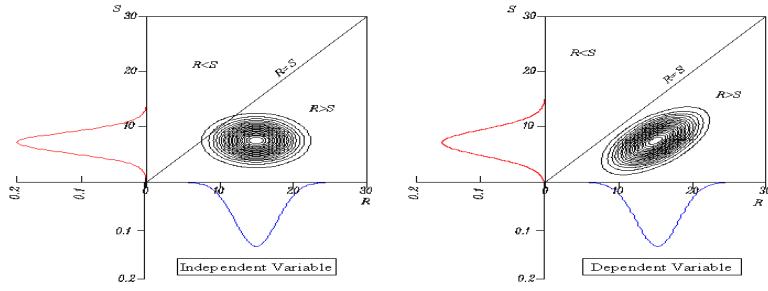
Figure 2-4. Joint probability density function

These methods, which take into account the real distribution of the variables, are called level III probabilistic methods. In Monte Carlo simulation method a large sample of values of the basic variables is generated and the number of failures is counted. The number of failures equals:

$$N_f = \sum_{j=1}^{N} 1\left(g\left(x_j\right)\right) \qquad (2.8)$$

in which, N is the total number of simulations, $1(g((x))$ is counter function, its value reset to 1 as the LSF is smaller than or equal to zero. The probability of failure can be estimated by:

$$P_f = \frac{N_f}{N} \qquad (2.9)$$

The coefficient of variation of the failure probability can be estimated by:

$$V_{P_f} = \frac{1}{\sqrt{P_f N}} \qquad (2.10)$$

in which, P_f denotes the estimated failure probability. The accuracy of the method depends on the number of simulations. The relative error made in the simulation can be written as:

$$\varepsilon = \frac{\dfrac{N_f}{N} - P_f}{P_f} \qquad (2.11)$$

The expected value of the error is zero. The standard deviation is given as:

$$\sigma_\varepsilon = \sqrt{\frac{1 - P_f}{N P_f}} \qquad (2.12)$$

For a large number of simulations, the error is normal distributed. Therefore, the probability that the relative error is smaller than a certain value E can be written as:

$$P(\varepsilon < E) = \Phi\left(\frac{E}{\sigma_\varepsilon}\right) \qquad (2.13)$$

$$N > \frac{k^2}{E^2}\left(\frac{1}{P_f} - 1\right) \qquad (2.14)$$

The probability of the relative error E being smaller than $k.\sigma_\varepsilon$ now equals $\Phi(k)$. For desired value of the k and E the required number of simulations is given by:

$$P(\varepsilon < E) = \Phi(\frac{E}{\sigma_\varepsilon}) \qquad (2.15)$$

$$N > \frac{k^2}{E^2}(\frac{1}{P_f} - 1) \qquad (2.16)$$

Requiring a relative error of E=0.1 lying within the 95% confidence interval (k=1.96) results in:

$$N > 400(\frac{1}{P_f} - 1) \qquad (2.17)$$

The above equation shows that the required number of simulation and thus the calculation time depend on the probability of failure to be calculated. Most structures in civil engineering hydraulic and river engineering possess a relatively high probability of failure (i.e.a relatively low reliability) compared to structural components/system, resulting in reasonable calculation times for Monte Carlo simulation. The calculation time is independent of the number of basic variables and therefore Monte Carlo simulation should be favoured over the Riemann method (CUR 190, 1997) in case of a large number of basic variables (typically more than five). Furthermore, the Monte Carlo method is very robust, meaning that it is able to handle discontinuous failure spaces and reliability calculation in which more than one design point is involved.

$$P_f = P(Z < 0) = \Phi(-\beta)$$
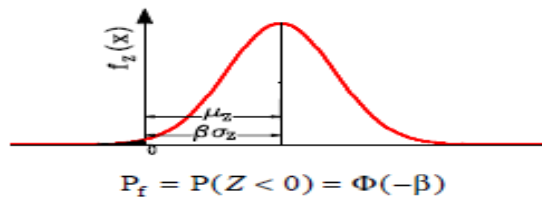
Figure 2-5. Probability density of the Z-function

If the reliability function Z is a sum of a number of normal distributed variables, then Z is also a normal distributed variable. The mean value and the standard deviation can easily be computed with these equations:

$$Z = \sum_{i=1}^{n} a_i x_i \qquad (2.18)$$

$$\mu_z = \sum_{i=1}^{n} a_i \mu_{xi} \qquad (2.19)$$

$$\sigma_Z = \sqrt{\sum_{i=1}^{n} \left(a_i \sigma_{x_i}\right)^2} \qquad (2.20)$$

This is the base of the level II probabilistic calculation. The level II methods approximate the distributions of the variables with normal distributions and they estimate the reliability function with a linear first order Taylor polynomial, so that the Z-function is normally distributed. If the distribution of the Z-function is normal and the mean value and the standard deviation are known, it is easy to determine the failure probability. By computing β as μ divided by σ it is possible to use the standard normal distribution to estimate the failure

21

probability. There are tables available for the standard normal distribution in the handbooks for statistics (Van Gelder, 2008).

2.1.2   **Nonlinear Z-function and design value**

In case of a non linear Z-function it will be estimated with a Taylor polynomial:

$$Z(\vec{x}) \approx Z(\vec{x}^*) + \sum_{i=1}^{n} \frac{\partial Z}{\partial x_i} \cdot (x_i - x_i^*) \tag{2.21}$$

The function is depending of the point where it will be linearised. The mean value and the standard deviation of the linear Z-function are:

$$\mu_Z \approx Z(\vec{x}^*) + \sum_{i=1}^{n} \frac{\partial Z}{\partial x_i} \cdot (\mu_{x_i} - x_i^*) \tag{2.22}$$

$$\sigma_Z = \sqrt{\sum_{i=1}^{n} \left(\frac{\partial Z}{\partial x_i} \cdot \sigma_{x_i} \right)^2} \tag{2.23}$$

If the reliability function is estimated by a linear Z-function in the point where all the variables have their mean value ($X_i^* = \mu_{x_i}$) we speak of a Mean Value Approach.

The so-called design point approach estimates the reliability function by a linear function for a point on $Z = 0$ where the value β has its minimum. Finding the design point is a minimising problem. For this problem there are several numerical solutions which will not be discussed here.

$$Z(\vec{x}) \approx Z(\vec{x}^*) + \sum_{i=1}^{n} \frac{\partial Z}{\partial x_i} \cdot (x_i - x_i^*) \tag{2.24}$$

If a first order approximation is applied (FORM) the failure function Z is linearised as:

$$Z_i^{lin} = Z_i(X_1^*, X_2^*, X_3^*, ... X_n^*) + \sum_{j=1}^{n} (X_j - X_j^*) \cdot \left(\frac{\partial Z}{\partial X} \right)_{X_j = X_j^*} = 0 \tag{2.25}$$

Z_i^{lin} : Linearized reliability functions of Z_i in $\left\{ X_j^* \right\}$;

$\left(\dfrac{\partial Z}{\partial X} \right)_{X_j = X_j^*}$ is gradient vector at the design point $\left\{ X_j^* \right\}$, determined by partial derivative of

Z_j with respect to X_j, evaluated in $X_j = X_j^*$. The mean value and standard deviation of Z_i^{lin} are:

$$\mu(Z_i^{lin}) = Z_i(X_1^*, X_2^*, X_3^*, ... X_n^*) + \sum_{j=1}^{n} (\mu_{Xj} - X_j^*) \cdot \left(\frac{\partial Z}{\partial X} \right)_{X_j = X_j^*} \tag{2.26}$$

$$\sigma_{(Z_i^{lin})}^2 = \sum_{j=1}^{n} \sigma_{X_j}^2 \cdot \left(\frac{\partial Z_i}{\partial X} \right)_{X_j = X_j^*}^2 \tag{2.27}$$

If mean values $X_1^* = \mu_{(X_j)}, ..., X_n^* = \mu_{(X_n)}$ are situated, a so called mean value approximation

of the probability of failure is obtained. If the failure boundary is nonlinear, a better approximation can be achieved by linearization of the reliability function at the design point. The design point is defined as the point on the failure boundary in which the joint probability density is maxima. Therefore, the design point can be obtained by:

$$X_j^* = \mu_{X_j} - \alpha_j . \beta . \sigma_{X_j} \tag{2.28}$$

where, reliability index and influence factor of variable number jth to failure probability of component ith can be determined by:

$$\beta = \frac{\mu(Z_{lin})}{\sigma(Z_{lin})} \tag{2.29}$$

$$\alpha_j = \frac{\sigma(X_j)}{\sigma(Z_i^{lin})} \cdot \frac{\partial Z_i}{\partial X_j} \tag{2.30}$$

$$P_f = \Phi(-\beta) \tag{2.31}$$

The design point can be determined analytically by an iterative procedure (Vrijling et al., 2002). It can be seen from Figure 2-6 that the reliability index β represents the length of this shortest distance vector whereas the sensitivity factors α_j characterize the directional cosines of this vector with respect to the coordinate axes.
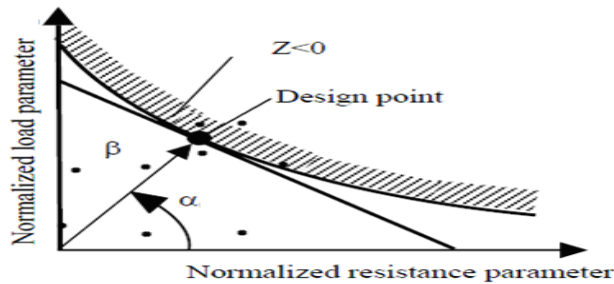
Figure 2-6. Determination of the design point in standard normalized space

2.1.3 Non normally distributed basic variables

If the basic variables of the Z-function are not normally distributed, the Z-function will be unknown and probably non-normally distributed. To cope with this problem the non normally distributed basic variables in the Z-function can be replaced by normally distributed variable. In the design point the adapted normal distribution must have the same as the real distribution. Because the normal distribution has two parameters one condition is not enough to find the right normal distribution. Therefore, the value of the adapted normal probability density function must also have the same value as the real probability density function as shown in Figure 2-7 (Van Gelder, 2008).

The two conditions give a set of two equations with two unknowns which can be solved:

$$\left. \begin{array}{l} F_N(x^*) = F_x(x^*) \\ f_N(x^*) = f_x(x^*) \end{array} \right\} \Rightarrow \mu_N, \sigma_N \tag{2.32}$$

This method is known as the Approximate Full Distribution Approach (AFDA).
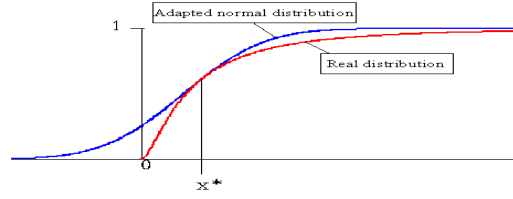
Figure 2-7. Adapted normal distribution

2.1.4 Monte Carlo Method

Monte Carlo simulation is a powerful analysis tool that involves a random number generation and simulates the behaviour of a variable when the data is insufficient to make decisions. The random number generation is based on a probability density function that defines the variable variation. Randomness is used to describe events whose outcomes are uncertain; random variables count or measure that is of interest to analyse.

The first step to the Monte Carlo process is to build a mathematical model with a set of relationships that simulates a real system. Then it is necessary to define the inputs and outputs variables. When the inputs and outputs are restricted to one value (each parameter takes only one value), we are dealing with a deterministic model. On the other hand, when the inputs and outputs are represented by random numbers or a probability density function, the model is known as stochastic or probabilistic.

Monte Carlo simulation combines the principles of probability and statistics with the expert opinion and data sources to quantify the uncertainty associated with the real systems. The Monte Carlo simulation method uses the possibility of drawing random number from a uniform probability density function between zero and one. Each continuous variable is replaced by a large number of discrete values generated from the underlying distributed, these values are used to compute a large number of values of function Z and its distribution.

$$F_{X_i}(x) = X_u \tag{2.33}$$

X_i is the uniformly distributed variable between zero and one, $F_X(x)$ is the non-exceedence probability $P(x < X)$. Thus, for the variable X:

$$X = F_X^{-1}(x_u) \tag{2.34}$$

$F_X^{-1}(x_u)$ is inverse of the probability distribution function of X.

To draw a value out of a joint probability density function, the function must be formulated as the product of the conditional probability distributions of the base variables. i.e.:

$$F_{\vec{X}}(\vec{X}) = F_{X_1}(X_1).F_{X_1|X_2}(X_2 | X_1)....F_{X_n|X_1,X_2,..X_{n-1}}(X_n | X_1, X_2,..X_{n-1}) \tag{2.35}$$

By taking n realizations of the uniform distribution between zero and one, a value can be determined for every X_i.

$$X_1 = F_{X_1}^{-1}(X_{u_1}) \tag{2.36}$$

$$X_2 = F_{X_2|X_1}^{-1}(X_{u_2}|X_1) \tag{2.37}$$

$$X_n = F_{X_n|X_1,X_2,...,X_n}^{-1}(X_{u_n}|X_1, X_2,..., X_{n-1}) \tag{2.38}$$

This corresponds to equation(2.38). By inserting the values for the reliability functions one can check whether the obtained vector ($X_1, X_2, ..., X_i$) is located in the safe area. By repeating this procedure a large number of times, the probability of failure can be estimated with:

$$P_f = n_f / n \tag{2.39}$$

in which, n is the total number of simulations and n_f is the number of simulations, for which $Z < 0$ (Van Gelder 1996). There are also several serious questions of convergence and of randomness in the generated variables. Several so-called variance reduction schemes can be effective in improving convergence and reducing computational effort. Fishman (1995) provides one of many treatments of the method. Monte Carlo simulation with variance reduction is particularly helpful in improving the accuracy of first order reliability method results.

2.1.5   Fault Tree Analysis

Fault tree and influence diagrams are techniques for describing the logical interactions among a complex set of events, conditions. Formal calculation of the failure risk can be determined by incorporating the fault tree analysis (Henly and Kumamto 1981; Ang and Tang 1984; Yen and Tung 1993).

Fault trees start with an undesired top event (Figure 2.8). The fault tree contains the conditions that must be met for the failure to occur. For a hydraulic structure the top event is inundation. There are four main intermediate events to lead to the top event: Geotechnical, Hydrological, Structural and Mechanical. The analyst develops the tree from top down, moving from condition to condition. In the usual formulation, the conditions at each stage are preferably independent and must encompass all the conditions that could lead to the next stage.

Influence diagrams can also be used in engineering practice. The diagram displays the relations between various events and conditions in a system. The direction of the arrows and other conventions represent the dependencies between the objects.

2.1.6   Uncertainty Analysis

Uncertainties are introduced in probabilistic risk analysis when we deal with parameters that are not deterministic (exactly known), hence uncertain. Two groups of uncertainties can be distinguished in Figure 2-9.

- o *Natural variability (Uncertainties that stem from known (or observable) populations and therefore represent randomness in samples).*
- o *Knowledge uncertainties (Uncertainties that come from basic lack of knowledge of fundamental phenomena).*

Natural variability cannot be reduced, while knowledge uncertainties may be reduced. Natural variability can be subdivided into natural variability in climatic, geomorphologic, hydrologic, seismic and structural. Knowledge uncertainty can be subdivided into model, operational and data uncertainty. Data uncertainty itself can be subdivided into statistical analysis of data and in measurement error and in distribution type uncertainty. Also the model uncertainty can be subdivided into formulation, parameter and numerical uncertainties.
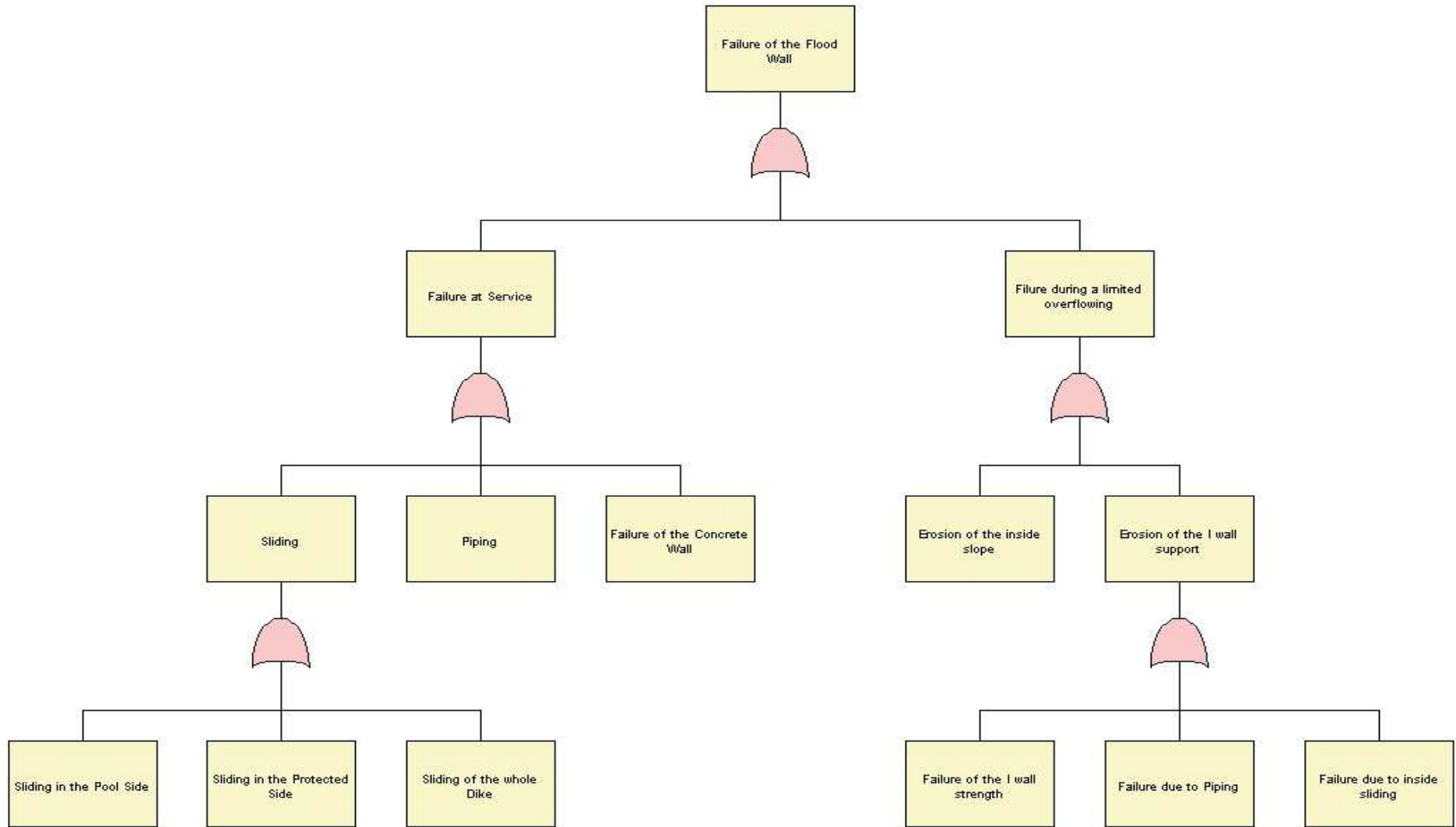
Figure 2-8. Fault tree of most expected failure mechanisms of a floodwall in New Orleans. (Rajabalinejad, 2009)
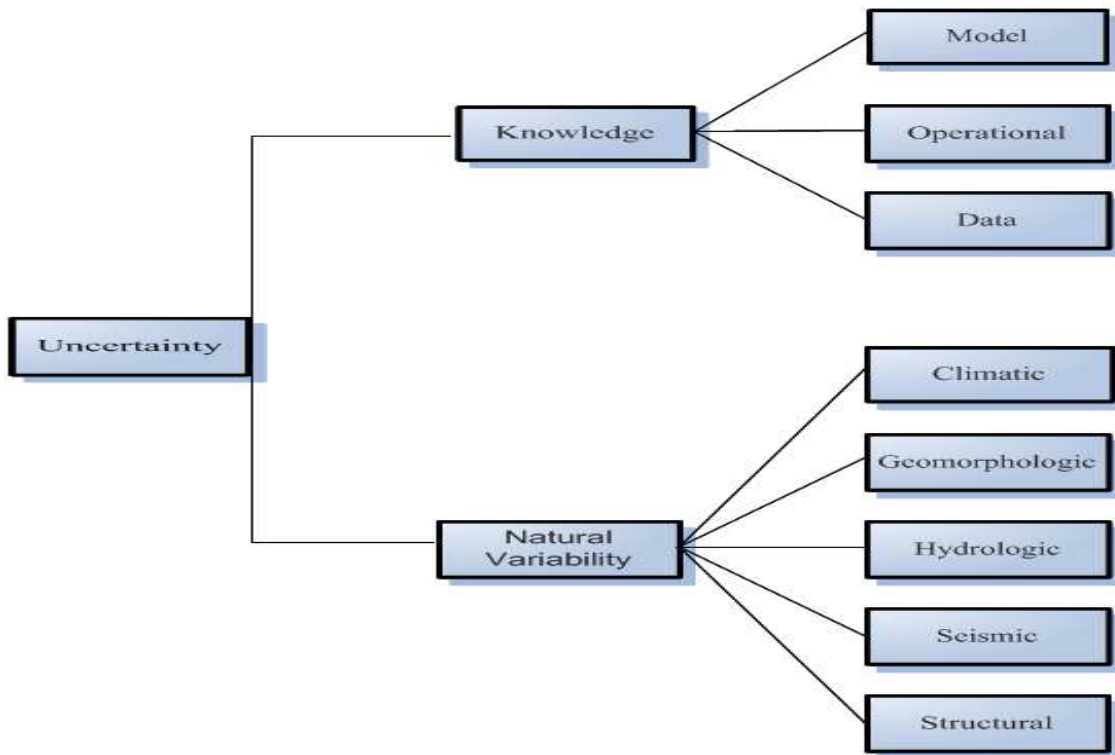
Figure 2-9. Groups of uncertainties

2.1.6.1   *Bootstrap Sampling*

The general form of a LSF equation was previously presented in section 2.1.1. The limit state equation model was created based on the multivariate regression analysis method. The method is exposed to parameter uncertainty when limited numbers of data are taken into account. The fewer data applied in the analysis the larger the parameter uncertainty. A parameter of a distribution function is estimated from the data and thus can be considered a random variable (Van Gelder, 2000). The parameter uncertainty can then be the probability distribution function of the parameter.

The bootstrap method is a fairly easy tool to calculate the parameter uncertainty. Bootstrapping methods are described by Erfan (1982) and Erfan and Tibshirani (1993). If we have dataset $X = (X_1, X_1, ..., X_n)$, we can generate a bootstrap sample X^* which is a random sample of size n drawn with replacement from the dataset X. The following bootstrap algorithm which can be used for estimating parameters uncertainty was reported by Van Gelder (2000).

- o *Select B independent bootstrap samples $(X_1^*, X_2^*, ..., X_B^*)$, each consisting of n data values drawn with replacement from X .*
- o *Evaluate the bootstrap corresponding to each bootstrap sample;*
- o $\theta^*(b) = f(X_b^*)$ *for* $[b = 1, 2, ..., B]$ *(2.40)*
- o *Determine the parameter uncertainty by the empirical distribution function of θ^**

The bootstrap samples of the observed data are normally generated with the Matlab programming software for many random values. It is assumed that if a set of random samples could be draw many times on data that come from the same source, the maximum likelihood estimates of the parameters would approximately follow a normal distribution.

27

2.2 LEAST SQUARES ESTIMATION

2.2.1 Introduction

The least square method is a very popular technique used to compute estimations of parameters and to fit a function to the data (Abdi, 2010). At the present time, the least square method is widely used to find or estimate the numerical values of the parameters to fit a function to a set of data and to characterize the statistical properties of estimates. It exists with several variations. Least square has different variants for estimation such as; the ordinary least squares estimation (OLSE), weighted least squares estimation (WLSE), alternating least squares estimation (ALSE), best linear unbiased estimation (BLUE), maximum likelihood estimation (MLE) and partial least squares estimation (PLSE).

2.2.2 Criteria

2.2.2.1 Unbiasedness

The estimator x is said to be unbiased if and only if the mathematical expectation of the estimation error is zero. An estimator is therefore unbiased if the mean of its distribution equals x.

$$E\{\hat{x}\} = x \quad \text{for all } x \tag{2.41}$$

where, $E\{.\}$ denotes the expectation operator. This implies that the average of repeated realizations of $\hat{\varepsilon}$ will tend to zero on the long run. An estimator which is not unbiased is said to be biased and the difference $E\{\hat{\varepsilon}\} = E\{\hat{x}\} - x$ is called the bias of the estimator. The size of the bias is therefore a measure of closeness of $\hat{x}$ to x. The mean error $E\{\hat{\varepsilon}\}$ is a measure of closeness that makes use of the first moment of the distribution of $\hat{x}$ (Amiri 2007).

2.2.2.2 Minimum Variance

Here, one of the most important and useful concepts in estimation is introduced. Minimum variance estimation can give the best option in a probabilistic method to find the optimal estimate. In particular, minimal variance estimation and maximum likelihood estimation will be explored, and a connection to the least squares problem (Crassidis et al, 2004). A second measure of closeness of the estimator to x is the mean squared error (MSE), which is defined as:

$$MSE = E\left\{\|\hat{x} - x\|^2\right\} \rightarrow \min \tag{2.42}$$

Where $\|.\|$ is a vector norm. If we were to compare different estimators by looking at their respective MSEs, we would prefer one with small or the smallest MSE. This is a measure of closeness that makes use also of the second moment of the distribution of $\hat{x}$. The best estimator in the absence of biases therefore is of minimum variance.

2.2.3 Estimation Methods

In this section the theory of the least square methods in engineering application is presented. From experience we know that various uncertain phenomena can be modelled as a random variable (or a random vector), namely y. An example is the uncertainty in instrument readings due to measurement errors. The randomness of y is expressed by its probability density function (PDF). In practice our knowledge of the PDF is incomplete. The PDF can usually be indexed with one of more unknown parameters. The PDF of a random m-vector y is denoted as $f_y(y \mid x)$, in which x is an n-vector of unknown parameters to be estimated.

The approach is to take an observation for the m-vector y and to use this information in order to estimate the unknown n-vector. The observation y as a realization of y with PDF $f_y(y \mid x)$ contains information about x, which can be used to estimate its entries.

Four different estimation methods will be treated in section 2.2.3.1 to 2.2.3.4. They are ordinary least squares estimation (OLSE), weighted least-squares estimation (WLSE), best linear unbiased estimation (BLUE) and maximum likelihood estimation (MLE). The methods differ not only in the estimation principles involved, but also in the information that is required about the PDF $f_y(y \mid x)$. WLSE is applied when we only have information about the first moment of the distribution. BLUE is a method which can be applied when we have information about the first two moments of the distribution. MLE is used if we know the complete structure of the PDF $f_y(y \mid x)$. An important example for which the complete structure of the PDF is known is the multivariate normal distribution, i.e. as $y \sim N_m(Ax, Q_y)$. From now on we will refer to the linear system of equations as the linear model $y = Ax + e$.

$$E\{y\} = Ax, \quad W, \quad D\{y\} = Q_y \tag{2.43}$$

Where y is the m-vector of (stochastic) observables like depth, length and width, A is the $m \times n$ design matrix, x is the n-vector of explanatory observables like Fr_N, R, d_{50}, G_s, and W and Q_y are the $m \times m$ weight matrix and covariance matrix of the observables, respectively. The design matrix A is assumed to be of full column rank, i.e., $\mathrm{rank}(A) = n$, provided that $m \geq n$, W and Q_y are symmetric and positive-definite. Again $E\{.\}$ denotes the expectation operator, and $D\{.\}$ represents the dispersion operator. The above parametric form of the functional model is referred to as a Gauss-Markov model when y is normally distributed, $y \sim N_m(Ax, Q_y)$.

2.2.3.1 *Ordinary Least Squares Estimation (OLSE)*

The oldest (and still most frequent) use of OLSE was linear regression, which corresponds to the problem of finding a line (or curve) that best fits a set of data. In the standard formulation, a set of N pairs of observations (X_i, Y_i) is used to find a function giving the value of the dependent variable y from the values of an independent variable x. With one variable and a linear function, the prediction is given by the following equation:

$$\hat{Y} = a + bX \tag{2.44}$$

This equation involves two free parameters which specify the intercept a and the slope b of the regression line. The least square method defines the estimate of these parameters as the values which minimize the sum of the squares (hence the name least squares) between the measurements and the model (i.e., the predicted values). This amounts to minimizing the expression:

$$\varepsilon = \sum_{i=1}^{n}(Y_i - \hat{Y}_i)^2 = \sum_{i=1}^{n}[Y_i - (a + bX_i)]^2 \tag{2.45}$$

where, ε is the standard error which is the quantity to be minimized. This is achieved using standard techniques from calculus, namely the property that a quadratic (i.e., with a square) formula reaches its minimum value when its derivatives vanish. Taking the derivative of ε with respect to a and b and setting them to zero gives the following set of equations (called the normal equations):

$$\frac{\partial \varepsilon}{\partial a} = \sum_{i=1}^{n} -2(Y_i - a - bX_i) = 0 \tag{2.46}$$

$$\frac{\partial \varepsilon}{\partial b} = \sum_{i=1}^{n} -2X_i(Y_i - a - bX_i) = 0 \tag{2.47}$$

Solving these 2 equations gives the least square estimates of a and b as:

$$a = \mu_Y - b\mu_X \tag{2.48}$$

$$b = \frac{\sum(Y_i - \mu_Y)(X_i - \mu_X)}{\sum(X_i - \mu_X)^2} \tag{2.49}$$

μ_Y and μ_X denoting the means of X and Y. OLSE can be extended to more than one independent variable (using matrix algebra) and to non-linear functions.

2.2.3.2 *Weighted Least-Squares Estimation (WLSE)*

If $E\{y\} = Ax$, and A a $m \times n$ matrix of $\text{rank}(A) = n$, be a linear model and let W be a symmetric and positive-definite $m \times m$ weight matrix $(W = W_T > 0)$. Then the weighted least-squares solution of the system is defined as:

$$\hat{x} = \arg \min_{x \in R^n}(y - Ax)^T W(y - Ax) \tag{2.50}$$

The difference $\hat{e} = y - A\hat{x}$ is called the (weighted) least-squares residual vector. Its squared (weighted) norm $\|\hat{e}\|_W^2 = \hat{e}^T W \hat{e}$ is a scalar measure for the inconsistency of the linear system. Since the mean of y depends on the unknown x, also the PDF of y depends on the unknown x.

The problem of determining a value for x can thus now be seen as an estimation problem, i.e. as the problem of finding a function G such that $\hat{x} = G(y)$ can act as the estimate of x and $\hat{x} = G(y)$ as the estimator of x. The weighted least squares estimator is given as.

$$\hat{x} = (A^T W A)^{-1}(A^T W y) \tag{2.51}$$

Which a linear estimator is since all the entries of $\hat{x}$ are linear combinations of the entries of y. The least squares estimator $\hat{y} = A\hat{x}$ of observables and $\hat{e} = y - \hat{y}$ of residuals follow from equation $y = Ax + e$ (Teunissen et al., 2005).

$$\hat{y} = A \ (A^TWA)^{-1} A^TW \ \text{y=P y} \tag{2.52}$$

In linear algebra and functional analysis, a projection is a linear transformation P from a vector space to itself such that $P^2 = P$. where, $P = A \ (A^TWA)^{-1} A^TW$ is so called hat matrix since it transforms or projection y into $\hat{y}$.

The estimate of the error term e (also known as the residual) termed $\hat{e}$ is:

$$\hat{e} = (I_m - A \ (A^TWA)^{-1} A^TW) \ y = (I_m - P) \ y \tag{2.53}$$

To get some insight into the performance of an estimator, we need to know how the estimator relates to its target value. Based on the assumption $E\{\hat{e}\} = 0$, the expectations of $\hat{x}$, $\hat{y}$ and $\hat{e}$ follow as:

$$E\{\hat{x}\} = x , \quad E\{\hat{y}\} = y = Ax , \quad E\{\hat{e}\} = E\{e\} = 0 \tag{2.54}$$

This shows that the WLSE is a linear unbiased estimator. Unbiasedness is clearly a describable property. It implies that on the average the outcomes of the estimator will be on target. Also $\hat{y}$ and $\hat{e}$ are on target on the average.

In order to obtain the covariance matrix of $\hat{x}$, $\hat{y}$ and $\hat{e}$, we need the covariance matrix of e or observables y, namely Q_y. The covariance matrixes of $\hat{x}$, $\hat{y}$ and $\hat{e}$ will be denoted respectively as $Q_{\hat{x}}$, $Q_{\hat{y}}$ and $Q_{\hat{e}}$. We can derive that:

$$\begin{cases} Q_{\hat{x}} = (A^TWA)^{-1} A^TWQ_yWA \ (A^TWA)^{-1} \\ Q_{\hat{y}} = P \ Q_y P^T \\ Q_{\hat{e}} = (I_m - P) \ Q_y (I_m - P)^T \end{cases} \tag{2.55}$$

The mean and covariance matrix of an estimator come together in the mean square error of the estimator. As before, let $\hat{\varepsilon} = \hat{x} - x$ be the estimation error. Assume that we measure the size of the estimation error by the expectation of the sum of squares of its entries:

$$E\{\hat{\varepsilon}^T\hat{\varepsilon}\} = E\{\|\hat{x} - x\|^2\} \tag{2.56}$$

This is called the mean squared error (MSE) of the estimator. It can easily be shown that the MSE is decomposed as:

$$E\{\|\hat{x} - x\|^2\} = E\{\|\hat{x} - E\{\hat{x}\}\|^2\} + E\{\|x - E\{\hat{x}\}\|^2\} \tag{2.57}$$

The first term on the right hand side is the trace of the covariance matrix of the estimator and second term is the squared norm of the bias of the estimator. But since the WLSE is unbiased the second term vanishes as a result of which the MSE of the WLSE reads:

$$E\{\|\hat{x} - x\|^2\} = E\{\|\hat{x} - E\{\hat{x}\}\|^2\} \tag{2.58}$$

In weighted least square one important criterion which shows the inconsistency of the linear model of observation equations is the quadratic form (square norm) of the residuals which is given as:

$$\|\hat{e}\|_W^2 = \hat{e}^T.W.\hat{e} = (y^T.W.y) - (y^T.W.A)(A^T.W.A)^{-1}(A^T.W.y) \tag{2.59}$$

2.2.3.3   *Best Linear Unbiased Estimation (BLUE)*

The weighted least square approach was introduced as an interesting technique for solving an inconsistent system of equations. The method itself is a deterministic principle, since to concepts from probability theory is used in formulating the least squares minimization problem. In order to select an optimal estimator from the class of linear unbiased estimators (LUE), we need to define the optimality criterion. As optimality criterion we choose the minimization of the mean square error (MSE). The estimator which has the smallest mean square error is called the best linear unbiased estimator (BLUE). Such a minimization problem results in the smallest possible variance for estimators as:

$$E\left\{\|\hat{x} - x\|^2\right\} = E\left\{\|\hat{x} - E\{\hat{x}\}\|^2\right\} \equiv \min \tag{2.60}$$

If the covariance matrix Q_y of the observables is known, one could use the best linear unbiased estimation (BLUE) by taking the weight matrix to be the inverse of the covariance matrix namely taking $W = Q_y^{-1}$ in equations (2.51), (2.52) and (2.53), with this the BLUE estimator of x, y and e in equation $y = Ax + e$ read:

$$\begin{cases} \hat{x} = (A^T Q_y^{-1} A)^{-1} A^T Q_y^{-1} y \\ \hat{y} = A \ (A^T Q_y^{-1} A)^{-1} A^T Q_y^{-1} \ y \\ \hat{e} = (I_m - A \ (A^T Q_y^{-1} A)^{-1} A^T Q_y^{-1}) y \end{cases} \tag{2.61}$$

Substitution of $W = Q_y^{-1}$ into equation(2.55), and $P = A \ (A^T Q_y^{-1} A)^{-1} A^T Q_y^{-1}$, yields the covariance matrix of the BLUE estimator as:

$$\begin{cases} Q_{\hat{x}} = (A^T Q_y^{-1} A)^{-1} \\ Q_{\hat{y}} = (A \ (A^T Q_y^{-1} A)^{-1} A^T Q_y^{-1}) \ Q_y = P \ Q_y \\ Q_{\hat{e}} = (I_m - A \ (A^T Q_y^{-1} A)^{-1} A^T Q_y^{-1}) \ Q_y = (I - P) \ Q_y \end{cases} \tag{2.62}$$

It can be shown that of all linear unbiased estimators, the BLUE estimator has minimum variance. It is therefore a minimum variance unbiased estimator. The BLUE is also sometimes called the Probabilistic Least Square Estimator. The property of minimum variance is also independent of the distribution of y. From the BLUE estimators, the inconsistency criterion of the linear model of observation equation expressed by the quadratic form of the residuals is given as:

$$\|\hat{e}\|_W^2 = \hat{e}^T Q_y^{-1} \hat{e} = (y^T Q_y^{-1} y) - (y^T Q_y^{-1} A)(A^T Q_y^{-1} A)^{-1}(A^T Q_y^{-1} y) \tag{2.63}$$

The preceding square norm of the residual will play an important role in the section of detection and validation.

In the weighted least squares the weight matrix W plays the role of a metric tensor in a vector space. The BLUE estimators take the weight matrix as the inverse of the covariance matrix. Therefore, the covariance matrix of the observables is closely related to the metric tensor. We have thus some probabilistic interpretations in our vector space. For example, if the covariance between observables are zero, this means that the standard vectors having no projection on each other. If in addition the variances are equal, this means that the basis vectors are normal. Therefore, we take the weight matrix as inverse of covariance matrix the definition of the minimum distance (minimum norm) in the vector space obtained from weighted least square will coincide with the definition of minimum variance in the stochastic model (space) obtained from BLUE.

Example:

We now consider a simple example of the application of the weighted least squares estimation and the BLUE. Assume that we consider the simplest problem of linear regression. Let us assume that the parameters of the line $y = ax + b$ are unknown (i.e. the offset b and slope a). They are to be estimated using the observables $y_i (i = 1, .., 4)$ measured at the fixed positions on the x-axis as x_i $(i = 1, .., 4)$. Further, assume that the observables are uncorrelated with the same precision 0.1, 0.15, 0.20 and 0.25. The observables y_i are $y = [2.85\ 4.08\ 4.92\ 6.17]^T$. The design matrix A is the coefficients of the observation. The problem is now solved using WLSE and BLUE as follows:

WLSE: For this case we may consider the same weights for the observables, namely:

$$W = \begin{bmatrix} 1 & 0 & 0 & 0 \\ 0 & 1 & 0 & 0 \\ 0 & 0 & 1 & 0 \\ 0 & 0 & 0 & 1 \end{bmatrix} \qquad A = \begin{bmatrix} 1 & 1 \\ 2 & 1 \\ 3 & 1 \\ 4 & 1 \end{bmatrix} \qquad Q_y = \begin{bmatrix} 0.01 & 0 & 0 & 0 \\ 0 & 0.0225 & 0 & 0 \\ 0 & 0 & 0.04 & 0 \\ 0 & 0 & 0 & 0.0625 \end{bmatrix}$$

In matrix form we get (this is $y = Ax + b$) and with the covariance matrix equations (2.55) as:

$$\hat{x} = (A^T W A)^{-1} A^T W y = \begin{bmatrix} \hat{a} \\ \hat{b} \end{bmatrix} = \begin{bmatrix} 1.080 \\ 1.805 \end{bmatrix} \qquad Q_{\hat{x}} = \begin{bmatrix} 0.0071 & -0.0135 \\ -0.0135 & 0.0312 \end{bmatrix}$$

$$\hat{y} = A\hat{x} = \begin{bmatrix} 2.8850 \\ 3.9650 \\ 5.0450 \\ 6.1250 \end{bmatrix} \qquad Q_{\hat{y}} = \begin{bmatrix} 0.0114 & 0.0050 & -0.0013 & -0.0076 \\ 0.0050 & 0.0058 & 0.0066 & 0.0074 \\ -0.0013 & 0.0066 & 0.0146 & 0.0225 \\ -0.0076 & 0.0074 & 0.0225 & 0.0376 \end{bmatrix}$$

$$\hat{e} = y - \hat{y} = \begin{bmatrix} -0.0350 \\ 0.1150 \\ -0.1250 \\ 0.0450 \end{bmatrix} \qquad Q_{\hat{e}} = \begin{bmatrix} 0.0074 & -0.0079 & -0.0063 & 0.0069 \\ -0.0079 & 0.0149 & -0.0059 & -0.0011 \\ -0.0063 & -0.0059 & 0.0306 & -0.0185 \\ 0.0069 & -0.0011 & -0.0185 & 0.0127 \end{bmatrix}$$

BLUE: For the BLUE we may the weight matrix as the inverse of the covariance matrix as:

$$A = \begin{bmatrix} 1 & 1 \\ 2 & 1 \\ 3 & 1 \\ 4 & 1 \end{bmatrix} \qquad Q_y = \begin{bmatrix} 0.01 & 0 & 0 & 0 \\ 0 & 0.0225 & 0 & 0 \\ 0 & 0 & 0.04 & 0 \\ 0 & 0 & 0 & 0.0625 \end{bmatrix} \qquad W = Q_y^{-1} = \begin{bmatrix} 100 & 0 & 0 & 0 \\ 0 & 44.44 & 0 & 0 \\ 0 & 0 & 25 & 0 \\ 0 & 0 & 0 & 16 \end{bmatrix}$$

With the BLUE estimator equations (2.61) and the covariance matrix equations (2.62) as:

$$\hat{x} = (A^T Q_y^{-1} A)^{-1} A^T Q_y^{-1} y = \begin{bmatrix} \hat{a} \\ \hat{b} \end{bmatrix} = \begin{bmatrix} 1.089 \\ 1.785 \end{bmatrix} \qquad Q_{\hat{x}} = \begin{bmatrix} 0.0056 & -0.0099 \\ -0.0099 & 0.0229 \end{bmatrix}$$

$$\hat{y} = A\hat{x} = \begin{bmatrix} 2.8850 \\ 3.9650 \\ 5.0450 \\ 6.1250 \end{bmatrix} \qquad Q_{\hat{y}} = \begin{bmatrix} 0.0087 & 0.0044 & 0.0001 & -0.0042 \\ 0.0044 & 0.0057 & 0.0070 & 0.0083 \\ 0.0001 & 0.0070 & 0.0139 & 0.0207 \\ -0.0042 & 0.0083 & 0.0207 & 0.0332 \end{bmatrix}$$

$$\hat{e} = y - \hat{y} = \begin{bmatrix} -0.0237 \\ 0.1172 \\ -0.1319 \\ 0.0289 \end{bmatrix} \qquad Q_{\hat{e}} = \begin{bmatrix} 0.0013 & -0.0044 & -0.0001 & 0.0042 \\ -0.0044 & 0.0168 & -0.0070 & -0.0083 \\ -0.0001 & -0.0070 & 0.0261 & -0.0207 \\ 0.0042 & -0.0083 & -0.0207 & 0.0293 \end{bmatrix}$$

Comparing the results of the two models, we see the estimates of BLUE are more precise than the WLSE estimates.

2.2.3.4   *Maximum Likelihood Estimation (MLE)*

Rather than relying on the first two moments of a distribution one can also define what closeness mean in term of the distribution itself. As a third measure of closeness we therefore consider the probability that the estimator $\hat{x}$ resides in a small region entered at x. If we take this region to be a hyper sphere with a given radius r, the measure is given as:

$$P(\|\hat{x} - x\|^2 \le r^2) \rightarrow \max \tag{2.64}$$

The estimator x, which maximizes this probability, is therefore a maximum likelihood estimator. So far we have seen three different estimation methods at work: OLSE, WLSE and BLUE. These three methods are not only based on different principles, but they also differ in the type of information that is required of the PDF of y. For WLSE we only need information about the first moment of the PDF, the mean of y.

For BLUE we need additional information. Apart from the first moment, we also need the second (central) moment of the PDF, the covariance matrix of y. For the linear model, the two principles give identical results when the weight matrix is taken equal to the inverse of the covariance matrix. In this section we introduce the method of maximum likelihood estimation (MLE) which requires knowledge of the complete PDF.

The principle of the maximum likelihood (ML) method is conceptually one of the simplest methods of estimation. It is only applicable however when the general structure of the PDF is known.

Assume therefore that the PDF of $y \in R^m$, i.e. $f_y(y \mid x)$, is known apart from some n unknown parameters. Since the PDF will change when x changes, we in fact have a whole family of PDFs in which each member of the family is determined by the value taken by x. Since x is unknown, it is not known to which PDF an observed value of y, i.e. y_0, belongs. The idea now is to select from the family of PDFs, the PDF which gives the best support of the observed data.

For this purpose one considers $f_y(y_0 \mid x)$ as function of x. This function is referred to as the likelihood function of y_0 which produces, as x varies, the probability densities of all the PDFs for the same sample value y_0. Would x be the correct value, then the probability of y being an element of an infinitesimal region centered at y_0 is given as $f_y(y_0 \mid x)dy$. A reasonable choice for x, given the observed value y_0, is therefore the value which corresponds with the largest probability, $\max_x f_y(y_0 \mid x)$ and thus with the largest value of the likelihood function. The maximum likelihood estimator (MLE) of x is therefore defined as follows:

2.2.3.4.1   Definition (Maximum likelihood)

Let the PDF of the vector of observables $y \in R^m$ be parameterized as $f_y(y \mid x)$, with $x \in R^n$ unknown. Then the MLE of x is given as:

$$\hat{x} = \arg \max_{x \in R^n} f_y(y \mid x) \tag{2.65}$$

The computation of the maximum likelihood solution may not always be an easy task. If the likelihood function is sufficiently smooth, the two necessary and sufficient conditions for $\hat{x}$ to be a (local or global) maxima are:

$$\begin{cases} \partial_x f_y(y \mid \hat{x}) = 0 \\ \partial^2_{xx^T} f_y(y \mid \hat{x}) < 0 \end{cases} \tag{2.66}$$

with ∂x and $\partial^2_{xx^T}$ being the first and the second order partial derivatives with respect to x, respectively. Therefore, the gradient has to be zero and the Hessian matrix (the symmetric matrix of second-order partial derivatives) has to be negative definite. For more information see Teunissen et al. (2005).

In case of normally distributed data (Gauss-Markov model), the MLE estimators are identical to the BLUE ones. Let $y : N_m(Ax, Q_y)$, with x the n-vector of unknown parameters.

$$\hat{x} = (A^T Q_y^{-1} A)^{-1} A^T Q_y^{-1} y \tag{2.67}$$

The estimators $\hat{y}$ and $\hat{e}$ as well as their covariance matrices are also the same as those given for BLUE estimators (Section 2.2.3.3).

2.2.4   Hypothesis Testing

Hypothesis testing used for detection and validation data in linear models. Hypothesis testing is a statistical method for making inferential decisions about population based on information

provided by available sample data. The hypothesis testing may be useful in many engineering applications. For example engineering specifications often specify certain minimum values, such as the minimum yield strength of rebar. In reinforced concrete construction, the engineer would be interested in whether the available rebar satisfies the required minimum strength.

2.2.4.1   *Simple Hypotheses*

We consider two simple hypotheses. Using the Neyman-Pearson principle, we will test the null hypothesis against the alternative one. When the m-vector y has the probability density function(PDF) $f_y(y \mid x)$, we may define two simple hypotheses as $H_0 : x = x_0$ versus $H_a : x = x_a$. Each hypotheses pertains to a single distinct point in the parameter space. The objective is to decide, based on observations y of observables y, from which of the two distributions the observations originated, either from $f_y(y \mid x_0)$ or from $f_y(y \mid x_a)$. The SLR test as a decision rule reads (Teunissen et al., 2005). Reject H_0 if:

$$\frac{f_y(y \mid x_0)}{f_y(y \mid x_a)} < a \tag{2.68}$$

and accept otherwise, with a positive constant (threshold). It can be proved that the simple likelihood ratio test is the most powerful test.

2.2.4.2   *Powerful Test*

The simple likelihood ratio (SLR) test is derived based on the Neyman-Pearson testing principle. This principle states to choose among all tests or critical regions possessing the same size type I error α, the one for which the size of the type II error, β is as small as possible. Such a test with the smallest possible type II error is called the most powerful test.

2.2.4.3   *Generalized Likelihood Ratio*

In this section we address an important practical application of the Generalized Likelihood Ratio (GLR) test, namely hypotheses testing in linear models. In many applications, observed data are treated with a linear model; validation of data and model together. The goal is to make a correct decision to be able to eventually compute estimates for the unknown parameters of interest. This also provides us with the criteria such as reliability to control the quality of our final estimators.

The observables are assumed to have a normal distribution. In addition, different hypotheses differ only in the specification of the functional model. Misspecifications in the functional model have to be handled prior to variance component estimation. In this chapter, the stochastic model of the observables is not subject to discussion or decision. When testing hypotheses on misspecifications in the functional model, we consider two types of equivalent tests: the observation test and the parameter significance test. These types of hypothesis testing using the GLR are dealt with when the covariance matrix Q_y of the observables is completely known. This is called σ known. When the covariance matrix is known up to the variance of unit weight, i.e. $Q_y = \sigma^2 Q$, we will give some comments in the following

paragraph. This is referred to as σ^2 and is unknown. If the variance component σ^2 of the stochastic model is not known, which is the case for most of our applications, the principle of the least-squares can be used to estimate the unknown component. For this purpose we rely on the theory of least-squares variance component estimation (LS-VCE) developed by Amiri-Simkooei (2007). The least-squares estimate of the unknown σ^2 is:

$$\hat{\sigma}^2 = \frac{\hat{e}^T Q^{-1} \hat{e}}{m-n} \tag{2.69}$$

where $\hat{e}$ is the estimated least-squares residual vector and $m-n$ is the redundancy of the linear model $E\{y\} = Ax$. The preceding equation is of use when there is only one variance component in the model, which has been used in Chapters 6 and 7 of this thesis. However, the estimation of more unknown components of the stochastic model using LS-VCE leads to an iterative procedure presented by Amiri-Simkooei (2007).

2.2.5   **Outlier Detection**

2.2.5.1   *W-Test Statistic*

The following w-test statistic is used to screen the observables for the presence of outliers. In the linear model $E\{y\} = Ax$, when $m > n$, e.g. data is used more than once, if the covariance matrix Q_y of observables is diagonal, the expression for the w-test statistic reduces to a very simple form. The simple expression for the w-test statistic then reads (Teunissen 2000):

$$w_i = \frac{\hat{e}_i}{\sigma_{\hat{e}_i}} \tag{2.70}$$

$$\sigma_{\hat{e}_i} = \left(Q_{\hat{e}_o} \right)_{ii}^{1/2} \tag{2.71}$$

Equation (2.71) is the standard deviation of the least-squares residual i, for $i = 1, \ldots, m$. This quantity is also referred to as the normalized residual (Amiri, 2007).

The above test statistic has the standard normal distribution under the null hypothesis, which states that the observable i is free from gross errors (those that are not of the random nature). The goal of the w-test statistic is to screen the observed values (measurements) for the presence of outliers. We might find the observables that cannot fit the linear model and hence the w-test statistic is of use to identify such gross errors. The detected outliers can then be left out to repeat the estimation process for obtaining more reliable results on the parameters. This process is also referred to as 'data snooping'.

2.3   DISCUSSION AND CONCLUSION

Theories presented in this chapter are the main estimation approaches used in this thesis. Thus, descriptions presented earlier were rather simplified and straight forward, intentionally prepared to suit the content of this thesis.

The probabilistic method is all about to random variables and uncertainties analysis. The main probabilistic and reliability methods used in this dissertation are presented in this chapter. If the geometry of every component is known and the probability distributions of load and strength variables are determined, and limit state functions of the failure mechanisms are given, the probability of hydraulic structure systems can be calculated. This can be applied to technical management purposes to determine the safety levels of an existing system and to find out the weakest point of the system.

The failure probability of every mechanism is then calculated using the above reliability theory and simulation of random variables. Chapters 6, 7 and 8 of this thesis were principally carried out using the Level III Monte Carlo for simulation method (MCS) or Level II advance first order second moment (FORM).

For major frameworks of this thesis, we presented several approaches to establish a class of linear estimation algorithms, including: Ordinary least square estimation (OLSE), Weighted least square estimation (WLSE), Best linear unbiased estimation (BLUE) and Maximum likelihood estimation (MLE). These concepts are useful for the analysis of least squares estimation by combining probabilistic approaches. The least squares methods are considered as one the popular classical estimation methods among engineers because it gives lower failure probability for under design (Van Gelder, 2000).

In addition, the detection and validation of the linear model was introduced. The hypothesis testing in linear models, including the concept of testing simple hypothesis, and the w-test statistic were discussed.

The formulation of linear model parameter estimation using the four methods explained above have been presented. The best model which gives the most precise results is obtained using the BLUE method in chapter 6 and 7. Such a model requires a realistic covariance matrix of the observables, which can be estimated using LS-VCE (Equation(2.69)). The BLUE method not only is capable of estimating the parameters in the minimum variance sense, but also provides us with the realistic covariance matrix of the unknown parameters used for instance in Monte Carlo simulation. In addition, in case of normally distributed data (Gauss-Markov model), the MLE estimators were shown to be identical to the BLUE estimators.

Finally, the w-test statistic was introduced to identify the blunders (gross errors) of the observables. Our observables are suspected to the affected by the possible large errors (gross errors) which are not of stochastic nature. They need to be detected and removed from the analysis to obtain more reliable results. For this goal the 'data snooping' procedure introduced in Section 2.2.5.1 and chapter 6 and 7 can be used.

CHAPTER 3

FAILURE MECHANISMS OF LARGE DAMS

Over the centuries all human civilisations have been threatened by natural hazards such as hurricanes, floods, droughts, earthquakes, etc, claiming the lives of individuals or entire groups bound by their residence or profession. Many activities have been deployed to protect man against these hazards. Even today money is spent to avoid or prevent natural hazards, because the consequences in developed societies have increased considerably. Other more recent hazards are man-made and result from the technological progress in transport, civil, chemical and energy engineering (Vrijling, 2003), such as hazards from dams.

Engineering systems, components and devices are not perfect. A perfect design is one that remains operational and attains systems objective without failure during a preselected life. This is the deterministic view of an engineering system. This view is idealistic, empirical, and economically manufacturing, constructing and engineering analysis may far exceed economic prospects for such a system (Modarres, 1999). Therefore, practical and economical limitations dictate the use of not so perfect designs.

Designers, manufacturers and end users, however, strive to minimize the occurrence and recurrence of failures. In order to minimize failures in engineering systems, the designer must understand" Why" and "How" failure occurs. This would help them prevent failures. In order to maximize system performance and efficiently use resources economic optimizations is proposed. In the following, typical failure mechanisms of dams are first presented, with descriptions about failure models and the estimated loads.

3.1 FAILURE MECHANISMS

3.1.1 Introduction

The prevention of failures and the process of understanding why and how failures occur involve appreciation of the physics of failure. Failure mechanisms are the means by which failure occurs. To effectively minimize the occurrence of failures, the designer should have an excellent knowledge of failure mechanisms which may be inherently associated with the design or can be introduced from outside of the system. When failure mechanisms are known and appropriately considered in design, manufacturing, construction, production and operation, there probability can be "minimized" or the system can be "safeguarded" against them up to a certain level through careful engineering and economic analysis.

All potential failures in a design are generally not known or well understood. Accordingly, the prediction of failures is inherently a probabilistic problem. This chapter provides an overview of the application of the principal approaches to reliability for structural safety studies, failure modes and reliability analysis.

3.1.2 Estimating Loads

The three categories of loading conditions typically required in failure analysis are static, hydrologic, and seismic. Each of these loading conditions is briefly described in the following paragraphs. The discussion emphasizes the products needed by the designers, the range of extrapolation and the uncertainty of the structural response probability estimates. The technical details for developing the loads are not described, but may be found in numerous engineering textbooks and manuals. The responsibility for estimating load probabilities lies with the supporting scientists and the technical staff participating in the risk analysis. The parts of risk analysis shown in Figure 3-1.

Generally, load probabilities are estimated using the staged approach. The level of detail of the risk analysis determines the amount and quality of information used in the analysis. More detailed stages of risk analysis may require more detailed loading condition information.

Additional work on the loading conditions is performed only if warranted by the value added to the dam safety decision process (through the reduction or better description of uncertainty). Extra study cost should be weighed against the expected improvement in the quality of the dam safety decision. The failure of upstream dams could be considered as loading conditions in a risk analysis. The risk of multiple dam failures/incidents are addressed by assigning the cause of failure to the most upstream dam failure and including the resulting dam failures as consequences for that dam.
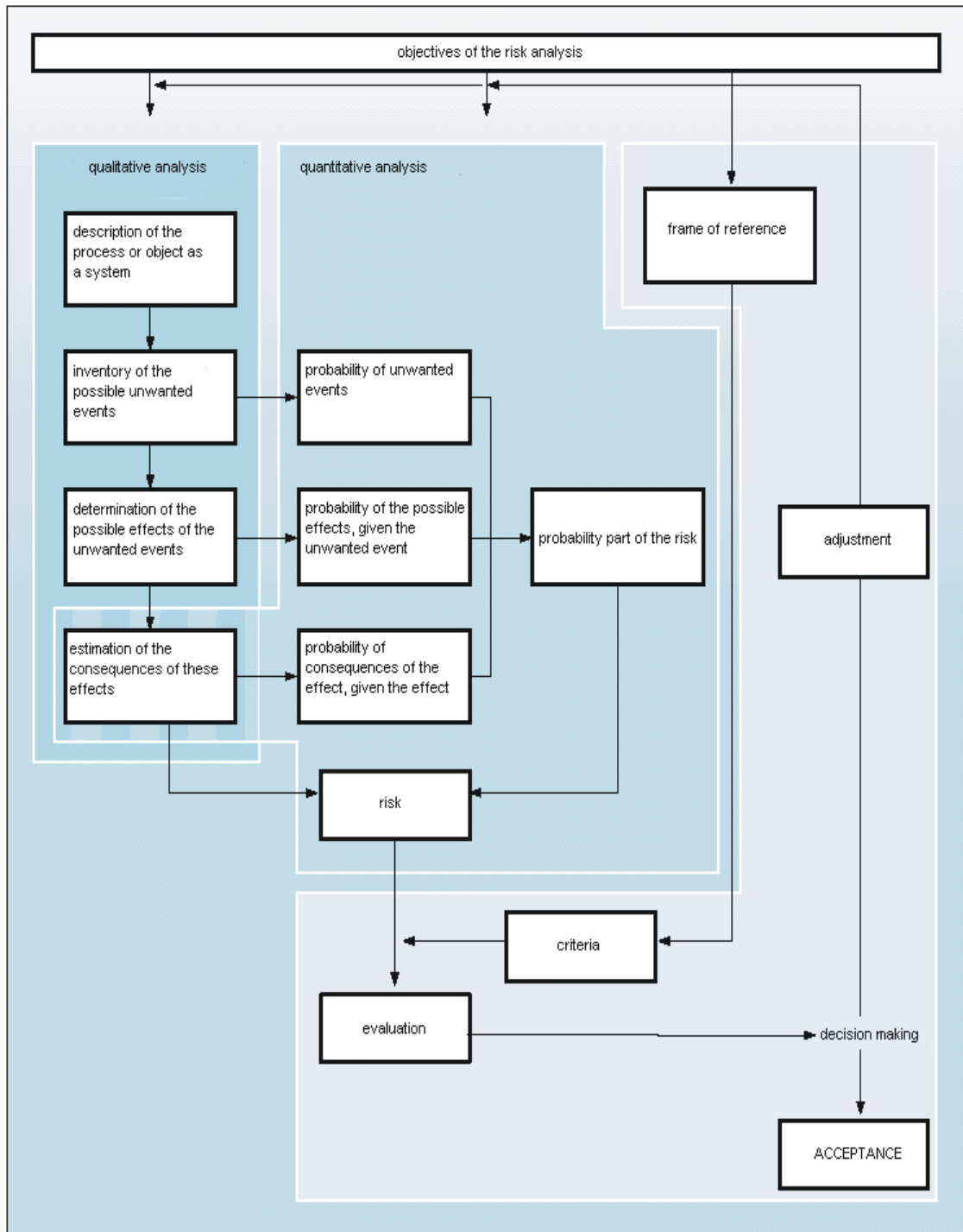
Figure 3-1. Parts of risk analysis (Vrijling, 2002)

3.1.2.1   *Hydraulic Loads*

The static loading condition encompasses a wide variety of specific loading conditions to which a dam is routinely exposed during the course of normal operation. These loads can include hydrostatic loads imposed by the reservoir, static and dynamic loads imposed by various operating components of the dam and its appurtenant structures, loads induced by landslides at the dam or on the reservoir rim, or by large hydraulic phenomena (overtopping, overturning, sliding, piping, seepage, erosion, cavitation) associated with water passing

41

through and around the dam (see Figure 3-2). Hydraulic failure may also include damage to spillway gates or operator errors associated with gates and spillways. Most static loading conditions are related to the reservoir level either in terms of the magnitude of the load, time of exposure to the load, or the potential for adverse consequences.
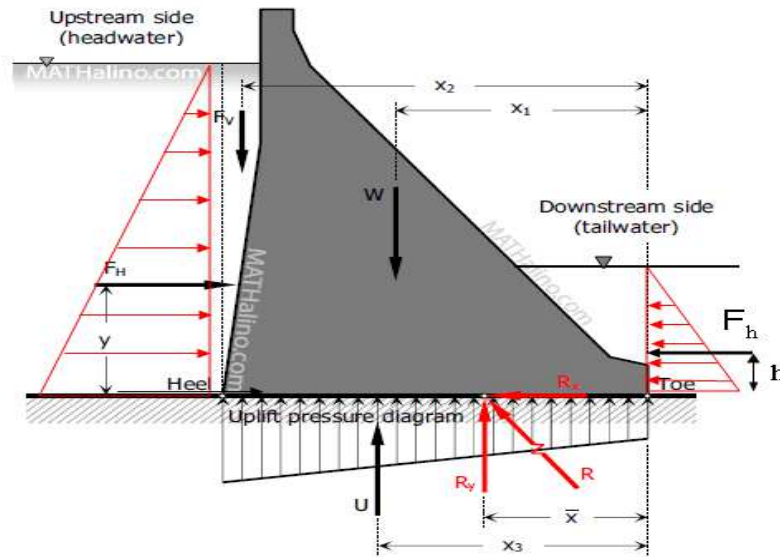
Figure 3-2 Main loads acting on a concrete dam [9]

3.1.2.2   *Hydrologic Loads*

The development of flood frequency relationships and reservoir inflow hydrographs are important inputs to the risk analysis process. For risk analysis, the focus of flood elevations shifts from a single maximum event, like the probable maximum flood, to describing a range of plausible inflow flood events. The products developed for a particular risk analysis depend on the level of study and the information available. In some cases, concurrent hydrographs are needed for tributaries located downstream of study dams so that flow conditions can be defined for analysis of the consequences of flood induced failure modes.

3.1.2.3   *Seismic Loads*

For utilization within a risk-based framework, seismic hazard evaluation must explicitly contain information on the frequency of occurrence (and/or exceedence) of relevant loading parameters. The currently accepted practice for evaluating and conveying seismic hazard information in this fashion is probabilistic seismic hazard assessment. The first step in any seismic hazard evaluation is source characterization. For use in risk analyses, both fault and areal sources should be incorporated into the hazard evaluation (USBR, 2003).

3.1.3   **Failure Model**

Failures are the result of the equilibrium of source stresses (loads) and strength conditions occurring in a particular scenario. The system has an inherent capacity to withstand such loads however, capacity may be reduced by specific internal or external conditions. When stresses surpass the capacity of the system a failure may occur (see Stress –Strength model shown in Figure 3-3).

Figure 3-3. Framework for modelling failure

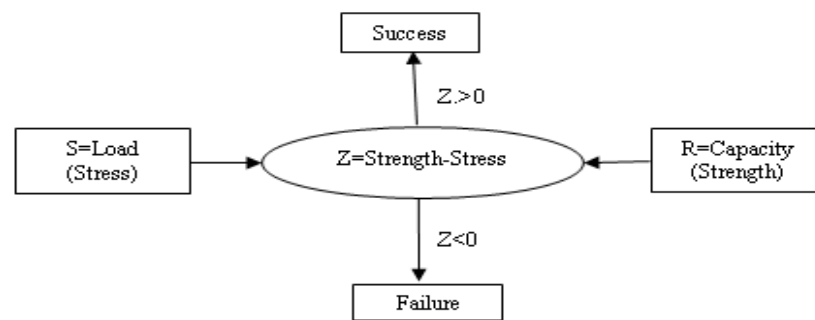Most published risk analyses for dam safety focus on four broad categories or modes of failure (Hartford, 2004):

o *Hydraulic failures due to abnormally high pool. These include among other things, overtopping and subsequent erosion of embankment dams, overturning of gravity dams and downstream sliding on a foundation.*

o *Mass movements. Due to extraordinary loads inadequate material properties or undetected geological features. These include among other things limiting equilibrium instability of embankment dams, settlement leading to overtopping, liquefaction of foundation soils, and abutment or foundation instabilities rapid drawdown failure of upstream face and reservoir landslides leading to overtopping.*

o *Deterioration and internal erosion. These include among other things development of sinkholes in the dam embankment, piping within the dam core and erosion of foundation soils of joints.*

o *Operator errors. Hydraulic failures may also be caused by operator errors associated with gates and spillway.*

The failure modes are of major importance in structural design and assessment. A structure can be seen as a series system where the reliability is defined by the weakest link. Figure 3-4 shows an example for failure of a hydraulic structure. As with any model if the failure modes identified are not the most essential, meaning that there are unidentified or neglected modes which will occur with higher probability, the outcome of the analysis will not reflect reality no matter the refinement of calculation methods or knowledge of input parameters. In most design and assessment of concrete dams the dam is treated as a rigid body when calculating stresses. This is an idealization with limitations and not considering these may lead to erroneous results.
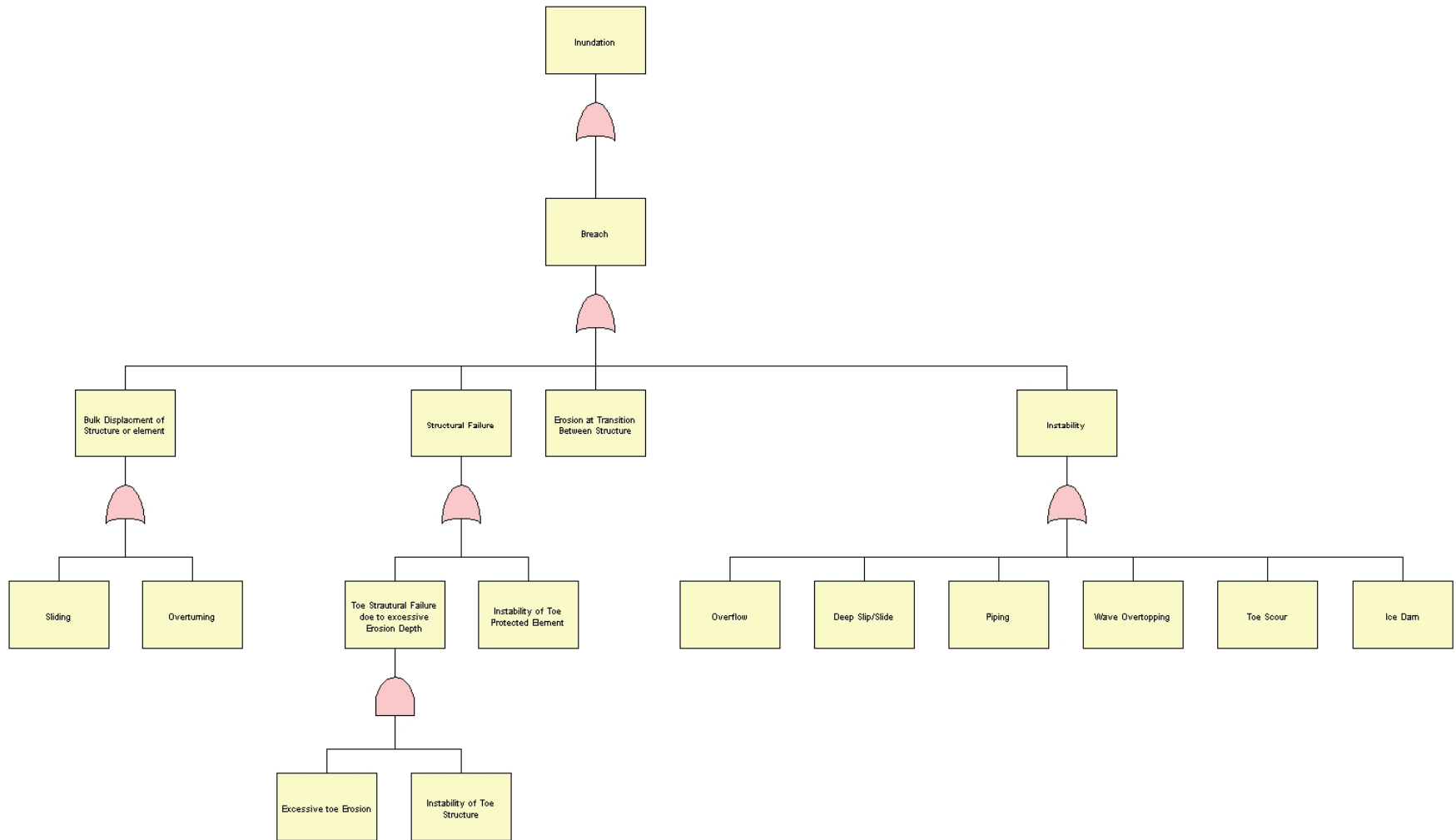
Figure 3-4. Fault tree analysis for structural failure (Flood site, 2006)

3.1.4 Observed Failure Modes of Dams

It is difficult to know if the failure modes described above are the "true" failure modes and if it is all possible failure modes. One possibility is to analyse known dam failures, but those do not necessarily cover all possible failure modes (the number of concrete dam failures is, luckily, not large enough to assume that all possible failure modes have been experienced). It can also be difficult to know the exact failure mode; especially long time after failure has occurred and for combined failure modes. It is still worth analysing but is not further discussed here. ICOLD bulletin 109 (1997), 99 (1995) and 111 (1998) mention two types of failure:

- o *Piping in the foundation. Occurred for dams on gravel or clay with no grout curtain*
- o *Overturning of blocks or sliding in the foundation*

3.1.4.1 Causes of Failure

As summarized by FEMA (2006) concrete dams fail for one or combinations of the following factors:

- o *Overtopping caused by floods that exceed the discharge capacity*
- o *Structural failure of materials used in dam construction*
- o *Movement and/or failure of the foundation supporting the dam*
- o *Settlement and cracking of concrete dams*
- o *Inadequate maintenance and upkeep*
- o *Deliberate acts of sabotage*

ICOLD Bulletin 99 (1995), gives a summary of dam failures and Figure 3-5 shows the reasons for concrete dam failures. Foundation problems are the most common cause, internal erosion and insufficient shear strength of the foundation each account for 21 percent of the failures. Of all concrete dam failures insufficient capacity of spillways during passage of maximum floods was the primary cause of about 22 percent of the dam failures and secondary cause in about 39 percent of the failures. Also, operation and human error will be extended in the case of the failures not mentioned by ICOLD.

According to ICOLD Bulletin 111 (1998), a concrete dam may withstand significant overtopping and the limiting factor in such conditions is the erosion of the foundation or abutments. Structural failure is usually due to weak foundation, structural deficiencies or sabotage. The failure of arch and buttress dams is usually assumed to be instantaneous. Gravity dams are assumed to have relatively short but not instantaneous failure time. The frequency of dam failures is approximately the same for all dam heights. The largest number of failure is among new dams, failures frequently occur within the first 10 years after construction and especially during first fill.
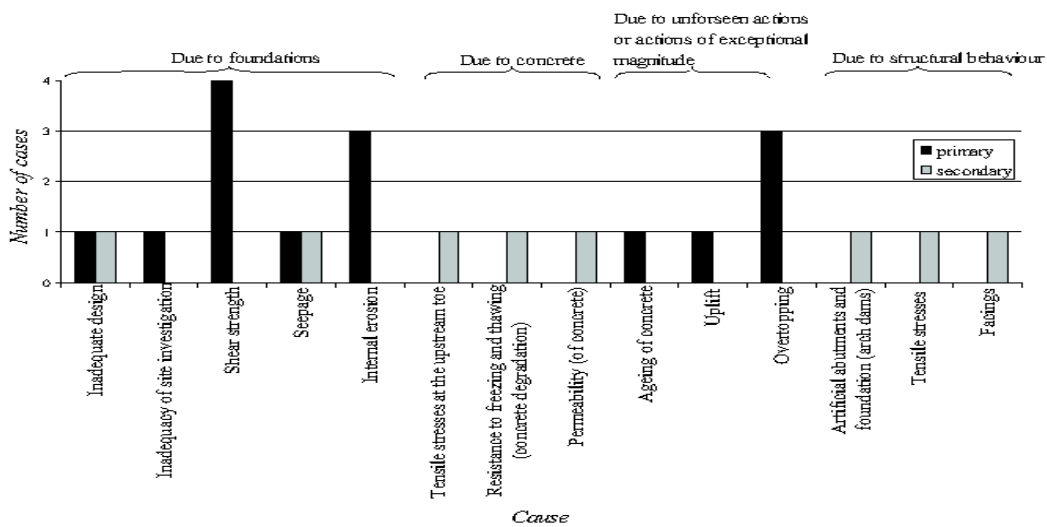
Figure 3-5. Cause of dam failures, after ICOLD Bulletin 99, (1995)

3.1.5 Failure Modes of Dam Spillways

Dam spillways failures can occur at any time in a dam's life; however, failures are most common when water storage for the dam is at or near design capacity. At high water levels, the water force on the dam is higher and several of the most common failure modes are more likely to occur. Failure of dam spillways may be caused by a combination of factors. It is important to be aware of the important causes of failures and the telltale signs that may foretell failure. A description of the major causes of spillway failures is given below:

- o *Overtopping. Overtopping caused by floods that exceed the discharge capacity.*

- o *Sliding. Sliding of the whole dam section or a monolith, or part thereof along the concrete to rock interface, lift joints (construction joint) in the dam body or along weak planes in the foundation.*

- o *Overstressing. Ultimate stresses exceed ultimate strength in foundation or dam body.*

- o *Overturning. Overturning of the whole monolith or part thereof. This failure mode is not explicitly accounted for in some guidelines, as will be shown later in this chapter.*

- o *Seepage and Piping. A hydraulic structure due to piping in the case the soil particles below the foundation are washed out due to excessive seepage.*

3.1.5.1 Overtopping

When water levels rise rapidly and without adequate warning due to flash floods, heavy rains, a landslide in the reservoir that creates a tsunami, or if a dam upstream collapses, overtopping occurs and rise in level of a reservoir exceeding the capacity or height of the spillways dam. If the spillways become blocked with debris, like silt, mud or trees, or the spillway gates are not operated properly and water can not be released, there is a danger that the water level in the reservoir will rise higher than the crest of the dam and spill over resulting overtopping.

- o *Insufficient freeboard leading to the flow of water over the crest and channel of the spillway dam in a manner not intended caused by the superelevation, steps or pools, obstructions and cross waves.*

- o *The energy dissipation arrangement at the end of a spillway has insufficient capacity to reduce the energy in the water to a safe level before it passes into the receiving*

46

watercourse. This can result in scour to the toe of the river downstream. Scour hole or erosional features can also develop further up the structure.

3.1.5.2   Sliding

The water impound in a reservoir and the silt accumulated behind the dam induces a horizontal force on the dam structure that is resisted by the shear strength of the base material in the foundation to prevent the sliding type of failure.

The stability analysis condition of a sliding mode of failure of a dam foundation follows the principles of the stability of sliding blocks. The limit equilibrium analysis methods consist of the calculation of the resisting and driving forces acting on the sliding surface, with the ratio of these two forces being the factor of safety of the dam.

3.1.5.3   Overturning

Overturning may occur if the stabilizing forces, mainly the self weight are less than the overturning forces. The overturning moments are calculated around the dam toe or some other relevant point, i.e. for lift joints in the dam body or other weak planes. Safety factors according to Table 3.1 are used to ensure the overturning stability (Westberg, 2007). According to RIDAS TA (Westberg, 2007) two criterions shall be fulfilled to ensure the overturning stability; the one described above, and that resultant forces fall within the mid third of the base area (Normal load case) or within the mid 3/5th of the base area.

Table 3.1. Safety factors of overturning according to RIDAS TA (Westberg, 2007)

Load case	Safety factor
Normal	1.50
Exceptional	1.35
Accidental	1.10

This criterion actually comes from the "cracked base criteria" mentioned above: if the resultant falls outside the mid third of the base area, tensile forces will occur in the upstream heel of the dam, resulting in full uplift pressure in the cracks thus appearing. A comprehensive review about overturning and different foundations of dams can be found in Novak, (2001) and Vischer (1998).

3.1.5.4   Overstressing

Overstressing will occur if the stresses induced in the dam body or foundation exceeds the material capacity. For buttress dams the front plate (head) will function as a cantilever beam, one possible failure mode is overstressing of the cantilever beam. This case is, however, not a global failure mode and will not be further discussed here. Stresses are often calculated based on "beam model" analysis using Navier's Equation.

As pointed out by Reinius (1962) the basic requirement behind Navier's equation, that plane cross-sections remain plane, is not fulfilled and larger stress concentrations will therefore occur at the heel and toe of the dam. Stresses from finite element analysis will represent the behaviour more accurately (Westberg, 2007).

It is usually assumed (cracked base analysis) that if tensile stresses calculated by rigid body analysis occur at the dam toe, a crack will form and water will percolate the crack, causing full uplift pressure along the whole crack length.

As pointed out in ICOLD bulletin 88 (1993), the concrete to rock interface has tensile strength that, for all practical purposes, is assumed to be zero. This is since joints or fractures may be located directly below the concrete/rock interface and the rock mass will then not be able to develop any tensile capacity (FERC, 2002). In RIDAS TA (2003) allowable stresses are determined case-specifically and there is no recommendations regarding safety factors.

3.1.5.5   *Seepage and Piping*

Currently, it is difficult to determine if and when a seepage problem will occur at the site of a dam. Advances over the past 30 years have incorporated defensive design measures into embankment dams minimizing the risk to piping problems. However, safety-threatening seepage incidents still occur at these dams as well as at dams constructed prior to this time. Increased knowledge of the mechanisms and factors that promote seepage is needed for reliable identification of those dams most likely to have piping problems. The objective of this work unit is to investigate and identify conditions in which seepage through and under embankment dams constructed on soil foundations causes piping and internal erosion of the embankment and foundation soils becomes critical. Performance parameters will be established for input into risk assessment with respect to seepage and piping (USACE, 1970).

Piping plays a big role in the failure of dams, embankment dams (Teton dam), dikes, and other flood defences. However, in this study the probability of failure by seepage and piping is not discussed in detail. However, there are explicit (analytical) limit state functions which can be approximately used to evaluate the probability of piping, which might be a case for further research.

3.2   DISCUSSION AND CONCLUSION

This chapter discussed mechanisms or failure modes of a dam for various combinations of hydraulic loading.

The most common modes or failure mechanism of large dams included flood overtopping, overturning, sliding, piping, seepage, erosion, cavitations, slope stability, earthquake, and failure of appurtenant works. The formation of a breach can occur in several ways, all of which need to be assessed and probabilities assigned. The ideal situation is that performance, parameters are assessed by relationships to a database of performance, including dams that have failed, experienced accidents and performed without incident. Failure mechanisms should be analysed with probabilistic modelling to fully define the phenomena of critical performance parameters such as variations in soil and rock characteristics, seepage, piping and other aspects for failure formation. Failure mechanisms of large dams were described from the risk and reliability methods point of view.

CHAPTER 4

DETERMINISTIC MODELS FOR PLUNGE POOLS

Downstream of free-falling jets (jet, ski-jump spillway, flip buckets) energy dissipation takes place in stilling basins, or more frequently, in plunge pools, usually excavated fully or partially in stream bed during dam construction, but sometimes only scoured by the action of the jet itself. Energy dissipation downstream from spillways is often necessary to protect the reservoir structure, and to avoid embankment erosion when high velocity water jets are present. Deposition of scour material downstream from reservoirs also increases the tail water depth, thus decreasing the total available head for power production. At the early stages of a project study, the estimation of the problems caused by the scour downstream of the reservoir must be addressed to check the feasibility of the project layout.

This chapter is organised as follows: first, the plunge pool structure is introduced; then a literature review on theoretical consideration for the plunge pools (flip bucket spillway, trajectory jet, energy dissipater, jet diffusion) and mechanisms characterizing the structures is carried out.; third, the incipient motions (forces) are discussed; forth, reviews of previous research are presented and fifth, the probabilistic approaches are introduced.

4.1   PLUNGE POOLS

4.1.1   Introduction

In recent years, due to the consideration of large and high reservoirs in narrow valleys, and higher standard dam safety, the general interest of hydraulic engineers for the dissipation of energy to be both economical and safe has grown considerably. Dams are also needed for

power generation, irrigation and flood protection. The use of a flip bucket spillway with a plunge pool as energy dissipator could satisfy both requirements of safety and economy. The flip bucket energy dissipater is able to direct the discharge jet at a relatively safe distance from the dam, and it has some economic advantage over other energy dissipators.

Energy dissipation at large dams with a significant design discharge often is accomplished by trajectory spillway in combination with a plunge pool which normally proves more economic than a stilling basin. The spillway plunge pool solution may be considered if geotechnical and geological conditions are sufficient and the developing scour is acceptable. The scour development is a significant concern because it may endanger the dam foundation and near hydraulic structure including the flip bucket. Steep valley sides may become unstable because their foot is eroded or spray is moistening the overload material, thus creating landslides.

The main question with respect to safety however is the size of the plunge pool scour including the scour depth. Today, it is common practice to introduce bottom aerators in high head spillway to reduce cavitation risk.

The flip bucket spillway energy dissipators can be used at sites which are rocky and not very erosive. In this case the plunge pool develops as a result of self excavation of the bed from the jet energy at the impact point. For the site in which the bed materials are not uniform at different layers and not strong enough to tolerate the high energy of the jet the construction of a pre-excavated plunge pool is necessary.

There are a number of studies that predict the depth of scour and describe design procedures for plunge pools. The equations which have been developed by various researchers are mainly based on model studies and on a few observations in prototypes. Due to the complex nature of the formation of the depth of scour and the large number of variables involved in the process, the range of prediction of the depth of scour using different equations available is very wide. Figure 4-1 shows a photo of the trajectory spillway in Karun3 dam in Iran with 205 m height.

Figure 4-1. Plunge pool on Karun Dam in Iran (IWPCO, 2006)

Since the three dimensional flow in a typical plunge pool has not yet been subjected to adequate mathematical descriptions and also due to the complex nature of the scour in the plunge pool which is generated by highly turbulent flows and secondary currents available the approach to describing plunge pool scour development is based on combining dimensional analysis and experiments. There is a need therefore to identify all the variables which might have some effect on scour geometry and choose those that are relevant.

The majority of previous studies on plunge pool scour have emphasized the development of equations of prediction of only the depth of scour. However, for the design of a plunge pool, or in this case to predict the scour shape, other elements of the geometry of scour pool need to be defined. The maximum width and length of the scour hole are variables which need to be involved in the analysis. The followings are the main objectives of the present study:

1- To develop a set of equations to predict the geometry of scour. The use of some variables such as total head and angle of the jet entry and tailwater depth is emphasized. The equation developed should be able to estimate the scour geometry for the design of plunge pool energy dissipators.

2- To obtain lab observation data related to mechanisms of scour and describe the effects of significant variables based on these observations.

3- To examine the effect of the size of the plunge pool and secondary currents within it on the geometry of the scour.

4.2   STRUCTURE DESCRIPTION

This chapter reviews theoretical aspects of the processes and mechanisms characterizing jet energy dissipation and scouring in the plunge pool downstream of a flip bucket spillway. Subjects covered in this review include geometry of jet trajectory, evaluation of jet energy at the bucket lip, and dissipation mechanisms in the plunge pool. Effects of gravel properties on the materials covered in this chapter are not directly applicable to the analysis of the data collected. However, having a knowledge of these theories helps in better understanding the mechanism and the effect of different parameters involved in the development of the scour hole.

A discussion of the relative significance of the different variables involved in the description of plunge pool scouring is also included. This discussion addresses the development of relevant dimensionless parameters to data experiments aimed at describing flow and scouring due to the flip bucket spillway.

4.2.1   Flip Bucket Spillway

A flip bucket spillway consists of a chute spillway, which conveys water from the reservoir to the bucket, and a flip bucket, which deflects the water jet a considerable distance away from the dam into the plunge pool. The flip bucket spillway and the trajectory basin are composed of five reaches as shown in Fig. 4.2, including: (1) approach chute spillway, (2) deflection and takeoff, (3) dispersion of water jet in air, (4) impact and scour of jet, and (5) tail water zone.

The length and slope of the chute spillway depend on the topographic and geologic conditions of the site and on the desired distance the water is to be thrown downstream of the reservoir. For the construction design of the flip bucket, a prime consideration is given to the total forces that are exerted on the bottom of the structure mainly from the centrifugal force of the curvilinear flow. The dynamic pressure exerted on the floor of the bucket is proportional to the square of velocity of the flow and inversely proportional to the bucket radius. An approximation equation for the pressure exerted on the bottom of the floor by centrifugal force of the deflecting flow given by the USBR (1977) is as follows:

$$P = 0.096 \, qV / R \tag{4.1}$$

In the above equations P is the normal dynamic pressure on the floor of the bucket in kilopascal, q is the unit flow rate in square meter per second, V is velocity at the bucket in meter per second and R is the radius of the curvature in meter. The USACE, (1970) recommends a method in which the total deflection angle and the angle of rotation from the beginning of the curve are used to calculate the pressure at every portion of the bucket. The relationship and the design curves are given in USACE, (1970).

4.2.2   Trajectory Jet

The high velocity flow at the end chute spillway is delivered some safe distance from the reservoir in the form of a trajectory jet by using the flip bucket. In regions where high wind velocities prevail if the spray from the jet could not be tolerated use of a flip bucket spillway may not be recommended. If the material at the point of impact of the jet is not strong enough against scouring or if it is characterized by the presence of different materials at different layers, the construction of a plunge pool with the riprap should be given consideration if using a flip bucket spillway.

The path which follows depends on the initial velocity of the jet at the lip, the difference in elevation between the bucket lip and the water surface level in the plunge pool and the deflection angle of the lip. To develop the equations defining the jet geometry, the projectile theory can be applied assuming that the jet is only under the influence of gravity, and that other influences such as air resistance, turbulence, etc. are ignored. Figure 4-2 shows the variables corresponding to the trajectory jets.

The following are the equations of jet throw distance, length of the jet, height of the jet, and the angle of the jet entry to the plunge pool, respectively, as developed from projectile motion:

$$X_j = V_j \cos\left\{ V_j \sin\alpha / g + \sqrt{((V_j \sin\alpha / g)^2 + 2h / g)} \right\} \tag{4.2}$$

$$L_j = -V_j^2 (\cos^2 \alpha) / g \int_{\theta_0 = \alpha}^{\theta_j = \beta} \sec^3 \theta \, d\theta \tag{4.3}$$

$$Y_j = V_j^2 \sin^2 \alpha / 2g \tag{4.4}$$

$$\beta = \arctan \sqrt{(\tan^2 \alpha + 2gh / V_j^2 \cos^2 \alpha)} \tag{4.5}$$

where, X_j is jet throw distance from the flip bucket lip to the point of impact in the plunge pool, V_j is velocity of the jet at the bucket lip, α is angle of the bucket lip, g is acceleration due to gravity, h is vertical drop height from the bucket lip to the water surface level in the plunge pool, L_j trajectory length of the jet from the lip to the plunge pool, Y_j is vertical rise height of jet, and β is jet entry angle to the plunge pool.
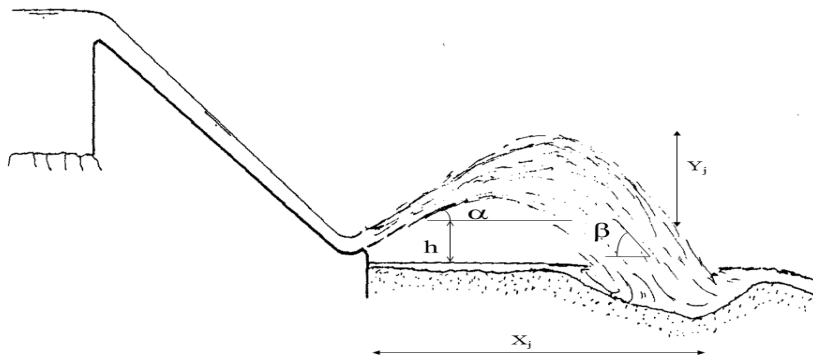
Figure 4-2. Schematic diagram of the flip bucket chute spillway, USACE, (1970)

4.2.3   **Energy Dissipator**

Dissipator of the kinetic energy generated at the base of a spillway is essential for bringing the flow into the downstream river to the normal condition in as short of a distance as possible. This is necessary not only to protect the riverbed and bank from erosion but also to ensure that the dam itself and adjoining structures like power house, canal and spillway are safe. Most of the jet energy needs to be dissipated before it reaches the channel downstream from the spillway. Some of the energy is employed in scouring the plunge pool bed. In order to describe the physical processes of the formation of the scour hole, the characteristics of the jet, as well as the geologic condition of the bedrock down the spillway, need to be studied. The jet loses part of its energy through its flight from the bucket lip to the pool due to expansion, internal turbulence processes and air resistance (Khatsuria, 2005).

However, most of the jet energy dissipates in the plunge pool as a result of jet impingement into the water mass and on the bedrock. The formation of the air bubbles at the point of the jet with the plunge pool cushions the dynamic forces of the jet as it moves into the tailwater, dissipating part of the energy. Resistance of the bed material to the impact of the jet dissipates additional energy. At the early stages of operation of the plunge pool energy dissipator, the bedrock acts as a flat plate, deflecting the incoming jet to the surrounding pool. The deflected jet acts on individual bed particles thus beginning scour. Initially the drag forces on the bed particles exceed the resistance to motion. As the scour hole increases in size an equilibrium condition is reached in which drag forces are balanced by gravity components of the sloping beds of the scour hole (Khatsuria, 2005).

The strength degree of fracture and properties of the bedrock at the jet impact point affect the rate, magnitude, shape and the extension of the scour hole in the plunge pool. The hydrodynamic forces of the jet and the pressure build up under the rock surface due to the penetration of the jet into the bedrock are two major causes of erosion of impinging jets. There are two distinctive regions of scour due to the trajectory jet: a region formed as direct result of the jet impingement, which is called live scour hole and a second region made of the surrounding areas where scouring is due to a recirculation and secondary flows, referred to as the outer pool.

When the bed material at one side of the live scour hole is more scour resistant than at the other side the development of the scour hole at that side may become partially confined and as a result asymmetrical recalculating and secondary flows in the plunge pool will distort the otherwise symmetric shape of the plunge pool. Bedrock with weak or open joints facilities

water penetration which in turn accelerates the build-up of internal pressure and produces faster breaking of the bed material (Amaian, 1994).

4.2.4   Jet Diffusion

A description of the jet dynamics including the distribution of the velocity and pressure in the plunge pool and the motion of the particle as a result of the jet impingement can be used for the analytical study of scour. Most of the studies currently available on jet scouring are vertical and horizontal jets under free submerged conditions: see Doddiah, Albertson and Thomas (1953), Altinbilek and Okyay (1973), Westrich and Kobus (1973), Beltaos and Rajaratnam (1974) and Rajaratnam and Beltaos (1977) for the vertical jets, and Ackermann and Undan (1970), Mih and Hoopes (1972), Rajaratnam and Pani (1974), Rajaratnam and Berry (1977), Rajaratnam (1981) for the horizontal jets and Hoffmans and Verhij (1997), (2009), (2011) for the scour manual and jet scour.

For free trajectory jets enter the plunge pool with an inclined angle and carry a significant amount of air bubbles as a result of their flight in the air and impingement at the pool. As the jet enters the pool the turbulent mixing of the incoming jet with the surrounding flows cause the velocity of the jet to the reduced consequently enlarging its size. These factors can appreciably diminish the jet energy available for erosion of the bed material. The structure of the impinging jet on a solid wall surface consists of four distinct flow regions as show in Figure 4-3 (Amaian, 1994). Immediately downstream of the impact point a potential core exists which rapidly diminishes in size in the downstream direction as a result of shear stress between the core and the surrounding fluids. The velocity in this region is equal to the initial velocity at the impact point.
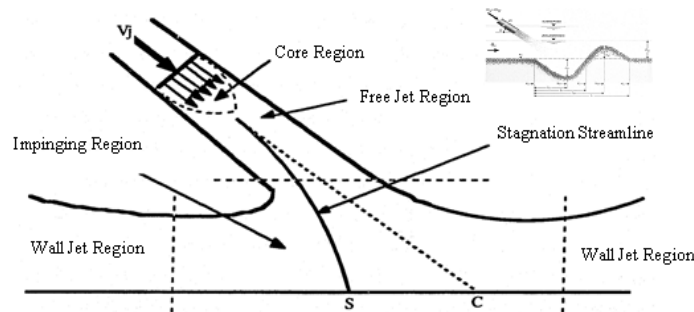

Figure 4-3. Definition Sketch of the impinging jet (Amaian, 1994)

After this transition zone the free jet region follows which extends to some distance above the wall. In this zone the flow is not affected by an increase of static pressure exerted from the wall and the velocity distribution shows similarity in profiles. Following the free jet region the impinging region forms in which the flow turns from its initial direction to the direction very close to parallel to the wall. After this point the pressure gradient gradually decreases and the wall jet region forms. This region consists of two different shear zones:

-A boundary layer near the wall in which the velocity changes from zero at the wall to some maximum value.

-A free shear region with a decrease in velocity and similarity profiles in velocity distribution.

For the normal jets flow is entirely axisymmetric for all the regions, whereas, in the case of oblique impinging jets, except for the free jet region in which the flow is symmetric, the other

regions do not possess an axisymmetric flow. Figure 4-3 shows that the stagnation point (s) dose not occur at the centreline of the incoming jet point c.

In order to study the extent of the local scour due to the jet impingement into the pool the flow pattern in the scouring area and its effect on scouring can be used as a basis for an analytical solution. The most severe hydrodynamic action from the impinging jets occurs at the impinging region where the pressure gradients as wall as the magnitude of shear stress are significant. The roughness of the wall is one of the parameters which has an effect on the flow filed at the impinging and wall jet zones. Empirical relationship for the shear stress distribution of smooth and walls are given by Kobus, Leister and Westrich (1979).

The permeability of the bed materials is another parameter that affects the pressure and velocity profiles in the deflection and wall jet zones. The stagnation pressure and the radial velocity as well as the resulting bed shear stress are reduced as the bed becomes more permeable. The energy of the incoming jet is dissipated by seepage through the permeable bed such that less energy is left for erosion and transport of the bed material.

4.3   INCIPIENT MOTION

The process of the removal of bed particles can be better understood by analysing the forces causing scour. When a fluid flow passes along a surface composed of solid particles if the hydrodynamic forces of flow which favor sediment motion become larger than the resistance forces on the particles then incipient motion and erosion of the bed materials will result. The concept of incipient motion of the bed particles is a very complex one. Initial motion is subject to the influence of several physical parameters such as the type of flow, bed slop, bed roughness, and physical properties of the bed material such as size distribution, shape, density, fall velocity, porosity, angle of repose of the sediments and so on (Vanoni 1975, Simons and Senturk 1977).

When the net hydrodynamic force on a particle reaches a value such that any slight increase causes the particle to move the critical or threshold condition is said to have been reached (Vanoni, 1975). At the critical condition values of velocity and shear stress are said to have their critical or threshold values. The initial motion of the particles can be defined by both the boundary shear stress on the grain or by the fluid velocity in the near of the particle. The choice of shear stress or velocity depends on the flow situations, type of problem and the availability of the data of critical conditions in the field.

In the regions of non-uniform flow or unsteady flow condition the use of shear stress as a variable to define the incipient motion is not suitable. In sediment transport problems, critical shear stress is the preferred criterion for incipient motion, whereas, in the design of riprap, the critical velocity is commonly used. The use of velocity for analyzing the incipient motion in riprap design is convenient because drag and lift forces are commonly expressed in terms of the fluid velocity. For laminar flow the initial motion condition can be defined very easily. As soon as flow exceeds the critical condition the bed particles start moving. For turbulent flow the immediate forces acting on the sediment particle fluctuate with time. Therefore, only a few particles may be in motion when flow is near the incipient motion. This is a main reason why it is difficult to exactly define a criterion for the incipient motion of the particle at turbulent flow.

4.3.1   **Hydrodynamic Forces**

It is easy to imagine that there is a critical value of the flow velocity at which a grain is no longer in equilibrium and starts to move. Figure 4-4 shows the forces acting on a grain. A drag force by the flow on a stone is easily imaginable. A lift force is mainly caused by the flow around a grain. The various flow forces on the grain cab can be expressed as follows.

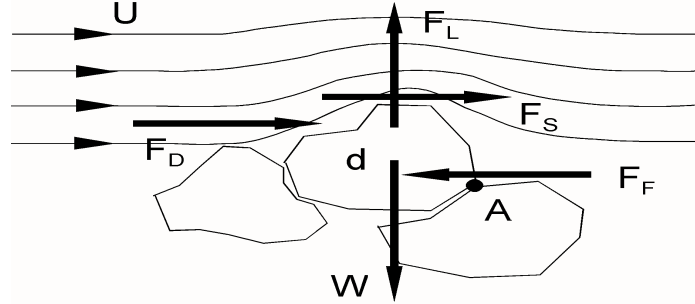
Figure 4-4 Forces on a grain flow (Schiereck, 2001)

The drag force is defined as the dynamic force of the fluid on a particle in the direction parallel to the bed. In general, the drag force on a submerged body consists of two components: shear drag (skin friction drag), which is related to boundary layer development, and pressure drag (form drag), which is due to pressure differences at zones of flow separations.

The lift force is a component of the hydrodynamic forces on the particle normal to the bed. The work of Einstein and Samni (1949) is one of the studies most frequently used to calculate the mean life force that is exerted by a turbulent flow on a bed particle.

$$\left.\begin{array}{l} \textit{Drag froce}\; : F_D = \dfrac{1}{2} C_D\; \rho_w\; u^2 A_D \\[2mm] \textit{Shear force}: F_F = \dfrac{1}{2} C_F\; \rho_w\; u^2 A_S \\[2mm] \textit{Lift force}\;\;\; : F_L = \dfrac{1}{2} C_L\; \rho_w\; u^2 A_L \end{array}\right\} \qquad F \propto \rho_w\; u^2\; d^2 \tag{4.6}$$

in which C_D, C_F and C_L are corresponding coefficients of drag, shear and lift forces, ρ_w is density of the fluid, u is fluid velocity, and A is a characteristic projected area of the particle perpendicular to the direction of flow. The drag coefficient is a function of particle shape and also of the flow characteristics at the vicinity of the particle as expressed by the Reynolds number $\mathrm{Re}_{(N)}$.

The lift force is balanced directly by the submerged weight, Shear and drag are balanced. The relation between load and strength can be expressed:

$$\rho_w\; u_c\; d^2\; \propto\; (\rho_s - \rho_w)\; g\; d^3 \tag{4.7}$$

The velocity used is the critical velocity. This leads to a dimensionless relation between load and strength (Schiereck, 2001):

$$u_c^2 \propto \left(\frac{\rho_s - \rho_w}{\rho_w} \right) g\; d = \Delta\; g\; d \;\; \Rightarrow \;\; u_c^2 = K\; \Delta\; g\; d \tag{4.8}$$

56

All formulae on grain stability come down to this proportionality. There are numerous formulae but there are two famous methods for the stability of stones in flowing water.

Izbash, (1930), expressed relation equation (4.9) as:

$$u_c = 1.2\sqrt{2\,\Delta\,g\,d} \quad or \quad \frac{u_c}{\sqrt{\Delta\,g\,d}} = 1.7 \quad or \quad \Delta\,d = 07\frac{u_c^2}{2g} \tag{4.9}$$

Shields (1963) assumed that the factors in determining the stability of the particles on a bed are the bed shear stress τ_b and the submerged weight of the particles. Shields gives a relation between a dimensionless shear stress and so-called particle Reynolds number.

$$\psi_c = \frac{\tau_c}{(\rho_S - \rho_w)\,gd} = \frac{u_{*c}^2}{\Delta gd} = f(\text{Re}_*) = f\left(\frac{u_{*c}d}{\upsilon}\right) \tag{4.10}$$

ψ_c is usually called the Shields parameter and is a stability parameter which is defined using a critical value of the velocity. The critical bed shear stress (or critical mobility parameter Ψ) can be obtained graphically, directly from the modified Shields diagram in or by using expressions that fit the Shields diagram (Hoffmans and Verhij 1997). Figure 4-5 illustrates the Shields relation.
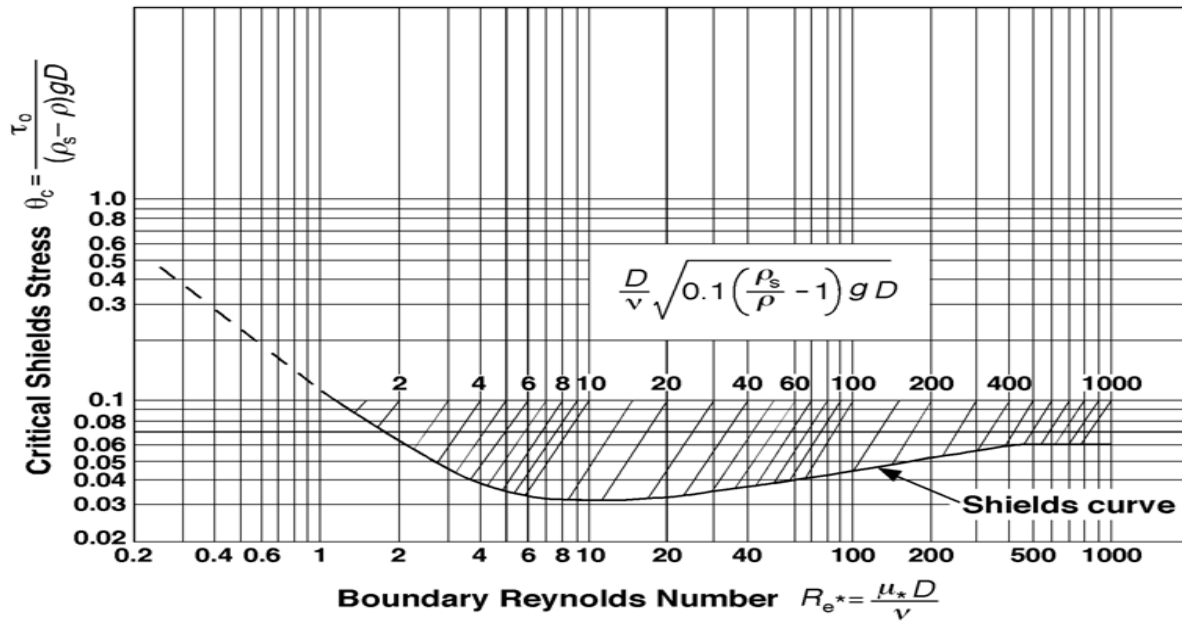

Figure 4-5. Shields diagram (Hoffmans and Verhij 1997).

4.4   PREVIOUS RESEARCH

There are a number of research studies in the area of plunge pool scour due to the different types of jets including vertical circular jets, horizontal two dimensional jets and submerged or free jets. A review of existing literature helps in better understanding the mechanisms and significance of different variables for specific conditions. The purpose of this section is to show the importance of the dissipation of the jet energy by giving an orderly review of the case histories of the damages caused by development of an excessive depth of scour

downstream of the reservoir and the methods used by different research studies to predict the size of scour hole and analysis with probabilistic methods.

In recent years the use of the free trajectory jets such as form flip bucket ski jump and free overall spillway and their associated plunge pools to dissipate the flow energy has increased. The safety of many dams has become endangered because of the lack of appropriate energy dissipator structure. In some cases, because the extent of the scour hole was grater than anticipated and the cost of the repair to ensure the safety of entire structure were relatively large. The following are case histories of some prototype dams with severe scour problems (Mason and Mice, 1984).

1. Alder Dam in the United States of America is $100\,m$ high with a flip bucket spillway capacity of $2,666\,m^3/s$. During the period 1945-1952 the extensive use of the spillway resulted in the development of $31\,m \times 37\,m \times 25\,m$ deep scour hole at the base of the hill below the bucket. In addition the deposition of the scour material into the river downstream caused an increase of the tailwater depth and as a result the loss of power output. The remedial work in 1952 used about 6,000 m^3 of material and reinforced concrete for the repair.

2. Tarbela Dam in Pakistan is another example of a flip bucket spillway that dissipated an insufficient amount of energy. The flip bucket chute service spillway was designed to pass flow of $17,420\,m^3/s$. The operation of this reservoir started in the spring of 1975. After two years of operation an excessive amount of scour which was $110\,m$ deep at the right side and $80\,m$ deep at the left side of the pool was discovered. The non uniformity of the bed material caused an asymmetric shape of the scour hole.

3. Picote Dam in Portugal is a $100\,m$ high arch dam with a discharge capacity of about $11000\,m^3/s$. Due to the flood of 1962 a $20\,m$ deep scour hole was formed. The deposited materials downstream of the scour hole produced a $15\,m$ high bar causing a significant reduction in the available head for power generation.

4. The Grand Rapids generating station in Canada with a spillway capacity of $4000\,m^3/s$ was completed in 1962. During the first four years of operation the spillway operated for longer periods than it was anticipated at the time of design. The depth of scour hole after four years of operation was 30% larger than it was anticipated for the entire life of the structure. The cost of remodeling which involved the extension of the chute $20\,m$ to the upstream face of the scour hole and also the construction of the dentate sill to direct the flow to the downstream edge of the scour hole for prediction of the bottom hole against further erosion was estimated to be 1 million dollars.

The studies of scour by impinging jets can be categorized into the following groups: vertical, horizontal and trajectory jets, submerged, or free jets, high or low drop jets, aerated, or nonaerated jets, and jets with various boundary configurations. The following paragraphs discuss some of these studies.

Altinbilek and Okyay (1973) investigated the local scour caused by the vertical submerged jet on a flat cohesion less bed. A rational method based on the application of an equation of continuity to describe the bed geometry and the transport capacity as a function of flow conditions and time was developed. The results of this study show that the ultimate depth of scour is a function of the jet Froude number, mean particle size diameter, jet thickness, jet velocity and the fall velocity of the sediment. The jet Froude number was defined as:

$$Fr = (U/\sqrt{gb}) \tag{4.11}$$

In which U is a velocity, g is the acceleration of gravity and b is the thickness of the jet.

Westrich and Kobus (1973) have shown that the momentum flux of the jet and the distance between the nozzle and the sediment determine the rate of scour. The flow velocity distribution and the fluctuation of pressure adjacent to the bed were found to have significant effect on the formation of the scour hole.

Doddih, Albertson and Thomas (1953) conducted a study of scour caused by circular solid and hollow jets issuing vertically downward impinging on an alluvial bed covered by a pool of water at different depths. The results of this study show that at large tailwater depths, the rate of scour and initial depth of scour were small, whereas for shallow tailwater depth the opposite is true. Also, they found that the magnitude of scour increases as the tailwater depth increases until the depth reaches a critical value. After this point any further increase of the tailwater depth reduced the depth of scour.

Rajaratnam and Beltaos (1977) performed experiments on the erosion of impinging circular turbulent air jets on loose beds of sand and polystyrene. The results show that the maximum depth of scour varies linearly with the logarithm of time and for an appreciable period of time the scour profile departs from the linear trend and reaches an asymptotic state. They concluded that for large impingement height characteristics of the scour hole in term of the drop height H is a function of $\left[Fr/(h/d) \right]$ in which Fr is the Froude number, equal to:

$$Fr = U_0 / \sqrt{g.d(\Delta\rho/\rho)} \tag{4.12}$$

where, ρ is the mass density of fluid and $\Delta\rho$ is the difference between the mass densities of the bed particles and the fluid, d is the diameter of the jet and U_0 is the velocity of the jet at the nozzle. For low values of h the length characteristics of the scour hole d were found to be mainly a function of Fr. In another study, Rajaratnam (1982) found that while there are similarities between the air-sand and water-sand systems there are also some differences between these two systems regarding the depth of scour and the radial extent of the scour hole. In both systems the maximum depth of scour and the radial extent of the scour hole are mainly a function of the parameter $\left[Fr/(h/d) \right]$, but for some values of this parameter the depth of scour in the water-sand system is smaller and the radial extent of the scour hole is much smaller than those in the air-sand system.

Beltaos (1976) conducted an experiment on the oblique impingement of plane turbulent jets by using air as the flop medium. A semi-empirical method was developed for the calculation of wall pressure and shear stress distribution in the impingement region. The results of this study show that the jet thickness grows linearly and the rate of divergence is independent of the impinging angle and included impingement height whereas it depends on the Reynolds number.

Blaisdell and Anderson (1991) performed experiments to develop criteria for the design of pipe plunge pool energy dissipators. The tests cover a range of flow discharges pipe heights from tailwater level and bed material sizes. The equations developed can be used to predict the time development and ultimate size of the scour hole and also to design the riprapped pipe plunge pool energy dissipators.

Son (1992) conducted a model study on the scour under submerged inclined jets by using spherical particles. The results of this study show that the Reynolds number of the jet is insignificant for the incipient motion of the bed particles. It was found that the effect of the width of the plunge pool can be neglected when the ratio of the width of plunge pool to the

size of the nozzle is greater than 4.5 and the effect of the width of the plunge pool varies as the tailwater depth changes. The research resulted in the development of equations predicting the maximum scour potential for two regions of jet diffusion; first, the region of flow establishment and second the established flow region. These equations were developed both from theoretical analysis and from regression analysis of the experimental data.

Johnston (1990) investigated the development of the scour hole in shallow tailwater depth formed by a horizontal triangular jet. In horizontal submerged rectangular jets and with shallow tailwater depth, the jet generally curves either toward the free surface or toward the bed. For this reason the scour formation is unstable. Three regimes of scour development have been described for this case.

Sobey, Johnston and Keane (1988) conducted experimental studies on the performance of horizontal round buoyant jet in shallow water. They found that the proximity of the bed and then free surface have significant effect on the flow pattern. At shallow tailwater depth the jet initially deflected toward the neighboring bed, where reduction of the jet momentum occurs and buoyancy gradually dominated the flow pattern causing the jet path to rise toward the free surface.

The scour due to free over flow of the crest of arch dams can cause severe damage to the foundation of the dam. Due to the almost vertical entry condition of the falling jet at the impact point to the pool the shape and location of a scour hole forms close to the toe of the dam the shorting of the seepage lines causes an increase in the seepage amount and consequently reduces the safety of the structure. Wang and Cheng (1990) estimated the maximum depth of scour caused by over falls flow by both theoretical and experimental approaches. The theoretical study is based on the momentum principle. Dimensional analysis was used to develop an equation based on the experimental data to predict the relative maximum depth of scour.

Most of the studies in the area related to the scour are due to free trajectory jets from flip buckets. A large number of equations have been developed to predict an ultimate depth of scour. However the type of method of approach and the number of variables involved in equations vary from study to study. Some equations have been simplified by ignoring the effect of some important variables due to either personal preferences in the choice of variable by different researchers or to problems in measuring and controlling the variables. The following is a brief discussion of some of these studies.

The general form of the scour, d_S measured from the tailwater surface is:

$$d_S = C \, q^X H^Y \beta^W / d_{50}^Z \tag{4.13}$$

where, C is a coefficient, β is the angle of the flip bucket with the horizontal, d_{50} is the particle size (mm), q is specific discharge (m^2/s), and H is the difference between upstream and downstream water levels (m). The range of the coefficient C and exponents x, y, z and w is: (Novak (2001)):

$$0.65 < C < 4.7 \quad , \quad 0.5 < x < 0.67 \quad , \quad 0.1 < y < 0.5 \quad , \quad 0 < z < 0.3 \quad , \quad 0 < w < 0.1$$

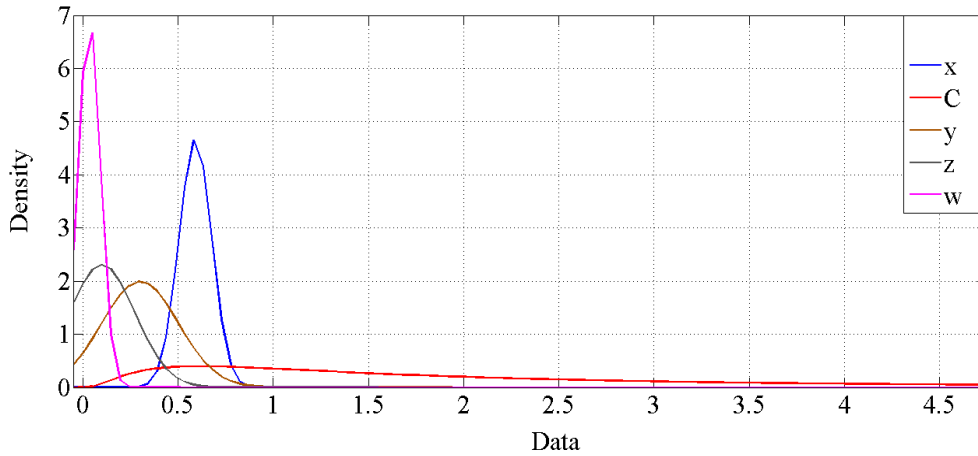Figure 4-6 shows the density function of the coefficient and parameters in equation(4.13).

Figure 4-6. Density function of the above given parameters

Thus the range of d_S is wide, as is only to be expected because equation(4.13) covers a wide range of structures with different designs, degree of entrainment, and geological conditions. Accepting the possibility of 100% errors a simplified equation by Martins (1975) with $x = 0.6$, $y = 0.1$, $w = z = 0$ and $C = 1.5$ can be used:

$$d_S = 1.5 \, q^{0.6} H^{0.1} \tag{4.14}$$

where, d_{cr} is the critical depth, and β_1 is the upstream angle of the scour hole, which is a function of the flip bucket exit angle β but does not vary widely ($14^o < \beta_1 < 24^o$ for $10^o < \beta < 40^o$).

Chee and Padiyar (1969) developed equations to predict the ultimate depth of scour and the scour hole configuration. In their study they found that the maximum depth of scour $d_S (m)$ depends on the spillway discharge $q (m^2/s)$ the head drop between the reservoir level and tailwater level in the plunge pool $H (m)$ and the mean particle size $d_{50} (m)$.

$$d_S = 2.126 \, q^{0.67}.H^{0.18} / d_{50}^{0.063} \tag{4.15}$$

Wart and Meel (1983) correlated the data collected from experience and literature using unit discharge and head as independent variables to estimate the scour hole depth in the plunge pool. The data were divided into two groups, high head which is greater than or equal $30(m)$ drop, and low head for the reservoirs with less than $30(m)$ drop. The equations for the depth of scour were accompanied by equations of 95 percent confidence and prediction intervals.

Coleman (1986) applied Veronese's scour formula. In which $d_S (m)$ is the vertical depth of scour below tailwater, $H (m)$ is the effective energy of jet entering the tailwater, and $q (m^2/s)$ is the unit discharge. This formula was developed to be applied to the vertical falling jets.

$$d_S = 1.9 \, H^{0.225}.q^{0.54} \tag{4.16}$$

Colman fond that Veronese's formula can reasonably estimate the limiting scour depth if d_S is measured in the direction of the tangent to the jet entry to the pool. The result of this study shows that the predicted value of the location of maximum depth of scour was further downstream from the observed results.

61

Mason and Arumugam (1985) examined the scour formulas which have been proposed to date with prototypes and models data of such prototypes to check the accuracies of individual equations and also show what variables were more significant. The result of this analysis shows that the unit flow rate, q, the head drop, H, and tailwater depth, d_w, are the most important variables for the estimation of ultimate depth of scour. For those equations in which the particle size is included the use of mean particle size d_{50}, gives better accuracy than using d_{90}. That study resulted in the development of an equation for the estimation of ultimate depth of scour by including the depth as an additional variable.

$$d_S = 3.27 \, q^{0.60} H^{0.05} d_w^{0.15} / (g^{0.3} . d_m^{0.06}) \tag{4.17}$$

Mason (1989) demonstrated that the head drop H, may not directly affect the scour depth, other than by varying the amount of air entrained in the plunge pool. This in turn affects the force on particles of bed material. An alternative expression that better described the scour process was therefore proposed.

$$d_S = 3.39 \, q^{0.6} (1+k)^{0.3} d_w^{0.16} / (g^{0.3} . d_m^{0.06}) \tag{4.18}$$

where, k is ratio of air to water, and calculated with this formula:

$$k = (1 - \frac{V_e}{V})(\frac{H}{b})^{0.446} \tag{4.19}$$

where V is the jet impact velocity, and the minimum jet velocity V_e required to entrain air and the thickness b at impact.

In recent years a number of model studies have been conducted at the Utah University Water Research Laboratory to predict the depth of scour below flip bucket spillways and under the vertical jets. Barfuss (1988) used energy of the jet at the flip bucket lip, E, instead of the total head for predicting the depth of scour below trajectory water jets. The jet energy is defined as follows:

$$E = \frac{V^2}{2g} + \frac{b}{2} + H_1 \tag{4.20}$$

where V is the velocity at the flip bucket lip, b is the thickness of the jet at the lip, H_1 is the drop height from the bucket lip to the water surface level in the plunge pool. Barfuss (1988) found that the scour hole is unstable at low tailwater depth, and at lower range of unit flow. In his formula d_{90} is the diameter of 90 percent of particle size.

$$d_S = 2.432 \, q^{0.66} E^{0.33} / (g^{0.33} . d_{90}^{0.32}) \tag{4.21}$$

Yildiz et al (1994), suggest that for applying this formula to spillways with flip buckets etc, it should be modified to:

$$d_s = 1.90 . q^{0.54} H_1^{0.225} \sin \theta \tag{4.22}$$

where θ is the jet impact angle at tail water surface.

Amanian (1994) developed a set of equations to predict the geometry of scour. He used some variables such as energy of the jet instead of the total head, the angle of the jet entry to the pool, and the tailwater depth is emphasized.

$$d_S = 0.25 \, q^{0.95} E^{0.65} (\sin \beta)^{0.6} / (H^{0.70} . d_{50}^{0.30}) \tag{4.23}$$

$$L_S = 2.40 \, q^{0.25} E^{0.40} H^{0.15} X_j^{0.40} / (d_{50}^{0.10} . (\sin \beta)^{0.2}) \tag{4.24}$$

$$W_S = W_b + 0.55 \, q^{1.50} E^{0.30} (\sin \beta)^{0.60} / (d_{50}^{0.50} . H) \tag{4.25}$$

where $q \, (m^2/s)$ is unit discharge, β is angle of the jet entering the plunge pool in degree, $H \, (m)$ is depth tailwater in the plunge pool, $X_j \, (m)$ is length of trajectory jet, $W_b \, (m)$ is width of the bucket lip, $L_S \, (m)$ and $W_S \, (m)$ is maximum length and width of the scour hole respectively.

Azmathullah (2005) performed experiments to develop equations to predict the ultimate depth of scour and the scour hole configuration. It was found that the geometry of scour hole downstream of the ski-jump bucket spillway. It is based on the approach of neural networks and it involved analysis of an extensive data base in order to obtain the depth, the location of maximum scour from the bucket lip, as well as the width of scour hole out of the given parameters of q, H, R, d_{50}, d_w and ϕ.

$$\frac{d_S}{d_W} = 6.914 (\frac{q}{\sqrt{g.d_W^3}})^{0.694} (\frac{H_1}{d_W})^{0.0815} (\frac{R}{d_W})^{-0.233} (\frac{d_{50}}{d_W})^{0.196} (\phi)^{0.196} \tag{4.26}$$

$$\frac{L_S}{d_W} = 9.850 (\frac{q}{\sqrt{g.d_W^3}})^{0.420} (\frac{H_1}{d_W})^{0.280} (\frac{R}{d_W})^{0.043} (\frac{d_{50}}{d_W})^{0.037} (\phi)^{0.346} \tag{4.27}$$

$$\frac{W_S}{d_W} = 5.420 (\frac{q}{\sqrt{g.d_W^3}})^{-0.015} (\frac{H_1}{d_W})^{0.551} (\frac{R}{d_W})^{0.139} (\frac{d_{50}}{d_W})^{0.242} (\phi)^{-0.160} \tag{4.28}$$

where $H \, (m)$ is the head between upstream reservoir water level and tail water level, $R \, (m)$ is radius of the bucket, $d_W \, (m)$ is tail water depth, ϕ is lip angle of bucket (radians).

4.5 DIMENSIONAL ANALYSIS

This section introduces the procedure of dimensional analysis and describes Buckingham's Π-theorem. In engineering the application of hydraulic and fluid mechanics in designs make much use of empirical results from a lot of experiments. This data is often difficult to present in a readable form. Even from graphs it may be difficult to interpret. This is a useful technique in all experimentally based areas of engineering. If it is possible to identify the factors involved in a physical situation, dimensional analysis can form a relationship between them.

4.5.1 Buckingham's Π-Theorem

The Buckingham P_i theorem is a rule for deciding how many dimensionless numbers (called Π's) to expect. The theorem states that the number of independent dimensionless groups is equal to the difference between the number of variables that make them up and the number of individual dimensions involved. The weakness of the theorem, from a practical point of view, is that it does not depend on the number of dimensions actually used, but rather on the minimum number that might have been used.

63

The Buckingham Π theorem is a key theorem in dimensional analysis. It is a formalization of Rayleigh's method of dimensional analysis. The theorem loosely states that if we have a physically meaningful equation involving a certain number, n, of physical variables, and these variables are expressible in terms of k independent fundamental physical quantities, then the original expression is equivalent to an equation involving a set of p=n−k dimensionless parameters constructed from the original variables: it is a scheme for dimensionless. This provides a method for computing sets of dimensionless parameters from the given variables, even if the form of the equation is still unknown. However, the choice of dimensionless parameters is not unique: Buckingham's theorem only provides a way of generating sets of dimensionless parameters and will not choose the most physically meaningful.

4.5.2   Equation for Scour Hole

An important objective of this model study was to develop an equation to describe the geometry of the scour hole. The development and the significance of the dimensionless variable (Π-terms) and some individual variables describing the geometry of the scour hole due to the flip bucket spillway were discussed in previous chapters. The aim of this section is to discuss and present the equation that resulted from this model study.

4.5.3   Dimensionless Equation in Plunge Pool

Due to the complexity of the problem and also the lack of theoretical explanation for the development of scour below the flip bucket spillway, the employment of the dimensional analysis is suggested both to reduce the number of variables and assist in the experimental design. Dimensional analysis provides a strategy for choosing relevant data and how it should be presented. Scour geometry depends on many variables that characterize the flip bucket and the plunge pool. With reference to Figure 4.7, illustration of some of these variables and their description follows.
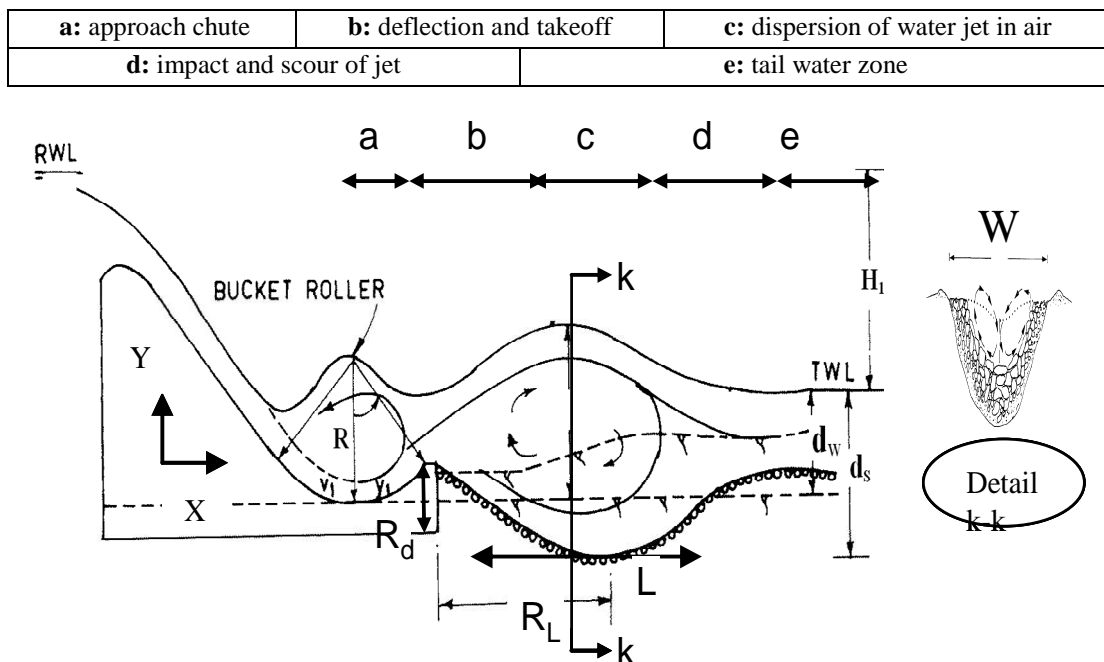
a: approach chute	**b:** deflection and takeoff	**c:** dispersion of water jet in air
d: impact and scour of jet		**e:** tail water zone

Figure 4-7. Scour profile and plunge pool characteristic (Khatsuria, 2005)

4.6   DEVELOPMENT OF EQUATION

The dependent variables d_S, L_S, W_S may be expressed in terms of other variables by the following functional.

$$d_S = f_1(q, H_1, d_{50}, G_S, V, \rho_W, \sigma_{50}, g, \mu_W, d_W, R, \theta) \tag{4.29}$$

$$L_S = f_2(q, H_1, d_{50}, G_S, V, \rho_w, \sigma_{50}, g, \mu_W, d_W, R, \theta) \tag{4.30}$$

$$W_S = f_3(q, H_1, d_{50}, G_S, V, \rho_W, \sigma_{50}, g, \mu_W, d_W, R, \theta) \tag{4.31}$$

The general form selected in this study for the equation relating a Π-term with a number of independent Π-term is in the product of powers of relevant Π-term, i.

$$\Pi_1 = c \ \Pi_2^{a_2} \ \Pi_3^{a_3} \ \Pi_4^{a_4} ..... \Pi_m^{a_m} \tag{4.32}$$

The value of parameters c, a_1, a_2, a_3,….., a_n which were obtained from a multiple regression analysis, can then be replaced back into equation (4.32). Applying the Buckingham Π-theorem, with V, d_w, ρ_w, g as repeating variables, equations above are transformed to:

$$\frac{d_S}{d_W} = f_1 \left(\frac{V}{\sqrt{g.d_W}}, \ \frac{H_1}{d_W}, \ \frac{d_{50}}{d_W}, \ \frac{\sigma_{50}}{d_W}, \ G_S, \ \frac{\mu}{\rho V d_W}, \ \frac{R}{d_W}, \ \theta \right) \tag{4.33}$$

$$\frac{L_S}{d_W} = f_2 \left(\frac{V}{\sqrt{g.d_W}}, \ \frac{H_1}{d_W}, \ \frac{d_{50}}{d_W}, \ \frac{\sigma_{50}}{d_W}, \ G_S, \ \frac{\mu}{\rho V d_W}, \ \frac{R}{d_W}, \ \theta \right) \tag{4.34}$$

$$\frac{W_S}{d_W} = f_3 \left(\frac{V}{\sqrt{g.d_W}}, \ \frac{H_1}{d_W}, \ \frac{d_{50}}{d_W}, \ \frac{\sigma_{50}}{d_W}, \ G_s, \ \frac{\mu}{\rho V d_W}, \ \frac{R}{d_W}, \ \theta \right) \tag{4.35}$$

Since the flow is a fully turbulent flow, the viscosity has a negligible effect on the local plunge pool scour; hence, equations above can be simplified to the form:

$$\frac{d_S}{d_W} = (Fr)^{\alpha_1} \ \left(\frac{H_1}{d_W}\right)^{\alpha_2} \ \left(\frac{R}{d_W}\right)^{\alpha_3} \left(\frac{d_{50}}{d_W}\right)^{\alpha_4} \ (\sin\theta)^{\alpha_5} (G_S)^{\alpha_6} \tag{4.36}$$

$$\frac{L_S}{d_W} = (Fr)^{\alpha_1} \ \left(\frac{H_1}{d_W}\right)^{\alpha_2} \ \left(\frac{R}{d_W}\right)^{\alpha_3} \left(\frac{d_{50}}{d_W}\right)^{\alpha_4} \ (\sin\theta)^{\alpha_5} (G_S)^{\alpha_6} \tag{4.37}$$

$$\frac{W_S}{d_W} = (Fr)^{\alpha_1} \ \left(\frac{H_1}{d_W}\right)^{\alpha_2} \ \left(\frac{R}{d_W}\right)^{\alpha_3} \left(\frac{d_{50}}{d_W}\right)^{\alpha_4} \ (\sin\theta)^{\alpha_5} (G_S)^{\alpha_6} \tag{4.38}$$

4.6.1   Physical Meaning

The physical meaning of the proposed model given in equation (4.29) to (4.31) closely conform to the mechanisms of the geometry of plunge pool subjected to depth, length and width. These equations explain that the scour depth (d_S), length (L_S) and width (W_S) of a plunge pool are a function of Froude number (Fr), differences up and down stream water level (H_1), specific gravity (G_S), bucket radius (R), lip angle (θ), normal water level (d_W) and mean particle size (d_{50}). Recall that the proposed model in this chapter was intentionally

developed to provide a better description about geometry of plunge pool. The proposed dimensionless limit state function analysis LSF model is created based on the multivariate regression analysis method and is presented in chapter 6. This model is designed to provide better visual views of the geometry of plunge pool. Thus these equations are comprehensive enough to illustrate the physical layout of geometry of plunge pool.

4.7   CONCLUSION

This chapter provided reviews on the theoretical aspects of the processes and mechanisms of damage modelling and characterizing jet energy dissipation and scouring in the plunge pool beneath a flip bucket spillway.

In addition, several research works related to plunge pool scour governed by different parameters were also presented. The review was meant at providing better understanding on the mechanisms and the effect of different parameters involved in the development of geometry of the plunge pool.

A discussion about the significance of different variables involved in the description of plunge pool scour was also included. This discussion addresses the development of relevant dimensionless parameters describing the flow and scours due to flip bucket spillway.

The purpose of this chapter was also to emphasize the importance of jet energy dissipation. Discussions were directed at the review of case histories of the damage caused by development of an excessive geometry of scour downstream of the reservoirs. Also, the methods used by different research studies to predict the geometry of scour hole were presented. The application of flip bucket plunge pools as energy dissipators was described as well.

CHAPTER 5

DETERMINISTIC MODELS FOR SUPERELEVATION

Flow in open channel bends is characterized by cross stream circulation which redistributes the velocity and the boundary shear stress and thereby shapes the characteristic bottom topography. River channels do not remain straight for any appreciable distance. The winding of channel platforms and the tendency to create a succession of shoals and depths have been of interest to hydraulicians, mathematicians and planners for more than a century. The physical explanation of shoals and deeps has been identified as the attenuation of the velocity filed by secondary flow. Secondary flow or currents occur in a plane normal to the local axis of the primary flow and are brought about by the interaction between the primary velocity with gross channel properties, resulting in spirals or vortexes (Krhoda, 1985).

The so-called centrifugal force caused by flow around a curve results in a rise in the water surface at the outside wall and a depression of the surface along the inside wall. This phenomenon is called superelevation. The problems associated with flow through open channel bends deserve special attention in hydraulic engineering. Water surface slopes have been frequently reported to be a function of the curvature. But due to the difficulties in operation, the theoretical basis of superelevation has been discussed thoroughly as reported in the literature. Furthermore, experience indicates that existing theory does not lead to good results.

In this chapter pressure models are described first, followed by the review of the previous research on mathematical models and superelevation in open channel bends.

5.1 LITERATURE REVIEW

The first work on mathematical modelling of flow in curved channels is based on the assumption of laminar flow assumed by Boussinesq 1868, Dean 1927 and many others. These analyses have also contributed to the understanding of the complex flow pattern in curved channels with turbulent flow, but the quantitative description is not good enough for most engineering purposes.

A mathematical analysis of the secondary flow in a uniform turbulent flow was carried out by Van Bendegom (1943 & 1947; the latter Engl. transl. 1963 & Allen (1977)). This analysis and the introduction of perturbation techniques (with the depth-radius of curvature ratio as small parameters) in the analysis of curved flow by Ananyan (1957; Engl. transl. 1965) and Rozowskii (1957; Engl. transl. 1961) suppose a large improvement of the understanding and mathematical description of the secondary flow and partly also its interaction with the main flow. Later on many solution methods of mathematical models of curved flows based on perturbation techniques have been published; for instance Yen (1965), De Vriend (1973, 1976, 1977& 1979), Ikeda (1975), Gottlib (1976) and Falcon (1979). In these perturbation methods it is assumed that the main flow distribution is unaffected by the secondary flow. De Vriend (1981a, 1981b) avoids this assumption, but his two-dimensional model only works well in mildly curved flows with vertical side walls.

Qualitatively, the influence of the secondary flow on the main flow (secondary flow convection) has been known for quite a while, but mathematical modelling of this effect, without excessive computational costs, has been lacking. Only recently Kalkwijk & De Vriend (1980) incorporated this effect into a two-dimensional depth integrated model for rivers with gently curved alignment and mildly sloping banks. For the case of channels with steep banks and of rectangular channels no simple two-dimensional model which includes secondary flow convection has been developed yet. Due to the fast improvement of computer capabilities fully three-dimensional flow computations have become feasible in the past decade. For curved channel flow the models can (so far) only cope with rectangular channels. Pratap & Spalding (1975), Leschziner & Rodi (1979), De Vriend & Koch (1981) report such computations. In combination with a thorough analysis these computations may contribute to an improved understanding of the flow in a bend. Presently, the three-dimensional models are not applicable in a morphological model, because the computational costs are far too high.

5.2 MATHEMATICAL MODEL

5.2.1.1 *Theory*

The water surface profile of flow in a channel bend is expressed implicitly by the equations of motion for the flow. Therefore, mathematical expressions for the free surface slopes along the longitudinal and transversal directions of the channel can be obtained from these equations each as a function of the velocity and stresses distribution of the flow.

A mathematical model of the flow in rivers with curved alignment can be described most conveniently in a curvilinear co-ordinate system. The co-ordinate system is chosen as follows: the s-axis coincides with the channel axis, the n-axis is horizontal and perpendicular to the s-axis and the z-axis is vertical and positive upwards. In this co-ordinate system the three-dimensional mathematical description of the flow is very comprehensive, but it can be

considerably simplified if only rivers of constant width are considered. In that case the n-axis will be straight. As a consequence of this simplification a number of small inertia and friction terms vanish in the mathematical model. It does not qualitatively or quantitatively influence the result of the analysis carried out in the following. Kalkwijk et al. (1980) give a three-dimensional mathematical description of the flow in a curvilinear co-ordinate system in which both horizontal co-ordinate axes are curved, but they avoid the comprehensive description of the friction terms. The main structure of the 3-D flow field in a curved open channel is outlined in Figure 5-1. Furthermore, it defines the (s, n, z) reference system, the centerline radius of curvature, r the flow depth $h = Z_S - Z_b$ where Z_S and Z_b are the elevations of the water surface and the bottom above a horizontal datum.
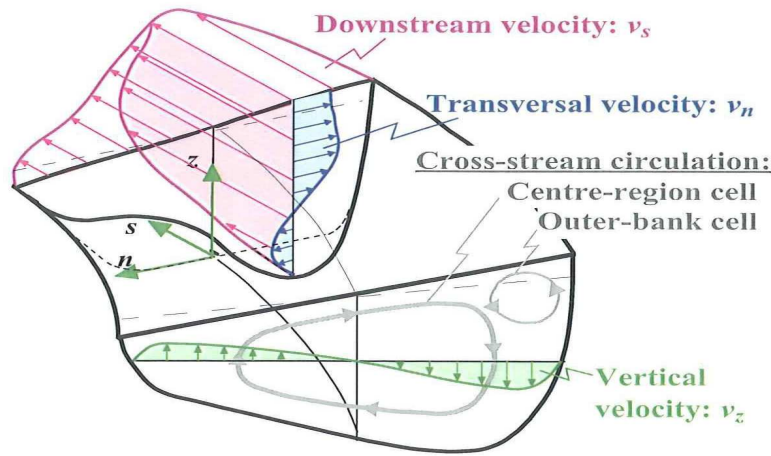
Figure 5-1. The curvilinear co-ordinate system (Blanckaert, 2003)

The steady incompressible turbulent flow can be described by four partial differential equations. Three dynamical equations (one for each direction) and one equation representing the conservation of mass. According to Rozowskii (1957) the equations read:

$$\frac{\partial U}{\partial t} + U \frac{\partial U}{\partial S} + V \frac{\partial U}{\partial n} + W \frac{\partial U}{\partial Z} + \frac{UV}{r} + \frac{1}{\rho} \frac{\partial P}{\partial S} = F_S \tag{5.1}$$

$$\frac{\partial V}{\partial t} + U \frac{\partial V}{\partial S} + V \frac{\partial V}{\partial n} + W \frac{\partial V}{\partial Z} - \frac{U^2}{r} + \frac{1}{\rho} \frac{\partial P}{\partial n} = F_n \tag{5.2}$$

$$\frac{\partial W}{\partial t} + U \frac{\partial W}{\partial S} + V \frac{\partial W}{\partial n} + W \frac{\partial W}{\partial Z} + g + \frac{1}{\rho} \frac{\partial P}{\partial Z} = F_Z \tag{5.3}$$

$$\frac{\partial U}{\partial S} + \frac{\partial V}{\partial n} + \frac{\partial W}{\partial Z} + \frac{V}{r} = F_Z \tag{5.4}$$

in which g is acceleration due to gravity, P is pressure U, V and W are velocity component in S, n and z direction, F_S, F_n and F_Z are friction terms, and ρ is density of fluid.

5.2.1.2   *Momentum Equation for Frictionless Flow*

The vast majority of work on the Navier–Stokes equations is done under an incompressible flow assumption for Newtonian fluids. Taking the incompressible flow assumption into

account and assuming constant viscosity, the Navier–Stokes equations will read (in vector form):

$$\rho(\frac{\partial V}{\partial t}+V.\nabla V)=-\nabla P+\rho v\ \nabla^2 V+f \tag{5.5}$$

f represents other body forces (forces per unit volume), such as gravity or centrifugal force.

$$\rho\ (\underbrace{\overbrace{\underset{\substack{\text{Unsteady}\\\text{acceleration}}}{\frac{\partial V}{\partial t}}+\underset{\substack{\text{Convective}\\\text{acceleration}}}{V.\nabla V}}^{\text{Inertia (per volume)}})=\overbrace{\underset{\substack{\text{Pr}essure\\gradient}}{-\nabla p}+\underset{Vis\cos ity}{\mu.\nabla^2.V}}^{\text{Divergence of stress}}+\underset{\substack{Other\ body\\forces}}{f} \tag{5.6}$$

Euler's equation (obtained from equation (5.5) after neglecting the viscous terms) is:

$$\rho\frac{D\vec{V}}{Dt}=\rho\vec{g}-\nabla P \tag{5.7}$$

In the steady flow a fluid particle will move along a stream line because, for steady flow, path lines and streamlines coincide. Thus in describing the motion of a fluid particle in a steady flow, the distance along a streamline is a logical coordinate to use in writing the equations of motion. Streamline coordinate also may be used to describe unsteady flow.

For simplicity, consider the flow shown in Figure 5-2, we wish to write the equations of motion in terms of the coordinate S, distance along a streamline, and the coordinate n, distance normal to the streamline. The pressure at the center is P. If we apply Newton's second law in the streamwise (the S) direction to the fluid element of volume $ds\ dn\ dz$, then neglecting viscous forces we obtain:

$$-\frac{1}{\rho}\frac{\partial P}{\partial S}-g\frac{\partial Z}{\partial S}=a_s \tag{5.8}$$

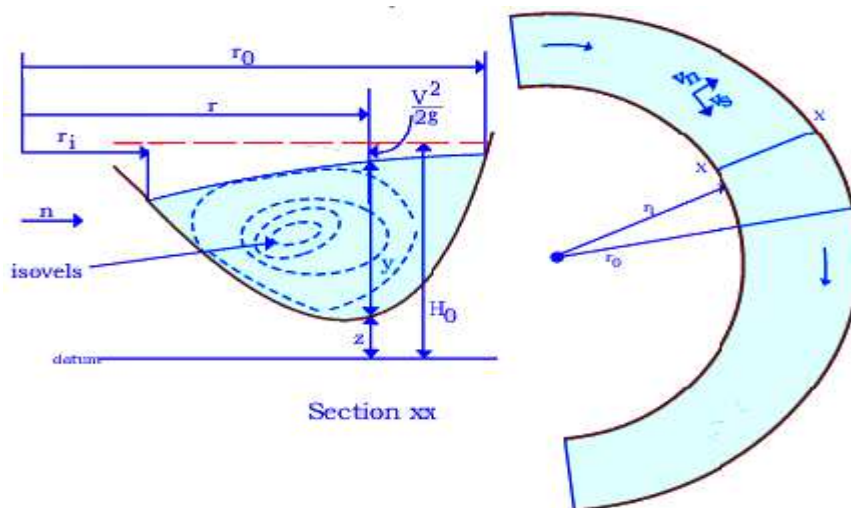Figure 5-2. Flow behavior at a channel bend

Along any streamline $V=V(S,t)$, and the material or total acceleration of a fluid particle in the streamwise direction is given by:

$$a_s = \frac{DV}{Dt} = \frac{\partial V}{\partial t} + V \frac{\partial V}{\partial S} \tag{5.9}$$

$$-\frac{1}{\rho} \frac{\partial P}{\partial S} - g \frac{\partial Z}{\partial S} = \frac{\partial V}{\partial t} + V \frac{\partial V}{\partial S} \tag{5.10}$$

For steady flow and neglecting body forces Euler's equation in the stream wise direction reduces to:

$$\frac{1}{\rho} \frac{\partial P}{\partial S} = -V \frac{\partial V}{\partial S} \tag{5.11}$$

To obtain Euler's equation in a direction normal to the streamline, we apply Newton's second law in the n direction to the fluid element. Again, neglecting viscous forces, we obtain:

$$-\frac{1}{\rho} \frac{\partial P}{\partial n} - g \frac{\partial Z}{\partial n} = a_n \tag{5.12}$$

The normal acceleration of the fluid element is toward the center of curvature of the streamline, in the minus n direction. Thus in coordinate system of Figure 5-2, the familiar centripetal acceleration is written:

$$a_n = -V^2 / r \tag{5.13}$$

For steady flow, where r is the radius of curvature of the streamline the Euler's equation normal to the streamline is written for steady flow as:

$$\frac{1}{\rho} \frac{\partial P}{\partial n} + g \frac{\partial Z}{\partial n} = \frac{V^2}{r} \tag{5.14}$$

For steady flow in a horizontal plan Euler's equation normal to a streamline becomes:

$$\frac{1}{\rho} \frac{\partial P}{\partial n} = \frac{V^2}{r} \tag{5.15}$$

Equation(5.15) indicated that pressure increases in the direction outward from the centre of curvature of the streamlines. This also makes sense, because the only force experienced by the particle is the net pressure force, the pressure field creates the centripetal acceleration. In regions where the streamlines are straight, the radius of curvature r is infinite so there is no pressure variation normal to straight streamlines.

If the pressure distribution is hydrostatics then $\partial(P + \gamma Z)/\partial S = -\gamma \, \partial h / \partial n$, since at all points, $P + \gamma Z = \gamma \, \partial h$ and then: (Henderson, 1989).

$$\frac{dh}{dn} = \frac{V^2}{gr} \tag{5.16}$$

$$\frac{dh}{dn} + \frac{V}{g} \frac{dV}{dn} = 0 \tag{5.17}$$

Combining equations (5.16) and (5.17) we obtain:

$$\frac{dV}{dn} + \frac{V}{r} = 0 \tag{5.18}$$

71

This is a general equation which is true for flow in closed conduits as well as in free surface flow. This equation indicate clearly that since V/r and V^2/gr are always positive, V decreases and h increases from the inner to the outer bank. This equation can be written as:

$$\frac{dV}{V} + \frac{dr}{r} = 0 \qquad (5.19)$$

Leading to the well known free vortex equation $V.r = C$ (Constant), and consider a rectangular channel bend, discharge per unit width $q = V.y$ and $y/r = q/c$. Modification to the bed profile to obtain the horizontal water surface in the bend we can write it as:

$$\frac{dy}{dr} = \frac{y}{r} \qquad and \qquad \frac{dy}{dr} = -\frac{dZ}{dr}\frac{1}{1-(Fr)^2} \qquad (5.20)$$

And it becomes clear that $Fr < 1$ the bed should fall toward the outside of the curve, as shown in Figure 5-3. From equations (5.20) we have:

$$\frac{dZ}{dr} = (Fr^2 - 1)\frac{dy}{dr} = (Fr^2 - 1)\frac{y}{r} \qquad (5.21)$$

$$\frac{dh}{dr} = \frac{dZ}{dr} + \frac{dy}{dr} = Fr^2\frac{dy}{dr} = Fr^2\frac{y}{r} = \frac{V^2}{gr} \qquad (5.22)$$

Finally, we obtain an explicit $z - r$ relationship by integration equation(5.21). This process is dependent on the choice of constants of integration implied in the choice of a bed level at some part of the section. Since the water surface is at its highest at the outer wall it is convenient to set the depth and bed level here at their original upstream value, the bed level falls or rises from this point according to Fr being greater or less than unity (Henderson, 1989).

If Z is defined as the height of the bed above the upstream bed level, y_o and V_o as the upstream value of y and V, r_o as the radius of the outer wall and E as the total energy referred to upstream bed level, then:

$$Z + y + \frac{V^2}{2g} = E = y_o + \frac{V_o^2}{2g} \qquad (5.23)$$

Also, with $C = V.r$, $q = V.y$ and $y = qr/C$, the above equation becomes:

$$Z + \frac{q.r}{V_o.r_o} + \frac{V_o^2.r_o^2}{2g.r^2} = E \qquad (5.24)$$

This equation defines the transverse bed profile and is in effect the integral of equation(5.21). If the radius of the curve is large, the average values of Fr, y and r may be used in equation (5.21) to give a straight line bed profile.
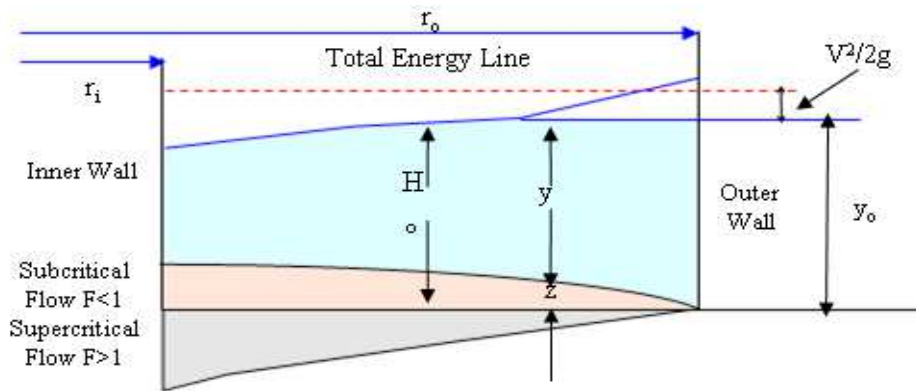
Figure 5-3. Transverse bed profiles required at a channel bend (Henderson, 1989)

5.2.2 **Superelevation**

Superelevation is defined as the difference in elevation of water surface between inside and outside wall of the bend at the same section.

$$\Delta y = y_0 - y_i \tag{5.25}$$

This is similar to the road banking in curves. The centrifugal force acting on the fluid particles, will throw the particle away from the centre in radial direction, creating centripetal lift. Superelevation in other words means a greater depth near the concave bank compared to near the convex bank of a bend. This phenomenon was first observed by Ripley in 1872, while he was surveying Red River in Louisiana for the removal of the great raft obstructing the stream.

5.2.2.1 *Transverse Water Surface Slope in Bends*

Gockinga was first to derive the following formula for determining the difference in elevation of the water surface on opposite sides of channel bends.

$$Y = 0.235 \, V^2 \log\left(1 - \frac{X}{r}\right) \tag{5.26}$$

in which $V \, (m/s)$ is the velocity, X is the distance at which Y is to be determined, r is the radius of the channel bend. But above equation is found to fit a particular stream to which it was designed. Also, he found that the transverse slope was twice greater than the longitudinal slope. He showed that the increased depth in bend is caused by the spiral flow induced by centrifugal force. Mitchell also derived another equation applicable for determining the cross profile of the Delaware River, at Philadelphia.

$$Y = 33\left(\frac{1100^2 - X^2}{1100}\right) + \frac{289}{r}\left(\frac{1100^2 - X^2}{1100^2}\right)2X \tag{5.27}$$

Ripley in 1926 arrived at the formulae based on field observations, having their own limitations.

$$Y = 1.445D\left(1 - \frac{4X^2}{T^2}\right) + 7.730\frac{D}{r}\left(1 - \frac{4X^2}{T^2}\right)X \tag{5.28}$$

73

$$Y = 1.65D\left(1 - \frac{4X^2}{T^2}\right) + 13.22\frac{D}{r}\left(1 - \frac{4X^2}{T^2}\right)X \tag{5.29}$$

in which, D is the mean depth of the channel in meters, T is width (above) of the channel in meters, X and Y are the co-ordinates of the cross profile of the channel, the origin begin in the center of the channel at the surface of the water, r is the radius of curvature in meters.

The above two equations when combined yield a simplified form in SI units. Figure 5-4 represents the general profile for equation given below (Thandaveswara, 1990).

$$Y = 1.935R\left(\sqrt{0.437 - \frac{X^2}{T^2}} - 0.433\right)\left(1 + \frac{17.52\,X}{r_o}\right) \tag{5.30}$$
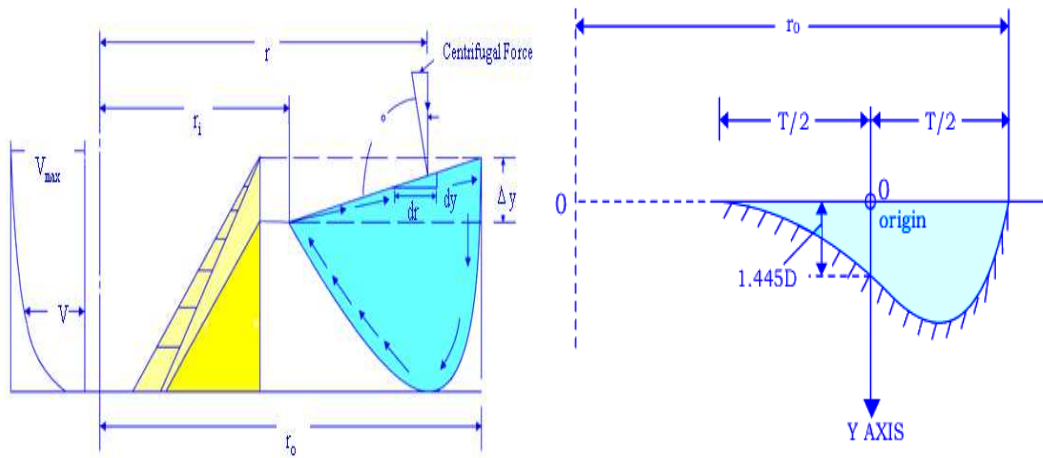
Figure 5-4. Cross section at the bend and model of the spiral flow as proposed

5.2.3 Profile for Equation

Grashof was the first to try an analytical solution for superelevation. He obtained the equation by applying Newton's second law of motion to every streamline and integrating the equation of motion.

$$Cenrifugal\ Force = \frac{T.V_{max}^2}{g\ r_c} \tag{5.31}$$

$$\frac{dy}{dr} = \left(\frac{T.V_{max}^2}{g\ r_c}\right)\bigg/T = \frac{V_{max}^2}{g\ r_c} \tag{5.32}$$

Assuming the boundary condition near inside wall of the bend and integrating the above equation reduces to the form.

$$dy = 2.3\frac{V_{max}^2}{g}\log\frac{r_0}{r_i} = 1.372\times10^{-3}\left(\frac{Q}{y}\right)^2 \tag{5.33}$$

where, r_i, r_0, r_c are the inner, outer and center radius of the bend, respectively. Woodward in 1920 assumed the velocity to be zero at banks and to have a maximum value at the center and

the velocity distribution varying in between according to parabolic curve. Using Newton's second law of motion he obtained the following equation for superelevation.

$$dy = \frac{V_{max}^2}{g}\left[\frac{20}{3}\frac{r_c}{b} - 16\left(\frac{r_c}{b}\right)^3 + \left(4\left(\frac{r_c}{b}\right)^2 - 1\right)^2 \ln\left(\frac{2r_c + b}{2r_c - b}\right)\right] = 3.628 \times 10^{-4}(\frac{Q}{y})^2 \tag{5.34}$$

Shukry in 1950 suggested the following equation for maximum superelevation based on free vortex flow and principle of specific energy. The forward velocity distribution and the water surface profile at the section of maximum surface depression may be estimated by the assumption of the theoretical free vortex distribution of velocity. By the law of free vortex motion the following expression can be written: $V = C/r$, where, V the forward filament velocity in the curve at a radial is distance r from the center of curvature and C is the so-called circulation constant in free vortex motion. Let E be the specific energy at any section and y the depth of flow at a distance r from the center of curvature. The average forward velocity and depth of flow is:

$$V = \frac{\int_{r_i}^{r_o}(C/r)dr}{r_o - r_i} = \frac{C}{r_o - r_i}\ln\frac{r_o}{r_i} \tag{5.35}$$

$$y_m = \frac{\int_{r_i}^{r_o} y.dr}{r_o - r_i} = \frac{\int_{r_i}^{r_o}\left(E - C^2/2g.r^2\right)dr}{r_o - r_i} \tag{5.36}$$

$$Q = V.y_m(r_o - r_i) = C(E - \frac{C^2}{2g.r_o.r_i})\ln\frac{r_o}{r_i} \tag{5.37}$$

If Q, r_o, r_i and E are given the constant C can be determined from Equations (5.37). Thus, the superelevation Δy of the water surface can be shown to be:

$$dy = \frac{C^2}{2g\ r_o^2\ r_i^2}(r_o^2 - r_i^2) \tag{5.38}$$

The above method was found to be reasonably accurate as long as the curve was greater than 90°. For smaller angles, Shukry assumed that C varies linearly with θ from $r.V_m$ at $\theta = 0^o$ to its full value at $\theta = 90^o$ suggested for circulation constant C, assuming it to vary linearly from 0° to 90°. Therefore, for any angle θ less than 90° the circulation constant can be multiplied by a correction factor equal to (Chow, 1959):

$$V.r = C.U_f = C\left[\frac{\theta}{90} + (1 - \frac{\theta}{90})(\frac{r.V_m}{C})\right] \tag{5.39}$$

where, V_m is the mean forward velocity in a straight channel. Superelevation in curved channels may also be determined by less accurate but simpler formulas which are based on the application of Newton's second law of motion to the centrifugal action in the curve. Chow assuming that all filament velocities in the bend are equal to the mean velocity V_c and that all streamlines have radius of curvature r_c the transverse water surface can be shown to be a straight line, and a simple formula for superelevation can be obtained:

$$dy_{max} = \frac{V_c^2}{2g}(\frac{2b}{r_c}) = 6.7958 \times 10^{-4}(\frac{Q}{y})^2 \qquad (5.40)$$

where, b is the width of the channel. For the channels other than rectangular, the bed width can be replaced by the water surface width T then:

$$dy_{max} = \frac{V_c^2}{2g}(\frac{2T}{r_c}) \qquad (5.41)$$

The above equation is only a first approximation and gives transverse profile as the straight line. This assumes that the rise and the drop of the water surface level from the normal level are equal on either side of center line of bend. As a better approximation, Ippen and Drinker (1962) obtained an equation for superelevation. The derivation of equation is based on the assumptions of free vortex or irrotational flow with the uniform specific head over the cross section and the mean depth in bend being equal to the mean approaching flow depth.

$$dy = \frac{V_c^2}{g}(\frac{T}{r_c})\left(\frac{1}{1-\frac{T^2}{4r_c^2}}\right) = 6.843 \times 10^{-4}(\frac{Q}{y})^2 \qquad (5.42)$$

The bends in nature will not have the symmetry due to entrance conditions, length of curvature and boundary resistance. Hence the above equation will not give accurate result. If the forced vortex condition exists with constant stream cross section and constant average specific energy, then equation for superelevation assumes the form:

$$dy = (\frac{V_c^2 T}{gr_c})\left(\frac{1}{1+\frac{T^2}{12r_c^2}}\right) \qquad (5.43)$$

The above equation is applicable to a smooth rectangular boundary with circular bend with the flowing fluid being ideal. Better results can be obtained by combining the effects of the free and forced vortex conditions simultaneously. The minimum angle of bend is to be 90° for applying the above equation in combination. For the smaller angles the difference in computed values from the above equation becomes larger than the actual ones.

Apmann in 1973 (Ranga, 1981) analysed data from laboratory and filed channels of different shapes and developed the following equation.

$$dy = [(\frac{5}{4})\tanh(\frac{r_c.\theta}{b})\ln(\frac{r_o}{r_i})](\frac{V^2}{2g}) = 8.155 \times 10^{-4}(\frac{Q}{y})^2 \qquad (5.44)$$

Muramoto in 1967 (Thandaveswara, 1990) obtained an equation for superelevation based on the equations of motion.

$$dy = \left[\frac{S_o^2.r^4.g}{36C_1^2} - \frac{(C_1^2 + C_2^2)}{2g.r^2} + \frac{2S_o.C_2.r}{3C_1}\right]_{r_i}^{r_o} \qquad (5.45)$$

76

in which C_1 and C_2 are circulation constants obtained after integration. The special feature of above equation lies in including the effect of bed slope on superelevation.

Thus it can be observed from the above discussion that superelevation in a bend is a function of shape of the cross section, Reynolds number, approach flow, slope of the bed, Froude number, $\theta/180$, r_c/b and boundary resistance. The superelevation is also affected by the presence of secondary currents and separation.

5.3   CONCLUSIONS

As discussed in this chapter, the literature on open channel flow bends is vast. The primary interest for this chapter are described first, followed by the review of the previous research on mathematical models and superelevation in open channel bends and the effects of surface roughness and velocity, and how these may be represented through hydraulic models such as Momentum's equation, possibly with parameters that are flow dependent.

This research program has addressed issues associated with open channel bends at superelevation transitions through combined physical modeling and mathematical modeling investigations.

CHAPTER 6

PROBABILISTIC ANALYSIS OF PLUNGE POOLS

The main topic of this chapter is concerned with the reliability-based assessment of the geometry of the plunge pool downstream of a ski jump bucket. Experimental data obtained from a model of a flip bucket spillway in India has been used to develop a number of equations for the prediction of scour geometry downstream from a flip bucket spillway of a large dam structure. The accuracy of the developed equations was examined both through statistical and experimental procedures with satisfactory results. In addition, reliability computations have been carried out using the Monte Carlo technique.

The main conclusions are that structural reliability analysis can be used as a tool in the dam safety risk management process and that the most important factors for further analysis are erosion, friction coefficient, uplift and self-weight.

6.1 INTRODUCTION

Hydraulic design is subject to uncertainties due to the randomness of natural phenomena, data sample limitations and errors, modeling reliability and operational variability. Uncertainties can be measured in terms of the probability density function, confidence interval, or statistical moment such as standard deviation or coefficient of variation of the stochastic parameters. In recent years, reliability analysis and probabilistic methods have found wide application in hydraulic engineering. Development of reliability-based analysis methods for engineering application can be found in literature (Tung and Mays 1980). Several applications of the methods to hydraulic design have also been reported in the

literature (Yen and Tung 1993; Vrijling 2001; Ang and Tang 2007). This allows us to determine the true probability of the component failure and of the whole system.

Energy dissipation downstream of large dams is a serious concern. Trajectory spillways or so-called ski jumps are employed whenever the velocity at the dam foot is in excess of typically 20 m/s because of problems with stilling basins in terms of cavitations, abrasion and uplift. Ski jumps are currently widely used because they appear to be the only hydraulic element allowing for the technically sound and the hydraulically safe control of large quantities of excess hydraulic energy during flood events (Vischer and Hager 1998).

In the present study, the probabilistic method will be used for estimating geometry of plunge pool downstream of a ski jump bucket. The Probabilistic Design method is an approach that can provide a better understanding of the failure mechanisms and their occurrence probabilities as well as the consequences of failure of such important infrastructure.

6.1.1   Data Collection

In this chapter the experimental values reported by Azmathullah, (2005) is utilised. This data relates to the measurements of scour parameters at the Central Water and Research Station (CWPRS), Pune, India. In addition, probability density functions about this data are presented in Figure 6-2 to Figure 6-1 (data set with 95 observations, see Appendix 1.B).

New hydraulic model studies were therefore conducted on three different bucket designs. The three hydraulic models simulated the dams across rivers Subarnarekha, Ranganadi, and Parbati Rivers in India.

The first dam was $52\,m$ high and $720\,m$ long. Its spillway consisted of 13 spans of $15\,m$ wide each with crest at elevation $177\,m$. Radial gates of size $15\,m \times 15\,m$ regulated the flow over this spillway. The design outflow flood was $26150\,m^3/s$. This corresponded to a maximum water level at an elevation of $192.37\,m$. The ski-jump bucket with bucket radius of $25\,m$ and lip angle of $32.5°$ was provided at the toe for energy dissipation.

The second dam was $60\,m$ high, made up of concrete with a rock fill portion on its right side. It had an overflow spillway with seven spans of $10\,m$ widths and $12\,m$ height. The spillway catered to a maximum outflow flood of $12500\,m^3/s$. This corresponded to the maximum water level of $568.3\,m$ and the full reservoir level of 567m with the crest level of the spillway at $544\,m$. It had a bucket radius of $18\,m$ with $35°$ as the lip angle.

The third dam spillway was 85m high. It was designed to pass a maximum discharge of $1,850\,m^3/s$ at the full reservoir level of $2,198\,m$ elevations. It had three spans, $6\,m$ wide and $9\,m$ height, separated by $6\,m$ thick piers and fitted with radial gates. An apron and a plunge pool along the downstream side fronted the bucket, which had a bucket radius of $28\,m$ with the lip angle of $30°$.
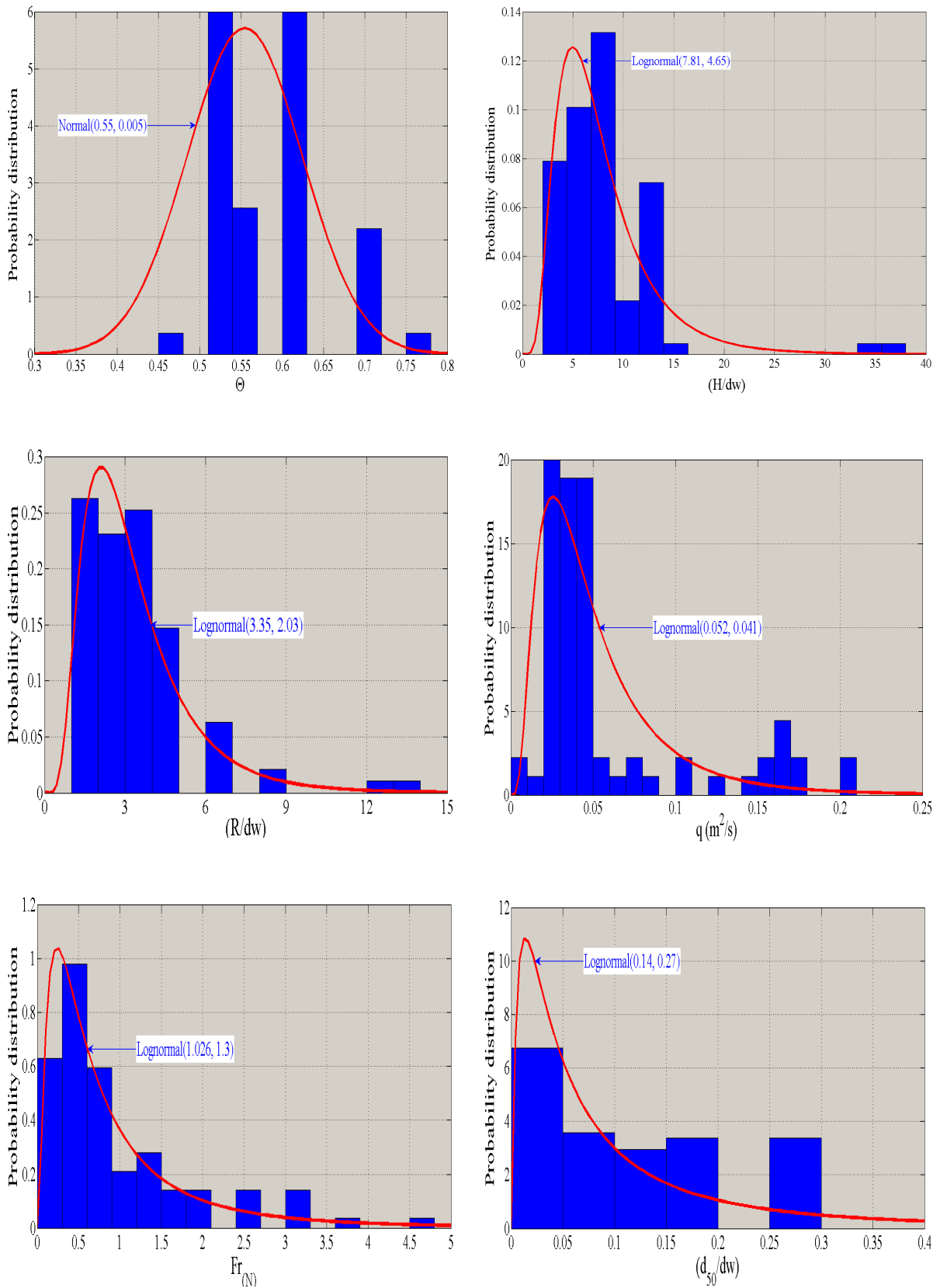
Figure 6-1. Probability distribution functions of observed data $(n = 95)$
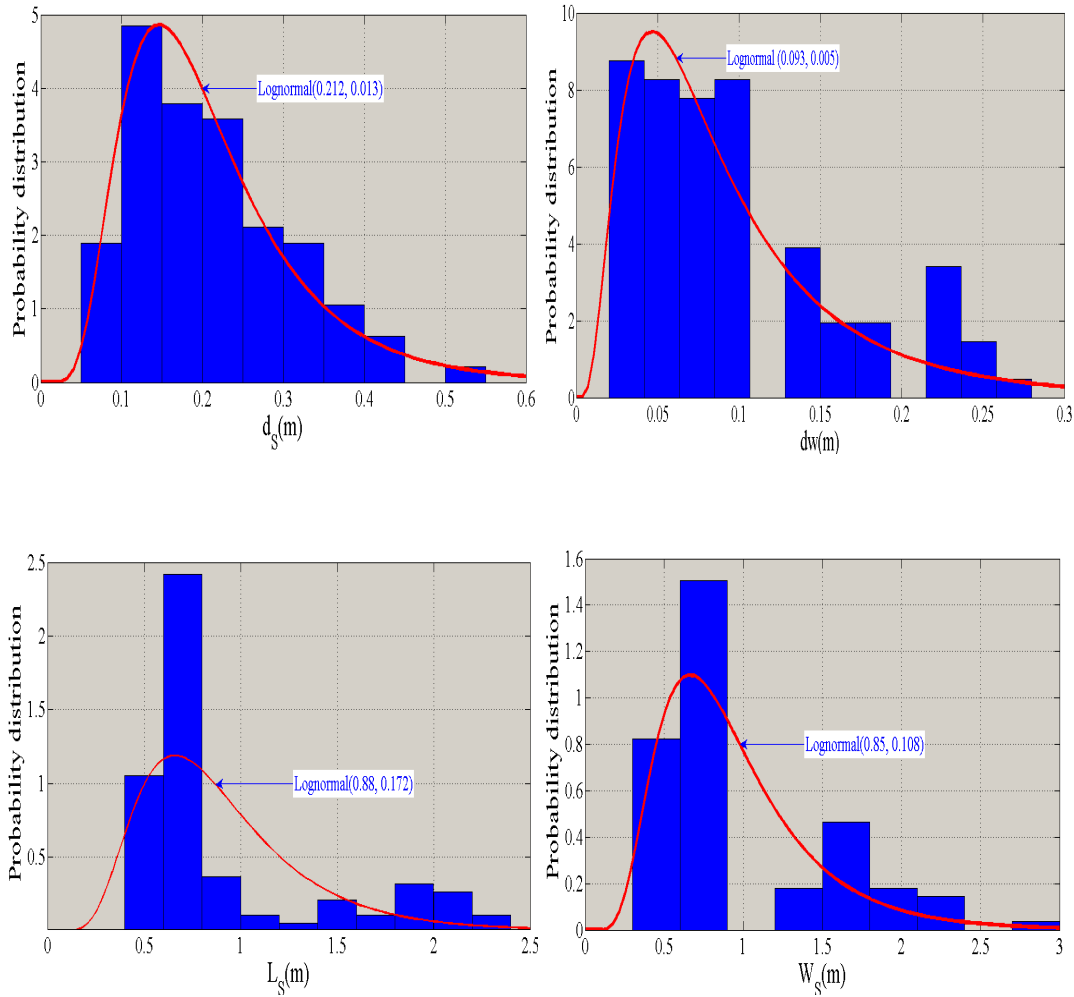
Figure 6-2. Probability distribution functions of observed data $(n = 95)$

6.1.2 Formulation and Statistical Regression

Empirical estimation methods are common in all specialities within civil engineering. Typically, data are collected and used to obtain values for coefficients of a function. Frequently, least-squares-regression analysis is used in fitting model coefficients. Standard regression theory assumes a linear structure (Amiri 2007):

$$\hat{Y} = \alpha_1 + \alpha_2 X_2 + \alpha_3 X_3 + \dots + \alpha_i X_i \tag{6.1}$$

in which $\hat{Y}$ = predicted value of the criterion (dependent) variable Y; X_i = predictor (independent) variables; α_i = sample estimates of the partial-regression coefficients. Instead of linear regression, also a power model is frequently used.

$$\hat{Y} = \alpha_1 (x_2)^{\alpha_2} (x_3)^{\alpha_3} \dots (x_i)^{\alpha_i} \tag{6.2}$$

The power model is widely used in engineering as the structure for empirical models. The coefficients are fitted using a logarithmic transformation of the data. The logarithmic

transformation leads to an unbiased model. Equations(6.1) and (6.2) are used for many engineering design problems. It is frequently used in hydraulic and hydrologic engineering.

Equation (6.2) is typically fitted to measured data by taking the logarithms of the variables and expressing them in a relationship with the linear structure of equation(6.3):

$$Ln\hat{Y} = Ln\,\alpha_0 + \alpha_1 Ln\,X_1 + \alpha_2 Ln\,X_2 + \dots\dots + \alpha_i Ln\,X_i \tag{6.3}$$

Equation (6.3) is now in the form of the linear model $E(y) = Ax$, where LnY plays the role of y, α_i's play the role of the unknown vector and the design matrix is made of the variables LnX. Goodness-of-fit statistics, follow from the correlation coefficient (r) and the standard error (σ). In assessing the accuracy and applicability of prediction equations, the characteristics of the residuals are important (McCuen 1990).

The BLUE estimators that were described in Chapter 2 can be used through $\hat{a} = (A^T Q_y^{-1} A)^{-1} A^T Q_y^{-1} y$ to obtain the unknown coefficients α_i's. The covariance matrix $Q_{\hat{a}} = (A^T Q_y^{-1} A)^{-1}$ can be obtained which explains the correlation coefficient (r) and the standard error (σ), of the coefficients α_i's.

In assessing the accuracy and applicability of prediction equations, the characteristics of the residuals are important (McCuen 1990). The above dimensionless groups of parameters were related to each other in the present study based on nonlinear regression using data of the measurements (Azmathullah 2005).

Equations(4.36), (4.37) and (4.38) can be fitted using least squares. The set of dimensionless equations with their original exponents obtained from regression analysis after a logarithmic transformation is shown in Table 6.1. This yielded the following correlation coefficients between a_1 to a_6 in the dimensionless equations for maximum scour depth, maximum scour length, and maximum scour width, in Table 6.2 to Table 6.4, respectively. The dimensionless groups of parameters were related to each other in the present study based on nonlinear regression. The set of dimensionless equations with their original exponents obtained from regression analysis is based on equations (6.4) to (6.6). This yielded the following equations in order to estimate the maximum scour depth, maximum scour width, and distance of maximum scour location from the bucket lip, respectively:

$$\frac{d_s}{d_w} = 9.02\,(Fr)^{0.90}\left(\frac{H_1}{d_w}\right)^{0.01}\left(\frac{R}{d_w}\right)^{-0.26}\left(\frac{d_{50}}{d_w}\right)^{0.08}(\sin\theta)^{0.50} \tag{6.4}$$

$$\frac{L_s}{d_w} = 7.191\,(Fr)^{0.36}\left(\frac{H_1}{d_w}\right)^{0.37}\left(\frac{R}{d_w}\right)^{0.12}\left(\frac{d_{50}}{d_w}\right)^{0.03}(\sin\theta)^{0.27} \tag{6.5}$$

$$\frac{W_s}{d_w} = 4.48\,(Fr)^{0.08}\left(\frac{H_1}{d_w}\right)^{0.57}\left(\frac{R}{d_w}\right)^{0.17}\left(\frac{d_{50}}{d_w}\right)^{0.13}(\sin\theta)^{-0.07} \tag{6.6}$$

A current prediction of the geometry of the scour hole around flip bucket spillway is based on dimensionless models. This chapter considers three dimensionless models to predict geometry of plunge pole.

The contribution of every parameter X_i can be established according to different tools described in Chapter 2. On the basis of these formula the linear or nonlinear relation of each variable, X_i regarding the least square estimation, can be calculated. The product moment

correlation defines a linear relation between two variables of X_i and predicted variable by equation(6.7).

$$\rho(X_i,Y) = \frac{Cov(X_i,Y)}{\sigma_{X_i}\sigma_Y} \qquad (6.7)$$

$$Cov(X_i,Y) = E(X_i,Y) - E(X_iY)E(Y) \qquad (6.8)$$

The partial correlation ratio of the predicted variable Y and base variable X_i is presented in Table 6.2 to Table 6.4. The density functions of coefficients $(\alpha_1,...,\alpha_i)$ in equation (6.4) are shown in Figure 6-3.
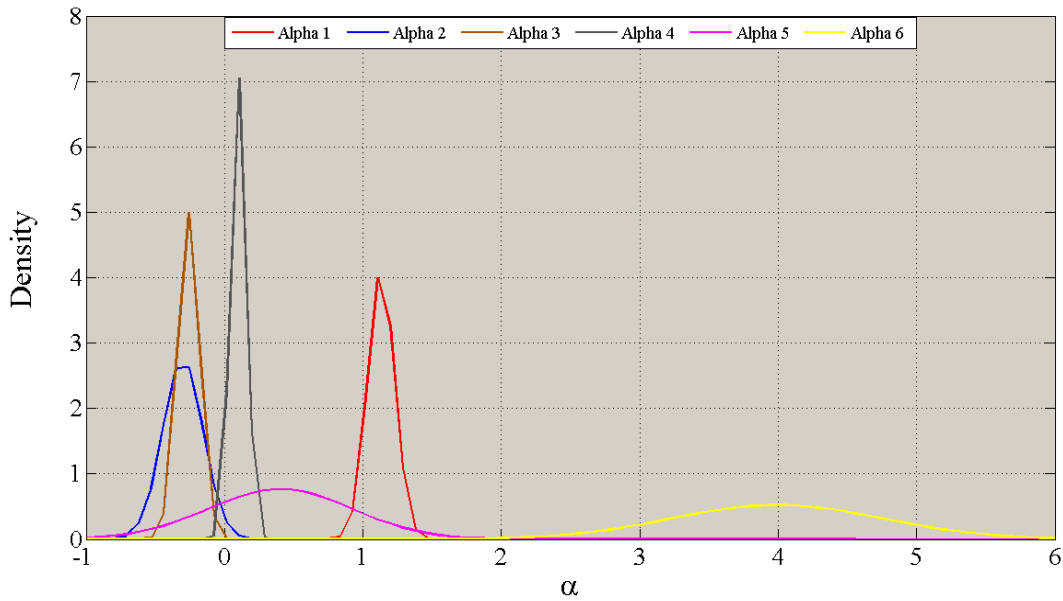

Figure 6-3. Density function of coefficients (α_i) for the first equation (6.4)

Statistical characteristics and comparison between predicted Y and observed X values, correlation coefficient, root mean square error, mean and standard deviation of plunge pool depth, length and width for the validation set are shown in Figure 6.4 and in Table 6.5. Also, standard residual and density function and multivariate density function of plunge pool depth, length and width for the validation set is qualitatively shown in Figure 6-5 to Figure 6-7, respectively. 75 percent of the data is used to calculate the model and 25% is used to validate the model and probability distributions functions (Gamma) are presented in Figure 6-8.

Table 6.1. Power coefficients of dimensionless equation

Coefficients	α_1	α_2	α_3	α_4	α_5
d_S/d_W	0.90	0.01	-0.26	0.08	0.50
L_S/d_W	0.36	0.37	0.12	0.03	0.27
W_S/d_W	0.08	0.54	0.17	0.13	-0.07

Table 6.2. Correlation coefficients of dimensionless equation (d_s / dw)

Data	α_1	α_2	α_3	α_4	α_5
α_1	1	-0.482	-0.185	-0.298	0.366
α_2	-0.482	1	-0.414	-0.249	-0.390
α_3	-0.185	-0.414	1	-0.105	-0.270
α_4	-0.298	-0.249	-0.105	1	0.535
α_5	0.366	-0.390	-0.270	0.535	1

Table 6.3. Correlation coefficients of dimensionless equation (L_s / dw)

Data	α_1	α_2	α_3	α_4	α_5
α_1	1	-0.594	-0.061	-0.566	0.163
α_2	-0.594	1	-0.496	0.323	-0.060
α_3	-0.061	-0.496	1	-0.288	-0.291
α_4	-0.566	0.323	-0.288	1	0.329
α_5	0.163	-0.060	-0.291	0.329	1

Table 6.4. Correlation coefficients of dimensionless equation (W_s / dw)

Data	α_1	α_2	α_3	α_4	α_5
α_1	1	-0.581	-0.105	-0.565	0.163
α_2	-0.581	1	-0.586	0.386	-0.022
α_3	-0.105	-0.586	1	-0.221	-0.316
α_4	-0.565	0.386	-0.221	1	0.319
α_5	0.163	-0.022	-0.316	0.319	1

Table 6.5. Statistical characteristic (X: Observed, Y: Predicted)

Y \ X	d_S/d_W	L_S/d_W	W_S/d_W	R-Square	μ_X	σ_X
d_S/d_W	Y=0.98X+0.15	--	--	0.98	3.416	2.844
L_S/d_W	--	Y=0.97X+0.48	--	0.976	11.94	6.516
W_S/d_W	--	--	Y=0.95X+1.05	0.95	12.577	8.339
μ_Y	3.491	12.02	12.972	--	--	--
σ_Y	2.808	6.409	8.166	--	--	--
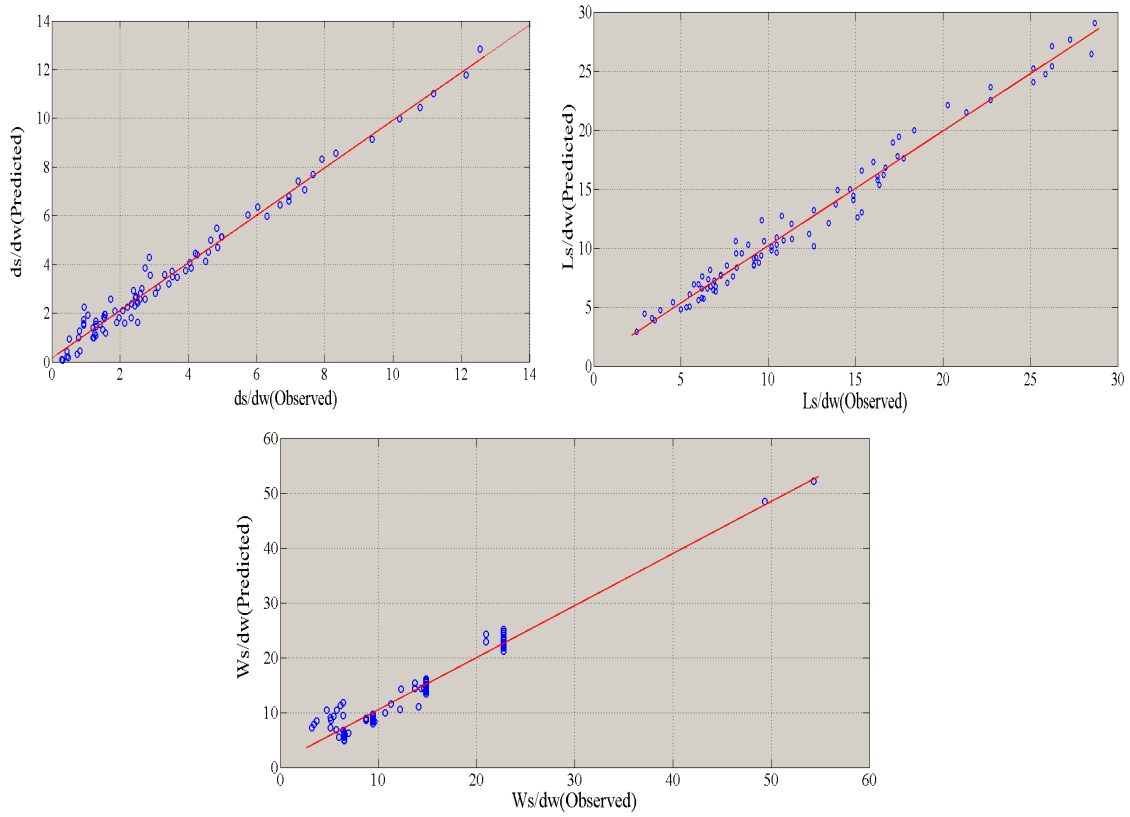
Figure 6-4. Observed versus predicted for depth (top left), length (top right) and width (bottom) of plunge pool
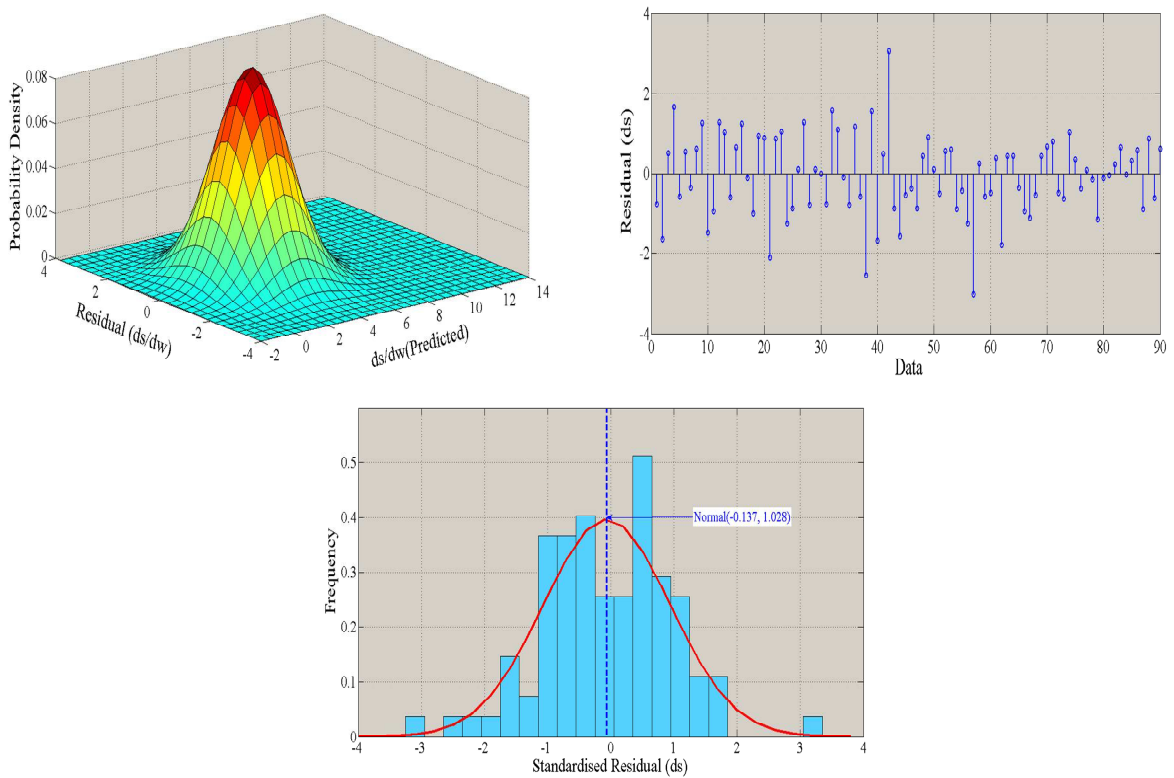
Figure 6-5. Multivariate density function for depth (top left), Depth residual (top right) and Histogram and density function residual, *ds* (bottom)
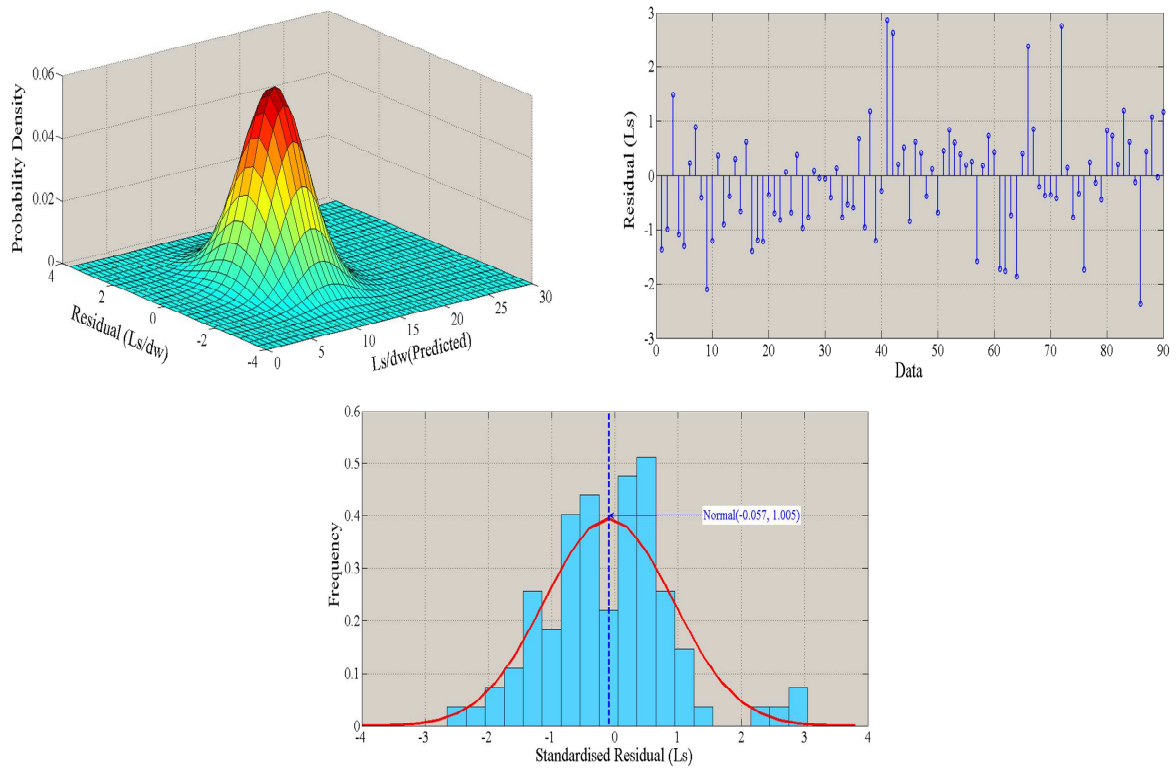
Figure 6-6. Multivariate density function for length (top left). Length residual (top right) and Histogram and density function residual, *Ls* (bottom)
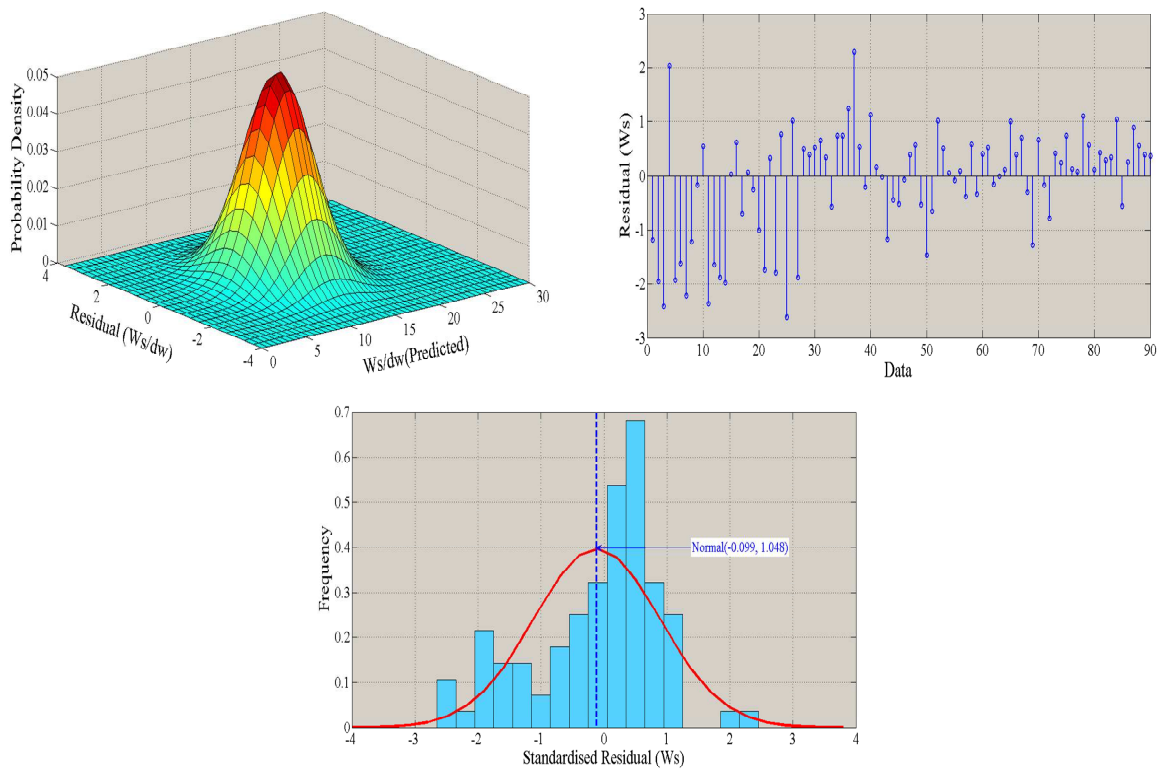
Figure 6-7. Multivariate density function for width (top left). Length residual (top right) and Histogram and density function residual, *Ws* (bottom)
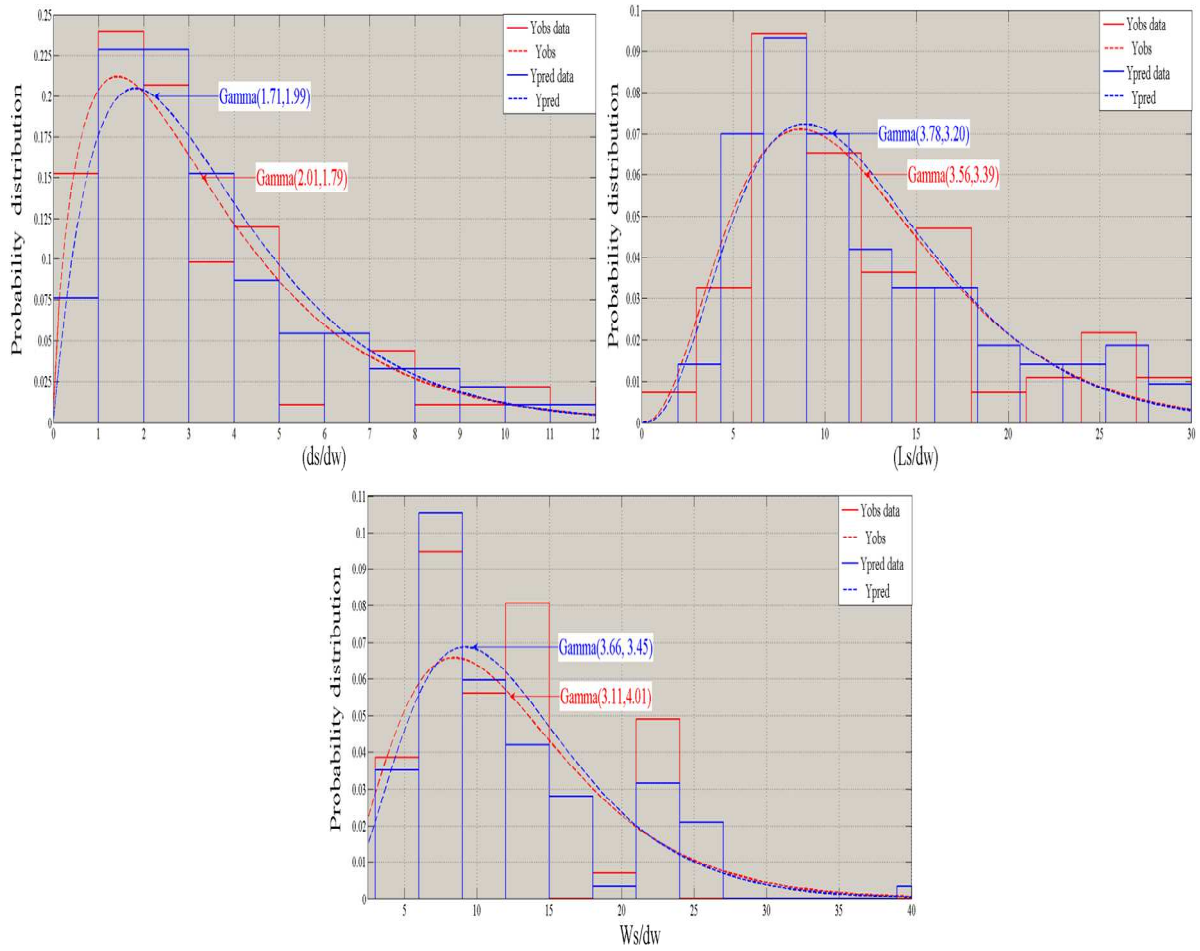
Figure 6-8. Comparison between probability distribution functions of the observed and predicted geometry (d_s, L_s, W_s) of the plunge pool
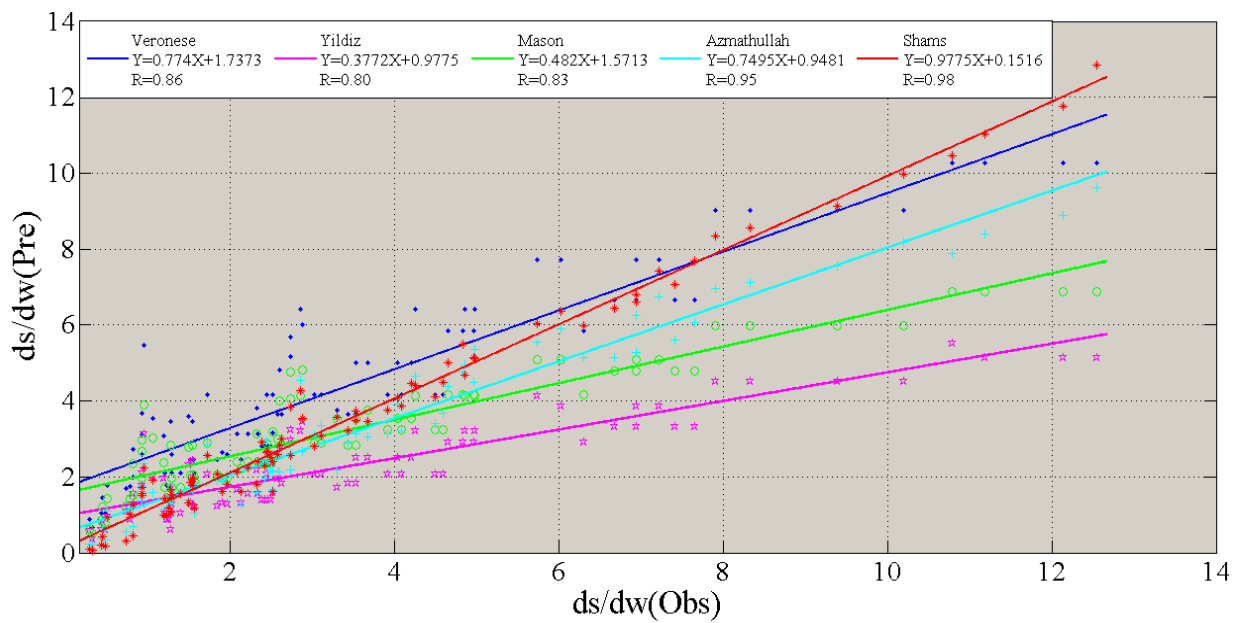
Figure 6-9. Comparison between the results of five different models

6.2   STRUCTURAL RELIABILITY ANALYSIS

Most hydraulic systems involve many subsystems and components whose performances affect the performance of the system as a whole. The reliability of the entire system is affected not only by the reliability of individual subsystems and components but also by the interactions and configurations of the subsystems and components. Many hydraulic structures involve multiple failure paths or modes, there are several potential paths and modes of failure in which the occurrence, either individually or in combination would constitute system failure. The hydraulic structural designer must verify, within a prescribed safety level, the serviceability and ultimate conditions, commonly expressed by the inequality $S < R$, where S represents the action effect and R the resistance. In Chapter 2 we explained tools of reliability analysis and failure probability methods.

Application of the simulation method for uncertainty analysis requires formulation of the performance function. In the case of a hydraulic structure, the performance function Z expressed in terms of the safety margin is presented in equations (6.9), (6.10) and (6.11) where, d_S is depth, L_S length and W_S width of the plunge pool and R_d, R_L, R_W are respectively resistance critical depth, critical length and critical width. Considering equation (2.1), the limit state functions can be written as:

$$Z_{d_S} = R_d - 9.019 \, (Fr_N)^{0.90} (\frac{H_1}{d_w})^{0.01} (\frac{R}{d_w})^{-0.26} (\frac{d_{50}}{d_w})^{0.08} (\sin\theta)^{0.50} \tag{6.9}$$

$$Z_{L_S} = R_L - 7.191 (Fr_N)^{0.36} (\frac{H_1}{d_w})^{0.37} (\frac{R}{d_w})^{0.12} (\frac{d_{50}}{d_w})^{0.03} (\sin\theta)^{0.27} \tag{6.10}$$

$$Z_{W_S} = R_w - 4.48 \, (Fr_N)^{0.08} (\frac{H_1}{d_w})^{0.57} (\frac{R}{d_w})^{0.17} (\frac{d_{50}}{d_w})^{0.13} (\sin\theta)^{-0.07} \tag{6.11}$$

In this case, estimates of the reliability index of the geometry of plunge pool are generated for different resistances between ($0.2 - 40 \, m$), for depth, length and width, respectively. The main resistance and load parameters are as presented in Table 6.6. The main analysis was made considering the above random variables. The possible failure mechanism is an unstable scour hole with the above given limit state functions. Equation (6.9) to (6.11) are nonlinear; therefore, a simulation technique, such as Monte Carlo analysis can be used to determine reliability. The summary of results is indicated in Table 6.7 to Table 6.9.

Table 6.6. Basic variable characterizing the plunge pool

Variable	$q(m^3/s.m)$	$H_1(m)$	$R(m)$	$d_{50}(mm)$	θ	$d_w(m)$
μ	0.052	0.633	0.258	0.006	0.550	0.097
σ	0.041	0.459	0.161	0.00002	0.005	0.068
Distribution	LN	LN	N	LN	N	LN

Table 6.7. Design points and reliability for $Z_S = R_S - (d_S/d_w)$

$R_d(m)$	H_1	R	θ	d_{50}	d_w	q	d_S	$P_{(Z)}$	β
0.2	0.711	0.274	0.515	0.006	0.283	0.023	0.0588	0.997	-2.7
3	0.52	0.222	0.562	0.006	0.084	0.055	0.2520	0.55	-0.128
4	0.503	0.217	0.567	0.006	0.074	0.061	0.2976	0.44	0.146
6	0.48	0.21	0.575	0.006	0.062	0.07	0.3729	0.3	0.533
10	0.453	0.202	0.584	0.006	0.049	0.083	0.4943	0.154	1.02
14	0.435	0.197	0.591	0.006	0.042	0.092	0.5896	0.09	1.34
16	0.429	0.195	0.593	0.006	0.04	0.097	0.6384	0.07	1.47
20	0.418	0.191	0.598	0.006	0.036	0.104	0.7199	0.047	1.68
25	0.407	0.188	0.602	0.006	0.033	0.112	0.8109	0.029	1.89
30	0.398	0.185	0.606	0.006	0.03	0.119	0.9003	0.02	2.07
40	0.385	0.181	0.611	0.006	0.027	0.132	1.0576	0.0096	2.34

Table 6.8. Design points and reliability for $Z_L = R_L - (L_S/d_w)$

$R_L(m)$	H_1	R	θ	d_{50}	d_w	q	L_S	$P_{(Z)}$	β
0.2	0.146	0.18	0.461	0.006	1.805	0.024	0.365	1.000	-5.58
4	0.365	0.208	0.534	0.006	0.184	0.046	0.741	0.930	-1.51
6	0.413	0.212	0.545	0.006	0.135	0.05	0.814	0.830	-0.954
10	0.484	0.218	0.559	0.006	0.092	0.056	0.920	0.600	-0.257
12	0.511	0.22	0.564	0.006	0.08	0.058	0.959	0.503	-0.009
13	0.524	0.22	0.566	0.006	0.075	0.059	0.977	0.460	0.1
15	0.548	0.222	0.57	0.006	0.067	0.061	1.012	0.3840	0.296
20	0.599	0.225	0.579	0.006	0.054	0.064	1.078	0.246	0.688
25	0.641	0.227	0.585	0.006	0.046	0.068	1.141	0.160	0.993
30	0.679	0.229	0.59	0.006	0.04	0.07	1.187	0.107	1.24
40	0.742	0.232	0.599	0.006	0.032	0.075	1.274	0.051	1.63

Table 6.9. Design points and reliability for $Z_W = R_W - (W_S/d_w)$

| $R_W(m)$	H_1	R	θ	d_{50}	d_w	q	W_S	$P_{(Z)}$	β
0.2	0.103	0.179	0.998	0.006	0.499	0.056	0.102	1.000	-4.28
1	0.196	0.194	0.794	0.006	0.239	0.057	0.239	0.995	-2.56
5	0.376	0.211	0.63	0.006	0.113	0.057	0.566	0.800	-0.825
6	0.405	0.213	0.614	0.006	0.104	0.058	0.623	0.740	-0.628
9	0.477	0.218	0.579	0.006	0.086	0.058	0.775	0.580	-0.189
10	0.498	0.219	0.57	0.006	0.082	0.058	0.820	0.530	-0.075
12	0.536	0.221	0.555	0.006	0.075	0.058	0.905	0.450	0.122
15	0.587	0.223	0.538	0.006	0.068	0.058	1.018	0.360	0.363
20	0.66	0.227	0.516	0.006	0.059	0.058	1.189	0.250	0.675
25	0.722	0.23	0.499	0.006	0.054	0.058	1.342	0.180	0.916
40	0.874	0.232	0.467	0.006	0.043	0.059	1.720	0.080	1.42
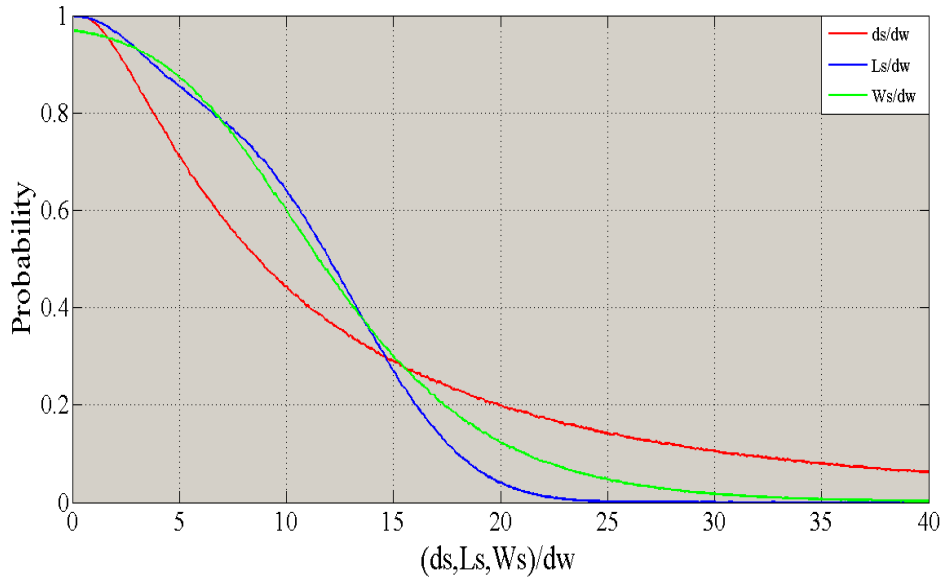
Figure 6-10. Probability of failure in plunge pool

6.3 DISCUSSION

It is very important that any designer should keep the downstream and upstream flow characteristics in mind before designing a conveyance structure such as a flip bucket spillway. For safety and stability of the structure, special attention must be given to monitor downstream scour holes.

The fitting of the power models of equations (4.36), (4.37) and (4.38) was carried out using the logarithmic transformation leading to an equation that has unbiased partial regression coefficients and provides unbiased estimates of d_S, L_S, W_S as was shown in Figure 6-4.

The residual prediction for depth and length and width are shown in Figure 6-5 to Figure 6-7, respectively. It shows a range of residuals of ±4 for depth and ±3 for length and width, therefore, the prediction can be considered as unbiased.

The statistical analysis of the data predicted by the equation developed in this study and comparison with observed values in this model (Table 6.5) show high values of the correlation coefficients (0.99, 0.98 and 0.95) and small values of the root mean square error (0.4, 0.998 and 1.823) which indicate that the equations developed herein accurately predict the scour geometry.

Comparison between Statistical characteristics and probability distribution functions of the observed and predicted geometry (d_S, L_S, W_S) of the plunge pool are presented in Figure 6-8. The maximum differences between coefficients of variations (CV) of the observed and predicted are 3.51%, 2.35% and 5.06% for d_S, L_S and W_S, respectively.

Comparisons between results of five hydraulic models (previously described in section 4.4) for design are shown in Figure 6-9. It can be seen that the correlation coefficient between observed (X) and predicted (Y) values using the proposed method of this chapter (see Figure 6.9, red line by Shams) are higher than that for the other methods.

91

Plunge pool reliability downstream of outlet spillway has been investigated using the Monte Carlo simulation techniques. It is based on the generation of random number for variables involved in the safety margin by assigning appropriate probability of failure shown in Figure 6-10. Failure probabilities decrease when the ratios d_S/d_w, L_S/d_w and W_S/d_w become larger.

6.4 CONCLUSION

In this study, the traditional empirical formulas used to obtain a prediction of the geometry of the scour hole with probabilistic multivariate regression and the analysis of reliability estimation of scour holes downstream of flip bucket spillways were presented.

It is based on the approach of probabilistic methods and involves analysis of an extensive data base in order to obtain the geometry of scour hole after the flip bucket spillway of the given parameters of q, H_1, R, θ, d_w and d_{50}.

Reliability analysis can provide a formal approach to the analysis of the performance of hydraulic structures, taking into account all uncertainties in models, load and strength variables.

Further analysis of the other components and prototype data should be carried out in order to find the weak links of the hydraulic structure. The vulnerability of a hydraulic structure can then be improved by strengthening these weak elements in the plunge pool.

In additional, statistical pattern recognition techniques have been employed to estimate the geometry of scour in plunge pools caused by high-velocity water jet impact. The results of an experimental study have been investigated considering probabilistic method. Appropriate dimensionless features have been selected using fluid mechanics concepts. Finally, the Best liner Unbiased Estimation (Minimum variance estimator) has been simplified to predict the geometry of scour hole.

The sum of the maximum of geometry of the plunge pool (depth, length and width) and the tail water depth can be computed using equations (6.4) to (6.6), which is based on solution of a set of six dimensionless parameters.

Equations (6.4) to (6.6) are based on fundamental principles of physics, mathematical modeling and validated by using measured scour data.

CHAPTER 7

PROBABILISTIC ANALYSIS OF SUPERELEVATION

This chapter deals with the Ziaran diversion dam in Iran. Data has been collected during previous studies of this dam. In particular one failure mechanism is investigated in this chapter in detail: overtopping by superelevation of the bend flume in the Ziaran Dam. This study focuses on the downstream water surface elevation during the flow considering the flume's actual discharge and roughness.

Superelevation in the Ziaran Flume has led to severe erosion of the bank and to undermining of the structure. Therefore, this study aims to cast lights on the cause of overtopping by superelevation. By means of direct observation on the flume's hydraulic performance, during full discharge and from generalization of the field data a more reliable prediction method of the magnitude of superelevation has become possible. The probabilistic analysis will show to have several advantages in comparison with deterministic analysis methods.

In this chapter, pressure models are first described, followed by a review of the previous research including mathematical models, superelevation in open channel bends, probabilistic design, uncertainty analysis and influence of uncertainties.

7.1   INTRODUCTION

Uncertainty and risk are central features in hydraulic structural engineering. Engineers can deal with uncertainty by ignoring it, by being conservative, by using the observation method or by quantifying it. In recent years, reliability analysis and probabilistic methods have found wide application in hydraulic engineering.

The so-called centrifugal force caused by flow around a curve results in a rise in the water surface at the outside wall and a depression of the surface along the inside wall. This phenomenon is called superelevation. The problems associated with flow through open channel bends deserve special attention in hydraulic engineering. Water surface slopes have been frequently reported to be a function of the curvature. But due to the difficulties in operation, the theoretical basis of superelevation has been discussed thoroughly by researchers. Furthermore, experience indicates that existing theory does not lead to good results at their present status.

In the present study, the probabilistic method will be used for estimating superelevation in the Ziaran Flume (Ziaran Dam in Iran). The probabilistic design method is an approach that can provide a better understanding of the failure mechanisms, its occurrence probabilities, as well as its consequences of failure of such important infrastructure.

7.2   ZIARAN DIVERSION DAM

The Ziaran diversion dam is a relatively small concrete dam near Tehran (Figure 7-1). The Ziaran dam was completed in 1976. The characteristics of the Ziaran dam are: Height $25\,m$; length $184\,m$, Reservoir volume about $225000\,m^3$, The Ogee spillway with controller, intake tower and outlet, stilling basin, transition and flume sections of the dam are shown in Figure 7-2.

The flume was designed for a peak flow of $30\,m^3/s$ with a height of $2.85\,m$, width of $5\,m$ for water conveyance to Qazvin city (Shams 1998). The flume has a concrete bend. The section of this bend is shown in Figure 7-3 with the characteristic parameters: $r = 30\,m$, $\theta = 26º$, $b = 5\,m$ and $H_b = 2.85\,m$.

Superelevation in the Ziaran Flume has led to severe erosion of the bank and has undermined the structure as seen in Figure 7-3. This flume was designed for steady and uniform flow using the Manning equation and the USBR standard and checked with other Iranian standards with a maximum discharge $30\,m^3/s$, $n = 0.014$, $b = 5\,m$ and $d = 2.35\,m$.

Originally, this bend had problems when operated at full capacity. Water was overtopping at the outer bank, undermining the structure, leading to severe erosion and to collapse of the bank. By direct observation of the flume and measurement of the flow characteristics such as discharge and water level in the automatic gauging station downstream, an analysis could be made to find the critical discharge as $27\,m^3/s$.
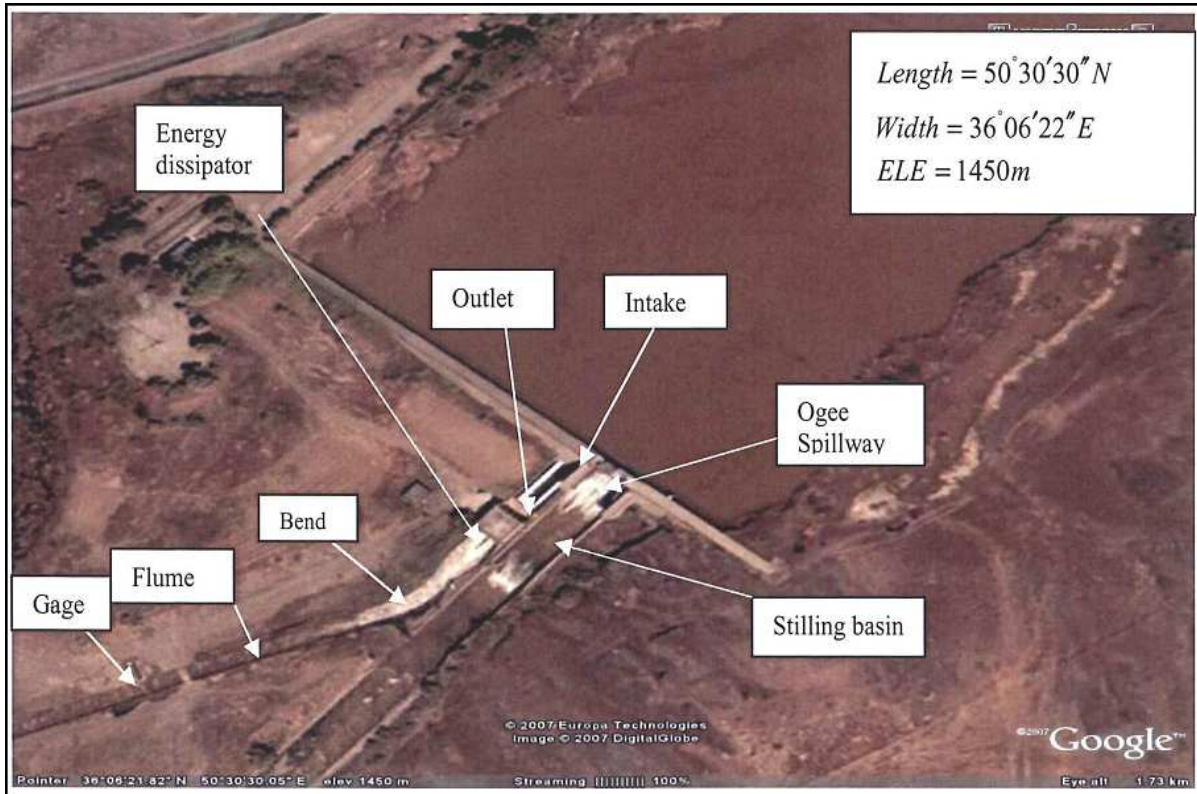
Figure 7-1. Ziaran diversion dam, Iran
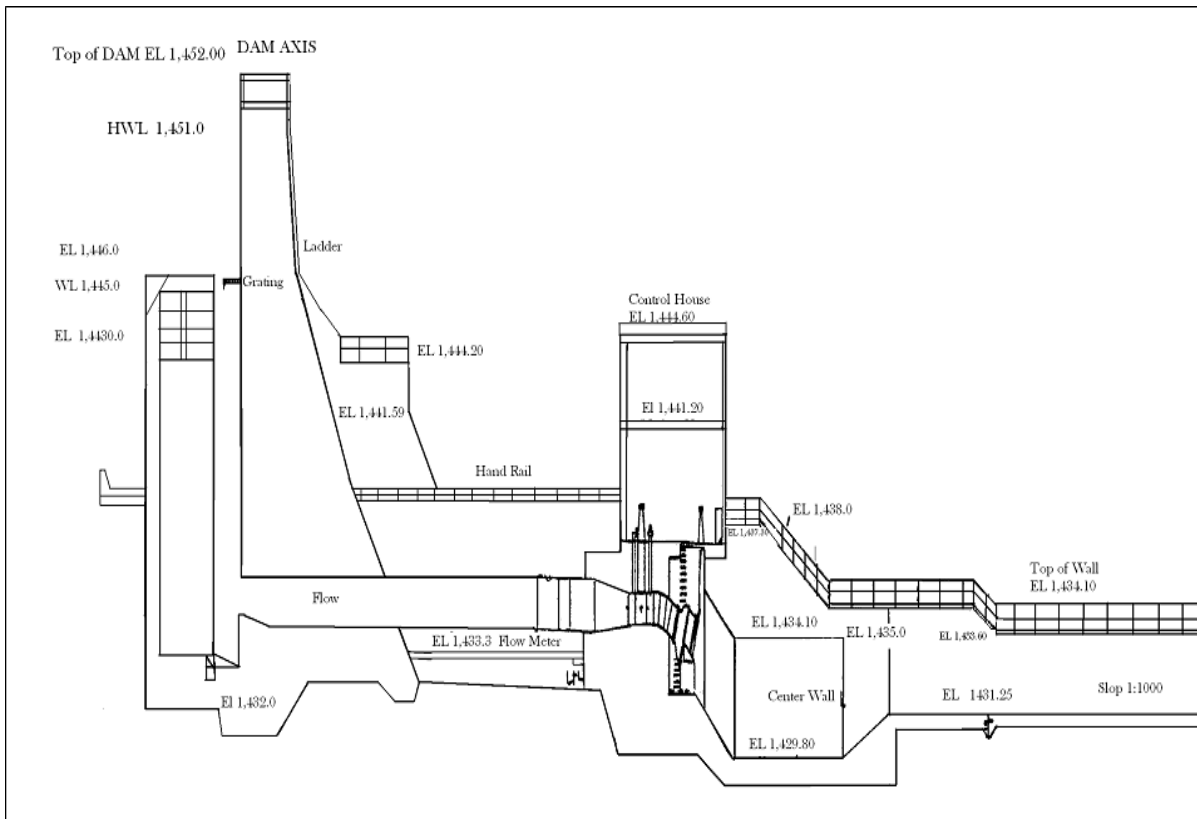
Figure 7-2. Profile of outlet works, Ziaran dam (Shams 1998)
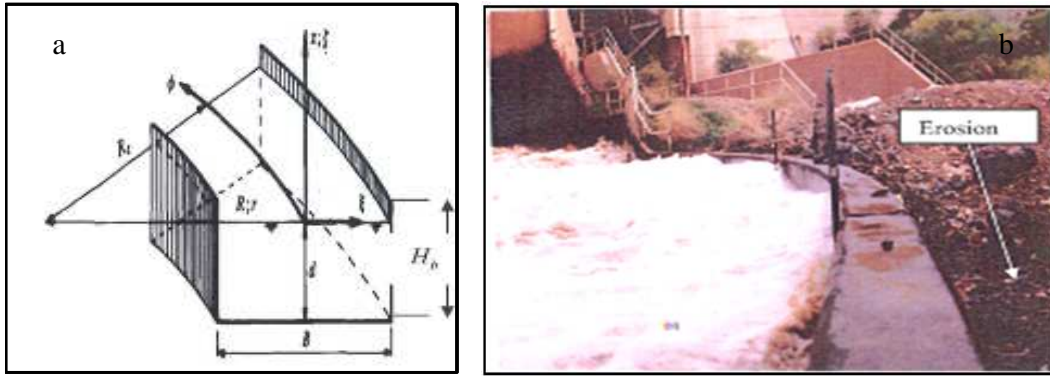
Figure 7-3. Erosion in bend channel (Shams, 2008)

7.2.1   Data Collection

Shams (1998) collected data from 173 experiments in Ziaran flume (Appendix 2). The hydraulic design implies the development of an energy based equation between one point in the flume downstream and one point in the bend centre that can be expressed as (Marengo 2006):

$$E = d_f + \frac{V^2}{2g} + S_f.L_{f-cb} + \sum_1^i k_i \frac{V^2}{2g} + dy_{cb} + Z_f \tag{7.1}$$

$$S_f = \frac{V^2.n^2}{R_f^{4/3}} \quad , \quad Q = A_f.V \tag{7.2}$$

$$E = d_f + \frac{Q^2}{2gA_f^2}(1 + \frac{2.g.n^2.L_{f-cb}}{R_f^{\frac{4}{3}}} + k_1 + k_2 + ... + k_i) + dy + Z_f \tag{7.3}$$

where, E (m) denotes the total head in the bend center in the outer bank, d_f (m) denotes the height of the water level, A_f (m^2) denotes the area of the flume (m^2), L_{f-cb} (m) denotes the distance between two points on the flume and bend center, dy (m) denotes the amount of superelevation in the flume center, n denotes the Manning friction factor, S_f denotes slope of the energy grade line, R_f (m) denotes the hydraulic radius, k_i denotes the dimensionless coefficients of local head losses and Z_f denotes the elevation of the bottom of the flume in meter above sea level.

$$E = \beta_1 Q^{\alpha_1} + \frac{Q^2}{2g(\beta_2 Q^{\alpha_2})^2}\left[\frac{2.g.L_{f-cb}.n^2}{(\beta_3 Q^{\alpha_3})^{\frac{4}{3}}} + 1.4\right] + \beta_4 Q^{\alpha_4} + Z_f \tag{7.4}$$

in which $\alpha_1, \beta_1, ..., \alpha_4, \beta_4$ are coefficients, which are fitted to the data. The parameters in equation (7.4) could be fitted by the data from Shams (1998). By referring to Table 7.1, parameters $(\alpha_1, \beta_1, ..., \alpha_4, \beta_4)$ could be approximated by normal distributions with mean values and standard deviations.

$$E = 0.2386\ Q^{0.6967} + 4.16\ L.n^2.Q^{-0.0397} + 0.0493\ Q^{0.6084} + 0.0167Q^{0.612} + Z_f \tag{7.5}$$

7.3 BEND OVERTOPPING RISK ANALYSIS

7.3.1 Fundamentals on Probabilistic Analysis Design

Structural hydraulic engineering reliability analysis is concerned with finding the reliability or probability of failure (or reliability index) of a structure or a system. The benefit of reliability analysis in hydraulic engineering can be summarized in the following points:

To highlight the uncertainties in design of these structures, reliability analysis plays a major role in considering the uncertainties influencing the design of hydraulic structures. For example, an optimum procedure for design of a spillway can be discussed where there are uncertainties with regard to a stability problem.

Allow the hydraulic engineer to quantify the effect of various failure preventive measures on these structures in order to develop an inspection and maintenance program. The reliability evaluation of most hydraulic structures, in particular an existing bend channel, the capacity-demand model is the simplest utilized, as the question of interest is the probability of failure related to a load event rather than the probability of failure within a time interval.

7.3.2 Uncertainty Analysis by Bootstrap Sampling

This section introduces the bootstrap method as a tool to treat parameters $(\alpha_1, \beta_1, \ldots, \alpha_4, \beta_4)$ uncertainty of the equation(7.4). By referring to

Table 7.2 and Figure 7-4 to Figure 7-7, parameters $(\alpha_1, \beta_1, \ldots, \alpha_4, \beta_4)$ could be very well approximated by normal distributions with mean values and standard deviations shown in

Table 7.2.

Also, coefficient of variations are between 0.8% to 1.5% and 1.3% to 1.8% for $(\alpha_1, \ldots, \alpha_4)$ and $(\beta_1, \ldots, \beta_4)$, respectively. This means that the degree of dispersion is low, which is preferable. Thus, the $(\alpha_1, \beta_1, \ldots, \alpha_4, \beta_4)$ values of the limit state equation are acceptable. Figures 7.4 to 7.7 show that the degree of dispersion is very small and correlation coefficients between these parameters are high. The bootstrap generation as shown in Figure 7-4 to Figure 7-7, seems to be close to normal distributions, but with some skewness in the right or left tail. This is acceptable for the parameter uncertainty checks of the limit state function equation. The maximum differences between the estimated results in Table7.1 and Table 7.2 are 1.3% and 1.8% for α_i and β_i, respectively. The estimated coefficients using the bootstrap and least square methods are in good agreements.

Table 7.1. Best linear unbiased estimation of coefficients used in equation (7.4)

	Variable	α_1	β_1	α_2	β_2	α_3	β_3	α_4	β_4
BLUE	μ	0.6969	0.2384	0.6935	1.1920	0.4775	0.2646	0.6039	0.0167
	σ	0.0004	0.0003	0.0005	0.0007	0.0008	0.0005	0.0011	0.0005
	Upper	0.6974	0.2387	0.6946	1.1935	0.4789	0.2658	0.6072	0.0168
	Lower	0.6964	0.2382	0.6927	1.1907	0.4756	0.2638	0.6024	0.0165
	Estimate	0.6967	0.2386	0.6958	1.1918	0.4861	0.2602	0.6012	0.0167

Table 7.2. Bootstrap uncertainty analysis of coefficients used in equation (7.4)

	Variable	α_1	β_1	α_2	β_2	α_3	β_3	α_4	β_4
Bootstrap	μ	0.6975	0.2385	0.6981	1.1896	0.4741	0.2673	0.5913	0.0172
	σ	0.0048	0.0029	0.0049	0.0020	0.0138	0.0080	0.0091	0.0004
	Upper	0.7070	0.2442	0.7077	1.2175	0.4952	0.2688	0.6092	0.0179
	Lower	0.6860	0.2328	0.6886	1.1617	0.4708	0.2554	0.5734	0.0164
	Estimate	0.7006	0.2367	0.6984	1.1854	0.4841	0.2607	0.5884	0.0172
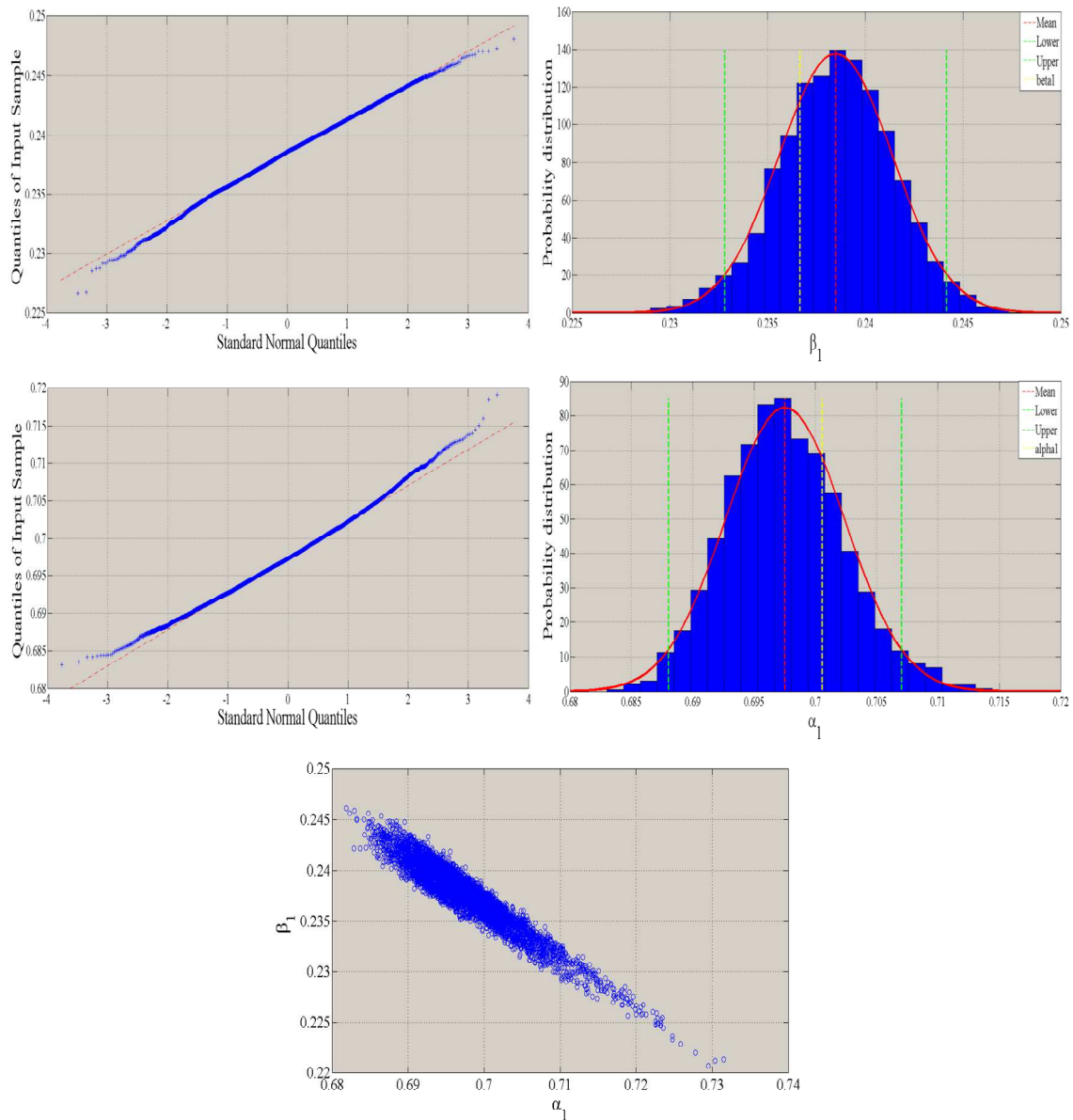
Figure 7-4. Normal quantile comparison and distribution function and correlation between α_1 and β_1
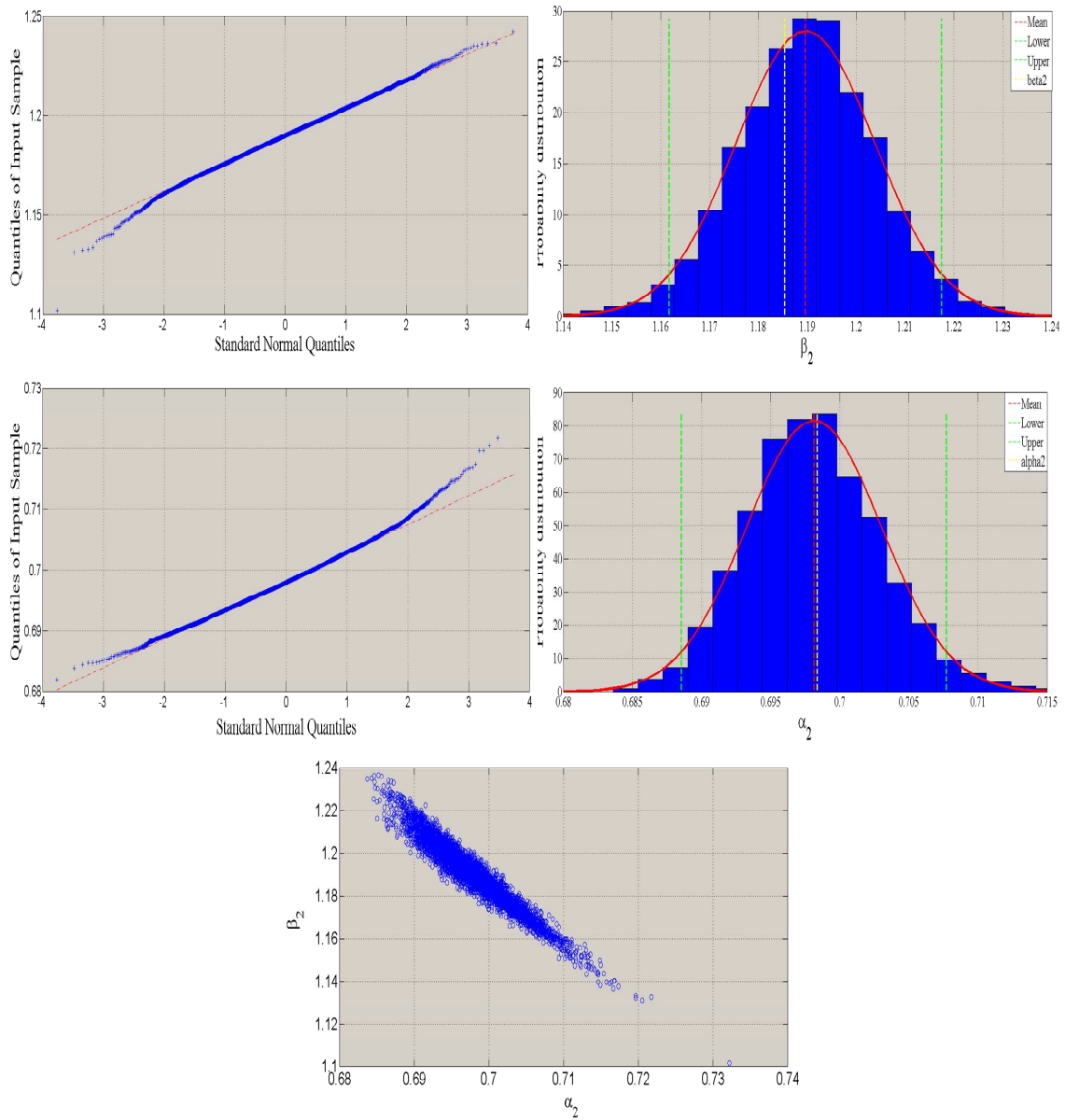
Figure 7-5. Normal quantile comparison and distribution function and correlation between α_2 and β_2
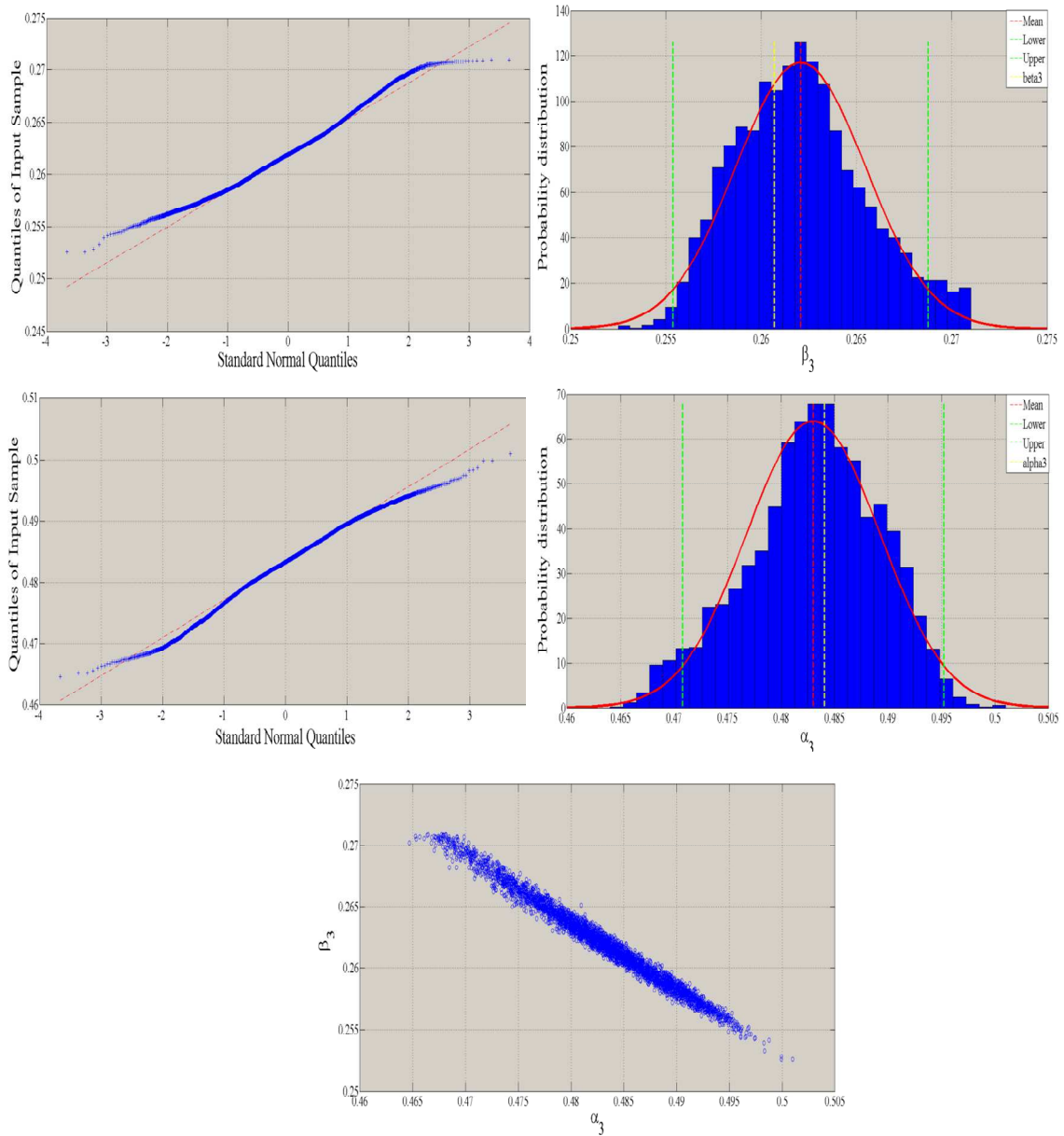
Figure 7-6. Normal quantile comparison and distribution function and correlation between α_3 and β_3
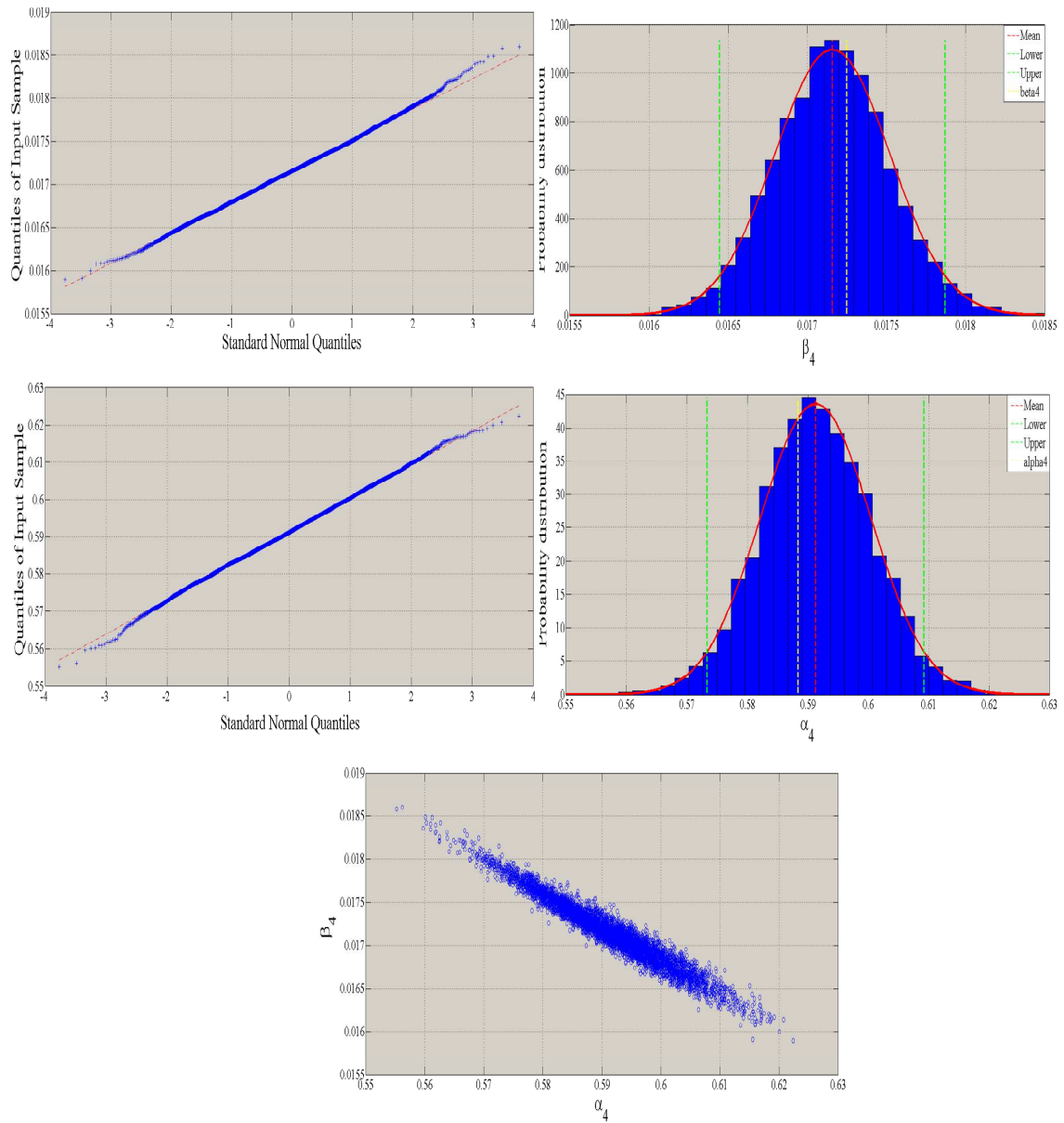
Figure 7-7. Normal quantile comparison and distribution function and correlation between α_4 and β_4

7.3.3   **Influence of Uncertainties**

The probabilistic analysis yields an expression of uncertainty in hydraulic model output that is responsive for analytical sensitivity analysis. Results of uncertainty analysis proved useful information in directing future data collection efforts in an attempt to reduce uncertainty in model output. For instance the channel roughness is a factor which influences the conveying capacity of channel.

Uncertainty analysis using the five hydraulic models (previously introduced in chapter 5.2.3) for open channel bends presented in this section is carried out with Monte Carlo simulation. The results of the Monte Carlo simulation for the effect of the parameters uncertainty in five hydraulics model are presented in Table 7.3 and also the comparison between coefficients of variation for five models are compared in Figure 7-8. In addition, two types of plots were prepared, histogram and probability density function as presented in Figure 7-9.

By referring to Table 7.3 and Figure 7-9 parameters for all models could be very well approximated by lognormal distribution with mean value, standard deviation and coefficient of variation $(Cv_1,...,Cv_5)$ for five different models. In these models the minimum and maximum differences between mean values are respectively for model Grashof and model Woodward and the minimum and maximum differences for standard deviation are respectively for models Grashof and Woodward. Table 7.3 presents the four extreme conditions for all models, and comparison with the general model. The response is close to the general models and lognormal distribution.

Table 7.3. Effect of uncertainties of the models coefficients on superelevation (dy)

dy (cm)	Ippen	Apmann	Chow	Grashof	Woodward
μ	5.5266	6.0147	5.4969	7.4881	3.7959
σ	7.6776	7.9444	7.6675	8.4180	6.1832
Cv_1	1.3903	1.3208	1.3892	1.1242	1.6290
$\mu + \sigma_\mu$	5.7806	6.2766	5.7778	7.6409	4.0895
$\sigma + \sigma_\sigma$	8.3064	8.5656	8.3077	8.8316	6.9205
Cv_2	1.4334	1.3648	1.4370	1.1558	1.6923
$\mu - \sigma_\mu$	5.3620	5.8855	5.3326	7.4357	3.6071
$\sigma - \sigma_\sigma$	7.1238	7.4245	7.0575	8.009	5.5773
Cv_3	1.3271	1.2615	1.3286	1.0771	1.5462
$\mu + 3\sigma_\mu$	6.1348	6.5678	6.1067	7.1880	4.4905
$\sigma + 3\sigma_\sigma$	9.4811	9.5976	9.4243	9.730	8.2422
Cv_4	1.5445	1.4643	1.5454	1.2446	1.8355
$\mu - 3\sigma_\mu$	4.8244	5.3869	4.8074	7.1443	3.040
$\sigma - 3\sigma_\sigma$	5.8548	6.2445	5.8379	7.1306	4.1815
Cv_5	1.2146	1.1593	1.2136	0.9981	1.3755
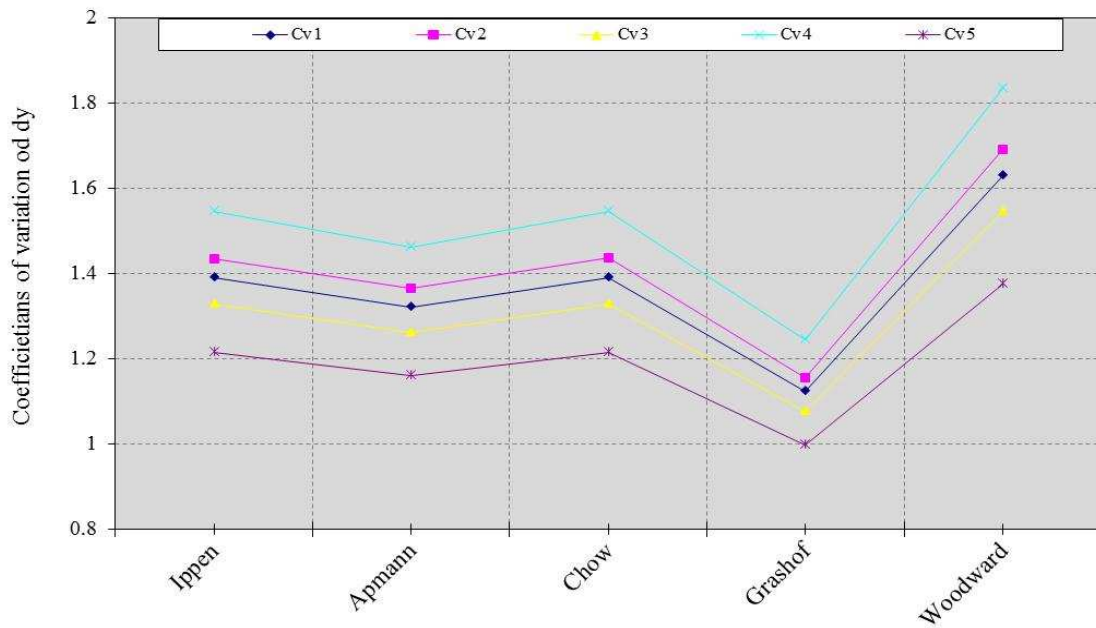
Figure 7-8. Coefficients of variation for five different models with different parameters($Cv_1,...,Cv_5$ are coefficient of variations)
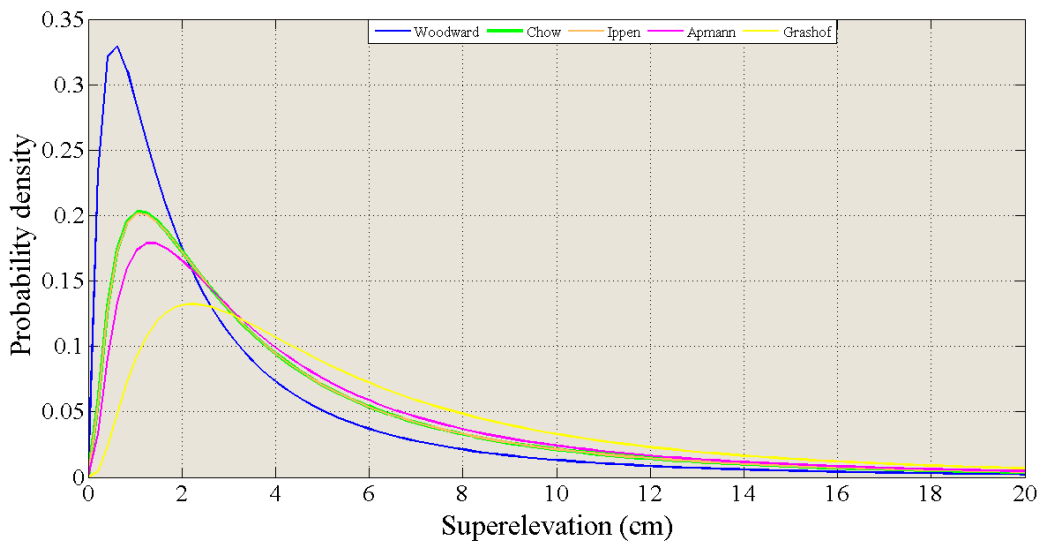
Figure 7-9. Probability density of superelevation in open channel bends for 5 models

7.3.4 Sensitivity Analysis

A tool related to uncertainty analysis is sensitivity analysis. Sensitivity analysis is used to determine the importance of different parameters and components of the model on the output of the model. If the response variable y depends on several variables, then the sensitivity of the response with respect to the variable or parameter is measured by the derivative of the response with respect to the variable or parameter.

Sensitivity analysis is sometimes a by product of a Monte Carlo uncertainty analysis. For example, if interest is in the sensitivity of the response to changes in variable, the values of the variables are selected using a probability method and then run through the model. The result is a set of input and output quantities. The importance of a variable is measured by the correlation or partial correlation between the variable and response. Variable with the greatest correlation indicates variable with great sensitivity.

There are five different positions on different parameters for evaluating effect of uncertainties of the total head ($E_1,...,E_5$) and superelevation ($dy_1,...,dy_5$) in an open channel bend. Here, the Monte Carlo uncertainty simulation for evaluating effect parameters is used. By referring to Table 7.4 and Table 7.5, and Figure 7-10 it can be noted that the maximum differences between the parameters estimated for total head and superelevation in open channel bends were very small. The effects of uncertainties were shown in Figure 7-11 for total head and superelevation, respectively. With the comparison of uncertainties, the estimated coefficients are in good agreement.

In summary, the parameters uncertainties for $\alpha_1, \beta_1, ..., \alpha_4, \beta_4$ have been tested using the bootstrap method. The analyses were carried out to see whether the bootstrapped samples might follow a normal distribution. Standard normal quantile plot or confidence interval could be used to measure the degree of dispersion relative to the mean value. Results from the bootstrap method were compared to those from the least square method. In these analyses both methods agreed to each other very well. Therefore, the coefficients of the limit state equation model were valid thus making the equation to be acceptable as well.

Table 7.4. Effect of uncertainties of the total head on different parameters

$E_1(m)$				$E_2(m)$		$E_3(m)$		$E_4(m)$		$E_5(m)$	
μ	σ_μ	σ	σ_σ	$\mu+\sigma_\mu$	$\sigma+\sigma_\sigma$	$\mu-\sigma_\mu$	$\sigma-\sigma_\sigma$	$\mu+3\sigma_\mu$	$\sigma+3\sigma_\sigma$	$\mu-3\sigma_\mu$	$\sigma-3\sigma_\sigma$
1.49	0.0005	0.537	0.0004	1.544	0.587	1.445	0.489	1.651	0.698	1.355	0.403

$E_1,...,E_5$ are total head with extreme conditions on different parameters in open channel bends.

Table 7.5. Effect of uncertainties of the superelevation on different parameters

$dy_1(cm)$				$dy_2\,(cm)$		$dy_3\,(cm)$		$dy_4\,(cm)$		$dy_5\,(cm)$	
μ	σ_μ	σ	σ_σ	$\mu+\sigma_\mu$	$\sigma+\sigma_\sigma$	$\mu-\sigma_\mu$	$\sigma-\sigma_\sigma$	$\mu+3\sigma_\mu$	$\sigma+3\sigma_\sigma$	$\mu-3\sigma_\mu$	$\sigma-3\sigma_\sigma$
6.733	0.174	2.29	0.124	6.512	1.967	6.694	2.138	6.896	2.319	6.160	1.967

$dy_1,...,dy_5$ are superelevation with extreme conditions on different parameters in open channel bends.
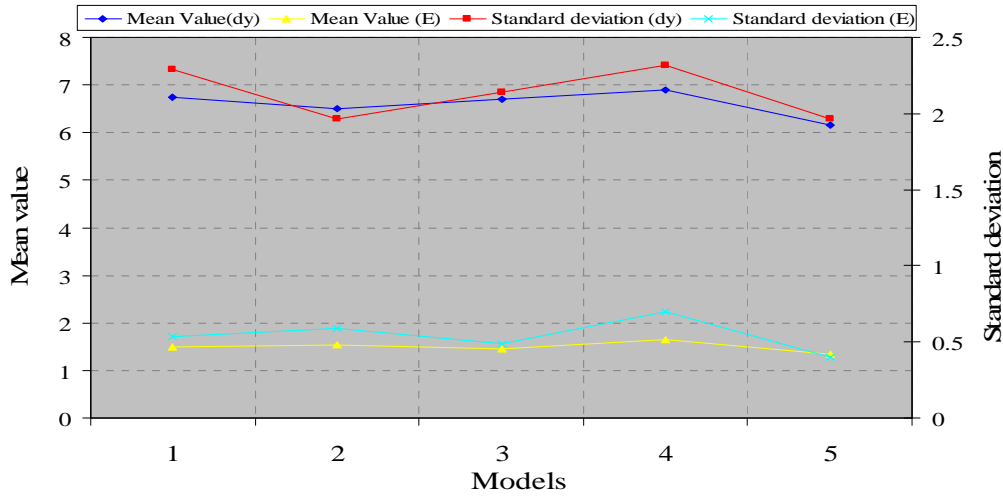
Figure 7-10. Differences between mean value and standard deviation for total head and superelevation
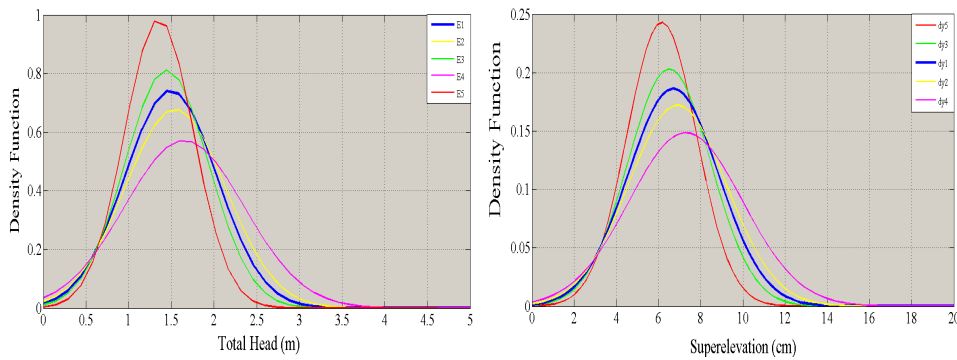
Figure 7-11. Distribution function for the effect of uncertainty in the total head (left). Distribution function for the effect of uncertainty in the superelevation (right)

7.3.5 **Probability of Exceedence for Bend Overtopping**

One of the components in the fault tree is the failure mode of bend overtopping. The limit state function of this failure mode is presented in equation(7.6), where H_b is height of the outer bank (outside wall), and E is the final total head in the center bend curve:

$$Z = H_b - E \tag{7.6}$$

Considering equation(7.6), the limit state function for the Ziaran dam can be written as:

$$Z = H_b - (0.2384\, Q^{0.6967} + 4.16\, L.n^2.Q^{-0.0397} + 0.0493\, Q^{0.6084} + dy + Z_f) \tag{7.7}$$

The conditional probability of bend failure analysis given Q is calculated by:

$$P_f = \int_{Q_1}^{Q_2} P_f(Q).f(Q).dQ \tag{7.8}$$

105

$$P_f = \sum_{i=1}^{N} P_f(Q_i).f(Q_i).\Delta Q_i \tag{7.9}$$

Failure probability calculations have been estimated for different water discharges. For a whole range of possible discharges, total failure probability of the superelevation is determined $(P_f = 0.053 \, per \, day)$. The main resistance and load parameter are as presented in Table 7.6 and Table 7.7 shows the design values of the canal height H_b, actual roughness coefficient n_A, superelevation dy, probability of failure P_f, reliability index β, for different discharges Q.

Table 7.6. Estimated mean and standard deviation of basic variables characterizing bend

Variable	H_b	dy	n	d	R	P	Q
μ	2.85	0.07	0.016	1.21	0.79	7.38	10.67
σ	-	0.023	0.0007	0.437	0.20	0.886	5.7
Distribution	D	LN	N	N	N	N	N

Table 7.7. Conditional probability of bend failure analysis given Q for different discharges and fixed H_b

$Q(m^3/s)$	$H_b(m)$	n_A	α_n	$dy(m)$	α_{dy}	β	P_f
30.23	2.85	0.016	0.511	0.007	0.860	-8.16	1
28.5	2.85	0.016	0.175	0.029	0.985	-2.66	0.996
27.8	2.85	0.016	0.106	0.049	0.994	-0.984	0.838
27.43	2.85	0.016	0.071	0.074	0.995	0.325	0.373
26.85	2.85	0.016	0.046	0.114	0.995	1.68	0.0468
26.69	2.85	0.016	0.042	0.125	0.996	1.97	0.0246
26.60	2.85	0.016	0.040	0.131	0.996	2.12	0.017
26	2.85	0.016	0.030	0.173	0.996	2.98	1.42×10^{-03}
25.40	2.85	0.016	0.025	0.215	0.997	3.66	1.24×10^{-04}
25.01	2.85	0.016	0.022	0.242	0.997	4.04	2.66×10^{-05}
23.34	2.85	0.017	0.015	0.362	0.998	5.29	6.05×10^{-08}
22.59	2.85	0.017	0.013	0.416	0.999	5.73	5.02×10^{-09}
19.37	2.85	0.017	0.008	0.657	1	7.16	0

7.4   ECONOMIC OPTIMIZATION

Firstly, the method of economic optimisation is presented as a framework for the derivation of an economically optimal level of risk. The derivation of the (economically) acceptable level of risk can be formulated as an economic decision problem. According to the method of economic optimisation, the total costs in a system (C_{tot}) are determined by the sum of the expenditure for a safer system (I) and the expected value of the economic damage $E(D)$. In the optimal economic situation the total costs in the system are minimised:

$$Min(C_{tot}) = Min(I + E(D)) \tag{7.10}$$

In this section the economic- mathematical model of Van Dantzig (1956) will be discussed. The method of economic optimisation was originally applied by van Danzig (1956) to determine the optimal level of flood protection (i.e. dike height) for Central Holland (this polder forms the economic centre of the Netherlands).

Assume that an existing channel has a height of h_0. The channel will be raised to an optimal height h. The costs involved with this elevation are a function of X. These costs can be assumed linearly with X by the relation:

$$\begin{cases} I = I_{h_0} + I_h.X \\ X = h - h_0 \end{cases} \tag{7.11}$$

The total investments in raising the channel (I) are determined by the initial costs (I_{h_0}) and the variable costs (I_h). The channel is raised by X, the difference between the new channel height (h) and the current channel height (h_0). The total costs are therefore given by the expression:

$$\begin{cases} E(D) = \dfrac{P_f.D}{r} \\ C_{tot} = I + E(D) \end{cases} \tag{7.12}$$

which is C_{tot} is the sum of construction costs, r is discount rate ($r = 0.015$) and D is damage costs which including the costs for material (gravel, sand and cement), damage to channel, spillway and Reconstruction, ($D = 100,000$ €). The optimal channel rise X_{opt} can be found by solving the equation $dC_{tot}(X)/dX = 0$ and gives for the height of channel the following result. The relation between the probability and investments, risk and total costs is shown in Figure 7-12.

The economical optimal channel height follows to be $H_{opt} = 3.03\ m$ with a corresponding probability of failure of $F(H_{opt}) = 2.76 \times 10^{-4}$ per year.
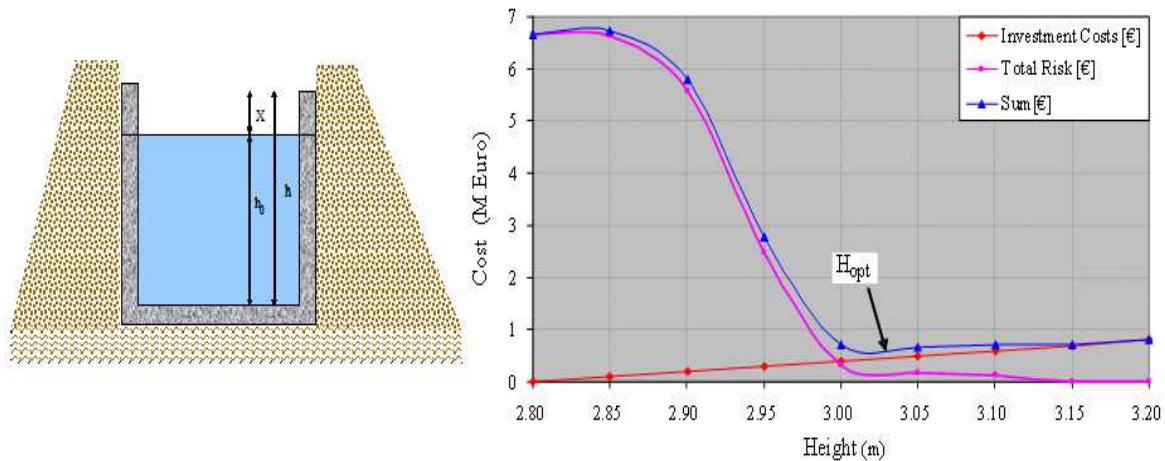
Figure 7-12. Simplified model for channel rise (left). Economic risk based optimal safety for height channel (right)

7.5   DISCUSSION

Table 7.7 shows that the probability of bend failure is very high (up to 0.373) when the discharge is $27.43 \, m^3/s$. Subsequently, overtopping from the outside channel bend will occur which accounts for erosion of the bank and the final undermining of the structure. The probability of failure P_f is shown in Figure 7-13 (right) for different discharges. In Figure 7-13 (left), the influence of the roughness coefficient shown by the PDF's in Figure 7-13 on the failure probabilities can be observed, with a change of about 10%.

The variation of superelevation may be expressed in terms of discharge rate and is a function of V^2. Figure 7-14 (left) shows the variations related to V^2 (Shams 1998).

It is very important that any designer should keep the upstream flow characteristics in mind before designing a conveyance structure after the outlet structure. It is required to take into full consideration that hydrodynamic turbulent pressure fluctuation is of great importance. Figure 7-14 (right) shows variation of superelevation as a function of the Reynolds number $\mathrm{Re}_{(N)}$ in the bend.

Relation between superelevation and velocity for seven models is shown in Figure 7-15, and comparison of superelevation for seven models with actual measurements presented in Figure 7-16. It shows that the field measurements of superelevation show higher values than the prediction methods. Some parts of actual measurements are 2-3 times bigger than other models (for example Woodward and Grashof). The reason of this difference might be caused by secondary flow.

Comparison of slope for seven models with actual measurements in Figure 7-16 is shown in Table 7.8. It shows that slop of two models (Red and blue line) are bigger than other models and the result of these models is close to measurements.

7.6 CONCLUSION

In this chapter, a probabilistic method for the analysis of superelevation in an open channel bend was presented and the conditional probability of overtopping failure was estimated.

The secondary flow has important role and has direct effect on the superelevation in open channel bends.

The presented case indicates that the existing theory cannot lead to exact results. For some models, there is an underestimation in the superelevation of a factor 3. For design the bends with this condition for safety, we need extra freeboard more than normal channel. Probabilistic modelling can provide a formal approach to the analysis of the performance of hydraulic structures, taking all uncertainties of the models, such as load and strength variables and uncertainties of the model coefficients $(\alpha_1, \beta_1, \ldots, \alpha_4, \beta_4)$ into account in Table 7.1 and Table 7.2, also in Figure 7-4 to Figure 7-7.

The detailed reliability analysis in this chapter has concentrated on one component in the failure analysis (overtopping). Further analysis of the other components should be carried out in order to find the weak links of the hydraulic structure. The vulnerability of a hydraulic structure can then be improved by strengthening these weak elements.

The probability of failure study in this research has demonstrated the need to improve the discharge capacity and the bank structure of the flume in the Ziaran dam.
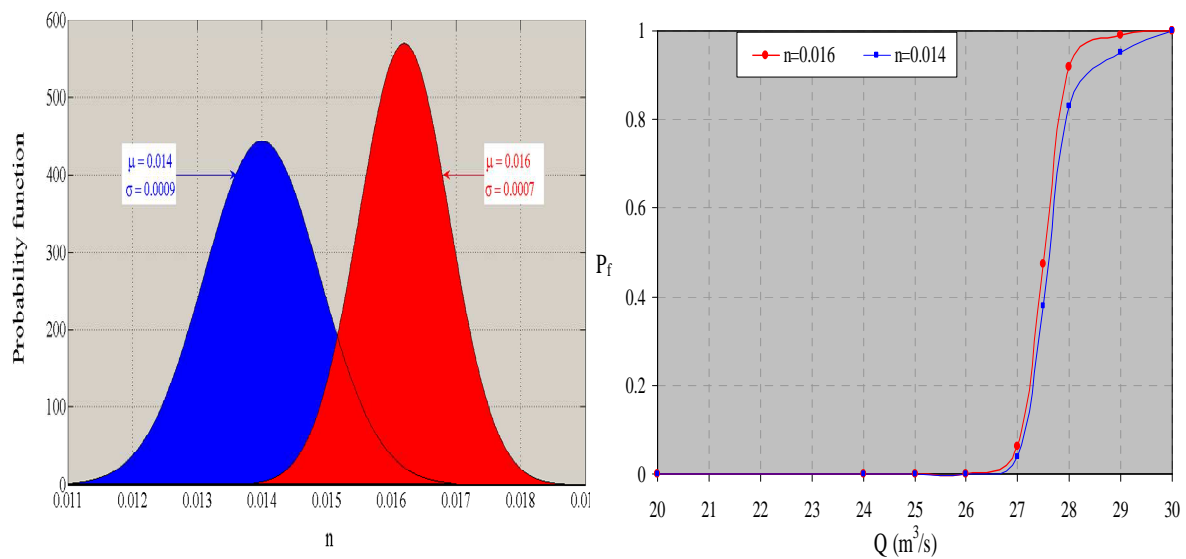
Figure 7-13. Pdf plots of roughness coefficient (left). Probability of failure as a function of discharge (right)
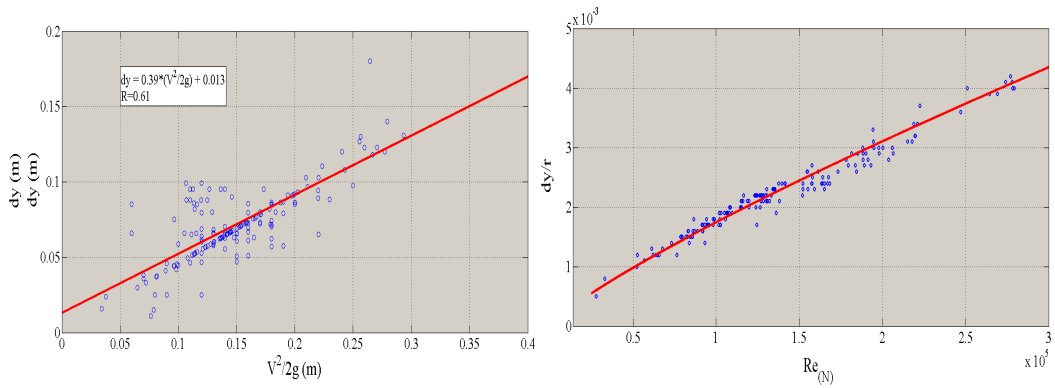
Figure 7-14. Regression of superelevation with dynamics pressure (left). Regression of dimensionless variable between dy/r and Re[-] (right).
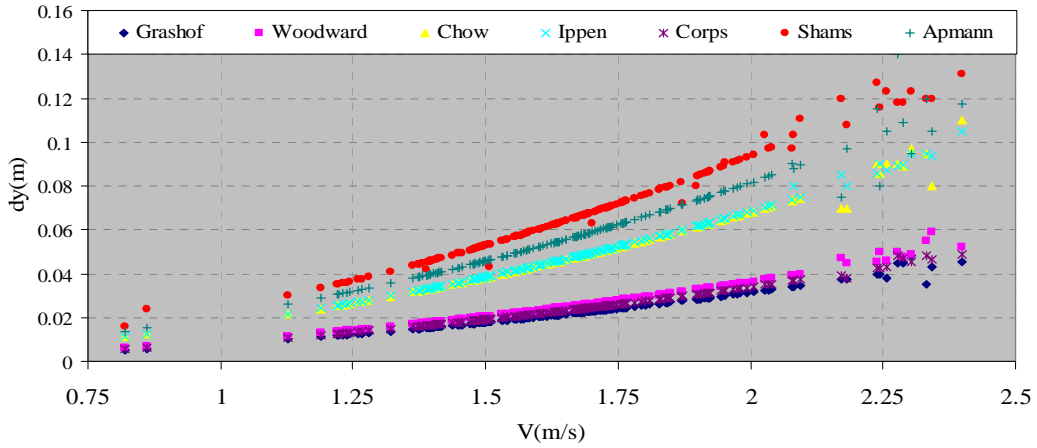
Figure 7-15. Relation between superelevation and velocity for seven models
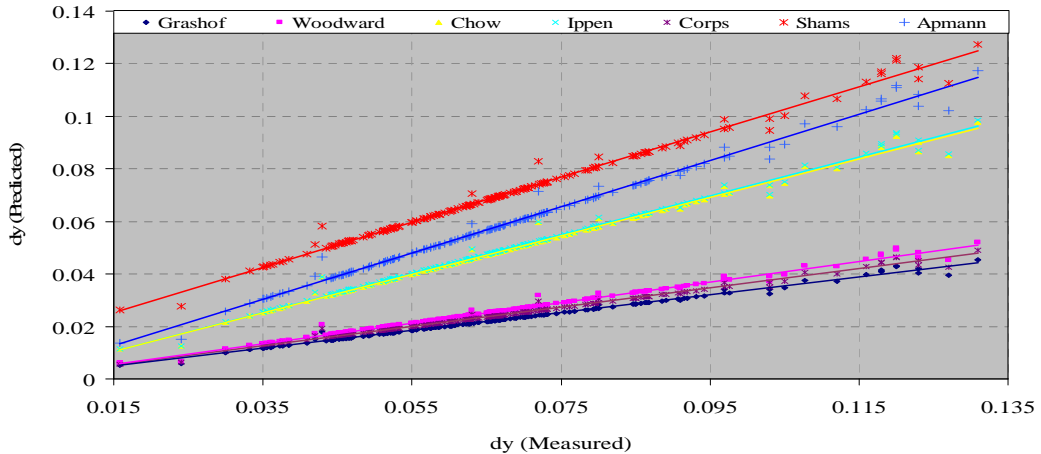
Figure 7-16. Comparison of superelevation for seven models with actual measurements

Table 7.8. Comparison of slopes for seven models with actual measurements in Figure 7-16

Model	Grashof	Woodward	Chow	Ippen	Corps	Shams	Apmann
Slope (^{o})	19	22	36	36	20	40	41

CHAPTER 8

HYDRODYNAMIC LOADINGS AFTER DAM BREAK

Assessing the vulnerability of buildings in flood-prone areas is a key issue when evaluating the risk induced by flood events, particularly because of its proved direct influence on the loss of life and economic damage during catastrophes. A comprehensive methodology for risk assessment of buildings subject to flooding is nevertheless still missing. Bearing this in mind, a new set of experiments have been performed at TU Delft with the aim of spreading more light on dynamics of flood-induced loads and their effects on buildings and to provide the CDF community with state of the art bench-marks. In this chapter, a brief overview is given of flood induced load on buildings, the new experimental work is then presented, together with results from preliminary analysis. Initial results suggest that the use of existing prediction methods might be unsafe and that impulsive loading might be critical for both the assessment of the vulnerability of existing structures and the design of new flood-proof buildings.

8.1 INTRODUCTION

Recent catastrophic events such as the Indian Ocean tsunami in 2004 (Kawata, 2005) and the New Orleans flood due to passage of hurricane Katrina in 2005 (FEMA 549, Figure 8-1) have focused the attention of politicians, economists and engineers worldwide on the need for the assessment of risk due to flooding of anthropized areas when estimating the potential life and economic losses of a catastrophic scenario.

While a huge effort is being devoted to the development of methodology for the definition of the hazard due to flooding (including flood-mapping of riverine and coastal areas), less is

known on the dynamics of flood-induced loads on buildings (Kelman and Spence, 2004) and a comprehensive methodology for damage assessment of buildings subject to flooding is still missing. In particular, new tools are needed for the evaluation of the fragility of civil structures to hydraulic loading.

In general, the structural vulnerability of buildings in flood flows is modelled based on the combination of water depth and flow velocity. Criteria have been derived based on data from historical floods, (see e.g. Clausen and Clark, 1990, Pistrika and Jonkman, 2009), but their empirical validation is relatively limited. The need to account for the large amount of uncertainties involved with such processes is motivating the recent orientation toward probabilistic approaches to risk assessment over the more established and simple deterministic ones. Bearing this in mind, a research project is being carried out with the aim of improving knowledge on hydrodynamic loading of buildings in flood-prone areas.
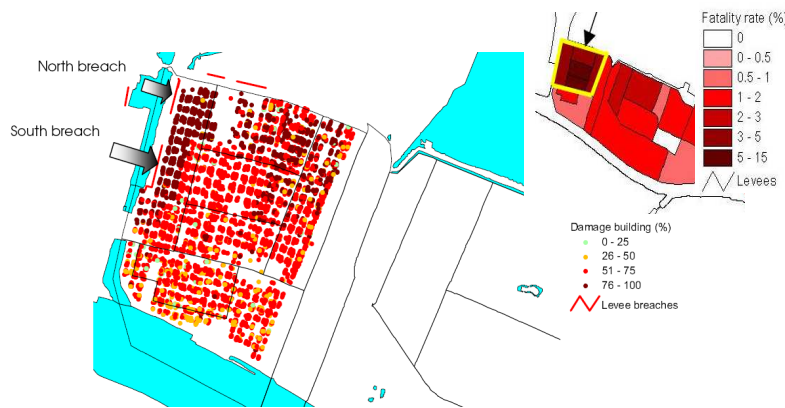
Figure 8-1. Percentage of building damage in the Lower Ninth Ward, New Orleans (main figure) and fatality rate (top-right),(Cuomo et al., 2008)

8.2 LITERATURE REVIEW

A dam-break wave is one of the most studied examples of unsteady flow in open channels. Catastrophes caused by the sudden failure of dams and the resulting wave have attracted physicists and scientists since the 19th century (Chanson, 2004).

8.2.1 Analytical Solutions

First attempts on solving the dam-break problem date back to 1892, when Ritter (1892) made important contributions and presented an analytical solution for the case of a dam-break wave problem for an inviscid fluid in a dry, horizontal rectangular channel with a semi-infinite reservoir extension. Major existing contributions to the analytical solution have been represented in the literature as follows:

Ritter (1892) derived an analytical solution for dry horizontal frictionless channels; the main feature of Ritter's solution is being self-similar (i.e., the solution only depends on the ratio x/t, in which x is location and t is time, see Leal et al. (2006));

Dressler (1952) took into account the influence of friction, based on a pertur-bation solution; his solution is non-self similar due to the effect of friction. Whitham (1955) utilized a friction model, quadratic in the flow velocity, and derived a parabolic water surface profile for the

bore front that is concave downward and asymptotically approaches a vertical face in the bore front. Stoker (1957) generalized Ritter's approach for wet initial downstream and like Ritter, reached a self-similar solution;

Lauber and Hager (1998) could reach a solution based on shallow water equations with friction slope in the source term. Fracarollo and Capart (2002) worked on mobile bed and derived a semi- analytical solution but were incapable of providing an explicit equation for wave celerity. Chanson (2005b and 2006) solved the Saint-Venant equations using the method of characteristics for a wide rectangular channel with a semi-infinite reservoir.

8.2.2 Experimental Research

Most studies have been geared towards investigating the initiation process of a dam-break flow and the flow features at the positive bore front. Most of the tests are performed in horizontal flumes or flumes with small angle. Also, the test flumes are supposed to be as long as possible to approach the assumption of an infinitely long channel in analytical solutions. Moreover, tests with dry or wet downstream and mobile or immobile beds have been performed to investigate the effect of various parameters on flow variables. A number of studies exist on dam-break experiments with fixed bed, such as those of Levin (1952), Dressler (1954), U.S. Army Corps of Engineers (1960, 1961), Estrade (1967), Chervet et al. (1970), Drobir (1971), Barr and Das (1980), Martin (1981), Miller and Chaudhry (1989), Bell et al. (1992), Franco (1996), Lauber and Hager (1998), Stansby et al. (1998), Leal (1999), Briechle and Kotenger (2002), Leal et al. (2002), Arnason (2005) and Nouri (2008).

8.2.3 Physical damage modeling

Flooding not only destroys human life, but also has a devastating effect on land use, infrastructures, plants and natural resources. The impact of a flooding on the environment relates not only to the landscape, but also to the man-made aspects of the environment. Researchers specializing in natural hazards have expressed a need for more complete documentation of losses, including both direct and indirect damage associated with flooding (Jonkman et al. 2008; Mileti 1999; National Research Council 1999; Heinz Center 2000).

Jonkman et al. 2008 presented a classification of various types of damages characterizing flood events and make a distinction between direct damages inside the flooded area and indirect damages that occur outside the flooded area (see Table 8.1) also described three categories for physical damage modelling in the Netherlands (Jonkman et al. 2008).

o *Direct physical damages*

o *Indirect economic losses*

o *Loss of life*

Direct damages are closely connected to a flood event and the resulting physical damage. The physical damage estimation includes two phases. The first phase is estimation of structural damage and second phase is the value pricing of this physical damage (Kelman et al. 2004).

8.3   FLOOD LOAD ON BUILDING

During extreme events, buildings laying in floodplains within high flood-induced hazard areas can be subjected to a series of loads including both hydrostatic and hydrodynamic loads see Figure 8-2 for example of impacts of floods.

1- Hydrostatic loads include:

- *Hydrostatic pressure on the vertical element of the structure*
- *Buoyancy on the horizontal element of the structure*

2- Hydrodynamic loads include:

2-1- Drag/Velocity-dominated (quasi-static) loads, including:

- *Flash floods (away from source banks/levee/breaches)*
- *Debris-flows (away from source)*
- *Storm surges (inland)*
- *Tsunami*
- *Non-breaking wave loads*

2-2- Inertia/acceleration-dominated (impulsive) loads:

- *Dam break, close to source*
- *Debris-flow, close to source*
- *Flash floods in the vicinity of banks/levee/breaches*
- *Storm surges (along the coast)*
- *Tsunami (along the cost and inland at the wave front)*
- *Breaking wave loads*

The above classes are described in detail in what follows. Here, it is worth mentioning that in most cases, different loads may co-exist and act on the same structure at the same time or at a different time during a single flooding event.

Figure 8-2. Tsunami Phenomena, Top-Left: North Fork of the KY River, March 1963; Top-Right: Melbourne flood, February 1972; Bottom-left Coastal flood in Walcott November 2007; Sumatra tsunami, December 2004), (Cuomo et al., 2008)

8.3.1   **Hydrostatic Loads**

The hydrostatic horizontal load $F_{hs}(N/m)$ derives from the difference in water level on the upstream and the downstream sides of the wall. Per unit width it is given by:

$$F_{hs} = (\rho.g) \big/ \left(2\left(h_{us}^2 - h_{ds}^2\right)\right) \tag{8.1}$$

in which $g\,(m/s^2)$ is the acceleration due to gravity, $h_{us}(m)$ and $h_{ds}(m)$ are the water depths, respectively upstream and downstream the wall and $\rho\left(kg/m^3\right)$ is the density of the fluid, which is a function of the amount of solid particles suspended within the flood.

8.3.2   **Buoyancy Loads**

When assessing the vulnerability of horizontal structural elements or the overall stability of a building, buoyancy should also be taken into account as it applies a potentially unbalanced uplift force and affects the resistance of gravity-based structures against sliding and overturning. Buoyancy (per unit length) can be easily estimated using:

$$F_v = \rho.g.V \tag{8.2}$$

in which g is the acceleration due to gravity, ρ is the density and V is the volume of water displaced by submerged structure. Equation (8.2) is found in FEMA (2000), Camfield (1980), FEMA (2008), amongst other literature.

8.3.3   **Hydrodynamic Loads**

Hydrodynamic loads derive from the combination of the inertia and drag and generally depend on both the kinematics of the flow and the geometrical and dynamic characteristics of structure. In practice, the following simplified expression is adopted for the hydrodynamic load per unit length:

$$F_D = C_D.\rho.b.h.u^2 \tag{8.3}$$

in which F_D is the total drag force acting in the direction of flow, $b.h$ is area of the structural element normal to the flow direction, the width of the object h is the water depth at the wall and u is the intensity of the velocity component orthogonal to the object and C_D is the drag coefficient, which varies depending on both building geometry and flow conditions.

Velocity is one of the major properties of dam break loading. By and large, velocity is taken as depending on the inundation depth, h. The expression for the velocity is $u = k\sqrt{gh}$. In which k is a constant coefficient. Different authors give different values for k (Murty, 1977; Kirkoz, 1981; FEMA, 2000; Iizuka & Matsutomi, 2000; Thurairajah, 2005).

Although the use of Equation (8.3) is recommended in many international standards and design codes, it doesn't nevertheless account for the contribution of inertia on the overall hydrodynamic force whose importance has been long known (see among others Morison et al., 1950). A more advanced formulation is that introduced by Kaplan et al. (1995) which reads:

$$F = \rho.h\left(C_D.g.u^2 + C_{I,1}.h.\frac{du}{dt} + C_{I,2}.u.\frac{dh}{dt} \right) \tag{8.4}$$

where, $C_{I,1}$ and $C_{I,2}$ are respectively the inertia coefficients for the contribution of the acceleration and the rise rate terms.

Written in the above form, the equation highlights the contribution of drag (first term on the right hand side) and inertia (second and third terms on the right hand side). Note that the contribution of inertia force is related to both variation in flow velocity (du/dt) and rise rate (dh/dt), both of which effects are known to be strongly correlated to damage to buildings in floods. Although more advanced than Equations(8.3), (8.4) it has been shown to underestimate most violent impulsive loading events (Cuomo et al. 2003).

8.3.4   Dam-Break and Tsunami-Induced Loads on Buildings

Recent catastrophic tsunami events have focused the attention of researchers worldwide on the need to assess the hydrodynamic loads exerted by tsunami on buildings. Among these, experiments by Arnason (2005) represent rare examples of tests concentrated on measuring loads exerted by dam break flow on isolated buildings. Results from the above experiments have been included in design standards including the recently published by FEMA (2008) in which the hydrodynamic force acting on an isolated building reached by a tsunami is given by:

$$F_D = 0.5C_D.\rho.b.h.u^2 \tag{8.5}$$

The authors of the FEMA guidelines suggest using a drag coefficient $C_D = 2$ when assessing the drag component of the load only but assuming $C_D = 3$ to account for the impulsive component of the loading, which implies:

$$F_{imp} = 1.5F_D \tag{8.6}$$

8.3.5   Short Wave-Induced Loads

When assessing hydrodynamic loads for use in design, short wave loads (period 1s < T < 10s) on buildings are usually accounted for separately. In the common practice, they are usually subdivided into loads exerted by non breaking, breaking and broken waves, the transition among the above conditions being mainly a function of the local wave height (H) to water depth (h) ratio. It should nevertheless be borne in mind that for walls exposed to wave loading, both the incident wave condition and the water depth in front of the structure might vary during the flood and it is therefore not easy to define boundaries for each loading condition.

A series of well established prediction methods for non-breaking wave loads are available to practitioners. Among these, Goda's (1974) prediction method for wave loads on caisson breakwaters represents a landmark in the evolution of physically rational approaches to the assessment of wave loads at walls. Takahashi et al. (1994) extended Goda's prediction method to include the effect of wave breaking. Within the PROVERBS research project, a

new design method was derived for the evaluation of wave forces on caisson breakwaters and was described in details in Oumeraci et al. (2001).

Since breaking is highly dissipative, force exerted by broken waves are assumed to be significantly less intense then for the breaking wave case. It is commonly assumed that after breaking, the wave propagates like a bore inshore and in-land, eventually transferring their residual kinetic energy to the structure at the time of impact (see Ramsden, 1993 and references therein).

8.3.6   Debris-Induced Loads

Debris-induced loads such as large rocks, cars, or other objects flowing in the water downstream represent a different kind of loading, both for their high level of unpredictability and their extreme danger. Among the rare studies carried out in this field, we will mention the recent work carried out by Haehnel and Daly (2002).

8.3.7   Load Combinations

As already mentioned, in most cases a structure is subjected to a combination of the loadings described above. An example calculation showing different degree of load combination acting on a vertical wall is given in Figure 8-3 from left to right and from top to bottom:

- o *hydrostatic pressure;*
- o *hydrostatic pressure + drag;*
- o *hydrostatic pressure + waves;*
- o *hydrostatic pressure + drag + waves;*
- o *Debris*
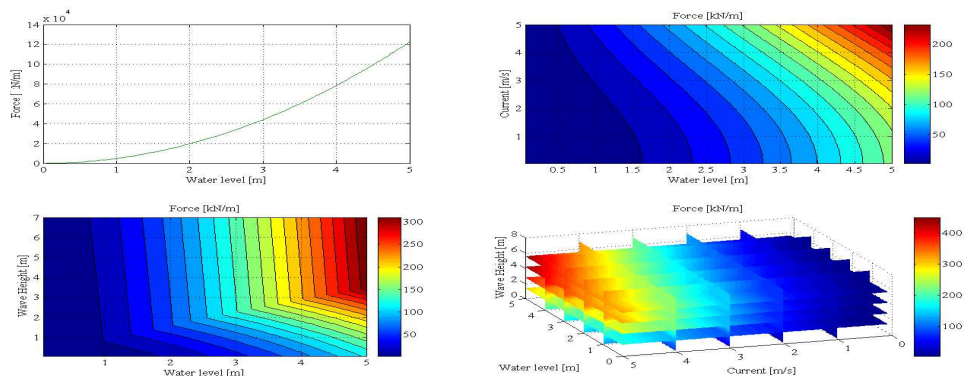
Figure 8-3. Example calculation showing the effect of the hydrostatic pressure (top-left) alone, and in combination with a steady current (top-right), waves (bottom-left), and both (bottom-right), (Cuomo et al., 2008).

Note that during a single flood event, the load felt by the wall might vary significantly within the sketched areas in Figure 8-3. For example, as the water reaches the base of the wall and starts rising, the wall will experience increasing hydrostatic pressure and drag force due to the current. If the structure is set in a coastal area, waves might as well reach the wall which will therefore experience loading from broken, breaking or pulsating waves as a function of the local wave height to water depth ratio, which can vary due to tide and storm surge variation

during a single flood. In other tsunamis cases, flash floods and dam break flows might drag along heavy objects as debris, with catastrophic effects on any structure laying along the path.

8.4 NEW PHYSICAL TESTS

A new set of dam-break 2D physical model tests were carried out in one of the wave-flume of the Hydraulic Laboratory of Delft University of Technology (TU Delft) with the aim of spreading more light on dynamics of flood-induced loads and their effects on buildings.

8.4.1 Experimental Set-Up and Measurement Instruments

Experiments were carried out in a 42 m long, 0.8 m wide and 1.0m high wave flume. A water column was stored in a 2.88m long, 0.67cm wide and 1.26cm high reservoir. To minimize the effect of the gate opening on the water tongue propagating downstream, the gate was operated by rotating a stiff metal plate around its top by pulling its bottom by means of a free-falling counterweight. The building was represented by a cubic structure (characteristic linear dimension of 18cm) and made out of thick aluminium to minimise its weight and maximise its stiffness (dynamics of model structure is discussed further in the following). The following sensors were housed in the model structure:

- o *1 accelerator*
- o *1 axial force transducer*
- o *11 pressure sensors*

In order to be able to effectively capture the sharpest impulsive events, data were logged continuously at high frequency (50 KHz), recording was initiated by monitoring the movement of the gate.
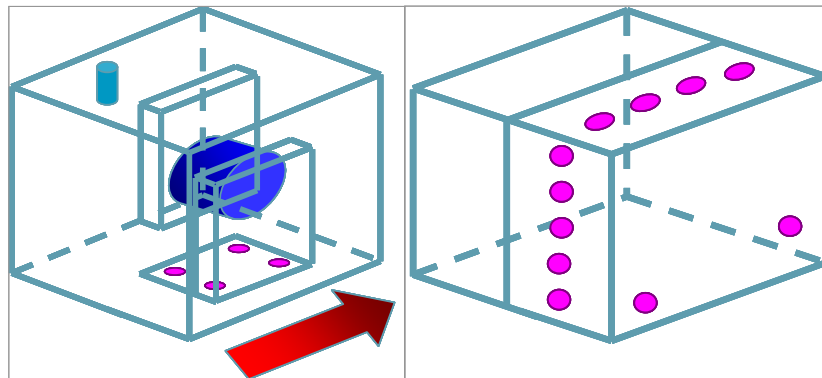
Figure 8-4. Sketch of model structure housing force transducer and acceleration (left) and pressure transducers (upstream, downstream, lateral and top side), (Cuomo et al., 2008)

8.4.2 Experimental Program

The experimental program covered a number of layouts and geometrical configurations, including (Figure 8-5):

- o *Single building layout (left): aimed at investigating the effect of building orientation and distance from the source;*

- ○ *City layout (top-right): aimed to investigate complex flow pattern and local amplification in urban environment*
- ○ *Debris layout (bottom-right): aimed to investigate the dynamics of the water-debris-structure interaction.*

Tested parameters included:

- ○ *Building orientation with respect to the main flow;*
- ○ *Water level in the reservoir;*
- ○ *Distance of the building from the gate;*
- ○ *Density and volume of debris,*
- ○ *Relative position within the "urban" environment;*

Each test was repeated three times for quality checking and to enhance the significance of the tests.
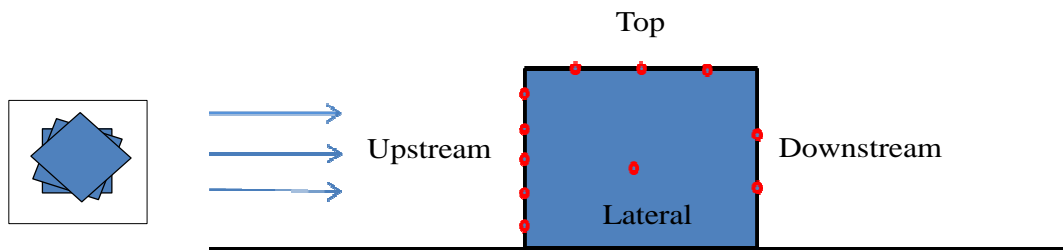
Figure 8-5. Model layouts used in the experiments

8.5 OBSERVATIONS DURING EXPERIMENTS

Tests investigated flood-induced loads on building subjected to a wide range of flow conditions. Example snapshots captured during testing of the single building (top) and city (bottom) layouts are given in Figure 8-6 showing respectively drag (top) and inertia (bottom) dominated loading phases. Vortex shredding and cavitation have also been observed (top-left).

8.5.1 Time History of Pressures

In the following, initial results from preliminary analysis performed on time histories recorded during the first set of the "single building layout" tests are presented. Data recorded during tests carried out with the structure located close to the gate only are presented in terms of effect of tested parameters and building orientation with respect to the direction of the main flow.

8.5.1.1 Upstream side

Figure 8-7 shows time histories of the pressure exerted on the upstream face of the cubic structure due to bores generated with impoundment depths of $h = 0.20, 0.40, 0.60, 0.80, 1.00$ and $1.20 \, m$, measured at the pressure sensors. A sudden rise is observed in the time history of

the exerted pressure, which corresponds to the impact of the bore front on the upstream face of the structure.

8.5.1.2 Top Side

Figure 8-8 shows the variation of the vertical distribution of the pressure exerted on the cubic structure from the impact of a bore generated by an impoundment depth of $h = 0.20$, 0.40, 0.60, 0.80, 1.00 and $1.20\,m$. It is observed that a negative pressure (suction) is exerted on the top sides of the structure. The pressure magnitude is less than the corresponding values for the upstream face of the structure.

8.5.1.3 Lateral Side

Lateral hydrostatic forces arise from the variation in pressure distribution with depth. The time histories of pressure exerted on the lateral side of the cubic structure due to bores generated with the different of the water depths and shows in Figure 8-9.

8.5.1.4 Downstream Side

shows time histories of pressure exerted on the downstream face of the cubic structure due to bores generated with impoundment depths of $h = 0.20$, 0.40, 0.60, 0.80, 1.00 and $1.20\,m$. It is observed that larger oscillations exist in the pressure time histories.
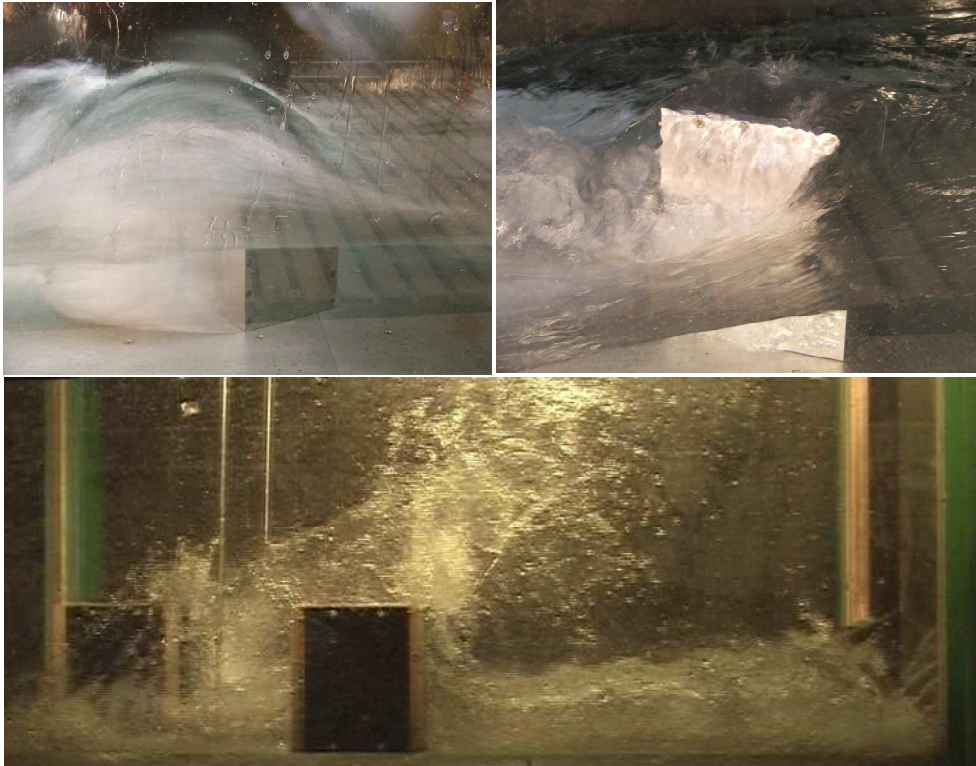
Figure 8-6. Snapshots captured during testing of the single building layout (top) and city layout (bottom).
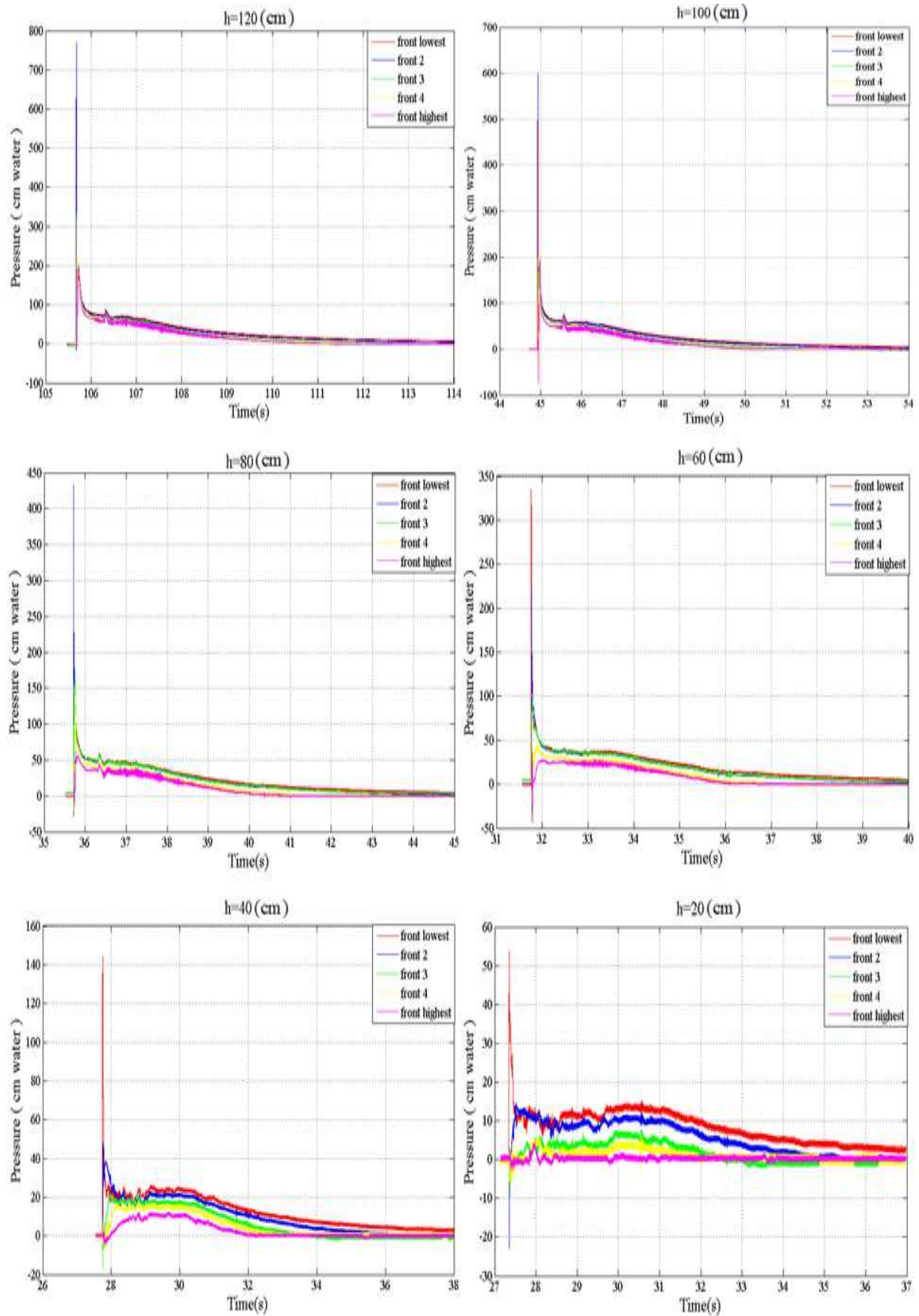
Figure 8-7 Time history of pressure on the upstream face (front) of the structure recorded during dam-break experiments with the different impoundment depths.
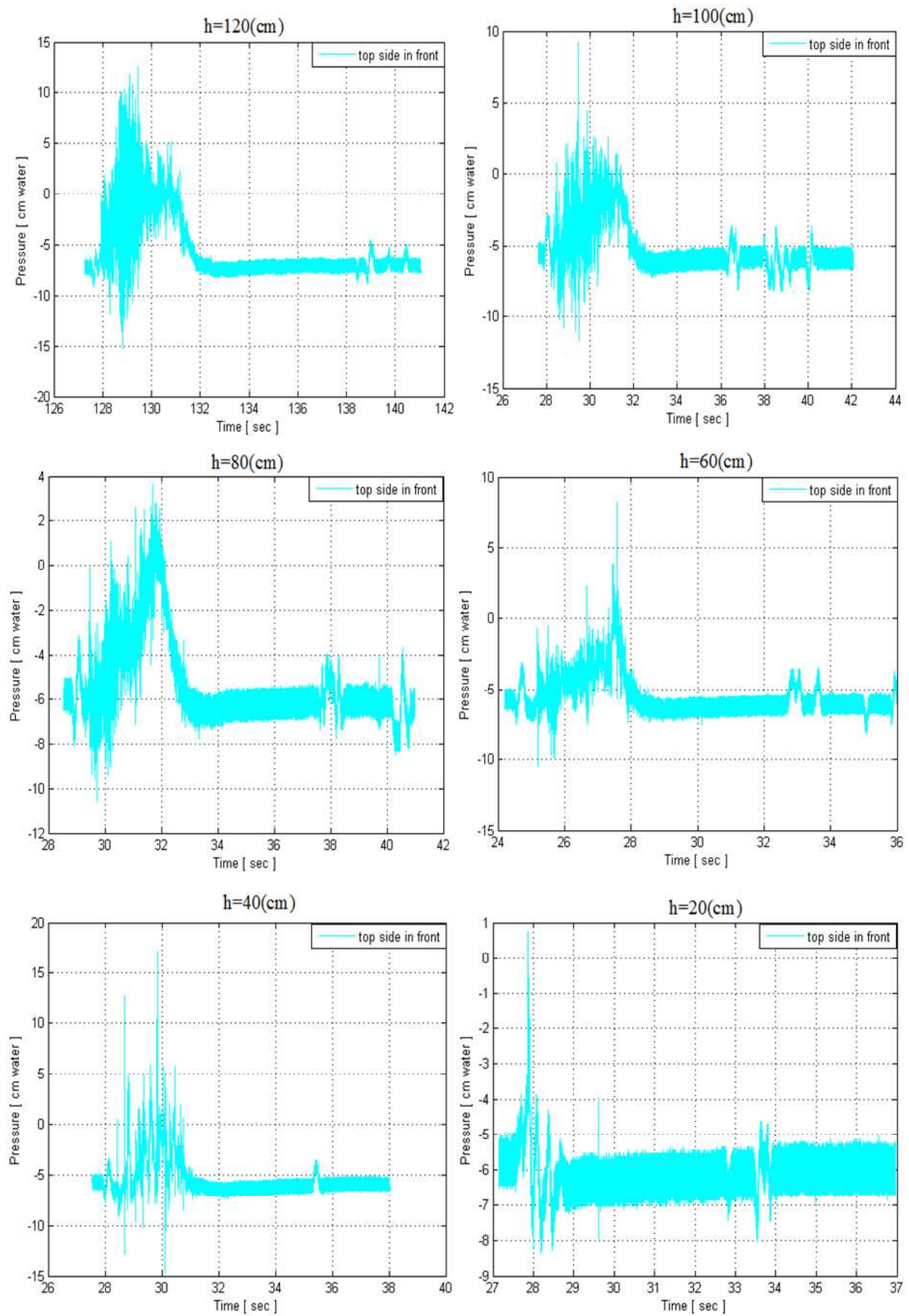
Figure 8-8 Time history of pressure on the top of the structure recorded during dam-break experiments with the different water level.
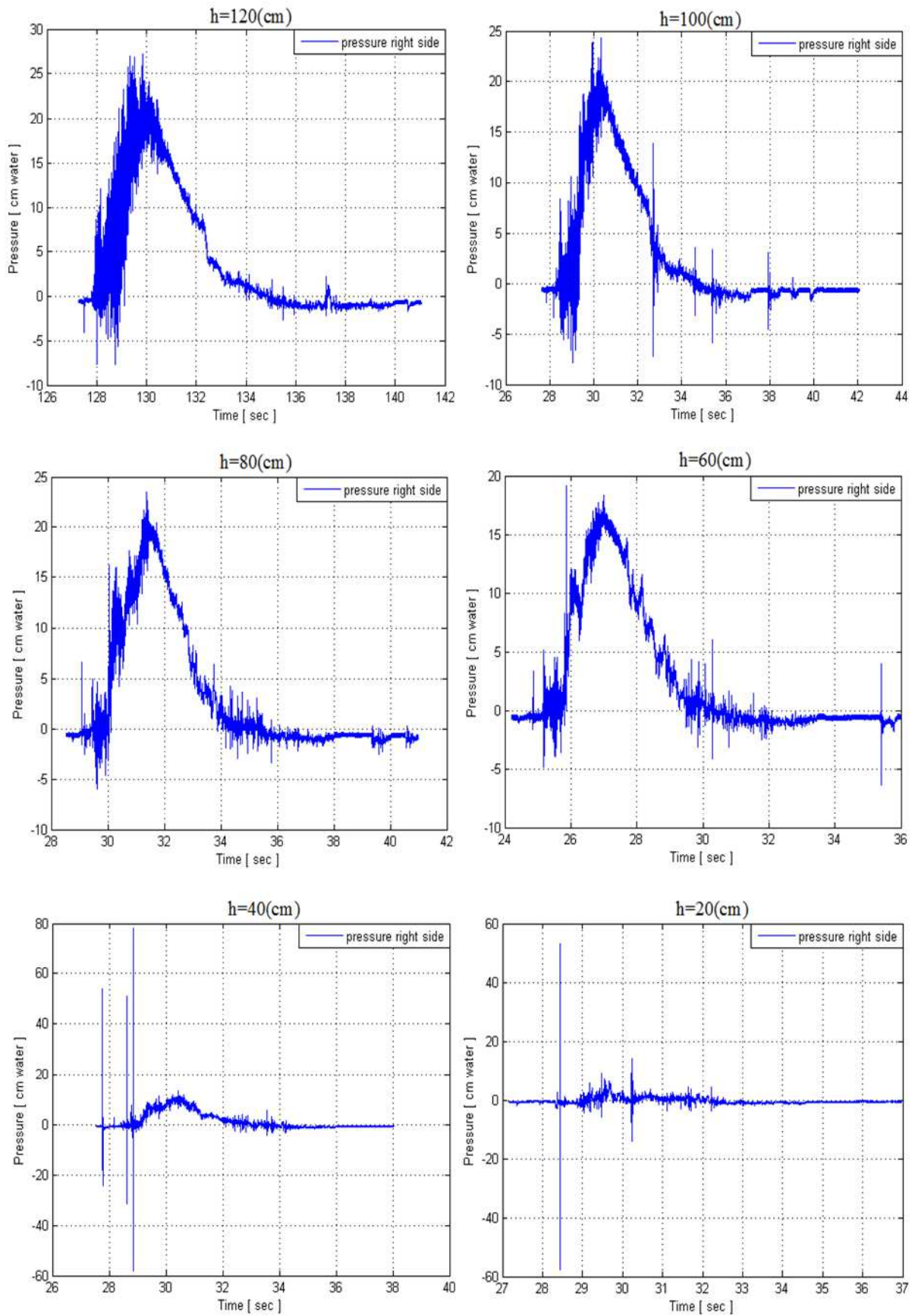
Figure 8-9 Time history of pressure on the right side of the structure recorded during dam-break experiments with the different impoundment depths.
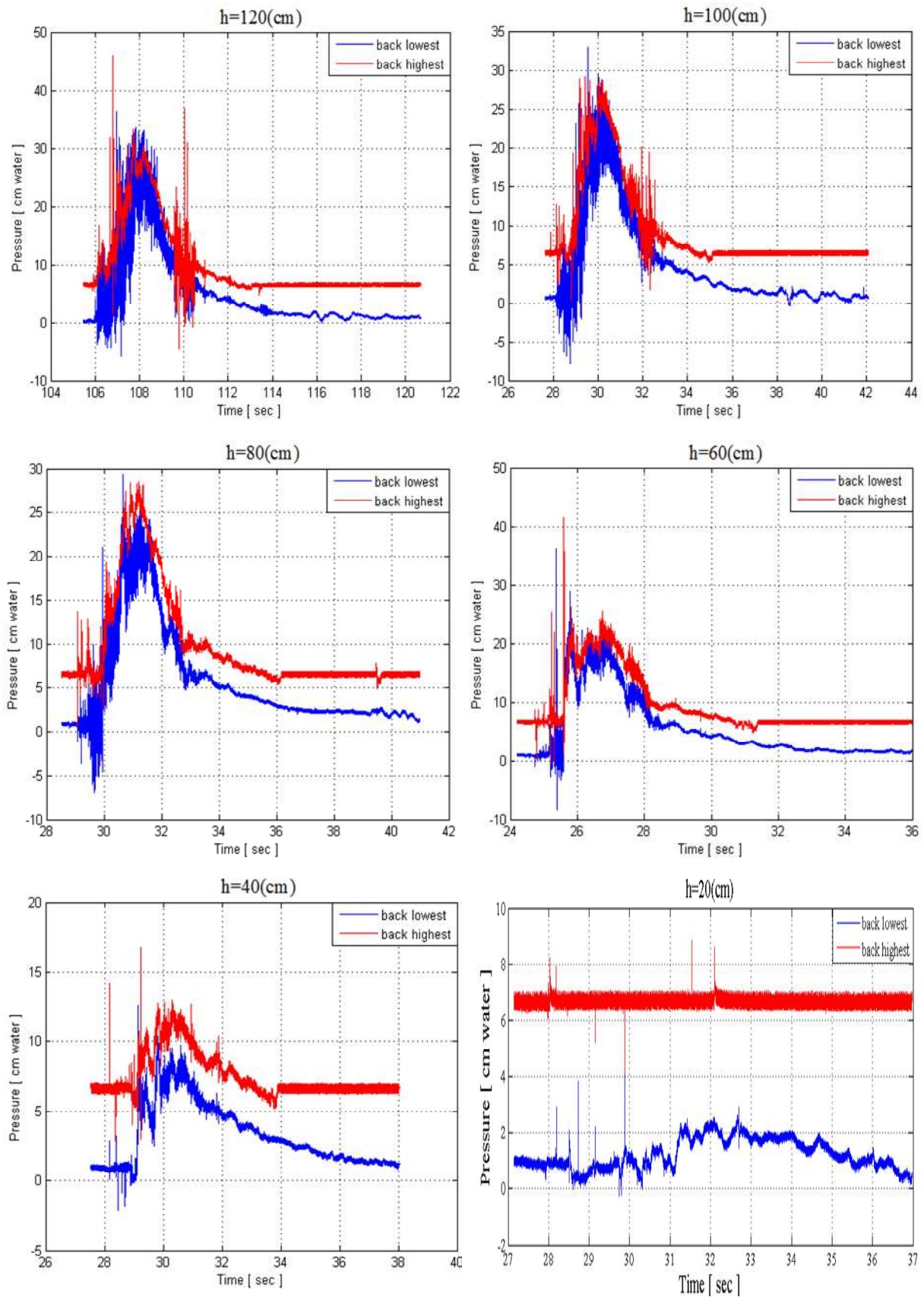
Figure 8-10 Time history of pressure on the back side of the structure recorded during dam-break experiments with the different impoundment depths.

8.5.2 Initial Results

An example of a force time-history (front side of the structure) recorded during dam break experiment presented in this section is shown in Figure 8-11 showing a sharp (inertia-dominated) peak (F_{imp}) followed by a less intense but longer lasting (quasi-static, drag-dominated load F_{qs^+}), (Cuomo et al., 2008). We refer to section 8.8 for further comparison with existing literatures.
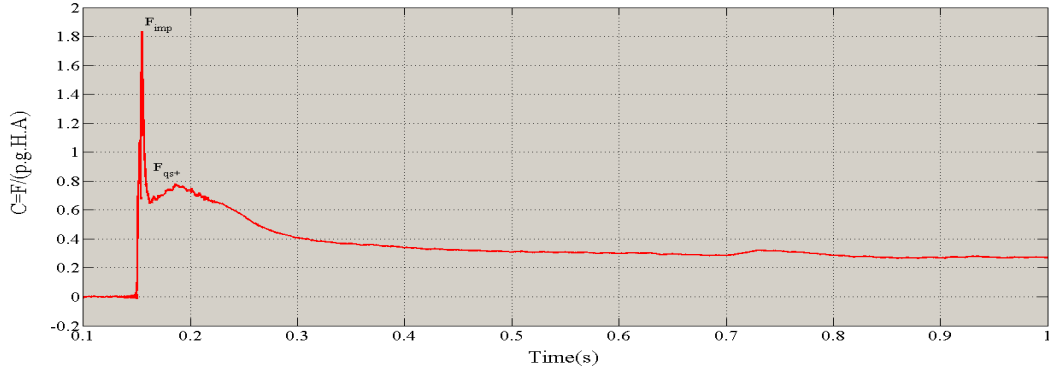
Figure 8-11. Example force time-history recorded during dam-break experiments.

8.6 QUASI-STATIC AND IMPULSIVE LOADS

Quasi-static loads are actually due to dynamic phenomena but remain constant for relatively long periods. Quasi-static F_{qs^+} and impulsive F_{imp} loads on the front face of the building are plotted respectively on the top and bottom side of Figure 8-13 as a function of the water level in the reservoir h, showing an increasing non-linear trend with linearly increasing h over the whole range of parameter tested. Best fit curves in Figure 8-13 over the range of parameter tested) obey the expression:

$$F_{qs^+} = a.\exp\left[-\left(\frac{h-b}{c}\right)^2\right] \qquad (8.7)$$

With a, b and c being best-fit empirical parameters summarised in Table 8.1, together with R-square of the corresponding fit.

Table 8.1. Summary of regression analysis and correlation coefficients for equation (8.7)

Load	Orientation	a (N)	$b(cm)$	$c(cm)$	R^2
F_{qs^+}	0°	254	127	68	0.99
F_{qs^+}	30°	222	131	70	0.99
F_{qs^+}	60°	126	169	101	0.99
F_{imp}	0°	535	115	53	0.99
F_{imp}	30°	441	119	54	0.99
F_{imp}	60°	233	138	70	0.99

125

8.7 EFFECT OF BUILDING ORIENTATION

The shape or floor plan of the propose building and its orientation to the direction of flow are factors affecting how it will perform in a flood. In principle, compact buildings offer less resistance to flowing water and are structurally more robust.

Figure 8-12 shows a range of plan configurations that will reduce the forces of floodwater on the house. Orientating the house across the flow can reduce the clearance between houses which increases the local velocity around the house.

These matters are complex and difficult to analyse because many factors relating to the building structure and flow of water come into play. The impact of structure and water flow are also highly dependent on the individual circumstances. Conventional houses have greater limitations than other types of buildings and are only suitable for areas of relatively low velocity.

Effect of building orientation with respect to the main flow direction on quasi-static and impulsive component of the loading is shown respectively at the left and right of Figure 8-13. As expected, the loading decreases more than linearly with increasing angle of inclination of the exposed face to the main flow direction.

The ratio of the impulsive to the quasi-static loads on the front face of the building is plotted in Figure 8-14 for increasing values of h. Best fit curves in Figure 8-14 obey the expression:

$$F_{imp} = \left(a \cdot h^3 + b \cdot h^2 + c \cdot h + d \right) \cdot F_{qs+} \tag{8.8}$$

$$F_{imp} = \left(-4.8 \times 10^{-6} \cdot h^3 + 9.45 \times 10^{-4} \cdot h^2 - 4.2 \times 10^{-2} \cdot h + 1.97 \right) \cdot F_{qs+} \tag{8.9}$$

where a, b, c and d are best-fit empirical parameters. Equation (8.9) is valid in the range $20 < h < 120 cm$ and has an overall $R^2 = 0.795$. For increasing h, the impulsiveness of the loading F_{imp} / F_{qs+} initially increases to reach a maximum of 2.5 at $h = 100 cm$, but then decreases. This is probably due to the fact that for water levels exceeding $h = 100 cm$, the flux has not developed (accelerated) enough at location of the building to become critical for the stability of the building.
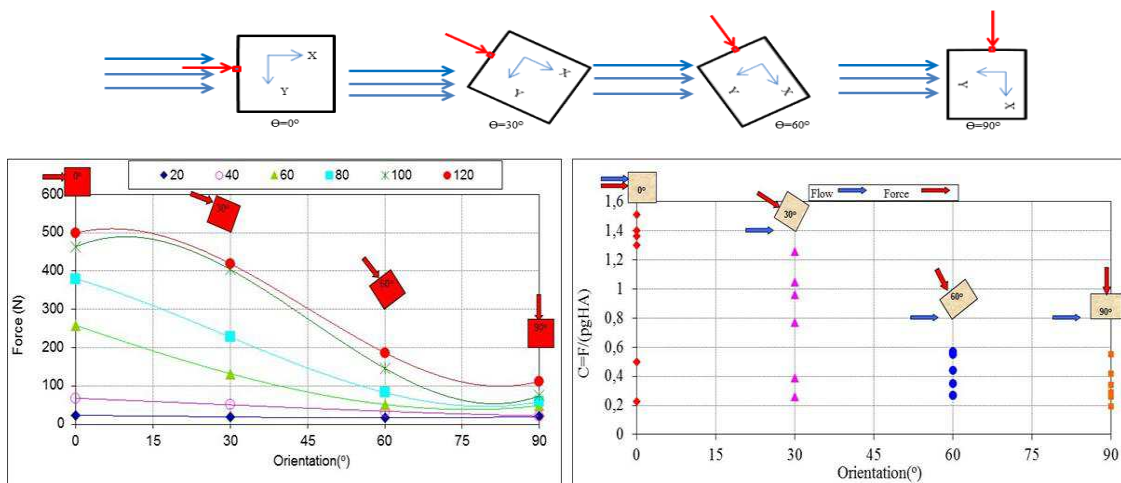
Figure 8-12 Effect of plan orientations that will reduce the forces of floodwater on the building with respect to the main flow direction.
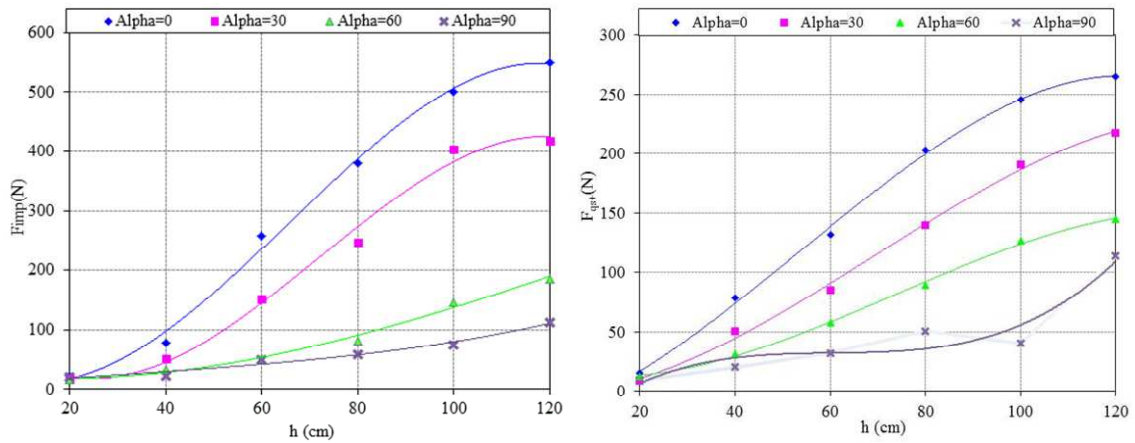
Figure 8-13. Effect of water level in the reservoir and angle of inclination of the building with respect to the main flow direction on quasi-static (right) and impulsive (left) loads.
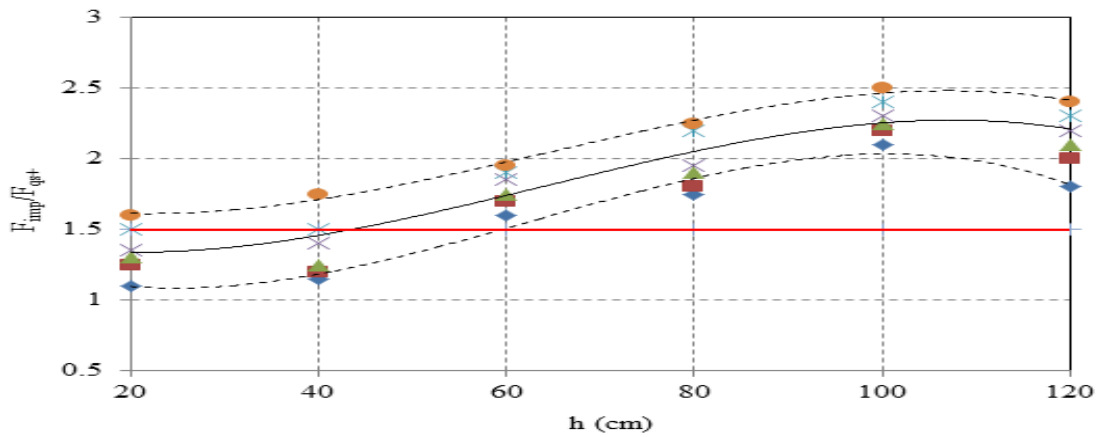
Figure 8-14. Impulsiveness of the loading as a function of the water level at rest in the reservoir. Best fit solid line obey Equation (8.8), 95% confidence bounds are also shown (dashed), together with prediction (red line) by Equation (8.6)

8.8   COMPARISON WITH PREVIOUS FINDINGS

When compared the initial result in Figure 8-11 with results from previous works, impulsive loading measured during the new set of experiments appear to be significantly higher than their corresponding quasi-static loads. In particular, Figure 8-14 shows impulsiveness ratio up to more than 2.5, confirming limitations in recommendations derived from previous studies such as that given by Equation (8.6), (also shown in Figure as a horizontal red line for comparison).

Discrepancies in the pressure between observation during the present tests and those carried out by Arnason (2005) and Nouri et al. (2007) are probably due to the difference in the dynamics of the experimental setup used in each case (see Figure 8-15). Indeed, looking at time-histories shown by previous authors, it appears likely that the experimental setup used in previous experimental work could have damped out most intense impacts as they were acting over a range of frequency higher than those corresponding to the natural frequency of vibration of the model structure.

127
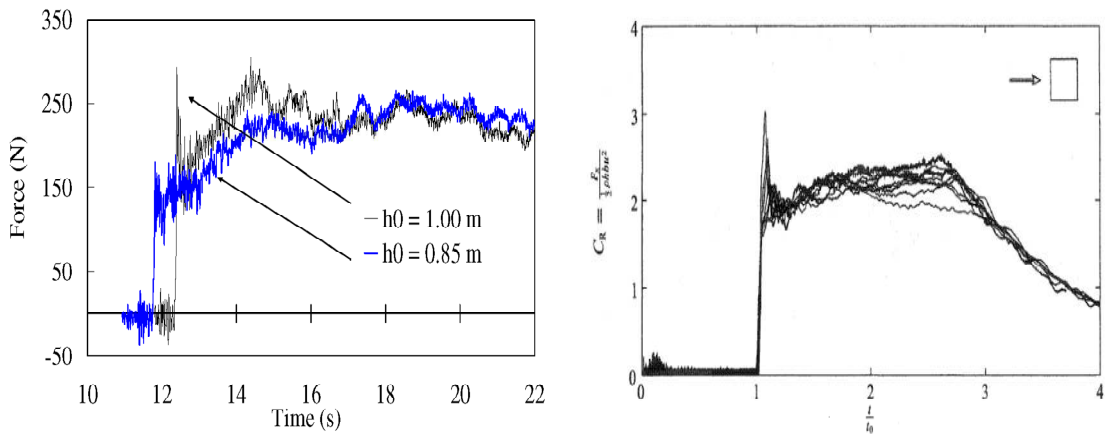
Figure 8-15. Non dimensionalized force history for the square column with one side facing in flow (Arnason, 2005), (right) and force-time history (Nouri, 2007), (left).
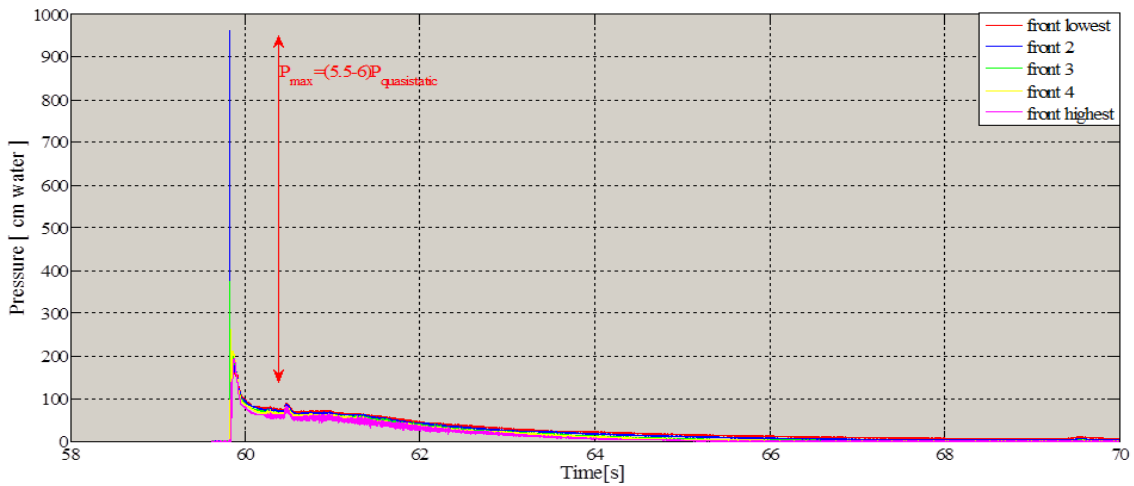
Figure 8-16. Example pressure time-history of a particularly impulsive event of an example pressure time-history of recorded during present experiments (h=120 cm)
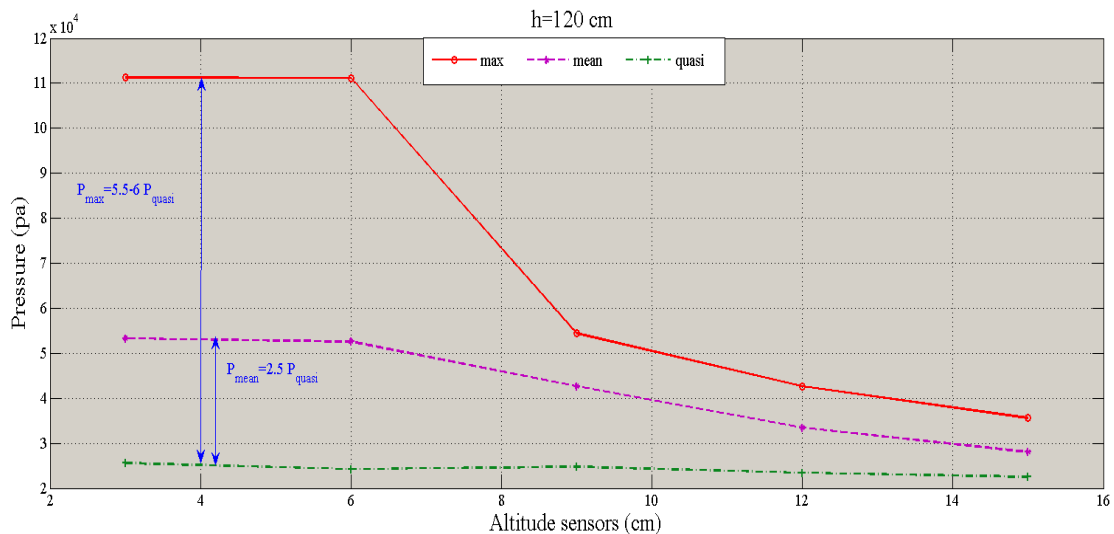
Figure 8-17. Relation between impulsive, quasi-static, dam mean value of pressure, for an example recorded during one of the laboratory experiments

128
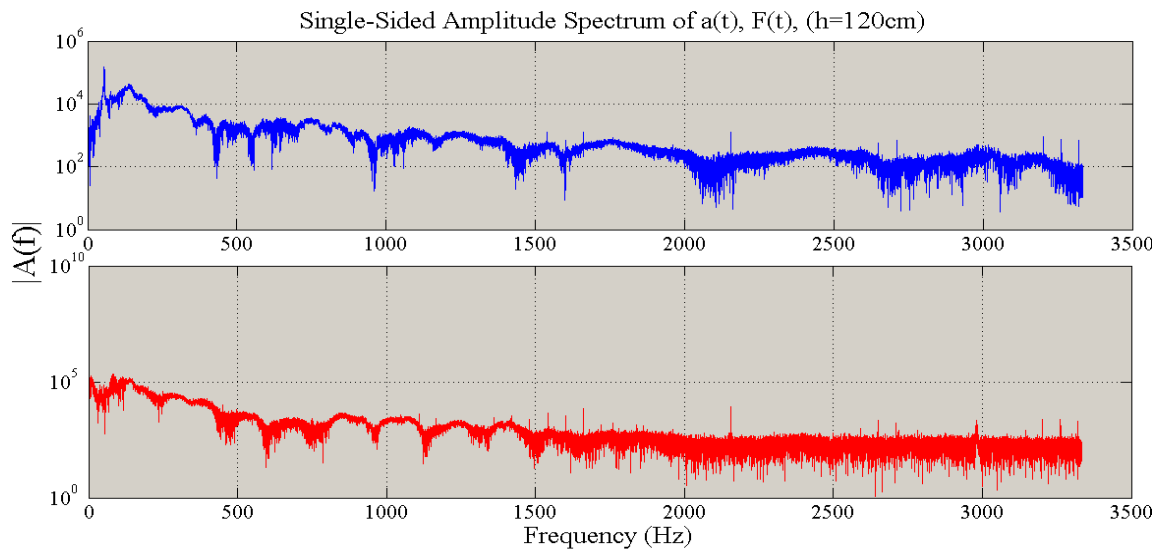
Figure 8-18. Single side amplitude spectrum of forces and accelerations time-history

8.8.1   Further Insights on Load Time -History

Further insight on the relative importance of impulsive loading on buildings can be derived by looking at pressure time-histories recorded during testing. Impulsive pressures up to 5.5-6 times their corresponding quasi-static components of the pressure sensor on different level are plotted on the Figure 8-16 and Figure 8-17. Relation between impulsive pressure and quasi-static pressure will depend on shape of pressure over height.

The dynamic response of a structure can affect the measured forces at the base in terms of magnitude and therefore, the time history of exerted forces. A typical time history of loading and acceleration observations can consist of several components. Most energetic component frequencies identified by wavelet transform of an example forces and accelerations time-history recorded during testing and plotting the single side amplitude spectrum of vibration of the buildings on Figure 8-18, and refer to Cuomo (2008).

8.9   CONCLUSIONS AND FURTHER WORK

Assessing the vulnerability of buildings in flood-prone areas is a key issue when evaluating the risk induced by flood events, especially for the strong correlation existing with loss of life during most catastrophic events. Nevertheless, while a huge effort has been devoted to the development of methodology for the definition of the hazard due to flooding, a comprehensive methodology for risk assessment of buildings subject to flooding is still missing.

Bearing this in mind, a new set of experiments have been performed at TU Delft with the aim of shedding more light on dynamics of flood-induced loads and their effects on buildings. Initial results suggest that impulsive loading might be significantly higher than those predicted by available prediction methods and should be regarded as potentially critical when assessing the vulnerability of existing structure and designing flood-proof buildings.

CHAPTER 9

Conclusions and Recommendations

The motivation behind the research presented in this thesis *Probabilistic Analysis of Failure Mechanisms of Large Dams* was to investigate the application of probabilistic methods in assessing the reliability of hydraulic structures especially dams. The work was first concentrated on interpreting data as random variables and probabilistic functions, through which uncertainties could be taken into account. Also, a framework for the reliability based model was developed in this thesis, aiming at optimizing the hydraulic structural dimensions and material properties.

Inspection tools can be considered as a primary mean that provides direct information to the end users on defects encountered by any civil engineering structures. There is a need to ensure that the design standards and criteria of dams meet contemporary requirements for operational and public safety as dams get older. If a dam is going to be constructed, then besides the safe-design concerns, cost is also an important issue. Reliability-based designs decrease the cost since risk is computed using a more realistic basis which reflects the probabilistic nature of all loading and resistance parameters. The main conclusions of this work relate to three aspects of dam failure are included below:

9.1   PROBABILISTIC ANALYSIS OF PLUNGE POOLS

- *The characteristics of plunge pool formation are the most important information during design stage in order to secure the dam spillway structure and downstream. They depend mainly on spillway operation, river morphology and natural topography of the plunge pool.*

- *A physical model is the most effective method for reproducing a comprehensive plunge pool formation and it in the plunge pool.*

o *Empirical formulas are able to predict only the ultimate scour depth and impact location, not the full extent of scour formation. However, they are useful for plunge pool pit design.*

o *For poor quality rock, the plunge pool formation is uncertain and unpredictable. Erosion can lead to serious problems of stability and outflanking of the structure. These risks increase in many ways if the structure has to be intensively used.*

o *The result of this scour erosion test is considered as an essential finding to provide hydraulic data for further investigation of scour problems and improvement of control structures, bank and downstream channel protection.*

o *statistical pattern recognition techniques have been employed to estimate the geometry of scour in plunge pools caused by high-velocity water jet impact. The results of an experimental study have been investigated considering two types of methods: (1) Deterministic method and (2) Probabilistic method. Appropriate dimensionless features have been selected using fluid mechanics concepts. Finally, the Best liner Unbiased Estimation (Minimum variance estimator) has been simplified to predict the geometry of scour hole.*

9.2   PROBABILISTIC ANALYSIS OF SUPERELEVATION

o *The main focus has been on flow and superelevation processes in curved channels using reliability modeling and mathematical expressions for evaluation of superelevation for flow in open channel bends can be obtained the equations of motion. With the aid of order of magnitude analysis based on experimental evidence, these expressions can be simplified for probabilistic methods.*

o *As water flows through a bend, a secondary circulation often develops, due to a local imbalance between the centrifugal force and the cross-channel pressure gradient. In our simulations, we have identified several parameters that influence the strength and development of the superelevation circulation.*

o *In particular, the superelevation circulation is influenced by the vertical profile of along channel velocity, the curvature of the topography, and the aspect ratio of the channel. Turbulent processes also influence the superelevation circulation. Due to the dependence on the vertical profile of along channel velocity, the superelevation is sensitive to changes in the channel topography, such as an obstruction inside the channel.*

9.3   HYDRODYNAMIC LOADINGS AFTER DAM BREAK

o *Assessing the vulnerability of buildings in flood-prone areas is a key issue when evaluating the risk induced by flood events, especially for his strong correlation with loss of life during most catastrophic events. Nevertheless, while a large effort is being devoted in the past to the development of methodology for the definition of the hazard due to flooding, where is limited insight in vulnerability of buildings.*

o *Initial results suggest that impulsive loading might be significantly higher than those predicted by available prediction methods. Impulsive loading should be regarded as potentially critical when assessing the vulnerability of existing structure and designing flood-proof buildings.*

o *Short duration impulsive loads might be important for the 1) Overall stability of buildings. 2) Resistance of structural and non-structural elements.*

o *Not accounting for impulsive loads in design and risk assessment might lead to underestimation of effective loading and thus life and economical losses.*

o *The physical model tests have been performed with the aim of: 1) Spread some lights on impulsive loads on buildings in flood prone areas. 2) Improve existing and provide designers with user friendly formulas for safe estimation of flood induced loading on buildings.*

o *The impulsive loading measured during the experiments appear to be significantly higher than their corresponding quasi-static loads. The impulsiveness ratio is more than 2.5*

o *Relative importance of impulsive pressure on buildings can be derived by looking at pressure time-histories recorded during testing. Impulsive pressures up to 5.5-6 times their corresponding quasi-static pressures were observed.*

Recommendations:

Recommendations to supplement this research are described in this section and focus on expanding the data base. Further research on superelevation this includes: increasing the number of experimental runs for different channel configuration; introducing additional radii of curvature into the study; and increasing the variety of bend angles investigated.

These modifications would enhance understanding of the controlling factors affecting superelevation. Moreover, this research has highlighted some of the weaknesses of the superelevation equation for predicting superelevation.

A good way to proceed may be to look for correlations between a limited number of parameters related to the superelevation, and the local mixing in real systems. From our studies, several promising parameters for such use can be identified. In order to obtain parameters valid for real flows, measurements in open channel flows would be needed for such studies in combination with laboratory-scale experiments and further reliability simulations.

The data collected in this investigation have led to the successful completion of the research objectives. However, further improvements could be made by expanding the dataset. An increase in the number of repetitions at each bend geometry and channel configuration would be useful in determining the experimental consistency and reliability of the results.

Failure mechanisms for dams were and are difficult to understand for engineer design. Although several knowledge gaps remain, it is expected that this thesis helps in understanding the behavior of the mechanism in reality assist in making safe decisions.

High hazard potential dams require an annual comprehensive inspection. Evaluation of the safety of existing hydraulic structures can be achieved using related information obtained from continuous monitoring.

Knowledge from literature and previous investigations documenting superelevation of open channel flows is very limited. This study has improved the understanding of some of the key factors which determine superelevation, although further research is required to improve this knowledge base.

More research is needed to improve the near real time surveillance of the dam break using monitoring data and collect data from real observations in the field.

For a better evaluation and comparison of the loads in the dam break analysis, we need to collect more data from tests in laboratory.

To better describe the dam break development, we need investigation of the 3D effects in numerical models for a more accurate dam break analysis, and flood propagation.

References

Abdi, H., (2010). The method of least squares. In N.J. Salkind., D.M. Dougherty., & B. Frey (Eds.): Encyclopedia of research design. Thousand Oaks (CA): Sage. pp. 705-708.

Ackermann, N.L., and Undan, R., (1977). Forces from submerged jets. Journal of the hydraulics division, ASCE 96(11), 2231-2240.

Almog, E., Kelham, P. and King, R,. (2011). Modes of dam failure and monitoring and measuring techniques. Environment Agency. ISBN: 978-1-84911-230-7.

Altinbilek, H.D., and Okyay. S., (1973). Localized scour in horizontal sand bed under vertical jets. Proceeding 15th congress of IAHR, Istanbul, Turkey, 99-106.

Amanian, N., (1993). Scour below a flip bucket spillway. Logan: Utah State University.

Amiri-Simkooei, A.R., (2003). Formulation of L1 norm minimization in Gauss-Markov models. Journal of Surveying Engineering, 129(1): 37–43.

Amiri-Simkooei, A.R., (2007). Least-squares variance component estimation. PhD thesis, Delft University of Technology. Delft, Netherlands, ISBN 10-90-804147-5-1.

Ananyan, A.K., (1957). Fluid flow in bends of conduits, in Russian, English translation: Israel Progress for Scientific Transl., Jerusalem 1965.

Ang, A.H.S., and Tang, W., (1994). Probability concept in engineering planning and design.Vol 1. John Wiley & Sons, New York.

Ang, A.H.S., and Tang, W., (2007). Probability concept in engineering emphasis on application to civil and environmental engineering. John Wiley & Sons, New York.

Arnason, H., (2005). Interactions between an incident bore and a free-standing coastal structure. PhD Thesis, University of Washington, 172 pages

References

Azmathullah, H.M., Deo, M.C., and Deolalikar, P.B., (2005). Neural networks for estimation of scour downstream of a ski-jump bucket. Journal of hydraulic engineering, Vol. 131, No. 10, ASCE, ISSN 0733-9429/2005/10-898–908.

Baecher, G.B., and Christian, J.T., (2003b). Reliability and statistics in geotechnical engineering. Wiley, Chichester, U.K.

Barfuss, S.L., (1988).Pre-excavation of rapped scour holes below flip bucket spillways. Civil and environmental engineering, Utah State University, Logan, Utah. 71p.

Beltaos, S., (1976). Oblique impingement of plane turbulent jets. Journal of hydraulic division, ASCE 102(9), 1177-1192.

Beltaos, S., and Rajaratnam, N., (1974). Impinging circular turbulent jets. Journal of the hydraulics division, ASCE 100(10), 1313-1328.

Blaisdell, F.W., and Anderson, C.L., (1991). Pipe plunge pool energy dissipator. Journal of hydraulic engineering, ASCE 117(3), 303-323.

Blanckaert, K. (2003). Secondary currents measured in sharp open-channel bends. Proceeding, River Flow 2002, Louvain, Belgium.

Blanckaert, K., (2002). Flow and turbulence in sharp open channel bends, PhD thesis, École polytechnic federal lausanne (EPFL), Lausanne, Switzerland.

Blanckaert, K., (2002a). Secondary currents measured in sharp open-channel bends. Proceeding River Flow, 2002, Louvain, Belgium.

Briene, M., Koppert, S., Koopman, A., Verkennis, A., 2002. Financiële onderbouwing kengetallen hoogwaterschade, NEI / Ecorys report I7435 (in Dutch).

Caraballo-Nadal, N,. Zapata-López, R., and Pagán-Trinidad, I., (2006). Building Damage Estimation due to Riverine Floods, Storm Surges and Tsunamis: A Proposed Methodology. Fourth LACCEI International Latin American and Caribbean Conference for Engineering and Technology (LACCET'2006). Mayagüez, Puerto Rico.

Chow, V. T., (1986). Open channel hydraulics. McGraw-Hill, New York.

Christian, J. T., Ladd, C. C., and Baecher, G. B., (1994). Reliability applied to slope stability analysis. J. Geotech. Eng., 120(12), 2180–2207.

Clausen, L. and Clark, P.B., (1990). The development of criteria for predicting dam break flood damages using modeling of historical dam failures. International conference on River Flood Hydraulics, pp. 369-380.

Cornell, C. A., (1972). First order analysis of model and parameter uncertainty. Proc., Int. Symposium on uncertainty in hydrologic and water resource systems, University of Arizona, Tucson, Ariz., 2:1245– 1272.

Cornell, C.A., (1969). Structural safety specifications based on second moment reliability analysis. Department of civil engineering, Massachusetts Institute of Technology, Cambridge, Mass.

References

Crassidis, J.L., Junkins, J.L., (2004). Optimal estimation of dynamic systems. Chapman &Hall/CRC, applied mathematics and nonlinear science series, ISBN 1-58488-391-X.

Cuomo, G., Allsop N.W.H. and McConnell K., (2003). Dynamic wave loads on coastal structures: Analysis of impulsive and pulsating wave loads. Proceeding of international conference on coastal structures, Portland, Oregon, USA.

Cuomo, G., Shams, G., Jonkman, S., and Van Gelder, P.H.A.J.M., (2008). Hydrodynamic loadings of buildings in floods. Proceeding of the 31th international conference on coastal structures, Hamburg, Germany.

Dean, W.R., (1927). Note on the motion of fluid in a curved pipe, Phil. Mag., S7, 4, no. 20, p. 208.

Demetracopoulos, A.C., (1994). Nonlinear-regression applied to hydrologic data,   journal of irrigation and drainage engineering-ASCE, 120: (3) 652-659 May-June.

Doddiah, D. Albertson M.L, and Thomas, R., (1953). Scour from jets. Proceeding 5th congress of IAHR, Minneapolis, Minnesota, 161-169.

Einstein, H.A., and Samni, E.A., (1949). Hydrodynamic forces on a rough wall. Review of modern physics 21(3), 520-524.

Falcon, A.M.A., (1979). Analysis of flow in alluvial channel bends, Ph. D. thesis, University of Iowa, Iowa, USA.

FEMA 549., (2006). Hurricane Katrina in the Gulf Coast. Building performance observations, recommendations, and technical guidance.

FEMA 646., (2008). Guidelines for design of structures for vertical evacuation from tsunamis.

FEMA., (2007). Federal guidelines for dam safety. www.fema.gov/hazard/damfailure.

FERC., (2002), Engineering guidelines for the evaluation of hydropower projects, Chapter III gravity dams. www.ferc.gov/industries/hydropower/safety/ guidelines/eng.

Fishman, G.S., (1995). Monte carlo: concepts, algorithms, and applications. Springer, New York.

Flannery. B. P., Teukolsky. S. A., and Vetterling. W. T., (1992). Numerical recipes. Cambridge University. Press, New York.

Goda, Y., (1974). New wave pressure formulae for composite breakwater. Proceeding of 14th ICCE, Copenhagen, Denmark, pp1702-1720. ASCE New York.

Gottlib, L., (1976). Three-dimensional flow pattern and bed topography in meandering channels, Hydrodynamic and hydraulic engineering. University of Technology Denmark, Series Paper 11.

Haehnel, R. H. and Daly S. F., (2002). Maximum impact force of woody debris on floodplain structures, US Army Corps of Engineers, Cold Regions Research and Engineering Laboratory, Report ERDC/CRREL TR-02-2.

Haffmans, G.J.C.M. & Booij, R., (1993). The influence of upstream turbulence on local scour holes. Proceeding of 25th IAHR congress, Tokyo, Japan.

Haffmans, G.J.C.M. & Verheij, H.J., (1997). Scour manual. Balkema, Rotterdam, The Netherlands.

Haffmans, G.J.C.M. & Verheij, H.J., (2009). Closure problem to jet scour. Journal of hydraulic research 47(1):100-109.

Haffmans, G.J.C.M. & Verheij, H.J., (2011). Jet scour. Proceedings of the institute of civil engineers, Maritime engineering, Volume 164, Issue MA4, 185-193.

Harrington, B,. (2012). Dam Break Analysis & Hazard Classifications. Maryland Dam Safety, Maryland, United State.

Hartford, D.N.D., and Baecher, G. B., (2004). Risk and uncertainty in dam safety. Tomas telford limited, Great Britan. ISBN: 0 7277 3270 6.

Hasofer, A. M., and Lind, N., (1974). Exact and invariant second-moment code format. Journal of engineering mechanics. 100(1), 111–121.

Heller, V., Hager, W.H,. and Minor, H.E., (2005). Ski jump hydraulics. Journal of hydraulic engineering. Volume 131, Issue 5, pp. 347-355.

Henderson. F.M., (1989). Open channels flow. Prentice-Hall, New Jersey, chapter 7.

Henley, E. J., and Kumamoto, H., (1981). Reliability engineering and risk assessment. Prentice-Hall, Englewood Cliffs, N.J. Haffmans, G.J.C.M., (1992). Two dimensional mathematical modeling of local scour holes. Doctoral thesis, Delft University of Technology, Delft, The Netherlands.

Hepler, T,. (2011). Overtopping Protection for Concrete Dams. National Dam Safety Program, Technical Seminar No. 20.

ICOLD., (1993). Bulletin 88: Rock foundations for dams. International Commission on large dams, Paris.

ICOLD., (1995). Bulletin 99: Dam failures. Statistical Analysis. International Commission on large dams, Paris.

ICOLD., (1997). Bulletin 109: Dams less than thirty meters high. International Commission on large dams, Paris.

ICOLD., (1998). Bulletin 111: Dam-break flood analysis. International Commission on large dams, Paris.

Ikeda, S., (1975). On secondary flow and bed profiles in alluvial curved open channels, Proceeding 16th IAHR Congress, Sao Paulo, Brazil, paper B14.

Ippen, A.T., and Drinker, P.A., (1962). Boundary shear stresses in curved trapezoidal channels, Proceeding of Journal hydraulic division, HY5, Part I, Vol 88, pp. 143 – 179.

IWPCO., (2006). Iran Water and Power Resources Development Co. www.iwpco.ir.

Johanston, A.J., (1990). Scour hole developments in shallow tailwater. Journal of hydraulic research 28(3), 341-354.

References

Jonkman S.N., Bockarjova M., Kok M., Bernardini P., 2008. Integrated hydrodynamic and economic modeling of flood damage in the Netherlands. Ecological Economics 66, pp. 77-90.

Jonkman, SN., Kok, M., Van Ledden, M., Vrijling, JK., (2008). Risk based design of flood defenses system- A preliminary analysis for the new Orleans metropolitan area. 4th International Symposium on Flood Defence: Managing Flood Risk, Reliability and Vulnerability.Toronto, Ontario, Canada, May 6-8, 2008

Kalwijk, J.P.T.H., & Vriend, H.J. DE., (1980). Computation of the flow in Shallow River bends, Journal of Hydraulic Research., 18, no. 4, p. 327.

Kawata Y. et al., (2005). Comprehensive analysis of the damage and its impact on coastal zones by the Indian Ocean tsunami disaster.

Kelman, I., Spence, R., (2004). An overview of flood actions on buildings. Journal of Engineering Geology, 73 (3-4), 297–309

Khatsuria, R.M., (2005). Hydraulics of spillways and energy dissipators. New York. Dakker, ISBN 0-8247-5789-0

Kobus, H., Leister, P., and Westrich, B., (1979). Flow field and scouring effects of steady and pulsating jets impinging on a movable bed. IAHR, Journal of hydraulic research 17(3), 175-192.

Krhoda, G.O., (1985). Flow behaviour in model open channel bends and implications for lateral migration in river. PhD thesis in Simon Fraser University, Vancouver, Canada.

Leschziner, M. & Rodi, W., (1979). Calculation of strongly curved open channel flow, Journal of hydraulic division, ASCE, Vol. 105, No. HY10, p. 1297.

Lopardo, R.A., Lopardo, M.C., and Casado, J.M., (2002). Local rock scours downstream large dams. Proceeding international workshop on rock scour due to high velocity jets, Lausanne, Switzerland, 55–58.

Manso, P. A., (2006). The influence of pool geometry and induced flow patterns on rock scour by high-velocity plunging jets. PhD thesis, Ecole Polytechnique Federal de Lausanne (EPFL). Lausanne, Switzerland.

Manso, P. A., Bollaert, E, F, R., and Schleiss, A, J., (2009). Influence of Plunge Pool Geometry on High-Velocity Jet Impact Pressures and Pressure Propagation inside Fissured Rock Media. Journal of Hydraulic Engineering, Vol. 135, No. 10, October 1, 2009. ©ASCE, ISSN 0733- 9429/2009/10-783–792

Marengo, H., (2006). Case Study: Dam safety during construction, Lessons of the overtopping diversion works at aguadilla dam. Journal of hydraulic engineering, 132(11), ASCE, 1121-1127.

Mason, P. J., and Arumugam, K., (1985). Free jet scours below dams and flip buckets. Journal of hydraulic engineering. 111(2), 220–235.

Mason, P.J., (1989). Effect of air entrainment on plunge pool scour. ASCE, Journal of hydraulic engineering.

Mason, P.J., Mice, M., (1984). Erosion of plunge pools downstream of dams due the action of free trajectory jets. Proceeding institute of civil engineers, Part 1, 523-537.

McCuen, R.H., Leahy, R.B., and Johnson, P.A., (1990). Problems with logarithmic transformations in regression. Journal of hydraulic engineering. ASCE, 116(3) 414-428.

Mih, W.C., and Hoopes, J.A., (1972). Mean and turbulent velocities for plane jet. Journal of the hydraulics division, ASCE 98(7), 1275-1294.

Modarres, M., Kaminskiy. M., and Krivtsov. V., (1999). Reliability engineering and risk analysis: A practical guide, Marcel Dekker, New York, N.Y.

Morison, J.R., O'Brien, M.P., Johnson J.W. and Schaaf, S.A., (1950). The force exerted by surface waves on piles, Trans. Am. Inst. Min. Engrs. 189 (1950), pp. 149–154.

N.C.D.E.N.R., (2007). Dam operation, maintenance and inspection manual. North Carolina Department of Environment and Natural Resources Division of Land Resources, Land Quality Section, North Carolina, United State.

Nouri Y., Nistor Y., Palermo D. and Saatcioglu M., (2007). Structural analysis for tsunami-induced force and debris impact. Proceeding of international conference in coastal structures 2007, Venice, Italy.

Novak, P., Mofta, A.I.B., Nalluri. C., and Narayanan, R., (2001). Hydraulic structures. Spon Press, Taylor & Francis Group, London and New York.

Oumeraci, H., Kortenhaus, A., Allsop, N.W.H., De Groot, M.B., Crouch, R.S., Vrijling, J.K. & Voortman, H.G., (2001). Probabilistic design tools for vertical break waters. ,Balkema, Rotterdam (392 pp).

Pistrika, A.K., Jonkman, S.N., (2009). Damage to residential buildings due to flooding of New Orleans after hurricane Katrina. Natural Hazards. Vol. 54 Issue 2, pp. 413-434.

Pratap, V.S. & Splanding, D.B., (1975). Numerical computation of the flow in curved ducts, Aeron. Quart., 26, part. 3, p. 219.

Rajabalinejad, M.R., (2009). Reliability methods for finite element models. PhD thesis, Delft University of Technology. Delft, The Netherlands, ISBN 978-1-58603-991-2.

Rajaratnam, N. and Beltaos, S., (1977). Erosion by impinging circular turbulent jets. Journal of the hydraulics division, ASCE 103(10), 1191-1205.

Rajaratnam, N., (1981). Erosion by plane turbulent jets. Journal of the hydraulic research, International association for hydraulics research 19(4), 339-358.

Rajaratnam, N., (2002). Erosion by submerged circular jets. Journal of hydraulic engineering. ASCE, 108(HY2), 262-267, 1982.

Rajaratnam, N., and Berry, B., (1977). Erosion by circular turbulent wall jets. Journal of the hydraulic research, International association for hydraulic research, Delft, The Netherlands, 277-289.

Rajaratnam, N., and Mazurek, K. A., (2002). Erosion of a polystyrene bed by obliquely impinging circular turbulent air jets. Journal of Hydraulic Research, 40(6), 709–716.

Rajaratnam, N., and Pani, B.S., (1974). Three dimensional turbulent wall jets. Journal of the hydraulics division, ASCE 100(1), 69-83.

Ramsden, J.D., (1993). Tsunamis: forces on a vertical wall caused by long waves, bores and surges on a dry bed. PhD thesis, California Institute of Technology, Pasadena, California, Report No. KH-R-54

Ranga Raju, K.G., (1981). Flow through open channels. Tata McGrow-Hill Publishing Company Limited, New Dehli.

Reinauer, R., and Hager, W.H., (1997). Supercritical bend flow. Journal of hydraulic engineering, 123(3), ASCE, 208-218.

Rozowskii, I.L., (1957). Flow of water in bends of open channels, in Russian, English translation: Israel Progress for Scientific Transl., Jerusalem 1961.

Schiereck, G.J., (2001). Introduction to Bed, bank and shore protection. Delft University of Technology. Delft, The Netherlands. ISBN 90-407-1683-8.

Schleiss, A, J., and Bollaert, E, F, R., (2002). Rock scour due to falling high velocity jets. Proceedings of the international workshop, Lausanne, Switzerland.

Shams, G.R. (1998). Superelevation in open channel bends. MS Thesis, Amirkabir University (Tehran polytechnic)., Tehran, Iran.

Shams, G.R., Van Gelder, P.H.A.J.M., and Vrijling, J. k., (2008). Probabilistic Description of scour hole downstream of flip bucket spillway of large dams. Technical Proceeding, International Conference on Dam and Water for Future (ANCOLD), Gold Coast, Australia.

Shams, G.R., Van Gelder, P.H.A.J.M., and Vrijling, J. k., (2008). Evaluation of superelevation in open channel bends with probabilistic analysis methods. World Environmental and water resources congress, Ahupua'a, EDITED BY Roger W. Babcock, Jr., Ph.D., P.E., Raymond Walton, Ph.D., P.E., Published by the American society of civil engineers, May 12–16, 2008. Honolulu, Hawaii.

Shukry, A., (1950). Flow around bends in an open flume. Transactions, American society of civil engineering, Vol. 115, pp.751-779.

Simons, D.B., and Senturk, F., (1977). Sediment transport technology. Water resources publications, Fort Collins, Colorado. 807p.

Sobey, R.J., Johanston, A.J, and keane, R.D., (1988). Horizontal round buoyant jet in shallow water. Journal of hydraulic engineering, ASCE 114(8). 910-929.

Son, K.I., (1992). Scour mechanism of large cohesion less bad materials under inclined submerged circular jet. Civil and environmental engineering, Utah State University, Logan, Utah. 158p.

Spendier, K., (2011). Dimensional Analysis, University of Colorado. Physics department. Colorado, United State,

Takahashi, S., Tanimoto, K. and Shimosako, K., (1994). A proposal of impulsive pressure coefficient for the design of composite breakwaters. Proceeding of Hydro-Port '94, Port and harbour research institute, pp 489-504.

Teunissen, P. J. G., (2000). Adjustment theory: An introduction, in series on mathematical geodesy and positioning. TU Delft, The Netherlands.

Teunissen, P. J. G., Simons, D.G., and Tiberius, C.C.J.M., (2005). Probability and observation theory. Publication of the faculty of aerospace engineering, AE2-E01, TU Delft, The Netherlands.

Teunissen, P.G. and Amiri-Simkooei, A.R., (2007). Least-squares variance component estimation. Journal of Geodesy. doi 10.1007/s00190-007-0157-

Thandaveswara, B.S., (1969). Characteristics of flow around a 90° open channel bend. M.Sc Engineering Thesis, Department of Civil and Hydraulic Engineering, Indian Institute of Science, Bangalore - 12, May 1969.

Tung, Y. K., and Mays, L. W., (1980). Risk analysis for hydraulic design. Journal of Hydraulic Division. American Society Civil Engineering, 106(5), 93–913.

U.S Bureau of Reclamation., (1977). Design of small dams. Second edition, revised reprint, Denver, Colorado, 816p.

U.S Bureau of Reclamation., (2003). Dam safety risk analysis methodology. Technical service center. Version 3.31, Denver, Colorado.

U.S. Corps of Engineers., (1970). Hydraulic design criteria. Revised 1-64, sheet 112-8, Prepared by U.S Army Engineer, Waterways experiment station, Vicksburg, Mississippi.

United Nation., (2000). Sustainable flood prevention. Economic commission for Europe, second meeting, The Hage, Netherlands

Van Bendegom, L., (1963). Some considerations on river morphology and river improvement, De Ingenieur, 59, no. 4, p. Bl-11, in Dutch, English translation: Nat. Res. Council of Canada, Tech. Transl. 1054.

Van der Heijden, F. and Duin, R.P.W. and de Ridder, D. and Tax, D.M.J., (2004) Classification, parameter estimation and state estimation: an engineering approach using matlab. John Wiley & Sons, Ltd, Chichester. ISBN 978-0-470-09013-8.

Van Gelder, P.H.A.J.M., (1996b). How to deal with wave statistical and model uncertainties in the design of vertical breakwaters. In H.G. Voortman, editor, Probabilistic Design Tools for Vertical Breakwaters; Proceedings Task 4 Meeting, Hannover, Germany, pages 1-13.

Van Gelder, P.H.A.J.M., (2000). Statistical methods for the risk-based design of civil structures. PhD thesis, TU Delft. Delft, The Netherlands, ISBN 90-9013452-3.

Van Gelder, P.H.A.J.M., Nadim, F., and Guedes Soares, C., (2010). Risk assessment of natural hazards with applications to landslides and abnormal waves. Safety and Reliability of Industrial Products, Systems and Structures – Guedes Soares (ed) © 2010 Taylor & Francis Group, London, ISBN 978-0-415-66392-2.

Van Gelder, P.H.A.J.M., Vrijling J.K., (2008). Probabilistic Design, Encyclopaedia of Quantitative Risk Assessment, (EQRAA), John Wiley & Sons, Ltd, Chichester.

Vanoni, V.A., (1975). Sedimentation engineering. ASCE Manual and reports on engineering practice No. 54.

Vischer, D. L., and Hager, W. H., (1998). Dam hydraulics, Wiley, Chichester, England.

Vriend, H.J. DE & Koch, F.G., (1978). Flow of water in a curved open channel with a fixed uneven bed, TOW report. R657-V/M1415-I, Delft Hyd. Lab. Delft University of Technology., Delft, the Netherlands.

Vriend, H.J. DE., (1973). Theory of viscous flow in curved shallow channels, Communications on Hydraulics 73-1, Department of Civil Engineering. Delft University of Technology. Delft, the Netherlands.

Vriend, H.J. DE., (1976). A mathematical model of steady flow in curved shallow channels, Communications on Hydraulics 76-1, Department of Civil Engineering. Delft University of Technology. Delft, The Netherlands.

Vriend, H.J. DE., (1978). Developing laminar flow in curved rectangular channels, Internal Report 2-78, Laboratory of fluid mechanics, Department of Civil Engineering. Delft University of Technology., Delft, the Netherlands.

Vriend, H.J. DE., (1979). Flow measurements in curved rectangular channels, Internal Report 9-79, Laboratory of fluid mechanics, Department of Civil Engineering, Delft University of Technology. Delft, The Netherlands.

Vriend, H.J. DE., (1981 a). Steady flow in shallow channel bends, Communications on hydraulics 81-3, Department of Civil Engineering., Delft University of Technology., Delft, the Netherlands.

Vriend, H.J. DE., (1981 b). Flow measurements in curved rectangular channels; Part II rough bottom, Internal Report 5-81, Laboratory of fluid mechanics., Department of civil engineering., Delft University of Technology., Delft, the Netherlands.

Vriend, H.J., (1977). A mathematical model of steady flow in curved shallow channels. Journal of hydraulic research., IAHR, 15(1), 37-54.

Vrijling, J.K. and Bruinsma J., (1980). Hydraulic boundary conditions. Proceeding International on hydraulic aspects of coastal structures; Developments in hydraulic engineering related to the design of the oosterschelde storm surge barrier in the Netherlands. Editors: A. Paape, J. Stuip, W.A.Venis, Delft University of Technology Press 1980, 109-133, ISBN 90-6275-0540, Delft, The Netherlands.

Vrijling, J.K., (1996). Probability in civil engineering. Delft University of Technology Press. Delft, The Netherlands.

Vrijling, J.K., (2001). Probabilistic design of water defence systems in the Netherlands. Journal of reliability engineering & system safety, 74(3), 337-344.

Vrijling, J.K., (2003). Safe dams and dikes, how safe? Dams and dikes in development, Proceedings Editors: H. Van Duivendijk, B. Schultz, C.J. VanWesten. 43-56.

Vrijling, J.K., P.H.A.J.M., (2002). Probabilistic design in hydraulic engineering. Delft University of Technology Press. Delft, The Netherlands.

Wang, S., (1987). Scouring of river beds below sluices and dams. Design of Hydraulic Structures. Proceeding international symposium on design of hydraulic structures, Colorado State University. Fort Collins, Colo., 295–304.

Wang, T.W., and Cheng, C.W., (1990). Maximum scour below dams caused by over fall flow. Proceeding of international conference, ASCE, Vol (1), 275-280.

Westberg, M., (2007). Reliability-based evaluation of concrete dams. PhD thesis, Lund University. Sweden. Report TVBK-1033, ISSN 0349-4969, ISRN: LUTVDG/TVBK-1033/07-SE (228).

Westich, B., and Kobus, H., (1973). Erosion of a uniform sand bed by continuous and pulsating jets. Proceeding 15th congress of IAHR, Istanbul, Turkey, 99-106.

Woodward, S.M., and Posey, C.J., (1941). Hydraulic of steady flow in open channels. John Wiley & Sons, New York.

Yang, C., Lin, B,. Jing C., and Liu, Y., (2010). Predicting near-field dam-break flow and impact force using a 3D model. Journal of Hydraulic Research (IAHR), Vol. 48, No. 6 (2010), pp. 784–792

Yanmaz, A.M., (2003). Reliability simulation of scouring downstream of outlet facilities, Turkish. Journal of engineering & environmental science. 65-7127.

Yanqing, L. and Yen, B. C., (2003). Comparison of risk calculation methods for a culvert. Journal of hydraulic engineering. Vol 129(2), 140-152.

Yen, B. C., and Tung, Y. K., (1993). Some recent progress in reliability analysis for hydraulic design. Reliability and uncertainty analysis in hydraulic design, B. C. Yen and Y. K. Tung, eds., ASCE, Reston, VA., 35–79.

Yen, B. C., Cheng, S. T., and Tang, W. H., (1980). Reliability of hydraulic design of culverts. Proceeding international conference on water resources development, IAHR, Asian Pacific Division. 2nd Congress, Taipei, Taiwan, 2, 991– 1001.

Yen, C.L., (1967). Bed configuration and characteristics of subcritical flow in a meandering channel, PhD. Thesis University of Iowa, Iowa City, USA.

Yildiz, D., and Üzücek, E., (1994). Prediction of scour depth from free falling flip bucket jets. Journal of Water power dam construction, 46(11), 50–56.

Zebell, D, A,. (2012). Overtopping Protection: How to Turn Your Dam Embankment into an Emergency Spillway. Proceeding of 51 Annual Association of Conservation Engineers (ACE) Conference. Chesterton, Indiana, United State.

Online Reference

[1]. http://www.aquavision-eng.ch/EN/Gebidem Dam_Scour.html

[2]. http://www.pakistanpaedia.com/mega/tarbela/pic_tarbela_spillway-1.gif

[3]. http://mw2.google.com/mw-panoramio/photos/medium/54190344.jpg

[4]. http://www.delange.org/RooseveltLake/Dsc00096.jpg

[5]. http://www.ideers.bris.ac.uk/shaken/taiwan_dam.html

[6]. http://firelink.monster.com/news/articles/14705-immediate-danger-has-passed-after-catastrophic-dam-break

[7]. http://web.mst.edu/rogersda/dams_of_ca/

[8]. http://www.usbr.gov/pn/about/Teton.html

[9]. http://www.mathalino.com/reviewer/fluid-mechanics-and-hydraulics/analysis-gravity-dam

List of Figures

List of Tables

Appendices

Appendix. 1.A.

Based on the P$_i$ Theorem and equations (6.4), (6.5) and (6.6), the scour equations are given as follows:

$$\frac{d_s}{d_w} = 9.02 \, (Fr)^{0.8968} (\frac{H_1}{d_w})^{0.0089} (\frac{R}{d_w})^{-0.2604} (\frac{d_{50}}{d_w})^{0.0801} (\sin\theta)^{0.5009} \tag{6.4}$$

By using the law of Torricelli : $\qquad V = \sqrt{2gH_1}$

where the discharge is defined with b_u as the thickness of the jet as: $\quad q = b_u V$

Rewriting Eq. (6.4) the scour depth is proportional to:

$$\frac{d_s}{d_w} \propto (\frac{q}{\sqrt{g.d_w^3}})^{0.8968} (\frac{V^2}{2gd_w})^{0.0089} (\frac{R}{d_w})^{-0.2604} (\frac{d_{50}}{d_w})^{0.0801} (\sin\theta)^{0.5009}$$

$$\frac{d_s}{d_w} \propto (\frac{b_u V}{\sqrt{g.d_w^3}})^{0.8968} (\frac{V^2}{2gd_w})^{0.0089} (\frac{R}{d_w})^{-0.2604} (\frac{d_{50}}{d_w})^{0.0801} (\sin\theta)^{0.5009}$$

$$\frac{d_s}{d_w} = 9.02 f\left(R, d_{50}, \theta\right) \cdot \left(\frac{b_u^{0.8968} V^{0.9146}}{2^{0.0089} g^{0.4573} d_w^{1.1738}} \right)$$

$$d_s \propto \sqrt{\frac{qV}{g}}.C_{A.d_s} \quad \text{with} \quad C_{A,d_s} = 9.02 f\left(R, d_{50}, \theta\right) \cdot C_{d-scour}$$

where: $C_{d-scour} = \left(\dfrac{b_u^{0.3968} g^{0.0427}}{2^{0.0089} V^{0.0854} d_w^{0.1738}} \right)$

Although the parameter C_{scour} depends on the width of the jet, the flow velocity and the tail water depth C_{scour} can be considered as a constant (the exponents 0.3968, 0.0854 and 0.1738 are about zero).

$$\frac{L_s}{d_w} = 7.191 \, (Fr)^{0.3549} (\frac{H_1}{d_w})^{0.3699} (\frac{R}{d_w})^{0.1142} (\frac{d_{50}}{d_w})^{0.0277} (\sin\theta)^{0.2742} \tag{6.5}$$

Rewriting Eq. (6.5) the scour length is proportional to:

$$\frac{L_s}{d_w} \propto (\frac{q}{\sqrt{g.d_w^3}})^{0.3549} (\frac{V^2}{2gd_w})^{0.3699} (\frac{R}{d_w})^{0.1142} (\frac{d_{50}}{d_w})^{0.0277} (\sin\theta)^{0.2742}$$

$$\frac{L_s}{d_w} \propto (\frac{b_u V}{\sqrt{g.d_w^3}})^{0.3549} (\frac{V^2}{2gd_w})^{0.3699} (\frac{R}{d_w})^{0.1142} (\frac{d_{50}}{d_w})^{0.0277} (\sin\theta)^{0.2742}$$

$$L_s \propto \sqrt{\frac{qV}{g}} . C_{A.L_s} \quad \text{with} \quad C_{A,L_S} = 7.191 f\left(R, d_{50}, \theta\right) \cdot \left(\frac{V^{0.095}}{2^{0.3699} g^{0.0474} d_w^{0.0438} b_u^{0.1451}} \right)$$

where: $C_{L-scour} = \left(\dfrac{V^{0.095}}{2^{0.3699} g^{0.0474} d_w^{0.0438} b_u^{0.1451}} \right)$

$$\frac{W_s}{d_w} = 4.48 \, (Fr)^{0.0807} (\frac{H_1}{d_w})^{0.5621} (\frac{R}{d_w})^{0.1675} (\frac{d_{50}}{d_w})^{0.1304} (\sin\theta)^{-0.0703} \tag{6.6}$$

Rewriting Eq. (6.6) the scour width is proportional to:

$$\frac{W_s}{d_w} = 4.48 \, (\frac{q}{\sqrt{g.d_w^3}})^{0.0807} (\frac{V^2}{2gd_w})^{0.5621} (\frac{R}{d_w})^{0.1675} (\frac{d_{50}}{d_w})^{0.1304} (\sin\theta)^{-0.0703}$$

$$\frac{W_s}{d_w} = 4.48 (\frac{b_u V}{\sqrt{g.d_w^3}})^{0.0807} (\frac{V^2}{2gd_w})^{0.5621} (\frac{R}{d_w})^{0.1675} (\frac{d_{50}}{d_w})^{0.1304} (\sin\theta)^{-0.0703}$$

$$W_s \propto \sqrt{\frac{qV}{g}} . C_{A.W_S} \quad \text{with} \quad C_{A,W_S} = 4.48 f\left(R, d_{50}, \theta\right) \cdot \left(\frac{V^{0.205} d_w^{0.01895}}{2^{0.5621} g^{0.1025} b_u^{0.4195}} \right)$$

where: $C_{W-scour} = \left(\dfrac{V^{0.205} d_w^{0.01895}}{2^{0.5621} g^{0.1025} b_u^{0.4195}} \right)$

Appendix. 1.B. Data collection used for prediction of geometry of plunge pool. This data relates to the measurements of scour parameters at the Central Water and Research Station (CWPRS), Pune, India and reported by Azmathullah, 2005.

Row	Fr	H_1/d_w	R/d_w	d_{50}/d_w	θ	Gs	d_s/d_w	L_s/d_w	W_s/d_w	d_w	d_s
1	0.799	3.049	2.4	0.024	0.472	2	3.299	6.668	5.099	0.1667	0.55
2	0.519	6.203	1.765	0.009	0.612	2	1.06	8.483	3.696	0.23	0.2439
3	0.463	9.512	4.06	0.013	0.698	2	1.497	13.468	6.133	0.15	0.2246
4	3.896	37.76	13.533	0.067	0.612	2	3.76	32.69	54.333	0.03	0.1128
5	0.121	8.035	3.588	0.012	0.698	2	0.741	5.739	5.412	0.17	0.1259
6	0.457	7.686	1.087	0.009	0.612	2	1.544	8.154	6.418	0.2337	0.3608
7	0.354	8.841	3.813	0.013	0.698	2	1.201	10.861	5.75	0.16	0.1922
8	1.347	12.255	6.294	0.28	0.524	2	4.259	24.371	20.979	0.0286	0.1218
9	0.663	4.844	2.038	0.116	0.524	2	3.435	10.48	8.734	0.0687	0.236
10	0.026	4.58	1.735	0.009	0.612	2	0.326	2.454	6.966	0.234	0.0762
11	0.518	7.588	2.256	0.011	0.612	2	0.932	8.13	4.722	0.18	0.1677
12	0.338	5.246	1.532	0.008	0.612	2	0.817	6.212	3.208	0.265	0.2165
13	0.167	7.723	3.389	0.011	0.698	2	0.825	7.961	5.111	0.18	0.1485
14	3.109	13.381	4.895	0.28	0.524	2	12.133	26.224	20.979	0.0286	0.347
15	0.362	4.518	2.62	0.116	0.524	2	1.294	7.278	8.734	0.0687	0.0889
16	0.206	2.991	1.4	0.05	0.524	2	1.235	5.3	6.5	0.1	0.1235
17	0.06	5.033	1.888	0.009	0.612	2	0.482	3.333	5.721	0.215	0.1037
18	0.505	4.64	2.038	0.116	0.524	2	2.342	9.17	8.734	0.0687	0.1609
19	0.457	7.686	1.087	0.009	0.78	2	1.544	8.861	6.418	0.2337	0.3608
20	1.646	8.412	3.204	0.183	0.524	2	7.41	16.018	13.73	0.0437	0.3238
21	0.038	7.537	3.427	0.011	0.698	2	0.288	2.912	5.169	0.178	0.0512
22	0.857	14.906	4.511	0.022	0.612	2	0.949	10.162	9.444	0.09	0.0854
23	0.064	4.369	1.624	0.008	0.612	2	0.439	3.512	6.52	0.25	0.1098
24	0.457	7.686	1.087	0.009	0.174	2	1.283	6.197	6.418	0.2337	0.2998
25	0.42	5.704	1.637	0.008	0.612	2	0.934	7.622	3.427	0.248	0.2317
26	4.634	34.945	12.303	0.061	0.612	2	3.542	30.797	49.394	0.033	0.1169
27	0.457	7.686	1.087	0.009	0.523	2	1.283	9.174	6.418	0.2337	0.2998
28	0.713	7.675	2.288	0.183	0.524	2	3.112	11.327	14.874	0.0437	0.136
29	0.166	7.723	3.389	0.011	0.698	2	0.825	7.961	5.111	0.18	0.1485
30	1.881	12.549	8.741	0.28	0.567	2	5.741	22.727	22.727	0.0286	0.1642
31	0.112	4.486	1.21	0.008	0.612	2	0.449	3.831	6.573	0.248	0.1113
32	0.663	4.844	3.639	0.044	0.567	2	2.579	10.189	9.461	0.0687	0.1772
33	0.378	3.015	2.5	0.08	0.567	2	1.516	6.7	6.5	0.1	0.1516
34	0.378	3.015	2.5	0.02	0.567	2	2.135	6.5	6	0.1	0.2135
35	3.109	13.381	8.741	0.28	0.567	2	10.787	28.671	22.727	0.0286	0.3085
36	0.505	4.64	3.639	0.116	0.567	2	2.084	9.316	9.461	0.0687	0.1432
37	0.206	2.991	2.5	0.08	0.567	2	0.512	4.55	6.5	0.1	0.0512
38	0.288	2.875	3	0.02	0.612	2	1.57	5.5	6.5	0.1	0.157
39	0.877	7.363	3.836	0.014	0.611	2	2.603	12.603	14.11	0.146	0.38
40	0.292	6.61	3.836	0.014	0.611	2	1.986	9.178	10.685	0.146	0.29
41	1.169	7.74	3.836	0.014	0.611	2	2.74	13.973	11.301	0.146	0.4
42	0.584	7.055	3.836	0.014	0.611	2	2.329	12.329	12.192	0.146	0.34
43	1.169	10.096	3.836	0.014	0.611	2	2.877	15.342	14.658	0.146	0.42
44	0.877	10.171	3.836	0.014	0.611	2	2.74	14.685	14.384	0.146	0.4
45	0.292	10.308	3.836	0.014	0.611	2	1.986	12.603	12.329	0.146	0.29
46	0.584	10.274	3.836	0.014	0.611	2	2.521	15.342	13.699	0.146	0.368
47	1.881	12.549	6.294	0.28	0.524	2	6.031	22.727	22.727	0.0286	0.1725

Row	Fr	H_1/d_w	R/d_w	d_{50}/d_w	θ	Gs	d_s/d_w	L_s/d_w	W_s/d_w	d_w	d_s
48	1.307	8.188	3.204	0.183	0.524	2	4.833	16.247	14.874	0.0437	0.2112
49	0.476	3.113	1.4	0.08	0.524	2	2.459	6	6.5	0.1	0.2459
50	0.288	2.875	1.8	0.08	0.524	2	1.297	6.3	6.5	0.1	0.1297
51	1.307	8.188	4.577	0.183	0.524	2	4.65	16.59	14.874	0.0437	0.2032
52	3.109	13.381	6.294	0.28	0.524	2	11.185	27.273	22.727	0.0286	0.3199
53	1.646	8.412	4.119	0.183	0.524	2	6.947	17.735	14.874	0.0437	0.3036
54	0.713	7.675	2.288	0.183	0.524	2	3.112	11.327	14.874	0.0437	0.136
55	0.288	2.875	2	0.08	0.524	2	1.207	6.2	6.5	0.1	0.1207
56	0.996	7.867	4.119	0.069	0.524	2	3.677	14.874	14.874	0.0437	0.1607
57	0.835	4.987	2.62	0.116	0.524	2	4.087	11.354	9.461	0.0687	0.2808
58	0.663	4.844	2.62	0.116	0.524	2	2.635	10.189	9.461	0.0687	0.181
59	1.307	8.188	4.119	0.183	0.524	2	4.97	16.247	14.874	0.0437	0.2172
60	0.476	3.113	1	0.08	0.524	2	2.394	7	6.5	0.1	0.2394
61	1.347	12.255	6.993	0.28	0.524	2	2.853	18.357	22.727	0.0286	0.0816
62	0.835	4.987	1.456	0.116	0.524	2	4.59	10.48	9.461	0.0687	0.3153
63	0.378	3.015	1.4	0.08	0.524	2	1.848	7	6.5	0.1	0.1848
64	0.996	7.867	4.577	0.183	0.524	2	3.529	14.874	14.874	0.0437	0.1542
65	1.881	12.549	4.895	0.28	0.524	2	6.944	20.28	22.727	0.0286	0.1986
66	0.713	7.675	4.577	0.183	0.524	2	1.721	10.755	14.874	0.0437	0.0752
67	0.362	4.518	1.456	0.116	0.524	2	1.965	6.55	9.461	0.0687	0.135
68	1.347	12.255	4.895	0.28	0.524	2	4.86	17.483	22.727	0.0286	0.139
69	0.288	2.875	1.4	0.08	0.524	2	1.405	6	6.5	0.1	0.1405
70	3.109	13.381	3.497	0.28	0.524	2	12.542	28.497	22.727	0.0286	0.3587
71	2.469	13.038	6.993	0.28	0.524	2	7.913	26.224	22.727	0.0286	0.2263
72	1.881	12.549	3.497	0.28	0.524	2	7.22	21.329	22.727	0.0286	0.2065
73	0.835	4.987	2.911	0.116	0.524	2	3.92	10.48	9.461	0.0687	0.2693
74	1.646	8.412	4.577	0.183	0.524	2	6.682	17.391	14.874	0.0437	0.292
75	0.362	4.809	2.038	0.116	0.524	2	1.905	7.278	9.461	0.0687	0.1309
76	0.713	7.675	4.119	0.183	0.524	2	2.444	15.103	14.874	0.0437	0.1068
77	0.996	7.867	2.288	0.183	0.524	2	4.208	13.844	14.874	0.0437	0.1839
78	0.835	4.987	2.038	0.116	0.524	2	4.499	9.753	9.461	0.0687	0.3091
79	0.476	3.113	2.5	0.08	0.524	2	2.43	6.9	6.5	0.1	0.243
80	1.347	12.255	3.497	0.28	0.524	2	4.979	17.133	22.727	0.0286	0.1424
81	0.663	4.844	1.456	0.116	0.524	2	3.531	9.607	9.461	0.0687	0.2426
82	1.646	8.412	2.288	0.183	0.524	2	7.65	16.705	14.874	0.0437	0.3343
83	0.362	4.518	2.911	0.116	0.524	2	0.936	7.278	9.461	0.0687	0.0643
84	0.996	7.867	3.204	0.183	0.524	2	4.039	14.874	14.874	0.0437	0.1765
85	0.505	4.64	2.62	0.116	0.524	2	2.221	9.461	9.461	0.0687	0.1526
86	0.206	2.791	1	0.08	0.524	2	1.255	5	6.5	0.1	0.1255
87	2.469	13.038	4.895	0.28	0.524	2	9.388	25.874	22.727	0.0286	0.2685
88	0.476	3.113	1.8	0.08	0.524	2	2.497	7.65	6.5	0.1	0.2497
89	0.515	4.702	1.475	0.044	0.524	2	2.516	8.186	9.587	0.0678	0.1706
90	0.713	7.675	3.204	0.183	0.524	2	3.032	9.611	14.874	0.0437	0.1325
91	0.378	3.015	1.8	0.08	0.524	2	1.56	6.85	6.5	0.1	0.156
92	1.307	8.188	2.288	0.183	0.524	2	6.304	16.362	14.874	0.0437	0.2755
93	2.469	13.038	6.294	0.28	0.524	2	8.329	25.175	22.727	0.0286	0.2382
94	2.469	13.038	3.497	0.28	0.524	2	10.192	25.175	22.727	0.0286	0.2915
95	0.206	2.791	1.8	0.08	0.524	2	0.785	5.5	6.5	0.1	0.0785

Appendix. 2 Data collection used for evaluation of superelevation in open channel bends
(Shams, 1998)

Row	Q(m^3/s)	Y(m)	V(m/s)	A(m^2)	dy (m)
1	1.6	0.39	0.821	1.95	0.016
2	3.18	0.52	1.223	2.6	0.035
3	3.51	0.59	1.190	2.95	0.033
4	3.8	0.6	1.267	3	0.038
5	5.04	0.8	1.260	4	0.037
6	5.75	0.8	1.438	4	0.048
7	7.08	0.95	1.491	4.75	0.052
8	8.99	1.13	1.591	5.65	0.059
9	11.98	1.3	1.843	6.5	0.080
10	13.37	1.49	1.795	7.45	0.076
11	10.45	1.34	1.560	6.7	0.057
12	12.61	1.46	1.727	7.3	0.070
13	12.1	1.4	1.729	7	0.070
14	11.85	1.4	1.693	7	0.067
15	12.28	1.4	1.754	7	0.072
16	12.3	1.4	1.757	7	0.072
17	11.71	1.35	1.735	6.75	0.071
18	12.16	1.35	1.801	6.75	0.076
19	9.53	1.16	1.643	5.8	0.063
20	9.58	1.16	1.652	5.8	0.064
21	9.34	1.25	1.494	6.25	0.052
22	7.02	0.95	1.478	4.75	0.051
23	5.87	0.81	1.449	4.05	0.049
24	5.57	0.8	1.393	4	0.045
25	5.59	0.8	1.398	4	0.046
26	5.36	0.78	1.374	3.9	0.044
27	6.15	0.85	1.447	4.25	0.049
28	9.21	1.13	1.630	5.65	0.062
29	9.24	1.13	1.635	5.65	0.063
30	9.21	1.14	1.616	5.7	0.061
31	9.38	1.15	1.631	5.75	0.062
32	8.14	1.03	1.581	5.15	0.059
33	8.01	1	1.602	5	0.060
34	7.28	0.95	1.533	4.75	0.055
35	6.22	0.88	1.414	4.4	0.047
36	7.32	0.95	1.541	4.75	0.056
37	7.44	0.95	1.566	4.75	0.058
38	8.53	1.06	1.609	5.3	0.061
39	9.77	1.17	1.670	5.85	0.065
40	9.75	1.19	1.639	5.95	0.063
41	13.89	1.51	1.840	7.55	0.079
42	16	1.68	1.905	8.4	0.085
43	16.04	1.62	1.980	8.1	0.092
44	15.71	1.54	2.040	7.7	0.098
45	19.25	1.92	2.005	9.6	0.094
46	17.81	1.87	1.905	9.35	0.085
47	18.09	1.88	1.924	9.4	0.087

Row	Q(m³/s)	Y(m)	V(m/s)	A(m²)	dy(m)
48	17.84	1.83	1.950	9.15	0.089
49	13.33	1.54	1.731	7.7	0.070
50	13.6	1.54	1.766	7.7	0.073
51	16.04	1.74	1.844	8.7	0.080
52	15.37	1.67	1.841	8.35	0.079
53	13.54	1.55	1.747	7.75	0.072
54	13	1.46	1.781	7.3	0.074
55	11.81	1.38	1.712	6.9	0.069
56	13.32	1.53	1.741	7.65	0.071
57	16.45	1.76	1.869	8.8	0.082
58	16.88	1.76	1.918	8.8	0.086
59	18.93	1.9	1.993	9.5	0.093
60	19.32	1.9	2.034	9.5	0.097
61	13.07	1.48	1.766	7.4	0.073
62	12.45	1.36	1.831	6.8	0.079
63	11.77	1.3	1.811	6.5	0.077
64	11.7	1.28	1.828	6.4	0.078
65	16.1	1.63	1.975	8.15	0.091
66	16.53	1.68	1.968	8.4	0.091
67	15.75	1.64	1.921	8.2	0.086
68	15.11	1.58	1.913	7.9	0.086
69	14.59	1.52	1.920	7.6	0.086
70	15.35	1.58	1.943	7.9	0.089
71	15.59	1.64	1.901	8.2	0.085
72	15.25	1.65	1.848	8.25	0.080
73	14.25	1.5	1.900	7.5	0.085
74	15.49	1.61	1.924	8.05	0.087
75	9.2	1.1	1.673	5.5	0.066
76	9.49	1.13	1.680	5.65	0.066
77	9.78	1.14	1.716	5.7	0.069
78	9.82	1.14	1.723	5.7	0.070
79	9.86	1.14	1.730	5.7	0.070
80	9.07	1.07	1.695	5.35	0.067
81	7.44	0.93	1.600	4.65	0.060
82	7.33	0.93	1.576	4.65	0.058
83	8.01	0.98	1.635	4.9	0.063
84	10.41	1.18	1.764	5.9	0.073
85	10.39	1.18	1.761	5.9	0.073
86	9.78	1.14	1.716	5.7	0.069
87	6.29	0.84	1.498	4.2	0.053
88	6.21	0.83	1.496	4.15	0.052
89	6.11	0.82	1.490	4.1	0.052
90	8.35	1.02	1.637	5.1	0.063
91	9.33	1.1	1.696	5.5	0.067
92	8.09	0.97	1.668	4.85	0.065
93	10.07	1.16	1.736	5.8	0.071
94	9.24	1.1	1.680	5.5	0.066
95	8.02	1	1.604	5	0.060
96	8.86	1.06	1.672	5.3	0.066

Row	Q(m³/s)	Y(m)	V(m/s)	A(m²)	dy(m)
97	9.03	1.08	1.672	5.4	0.066
98	9.03	1.07	1.688	5.35	0.067
99	10.21	1.16	1.760	5.8	0.073
100	9.71	1.12	1.734	5.6	0.070
101	9.06	1.07	1.693	5.35	0.067
102	9.38	1.1	1.705	5.5	0.068
103	8.69	1.03	1.687	5.15	0.067
104	5.11	0.75	1.363	3.75	0.044
105	4.29	0.67	1.281	3.35	0.038
106	4.09	0.66	1.239	3.3	0.036
107	4.03	0.66	1.221	3.3	0.035
108	3.88	0.63	1.232	3.15	0.036
109	4.69	0.71	1.321	3.55	0.041
110	8.02	0.98	1.637	4.9	0.063
111	9.03	1.07	1.688	5.35	0.067
112	9.02	1.07	1.686	5.35	0.067
113	8.42	1.02	1.651	5.1	0.064
114	9.08	1.08	1.681	5.4	0.066
115	8.83	1.06	1.666	5.3	0.065
116	7.44	0.94	1.583	4.7	0.059
117	7.31	0.94	1.555	4.7	0.057
118	6.97	0.91	1.532	4.55	0.055
119	7.46	0.96	1.554	4.8	0.057
120	7.6	0.97	1.567	4.85	0.058
121	7.01	0.91	1.541	4.55	0.056
122	6.93	0.9	1.540	4.5	0.056
123	6.7	0.89	1.506	4.45	0.053
124	6.64	0.88	1.509	4.4	0.053
125	6.11	0.84	1.455	4.2	0.050
126	6.35	0.86	1.477	4.3	0.051
127	6.39	0.86	1.486	4.3	0.052
128	6.43	0.86	1.495	4.3	0.052
129	8.76	1.04	1.685	5.2	0.067
130	8.88	1.06	1.675	5.3	0.066
131	8.12	1	1.624	5	0.062
132	7.15	0.91	1.571	4.55	0.058
133	6.69	0.91	1.470	4.55	0.051
134	7.44	0.94	1.583	4.7	0.059
135	6.36	0.86	1.479	4.3	0.051
136	5.42	0.77	1.408	3.85	0.046
137	5.44	0.77	1.413	3.85	0.047
138	5.43	0.77	1.410	3.85	0.047
139	5.43	0.77	1.410	3.85	0.047
140	5.68	0.81	1.402	4.05	0.046
141	5.56	0.8	1.390	4	0.045
142	5.59	0.8	1.398	4	0.046
143	5.58	0.8	1.395	4	0.046
144	5.67	0.8	1.418	4	0.047
145	5.62	0.75	1.499	3.75	0.053

Row	Q(m³/s)	Y(m)	V(m/s)	A(m²)	dy(m)
146	5.18	0.75	1.381	3.75	0.045
147	5.16	0.75	1.376	3.75	0.044
148	5.15	0.75	1.373	3.75	0.044
149	6.37	0.86	1.481	4.3	0.051
150	4.17	0.67	1.245	3.35	0.036
151	28.50	2.50	2.32	12.4	0.130
152	3.21	0.57	1.126	2.85	0.030
153	27.802	2.47	2.30	12.45	0.129
154	10.21	1.2	1.702	6	0.063
155	25.01	2.23	2.243	11.15	0.116
156	30.229	2.52	2.399	12.6	0.131
157	19.24	1.85	2.080	9.25	0.103
158	19.37	1.85	2.094	9.25	0.111
159	26.694	2.28	2.342	11.4	0.120
160	26.642	2.36	2.258	11.8	0.123
161	25.4	2.22	2.288	11.1	0.118
162	26.596	2.28	2.333	11.4	0.120
163	26.85	2.33	2.305	11.65	0.123
164	27.425	2.45	2.239	12.25	0.127
165	19.0274	1.83	2.079	9.15	0.097
166	22.59	2.07	2.183	10.35	0.108
167	23.34	2.15	2.171	10.75	0.120
168	25.407	2.23	2.279	11.15	0.118
169	16.98	1.74	1.952	8.7	0.091
170	19.256	1.9	2.027	9.5	0.103
171	12.55	1.34	1.873	6.7	0.072
172	14.42	1.52	1.897	7.6	0.080
173	6.184	0.82	1.508	4.1	0.043

Measurements Descriptions:

Qazvin plain irrigation network is placed in 150 Km west of Tehran. Totally 278 MCM volume of water is conveyed by 9 Km tunnel from Taleghan storage dam into Ziaran diversion dam and then convey to Qazvin irrigation network. Main canal and laterals have concrete lining and have cumulatively 1100 Km length. Maximum capacity of main canal is 30 m3/sec. Total irrigated area by this network is equal to 80,000 ha.

The instrument is used for the accurate determination of the current velocity in water ways, channels and rivers (Figure App2.1). The measurements are executed with the propeller mounted on the rod(s) or connected to a cable. Suspended from a wire the meter can be applied at great depth.

The stream channel cross section is divided into numerous vertical subsections. In each subsection, the area is obtained by measuring the width and depth of the subsection, and the water velocity is determined using a current meter. The discharge in each subsection is computed by multiplying the subsection area by the measured velocity. The total discharge is then computed by summing the discharge of each subsection.

Each streamgage is a tall metal tower out at the end of a concrete walkway (Figure App.2.2). On the right is the automatic streamgage. The tall tube is called a stilling well. On the top is

the instrument shelter. The white strip along the side is called a staff gage, marked like a ruler so someone can read how deep the water is.

Figure. App 2.1. Water discharge measurements - current meter on Ziaran channel

Figure. App 2.2. Automatic streamgage on Ziaran channel

.

List of Notation and Symbols

The following list covers the global symbols that have used in this thesis.

Mathematical Notation and Abbreviations

Abbreviations

OLSE: Ordinary least squares estimation

WLSE: Weighted least-squares estimation

BLUE : Best linear unbiased estimation

MLE : Maximum likelihood estimation

ALSE: Alternating least squares estimation

GLR: Generalized likelihood ratio

SLR: Simple likelihood ratio

RFA: Regional frequency analysis

LS-VCE: Least square variance component estimation

FORM: First order reliability method

SORM: Second order reliability method

FEMA : Federal emergency management agency

PRA : Probabilistic risk analysis

QRA : Quantitative risk analysis

Mathematical Notation

Chapter 2

R_m : Real Euclidean space of dimension m

$I = I_m$: Identity matrix of order m

$\det(.)$: Determinant of a matrix

$(.)^T$: Transpose of a matrix

H_0 : Null hypothesis

H_a : Alternative hypothesis

α : Type I error probability

A : $m \times n$ Design matrix of functional model $E\{y\} = Ax$

$(.)^{-1}$: Inverse of a matrix

$\|.\|$: Squared norm of a vector as

$diag(.)$: Diagonal elements of a matrix

$E\{.\}$: Expectation operator

β : Type II error probability

y : m-vector of observables

x : n-vector of unknown parameters

W : $m \times m$ Weight matrix

$\hat{x}$: n-vector (estimator of x)

163

$\hat{\varepsilon}$: n-vector of estimation error $\hat{\varepsilon} = \hat{x} - x$

$Q_{\hat{x}}$: Covariance matrix of $\hat{x}$

$Q_{\hat{e}}$: Covariance matrix of $\hat{e}$

μ : Mean value

σ : Standard deviation

S_f : Safety

$Z_{(x_i)}$: Limit state function

R_{r_i} : Strength or capacity

S_{s_j} : External force or demands

P_f : Probability of failure

$f_{(x)}$: Probability density function

$F(x)$: Probability distribution

μ_z : Mean value

$\hat{e}_0$: Least squares estimate of residuals under H_0

$\hat{y}$: Least squares estimator of observables

Q_y : $m \times m$ Covariance matrix of observables

$P\{x = x_0\}$: Probability that x will be equal to x_0

W_t : A $b \times b$ symmetric and positive definite matrix

$\sigma_{\hat{e}_i}$: Standard deviation of least-squares residual i

e : m-vector of measurement error

$\hat{e}$: Least-squares estimator of residuals

w : w-test statistic

σ_z : Standard deviation

β : Reliability index

α_i : Sensitivity factor

μ_R : Strength mean value

μ_s : Force mean value

σ_R : Strength standard deviation

σ_s : Force standard deviation

n : Total number of simulation

$Q_{\hat{y}}$: Covariance matrix of $\hat{y}$

n_f : Number of simulation

Q : $m \times m$ symmetric and positive definite matrix

W : A $m \times m$ symmetric and positive definite matrix

$f_y(y|x)$: Probability density function of observables y

$rank(.)$: Rank of a matrix (independent columns or rows of a matrix)

$N(\mu, \sigma)$: Normal distribution with mean μ and standard deviation σ

Chapter 4

P : Dynamic pressure $(N.m^{-2})$

q : Specific discharge $(m^2.s^{-1})$

V : Velocity $(m.s^{-1})$

R : Radius of the bucket (m)

X_j : Distance form the flip bucket (m)

L_j : Trajectory length (m)

Y_j : Vertical rise height of jet (m)

β : Jet entry angle $(radians)$

α : Angle of the bucket lip $(radians)$

g : Acceleration gravity $(m.s^{-2})$

F_V : Shear drag (N)

F_P : Pressure drag (N)

F_D : Total drag (N)

C_V, C_P, C_D : Coefficient of drag

ρ : Density of fluid (kg/m^3)

U : Fluid velocity $(m.s^{-1})$

A : Projected area (m^2)

F_L : Life force (N)

C_L : Life coefficient $[-]$

Fr : Froude number $[-]$

b : Thickness of the jet (m)

d : Diameter of the jet (m)

d_S : Scour depth (m)

d_{50} : Mean practical size (mm)

d_{cr} : Critical depth (m)

d_w : Normal water depth (m)

k : Ratio of air to water $[-]$

V_e : Minimum jet velocity $(m.s^{-1})$

E : Jet energy (m)

L_S : Length of scour hole (m)

W_S : Width scour hole (m)

V_j : Velocity of the jet at the flip bucket $(m.s^{-1})$

U_0 : Velocity of the jet at the nozzle $(m.s^{-1})$

σ_{50} : Standard deviation bed material (mm)

β_1 : Upstream angle of the scour hole $(radians)$

W_b : Width of bucket lip (m)

X_j : Length of trajectory jet (m)

ϕ : Lip angle $(radians)$

R : Bucket radius (m)

θ : Lip angle $(radians)$

G_S : Specific gravity

ρ_w : Density of water (kg/m^3)

ρ : Density of bed particle (kg/m^3)

μ_w : Dynamic viscosity $(Pa.s)$

H_1 : Height from bucket lip to the water surface level in plunge pool (m)

H_1 : Difference between upstream and downstream water level (m)

$\Delta\rho$: Differences between the mass densities of the bed particles (kg/m^3)

Chapter 5

r : Centerline radius of curvature (m)

X, Y : The co-ordinates of the cross profile

h : Flow depth (m)

Z_S : Elevation of water surface (m)

Z_b : Elevation of the bottom (m)

P : Pressure $(N.m^{-2})$

ν : Kinematic viscosity (m^2/s)

∇ : Divergence

f : Other body forces (N)

t : Time (s)

a_s : Acceleration component in s

a_n : Acceleration component in n

E : Total energy (m)

s, n, z : Curvilinear coordinate component $[-]$

F_S, F_n, F_Z : friction force in s, n, z direction (N)

r_0 : Outer radius wall (m)

r_i : Inner radius wall (m)

r_c : Central radius (m)

V_0 : Outer velocity wall $(m.s^{-1})$

V_i : Inner velocity wall $(m.s^{-1})$

V_c : Center velocity wall $(m.s^{-1})$

y_i : Inner water level (m)

y_0 : Outer water level (m)

dy : Superelevation (m)

b : Bottom width of the channel (m)

T : Top width of the channel (m)

C_1, C_2 : Circulation constant

S : Secondary flow

U, V, W : Velocity component in s, n, z direction $(m.s^{-1})$

Chapter 6

n : Number of observations

P : Dynamic pressure $\left(N.m^{-2}\right)$

q : Specific discharge $\left(m^2.s^{-1}\right)$

V : Velocity $\left(m.s^{-1}\right)$

R : Radius of the bucket (m)

X_j : Distance form the flip bucket (m)

L_j : Trajectory length (m)

Y_j : Vertical rise height of jet (m)

β : Jet entry angle $(radians)$

α : Angle of the bucket lip $(radians)$

g : Acceleration gravity $\left(m.s^{-2}\right)$

F_V : Shear drag (N)

F_P : Pressure drag (N)

F_D : Total drag (N)

C_V, C_P, C_D : Coefficient of drag

ρ : Density of fluid $\left(kg/m^3\right)$

U : Fluid velocity $\left(m.s^{-1}\right)$

A : Projected area $\left(m^2\right)$

F_L : Life force (N)

C_L : Life coefficient $[-]$

Fr : Froude number $[-]$

V_j : Velocity of the jet at the flip bucket $\left(m.s^{-1}\right)$

U_0 : Velocity of the jet at the nozzle $\left(m.s^{-1}\right)$

β_1 : Upstream angle of the scour hole $(radians)$

b : Thickness of the jet (m)

d : Diameter of the jet (m)

d_S : Scour depth (m)

d_{50} : Mean practical size (mm)

d_{cr} : Critical depth (m)

d_w : Normal water depth (m)

k : Ratio of air to water $[-]$

V_e : Minimum jet velocity $\left(m.s^{-1}\right)$

E : Jet energy (m)

L_S : Length of scour hole (m)

W_S : Width scour hole (m)

W_b : Width of bucket lip (m)

X_j : Length of trajectory jet (m)

ϕ : Lip angle $(radians)$

R : Bucket radius (m)

θ : Lip angle $(radians)$

σ_{50} : Standard deviation bed material (mm)

G_S : Specific gravity

ρ_w : Density of water $\left(kg/m^3\right)$

ρ : Density of bed particle $\left(kg/m^3\right)$

μ_w : Dynamic viscosity $(Pa.s)$

H_1 : Difference between upstream and downstream water level (m)

$\Delta\rho$: Differences between the mass densities of the bed particles $\left(kg/m^3\right)$

Chapter 7

$E, E_1,.., E_5$: Total head (m)

d : Water depth (m)

θ : Bed slop

Z_0 : Bed elevation (m)

α' : Kinetic energy correction coefficient

V : Velocity $\left(m.s^{-1}\right)$

r : Radius of curvature (m)

b : Width channel (m)

n : Manning coefficient

n_A : Actual manning coefficient

E_{cb} : Elevation in the bend center (m)

d_f : Height of the water level (m)

Q : Discharge in the flume $\left(m^3/s\right)$

A_f : Area of the flume $\left(m^2\right)$

P : Wetted perimeter (m)

dy_{cb} : Amount of superelevation (m)

H_b : Canal height (m)

Z : Limit state function

P_f : Probability function

$k_1, k_2, ..., k_i$: Dimensionless coefficients of the local head losses

Z_f : Elevation of the bottom of the flume

L_{f-cb} : Distance between flume and bend center (m)

C_{tot} : Total cost

β : Reliability index

$\text{Re}_{(N)}$: Reynolds number

S_f : Hydraulic slope

E_d : Economic damage

I_{h_0} : Initial cost

I : Investment cost

r : Discount rate

I_h : Variable cost

h_0 : Current channel height

h : Channel height

Chapter 8

$F_{h,static}$: Hydrostatic horizontal load (N)

h_{us} : Upstream water depth (m)

h_{ds} : Downstream water depth (m)

w : Width (m)

$F_{v,static}$: Hydrostatic vertical load (N)

F_{drag} : Drag force (N)

$C_{I,1}, C_{I,2}$: Coefficients for the contribution of the acceleration

C_D : Drag coefficient

h : Water depth (m)

u : Velocity $(m.s^{-1})$

F_h : Hydrodynamic force (N)

F_{h,qs^+} : Quasi static force (N)

F_{imp} : Hydrodynamic impact force (N)

Acknowledgements

I am also indebted to my Iranian friends Dr. Alireza Amiri Simkooei, Dr. Alireza Asadi, Dr, Mohammadreza Rajabalinejad, Dr. Hossein Mansouri, Dr. Shohre Shahnoori, Dr. Ali Heidary, Dr. Yahya Memarzadeh, Dr. Mehdi Nikbakht, Dr. Asadollah Shahbahrami, Dr. Masoud Shirazian, Dr. Alireza Davoudian Dehkordi, and all my friends in the Netherlands.

Curriculum Vitae

Gholamreza Shams Ghahfarokhi was born on April, 07, 1963 in Khorramabad, Iran. He obtained his Bachelor of Engineering the Esfahan University of Technology Iran (1995) and Master of Science in Hydraulic Engineering, from the AmirKabir University of Technology (Tehran Polytechnic) of Tehran, Iran (1998). His earlier backgrounds are Hydraulics and Hydrology. He developed himself as an expert in probabilistic methods and reliability analysis in hydraulic structures design and risk based modeling techniques through his PhD research at the section of Hydraulic Structure and Probabilistic Design at the Faculty of Civil Engineering and Geosciences of Delft University of Technology (TU Delft), The Netherlands, under the supervisions of Prof.drs.ir. J.K. Vrijling and Prof. dr.ir. P.H.A.J.M van Gelder (TU Delft). The PhD research was fully funded by The Iranian Ministry of Science, Research, and Technology. While working on the project, he has been involved in a number of research activities at the department of Hydraulic Engineering such as the EU project FLOODsite on safety against flooding in the Netherlands. Gholamreza Shams research interests are related to statistics, sensitivity and uncertainty analysis of environmental data, multivariate analysis of hydraulic loads on structural systems, reliability analysis and flood risk.